

Global Biogeochemical Cycles[®]



REVIEW ARTICLE

10.1029/2020GB006814

Key Points:

- Distributions, drivers, and depositional archives described for iron, zinc, copper, cadmium, molybdenum, barium, nickel, chromium, and silver
- Cadmium, barium, nickel, and chromium isotopes offer the most promise as paleoproductivity tracers, but key uncertainties remain
- Future priorities include quantification of “missing” flux terms, constraining circulation influences, and identifying sedimentary archives

Correspondence to:




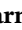
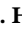

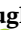







T. J. Horner, S. H. Little, T. M. Conway, and J. R. Farmer,
Tristan.Horner@whoi.edu;
susan.little@ucl.ac.uk;
tmconway@usf.edu;
jesse.farmer@princeton.edu

Citation:

Horner, T. J., Little, S. H., Conway, T. M., Farmer, J. R., Hertzberg, J. E., Janssen, D. J., et al. (2021). Bioactive trace metals and their isotopes as paleoproductivity proxies: An assessment using GEOTRACES-era data. *Global Biogeochemical Cycles*, 35, e2020GB006814. <https://doi.org/10.1029/2020GB006814>

Received 2 SEP 2020
 Accepted 20 MAY 2021

Bioactive Trace Metals and Their Isotopes as Paleoproductivity Proxies: An Assessment Using GEOTRACES-Era Data

T. J. Horner^{1,2} , S. H. Little³ , T. M. Conway⁴ , J. R. Farmer^{5,6} , J. E. Hertzberg^{7,8} ,
 D. J. Janssen⁹ , A. J. M. Lough^{10,11} , J. L. McKay¹² , A. Tessin¹³ , S. J. G. Galer⁶ ,
 S. L. Jaccard¹⁴ , F. Lacan¹⁵ , A. Paytan¹⁶ , K. Wuttig^{17,18} , and
 GEOTRACES–PAGES Biological Productivity Working Group Members¹⁹

¹NIRVANA Labs, Woods Hole Oceanographic Institution, Woods Hole, MA, USA, ²Department of Marine Chemistry & Geochemistry, Woods Hole Oceanographic Institution, Woods Hole, MA, USA, ³Department of Earth Sciences, University College London, London, UK, ⁴College of Marine Science, University of South Florida, FL, USA, ⁵Department of Geosciences, Princeton University, Princeton, NJ, USA, ⁶Max-Planck Institute for Chemistry, Mainz, Germany, ⁷Department of Ocean Earth & Atmospheric Sciences, Old Dominion University, Norfolk, VA, USA, ⁸Now at: International Ocean Discovery Program, Texas A&M University, College Station, TX, USA, ⁹Institute of Geological Sciences and Oeschger Centre for Climate Change Research, University of Bern, Bern, Switzerland, ¹⁰University of Southampton, National Oceanography Centre, Southampton, England, ¹¹Now at: School of Geography, University of Leeds, Leeds, England, ¹²College of Earth, Ocean, and Atmospheric Sciences, Oregon State University, Corvallis, OR, USA, ¹³Department of Geology, Kent State University, Kent, OH, USA, ¹⁴Institute of Earth Sciences, Université de Lausanne, Lausanne, Switzerland, ¹⁵LEGOS, University of Toulouse, CNRS, CNES, IRD, UPS, Toulouse, France, ¹⁶Institute of Marine Sciences, University of California Santa Cruz, Santa Cruz, CA, USA, ¹⁷Antarctic Climate and Ecosystems Cooperative Research Centre, University of Tasmania, Hobart, TAS, Australia, ¹⁸Now at: Federal Maritime and Hydrographic Agency (BSH), Hamburg, Germany, ¹⁹A Full list of working group members and their affiliations appears at the Appendix A section

Abstract Phytoplankton productivity and export sequester climatically significant quantities of atmospheric carbon dioxide as particulate organic carbon through a suite of processes termed the biological pump. Constraining how the biological pump operated in the past is important for understanding past atmospheric carbon dioxide concentrations and Earth’s climate history. However, reconstructing the history of the biological pump requires proxies. Due to their intimate association with biological processes, several bioactive trace metals and their isotopes are potential proxies for past phytoplankton productivity, including iron, zinc, copper, cadmium, molybdenum, barium, nickel, chromium, and silver. Here, we review the oceanic distributions, driving processes, and depositional archives for these nine metals and their isotopes based on GEOTRACES-era datasets. We offer an assessment of the overall maturity of each isotope system to serve as a proxy for diagnosing aspects of past ocean productivity and identify priorities for future research. This assessment reveals that cadmium, barium, nickel, and chromium isotopes offer the most promise as tracers of paleoproductivity, whereas iron, zinc, copper, and molybdenum do not. Too little is known about silver to make a confident determination. Intriguingly, the trace metals that are least sensitive to productivity may be used to track other aspects of ocean chemistry, such as nutrient sources, particle scavenging, organic complexation, and ocean redox state. These complementary sensitivities suggest new opportunities for combining perspectives from multiple proxies that will ultimately enable painting a more complete picture of marine paleoproductivity, biogeochemical cycles, and Earth’s climate history.

1. Introduction

The ocean plays host to three carbon “pumps” that redistribute climatically significant quantities of carbon dioxide (CO₂) from the atmosphere to the ocean interior and seafloor (Volk & Hoffert, 1985). These ocean carbon pumps—biological, carbonate, and solubility—influence Earth’s climate over timescales ranging from decades to millions of years (e.g., Khatiwala et al., 2019; Sigman et al., 2010; Volk & Hoffert, 1985). The biological pump refers specifically to the production of particulate organic carbon (POC) within the sunlit surface ocean (euphotic zone) and export of POC to the intermediate and deep ocean, where POC is

© 2021. The Authors.
 This is an open access article under the terms of the [Creative Commons Attribution License](https://creativecommons.org/licenses/by/4.0/), which permits use, distribution and reproduction in any medium, provided the original work is properly cited.

largely (but not wholly) regenerated. The biological pump is of particular interest as it connects the cycles of C to those of dissolved O₂, nutrients, and marine biology, and today accounts for as much as 70% of the carbon concentration gradient between the euphotic zone and the deep ocean (Sarmiento & Gruber, 2006).

The biological pump acts to redistribute CO₂ from the atmospheric/surface ocean carbon reservoir to the deep ocean and sediment carbon reservoirs via two steps. First, phytoplankton, photoautotrophic microbes, use sunlight (represented here by *hν*) to transform ambient dissolved inorganic carbon (DIC) into POC, represented here by CO₂ and a simple sugar (CH₂O), respectively, by the simplified reaction:

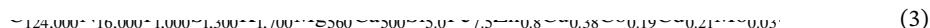


The second step requires that some fraction of the newly formed POC sinks into the ocean interior through a combination of biological and physical aggregation processes (e.g., Alldredge & Silver, 1988), where ultimately some POC may be buried in marine sediments. The resulting surface ocean DIC deficit promotes dissolution of atmospheric CO₂ into seawater to maintain air-sea CO₂ equilibrium, driving an overall reduction in the partial pressure of atmospheric CO₂ ($p\text{CO}_2$). Note that this definition of the biological pump neglects dissolved organic carbon export, which is comparatively understudied, though may account for as much as one-third of C export (e.g., Carlson et al., 2010; Giering et al., 2014). Importantly, Reaction (1) requires sunlight and can only occur in the euphotic zone of the ocean. In contrast, aerobic heterotrophic respiration can occur wherever POC and O₂ are present:



There are also a number of O₂-independent respiration pathways that are reviewed in detail elsewhere (e.g., Froelich et al., 1979).

While the representation of all POC as a simple sugar (CH₂O) is instructive for illustrating an important biotic transformation in the ocean, it is also simplistic; microbial biomass consists of dozens of bioactive elements that serve many essential functions (e.g., da Silva & Williams, 1991). The elemental stoichiometry of POC can thus be expanded to include a number of major and micronutrient elements, as illustrated by the extended Redfield ratio reported by Ho et al. (2003):



With this extended stoichiometry in mind, it is clear that Reactions (1) and (2)—the production and regeneration of organic matter, respectively—will not only generate gradients in the dissolved concentration of DIC and O₂, but will act on any bioactive element associated with POC cycling. These gradients will be steepest for those elements possessing shorter residence times and where biological uptake and regeneration are the most important processes driving their marine cycling. Likewise, such gradients may be almost absent for elements that possess long residence times or are primarily cycled by processes other than productivity.

For those bioactive metals where biological processes are dominant, the implication of Reactions (1) and (2) is that many of the elements listed in (3) may, in turn, be used as proxies of POC cycling and, potentially, paleoproductivity. Indeed, aspects of past ocean productivity that impact carbon and nutrient cycling are routinely reconstructed using the stable isotope compositions of carbon and macronutrient elements (N and Si; see Farmer et al., 2021). It thus follows that the abundance and isotopic compositions of bioactive trace metals cycled along with POC could also provide valuable information on past ocean productivity. However, in order to use bioactive trace elements and their isotopes (TEIs) as proxies for productivity, it is necessary to develop a comprehensive understanding of the marine behavior of these elements, including: mapping their distribution in the ocean; elucidating the drivers of their distribution; characterizing sources, sinks, and transformations associated with biological, physical and chemical (notably redox) reactions; and, recognizing if (and how) a given element is incorporated and preserved in marine sediments.

The wealth of new trace element and isotope data from the GEOTRACES program (e.g., Figure 1) now permits an assessment of whether certain bioactive TEI metals may serve as proxies for past ocean productivity. This contribution represents such an assessment. Our study synthesizes what is known about the processes governing the cycling of nine bioactive metals in seawater, explores the level of development and readiness of each isotope system to inform on aspects of past ocean productivity, and identifies areas where further

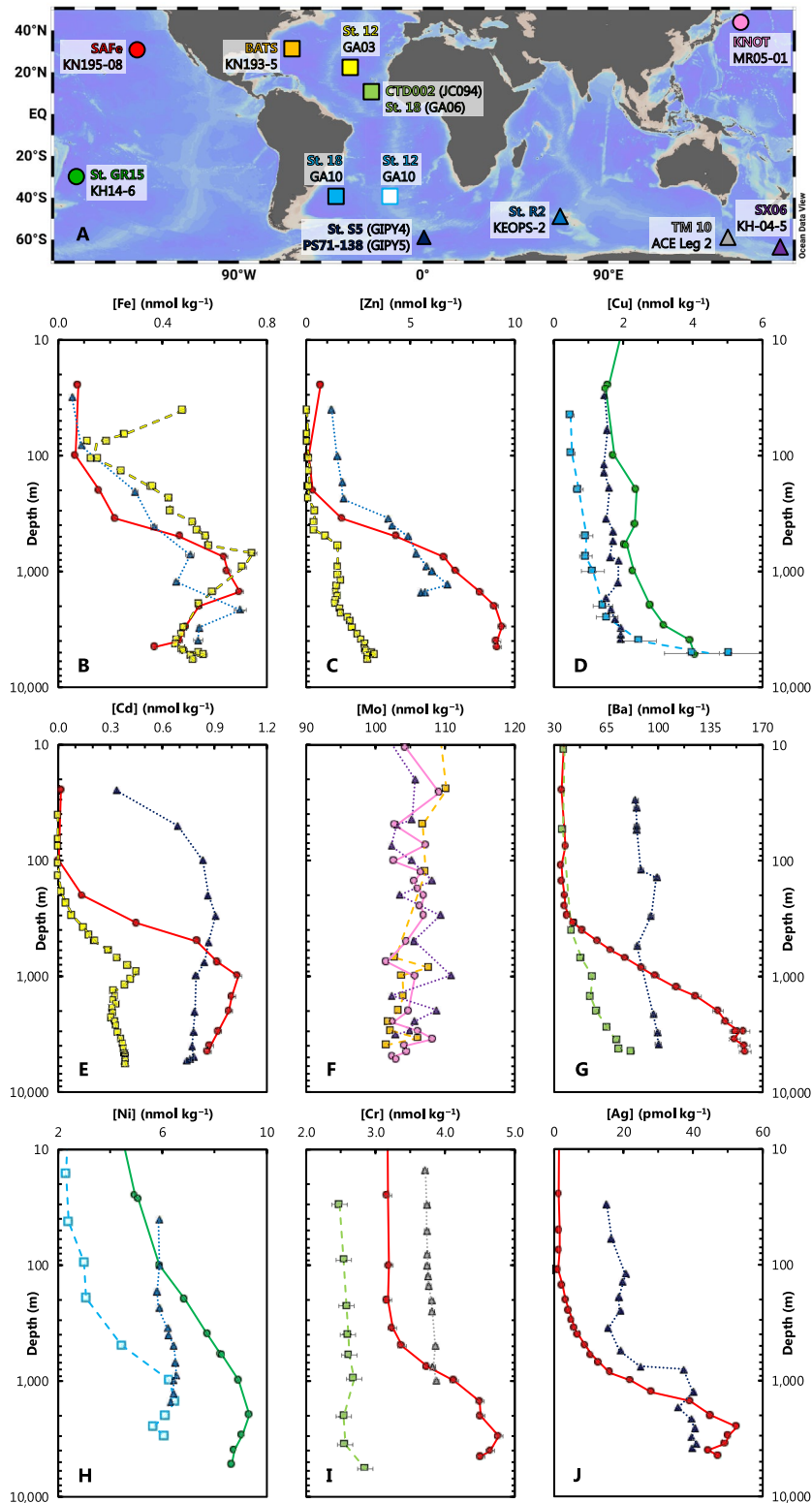


Figure 1.

research is most needed to improve our understanding of the geochemistry of trace metals in the past and present ocean. We base our assessment on publicly available results from the international GEOTRACES program (e.g., Mawji et al., 2015; Schlitzer et al., 2018). Our study is not intended to be a thorough review of all available techniques used to reconstruct paleoproductivity. Instead, we focus on bioactive metal isotope systems that are either recognized as micronutrients (such as those in Equation 3) or exhibit nutrient-like dissolved profiles in seawater, regardless of their nutritional status to phytoplankton (e.g., Ba, Cr, and Ag). This will not be the last word on the topic; our understanding of many of these metal isotope systems has rapidly evolved in recent years, and will continue to evolve as new data are generated.

2. Key Concepts

In this section, we introduce several key concepts to which we refer throughout the review. First, we provide definitions for reporting bioactive metal concentrations and isotope variations, and for the concept of paleoproductivity itself (Section 2.1). Second, we describe an idealized framework for reconstructing paleoproductivity based on the coupled cycling of bioactive trace metals and their isotopes (Section 2.2). Finally, we introduce a number of additional trace metal cycling processes that are important considerations when applying bioactive trace metal isotope systems to reconstruct productivity (Section 2.3).

The review sections are structured such that each bioactive metal isotope system is described similarly and systematically. The order in which metals are reviewed follows the extended Redfield ratio—Fe (Section 3), Zn (Section 4), Cu (Section 5), Cd (Section 6), and Mo (Section 7)—before describing the nonessential elements Ba (Section 8), Ni (Section 9), Cr (Section 10) and Ag (Section 11) in order of decreasing dissolved concentration in seawater. The review of each metal isotope system is organized around four questions:

1. What is the modern marine distribution of this trace metal isotope system?
2. Which biological, chemical, and physical processes are most important for maintaining this distribution?
3. Do any marine sediments capture the distribution of this trace metal isotope system?
4. What are the priorities for improving the utility of this trace metal isotope system to track paleoproductivity?

This structure results in some repetition of the main distributions, drivers, and sedimentary archives between individual isotope systems. This redundancy is deliberate: each section can be read independently without reference to the other bioactive trace metals. We close our review by assessing the “maturity” of each system based on a comparison to more established productivity proxies, offer suggestions for future studies, and discuss prospects for productivity reconstructions using bioactive trace metal isotope systems.

2.1. Definitions

2.1.1. Data Reporting Conventions

The isotope literature abounds with isotope notations (e.g., ϵ , δ), reference materials (e.g., IRMM, JMC, and NIST), and isotope ratio pairs (e.g., $^{57}\text{Fe}/^{54}\text{Fe}$ vs. $^{56}\text{Fe}/^{54}\text{Fe}$; $^{137}\text{Ba}/^{134}\text{Ba}$ vs. $^{138}\text{Ba}/^{134}\text{Ba}$). There are merits to each of these choices and we do not intend to review these here. However, we believe that the sheer number of ways in which trace metal isotope data have been reported can be confusing to scientists in other disciplines and this ultimately diminishes the reach and utility of isotope-based research. To avoid furthering this confusion, we have adopted a number of conventions that apply throughout this review, regardless of how literature data were originally reported. First, we use a single isotope notation throughout: “ δ ” (i.e., the delta notation; Equation 4). Second, we express all data relative to the most widely accepted standard

Figure 1. Overview of bioactive dissolved trace metal concentration distributions discussed in this review. A map showing locations of the representative depth profiles shown in both the lower panels and discussed throughout this review (Sections 3–11). The specific station (bold) and cruise identifier are given for each location; circles, squares, and triangles denote stations in the Pacific, Atlantic, and Southern Oceans, respectively. The lack of exemplar stations from the Indian Ocean reflects the current paucity of GEOTRACES-compliant campaigns in this basin. Two stations sampled from the Atlantic Sector of the Southern Ocean share the same symbol (St. S5 of GIPY4 at 57.55 S, 0.04 W; PS71-138 of GIPY5 at 61.00 S on the Zero Meridian), as do two stations from the Eastern Tropical North Atlantic (St. 18 of GA06 at 12.03 N, 28.98 W and CTD002 of JC094 at 9.28 N, 21.63 W). (b–j) Depth profiles of bioactive trace metal concentrations for Fe (b), Zn (c), Cu (d), Cd (e), Mo (f), Ba (g), Ni (h), Cr (i), and Ag (j). Profiles are shown in semi-log space to illustrate variations in the epi- and mesopelagic realm. Originators are cited in the Data Sources section. Map created using Ocean Data View (Schlitzer, R., <https://odv.awi.de>, 2018).

Table 1

Summary of Oceanic Dissolved Concentrations, Isotope Notation, Standards, and Isotopic Compositions, and Mean Ocean Residence Times for Trace Metals Discussed in This Review

Element	Dissolved concentration range (nmol kg ⁻¹)	$\delta^i\text{Me}$ and R	Standard used for $\delta^i\text{Me}$	Mean upper continental crust $\delta^i\text{Me}$ (‰)	Mean deep ocean $\delta^i\text{Me}$ (‰)	Range of deep ocean $\delta^i\text{Me}$ (‰)	Residence time estimates (kyr)
Fe	0.01–100 ^a	$\delta^{56}\text{Fe}$, $^{56}\text{Fe}/^{54}\text{Fe}$	IRMM-014 ^e	+0.1 ^m	Variable ^t	–2.4 to +1.5 ^t	0.004–0.6 ^{aa}
Zn	0.01–10 ^a	$\delta^{66}\text{Zn}$, $^{66}\text{Zn}/^{64}\text{Zn}$	JMC-Lyon ^f	+0.3 ^f	\approx +0.5 ^u	–0.2 to +0.6 ^u	1–11 ^{aa}
Cu	0.5–4 ^a	$\delta^{65}\text{Cu}$, $^{65}\text{Cu}/^{63}\text{Cu}$	NIST SRM 976 ^f	+0.1 ^f	\approx +0.7 ^v	+0.6 to +0.8 ^v	2–5 ^{aa}
Cd	0.00003–1.2 ^a	$\delta^{114}\text{Cd}$, $^{114}\text{Cd}/^{110}\text{Cd}$	NIST SRM 3108 ^g	0.0 ⁿ	\approx +0.3 ^w	+0.2 to +0.4 ^w	22–105 ^{aa}
Mo	100 ^b	$\delta^{98}\text{Mo}$, $^{98}\text{Mo}/^{95}\text{Mo}$	NIST SRM 3134 + 0.25‰ ^h	\leq 0.4 ^o	\approx +2.3 ^x	Homogeneous ^x	440 ^{ab}
Ba	35–160 ^a	$\delta^{138}\text{Ba}$, $^{138}\text{Ba}/^{134}\text{Ba}$	NIST SRM 3104a ⁱ	0.0 ^p	\approx +0.3 ^y	+0.2 to +0.4 ^y	8 ^{ac}
Ni	1.5–11 ^a	$\delta^{60}\text{Ni}$, $^{60}\text{Ni}/^{58}\text{Ni}$	NIST SRM 986 ^j	+0.1 ^q	\approx +1.3 ^z	+1.2 to +1.5 ^z	10–30 ^{ad}
Cr	1–7 ^c	$\delta^{53}\text{Cr}$, $^{53}\text{Cr}/^{52}\text{Cr}$	NIST SRM 979 ^k	–0.12 ^r	\approx +0.8 ^c	0.6–1.2 ^c	6 ^{ae}
Ag	0.0002–0.1 ^d	$\delta^{109}\text{Ag}$, $^{109}\text{Ag}/^{107}\text{Ag}$	NIST SRM 978a ^l	0.0 ^s	Unknown	Unknown	0.4 ^{af}

^aSchlitzer (2019); ^bMorris (1975); ^cSection 10 and references therein; ^dGallon and Flegal (2015); ^eDauphas et al. (2017); ^fMoynier et al. (2017) and references therein; ^gAbouchami et al. (2013); ^hNägler et al. (2014); ⁱHorner, Kinsley, and Nielsen (2015); ^jElliott & Steele (2017); ^kEllis et al. (2002); ^lWoodland et al. (2005); ^mGong et al. (2017); ⁿSchmitt et al. (2009a); ^oWillbold & Elliott (2017); ^pNan et al., 2018; ^qCameron et al. (2009); ^rSchoenberg et al. (2008); ^sUSGS reference material SCO-1 (Cody Shale) is used given paucity of representative data; Schönbachler et al. (2007); ^tSection 3 and references therein; ^uSection 4 and references therein; ^vSection 5 and references therein; ^wSection 6 and references therein; ^xData from Nakagawa et al. (2012) renormalized to NIST SRM 3134 + 0.25‰ based on Goldberg et al. (2013); ^ySection 8 and references therein; ^zYang et al. (2020); ^{aa}Hayes et al. (2018) and references therein; ^{ab}Miller et al. (2011); ^{ac}Dickens et al. (2003); ^{ad}Cameron & Vance (2014) and references therein; ^{ae}Wei et al. (2018); ^{af}Broecker and Peng (1982).

for each isotope system. For many isotope systems, the most widely accepted standard may have since been exhausted (e.g., JMC-Lyon for Zn). In those cases, there are usually cross-calibrated secondary materials that can be used to report new isotope data in terms of legacy materials (e.g., AA-ETH for Zn, Archer et al., 2017). Third, we report trace metal isotope data using the same isotope ratio pairs and reference materials as used in the GEOTRACES data products (e.g., Mawji et al., 2015; Schlitzer et al., 2018). We note that isotope data are a unitless ratio quantity (Coplen, 2011), though are commonly reported with “units” of ‰ (i.e., parts per one thousand):

$$\delta^i\text{Me}(\text{‰}) = \frac{R_{\text{sample}}}{R_{\text{standard}}} - 1 \quad (4)$$

where $\delta^i\text{Me}$ and R are listed for each element in Table 1. For clarity, all isotopic data reviewed here have been calculated using notation in Equation 4, and renormalized to the standards listed in Table 1, regardless of how the data originators reported their results.

We denote the concentrations of different species using square brackets (i.e., []). Unless specifically stated, all concentrations refer to dissolved species; for example, [Fe] denotes dissolved Fe concentrations, and [Me] denotes the concentration of a metal “Me” in a general case. Salient features of each trace metal isotope system are summarized in Table 1.

2.1.2. Paleoproductivity

We define paleoproductivity as the productivity of an ecosystem that contributes to the sequestration of atmospheric CO₂ as POC in the ocean interior and on the seafloor. Our definition of paleoproductivity is therefore analogous to that of net ecosystem productivity (NEP), which is defined as gross primary production minus autotrophic and heterotrophic respiration, and where gross primary production is the total autotrophic production of POC (or O₂; Equation 1; Sigman & Hain, 2012). If considering only the euphotic zone, NEP is equivalent to export production, which is an important component of the biological carbon pump (Boyd et al., 2019); indeed, changes in export production have been implicated as a major driver of variations in glacial–interglacial pCO₂ and hence climate (e.g., Berger et al., 1989; Boyle, 1988b; Broecker, 1982; Paytan, 2009). Many of these changes in past export production were inferred on the basis of variations in the cycling of major nutrients and their isotopes (e.g., N, Si; Farmer et al., 2021). The net consumption of

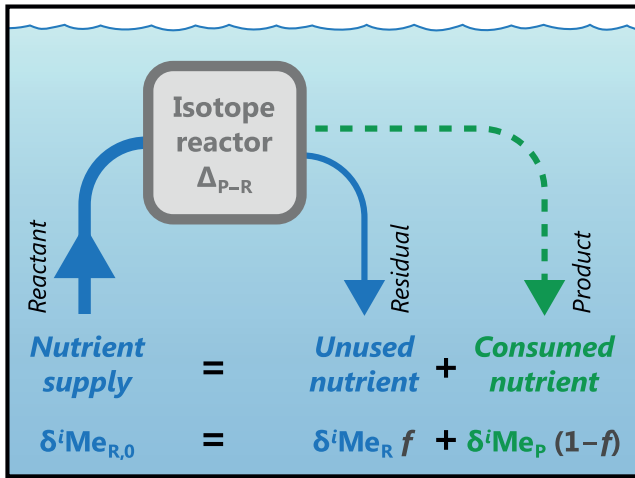


Figure 2. Overview of a single-process reactor with an isotope separation factor Δ_{P-R} . The reactor is assumed to follow the principles of isotope mass balance, in that the isotope composition of the residual unused nutrient ($\delta^i\text{Me}_R$) and consumed nutrient ($\delta^i\text{Me}_P$) sum to the isotope composition of metal initially supplied to the reactor ($\delta^i\text{Me}_{R,0}$).

nutrients can be interpreted in terms of export production by assuming a fixed proportionality between the major nutrients and C. This proportionality provides the connection linking major nutrient cycles to the sequestration of atmospheric CO_2 via biological productivity. In the next section, we outline how such a framework can be similarly applied to interpret the distributions of bioactive metals and their isotopes in terms of export productivity.

2.2. From Nutrients to Productivity

The cycling of nutrients is intimately connected with productivity; along with sunlight, nutrients are the fuel that powers the biological pump. In turn, the biological pump renders systematic changes in the concentration and isotopic composition of nutrients throughout the oceans. Assuming that these changes follow certain known rules, we can use bioactive metals and their isotopes as tracers of biological productivity in Earth's past. In this section, we describe how nutrient uptake can generate isotope variations in seawater and develop a framework for linking nutrients with productivity that applies to several of the isotope systems reviewed here.

2.2.1. The Isotope Reactor Model

Here we use an example whereby an hypothetical micronutrient metal “Me” is supplied to, and consumed within, an isotope reactor (Figure 2).

Though a simple, non-dimensional representation of myriad oceanographic processes, isotope reactor models have found utility in describing the marine behaviors of macro- (e.g., N; Sigman et al., 1999; Si, Reynolds et al., 2006) and micronutrients (e.g., Ba; Horner, Kinsley, & Nielsen, 2015; Cd, Abouchami et al., 2011; Cr, Scheiderich et al., 2015; Ni, Yang et al., 2020). Reactor models assume that a Me is only consumed within the reactor, and that consumption occurs as a single reaction with a fixed isotope separation factor, Δ_{P-R} , defined as:

$$\Delta_{P-R} \equiv \delta^i\text{Me}_P - \delta^i\text{Me}_R \quad (5)$$

where $\delta^i\text{Me}_P$ and $\delta^i\text{Me}_R$ are the stable isotope compositions of the product (phytoplankton) and reactant (dissolved nutrient), respectively (see Equation 4 for definition of $\delta^i\text{Me}$).

Following reaction, there may be a fraction of the initial micronutrient Me that remains unused, which we term f :

$$f = \frac{\text{Unused nutrient}}{\text{Nutrient supplied}} \quad (6)$$

where the nutrient terms represent quantities and f is unitless. (It follows that the fraction of nutrient consumed by phytoplankton equals $1-f$.) In systems where most nutrients are consumed, f will be close to zero. However, when productivity is limited by some other resource, such as another nutrient or light, systems will exhibit f that can approach the theoretical maximum of one.

The isotope composition of the residual nutrients and product phytoplankton will evolve over the course of a reaction. The precise nature of their evolution depends on three factors: The progress of the reaction, quantified in terms of the fraction of the initial reactant remaining (i.e., f); the magnitude and sign of Δ_{P-R} ; and, whether the system is “open” or “closed.” If the system remains open during the course of reaction, with the addition of new reactants balanced by the removal of product plankton and residual reactant, the system will follow Steady State behavior (SS). Alternatively, if the system is closed before and during the reaction, the system will follow Rayleigh Distillation (RD). We illustrate the effect of open-versus

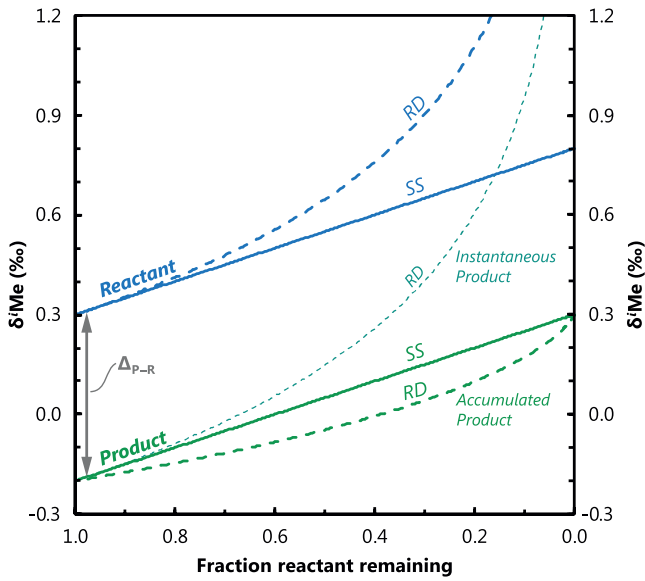


Figure 3. Isotopic evolution of an hypothetical metal (Me) in a reactor as a function of initial reactant remaining. The metal is supplied to a reactor with an initial composition, $\delta^i\text{Me}_{R,0}$, of +0.3‰, where it is reacted with an isotope separation factor, Δ_{P-R} , of -0.5‰ . The evolution of the reactants and products are shown for open-system behavior at SS (Steady State, solid lines; Equations 7 and 8) and closed-system RD (Rayleigh Distillation, dashed lines; Equation 9) for both the Instantaneous (Equation 10) and Accumulated Products (Equation 11). This example illustrates that the isotope evolution of the residual reactant is strongly dependent on whether the system is open or closed during the course of the reaction.

closed-system behavior using an example in which a reactant metal, possessing an initial isotope composition, $\delta^i\text{Me}_{R,0}$, of +0.3‰ is reacted to form a product assuming $\Delta_{P-R} = -0.5\text{‰}$ (Figure 3).

If Me supply and removal from the system are continuous, the system is considered open and will follow the lines marked SS (Figure 3). The SS scenario applies if the residual reactant Me is exported along with Me consumed by plankton, and that the sum of these removal terms are exactly balanced by Me resupply to the reactor. To define SS behavior, we draw on the simplifying approximations described by Johnson et al. (2004), whereby the the isotope composition of the SS product follows:

$$\delta^i\text{Me}_P \approx \delta^i\text{Me}_{R,0} + f\Delta_{P-R} \quad (7)$$

Because of this simplification, the isotope composition of the SS reactants, $\delta^i\text{Me}_R$, at any value of f is simply:

$$\delta^i\text{Me}_R \approx \delta^i\text{Me}_P - \Delta_{P-R} \quad (8)$$

and thus the reactant isotope composition will not exceed $\delta^i\text{Me}_{R,0} - \Delta_{P-R}$.

If the reactor is closed before and during reaction, the system will follow the lines marked RD (Figure 3). We define RD using the simplifying approximations of Mariotti et al. (1981). These approximations are unlikely to introduce significant systematic errors for the metals discussed here since they exhibit modest isotope variations (see Hayes, 2004). Unlike SS, the RD residual reactant isotope composition can evolve to extremely fractionated isotope compositions as $f \rightarrow 0$:

$$\delta^i\text{Me}_R \approx \Delta_{P-R} \ln f + \delta^i\text{Me}_{R,0} \quad (9)$$

The RD product formed at any point in the reaction is always offset from the reactant by -0.5‰ . This is termed the instantaneous product, $\delta^i\text{Me}_{IP}$ (Figure 3), defined as:

$$\delta^i\text{Me}_{IP} \approx \delta^i\text{Me}_R + \Delta_{P-R} \quad (10)$$

The RD Accumulated Product, $\delta^i\text{Me}_{AP}$, represents the integration of the instantaneous products formed up until that point in the reaction, given by:

$$\delta^i\text{Me}_{AP} \approx \frac{\Delta_{P-R} \ln f}{f-1} + \delta^i\text{Me}_{R,0} \quad (11)$$

Regardless of whether the system follows SS or RD behavior, the first product formed will exhibit $\delta^i\text{Me}_P$ offset from $\delta^i\text{Me}_{R,0}$ by Δ_{P-R} (double-ended arrow in Figure 3). Likewise, at $f = 0$, $\delta^i\text{Me}_P = \delta^i\text{Me}_{R,0}$.

2.2.2. From Reactors to Relative Nutrient Utilization

The isotope reactor models may be used to interpret metal isotope variations in the geological record in terms of Me supply and demand in the surface ocean. This is possible if one considers the reaction progress term in the reactors as being analogous to the fraction of initially supplied nutrient left unconsumed by phytoplankton (i.e., f). A benefit of this approach is that it does not require the initial concentration of metal supplied to the reactor ($[\text{Me}_{R,0}]$) to be known, only its initial isotope composition, $\delta^i\text{Me}_{R,0}$. However, the models do require assuming that the isotope separation factor during Me removal from seawater (Δ_{P-R}) and $\delta^i\text{Me}_{R,0}$ have remained constant over time. If these assumptions are justified, the reactor framework enables estimation of f from the Me isotope composition of either the residual reactants (seawater) or products (exported Me). For example, if a sedimentary archive were to accurately capture $\delta^i\text{Me}_R$ (the isotope

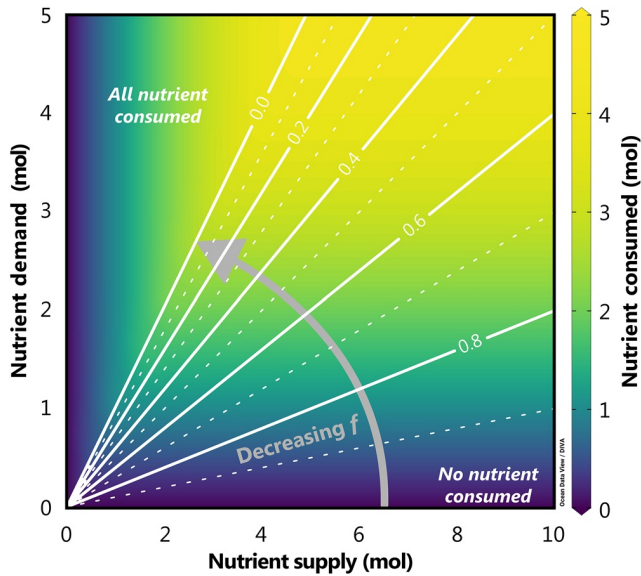


Figure 4. Relationships between nutrient demand, supply, and consumption. The y- and x-axes represent combinations of nutrient demand and supply, respectively. The total nutrient consumed by phytoplankton for each combination is illustrated by the shading; productive systems exist in the upper-right portion of the figure, where nutrient supply and demand are high, and unproductive systems are found close to the figure axes, where supply and demand are mismatched. Between these two extremes are moderately productive systems. The fraction of nutrients unused in these systems, f , is shown by the contour lines. This figure illustrates that f cannot be used in isolation to estimate productivity.

composition of a metal following reaction), f can be calculated assuming RD using:

$$\ln f \approx \frac{(\delta^i \text{Me}_R - \delta^i \text{Me}_{R,0})}{\Delta_{P-R}}, \quad (12)$$

or, if the reaction follows SS, using:

$$f \approx \frac{(\delta^i \text{Me}_R + \Delta_{P-R} - \delta^i \text{Me}_{R,0})}{\Delta_{P-R}}. \quad (13)$$

Likewise, f can be estimated from the isotope composition of exported products, $\delta^i \text{Me}_P$, assuming SS behavior using:

$$f \approx \frac{(\delta^i \text{Me}_P - \delta^i \text{Me}_{R,0})}{\Delta_{P-R}}, \quad (14)$$

There is no equivalent approximation for computing f from $\delta^i \text{Me}_{AP}$ assuming Rayleigh Distillation.

Equations 12–14 illustrate how metal isotope compositions can be used to calculate f . However, f is a measure of the relative utilization of nutrients in a system, and does not confer direct information about the size and thus total productivity of that system. This point is illustrated in the example shown in Figure 4, where we plot the demand for a nutrient by phytoplankton in a reactor against the initial quantity of nutrient supplied to the reactor (i.e., both axes represent quantities), with contours representing various f . These lines illustrate that a wide range of possible nutrient consumptions—and thus net ecosystem production—are possible for any value of f . Put another way, if all that was known about a system was f , it would be difficult to determine the productivity of that system.

Interpreting f in terms of ocean productivity requires an independent constraint on the nutrient supply, unused nutrient, or consumed nutrient (Figure 4). A common and powerful approach is to use the flux of bioactive metals to sediments as an indicator of past nutrient consumption (e.g., Brumsack, 2006; Eagle et al., 2003; Tribovillard et al., 2006). By assuming a fixed Me:C stoichiometry, bioactive metal fluxes can then be interpreted in terms of C export productivity. The isotope composition of Me is then used as an indicator of the balance between supply and demand for Me in that system (i.e., f), which is sensitive to factors such as ocean circulation and ecosystem structure (e.g., François et al., 1997). These approaches are especially powerful when the constraints on export and f are derived from the same Me system—barite mass accumulation rates and $\delta^{138}\text{Ba}$ (e.g., Bridgestock et al., 2019), [Cd] and $\delta^{114}\text{Cd}$ (e.g., Georgiev et al., 2015), [Zn] and $\delta^{66}\text{Zn}$ (e.g., Kunzmann et al., 2013)—since this minimizes potential confounding influences from other metal cycling processes, discussed next.

2.3. Other Trace Metal Cycling Processes

The framework outlined in Section 2.2 represents an idealized situation that implicitly assumes that phytoplankton productivity dominates the marine cycling of a trace metal. As we show in subsequent sections, many other processes cycle the bioactive trace metals and their isotopes in the marine realm; indeed, depending on the metal and the type of process, other factors—not directly related to productivity—may even dominate the cycling of that metal. Below, we introduce a number of these processes, which we group into three broad categories: biological, chemical, and physical. While these three categories of cycling processes may appear as insurmountable obstacles to the reliable application of a metal isotope system to reconstruct paleoproductivity, there are two reasons to be optimistic. First, that so many cycling processes are now

recognized highlights how far our understanding of trace metal geochemistry has evolved in recent years. Second, the multiple sensitivities of these metal systems to various ocean processes means that bioactive metals and their isotopes may be applied in concert to constrain multiple aspects of past ocean chemistry. Multi-proxy approaches are a familiar feature of the paleoredox landscape and are likely to become increasingly common for constraining paleoproductivity (e.g., Cd and Zn, John et al., 2017, Sweere et al., 2020; Cd and Cr, Frei et al., 2020).

2.3.1. Biological

Biological processes exclusive of productivity can play an important role in marine trace metal behavior. The example in Section 2.2 assumes that organisms exhibit inflexible Me:C stoichiometries, whereas in reality many marine microbes appear to have wide tolerances for the intracellular proportions of certain trace elements compared to those of C, N, and P. The physiological mechanisms enabling these wide tolerances, and the feedback interactions that drive them, are beyond the scope of this review, and are discussed in detail elsewhere (e.g., Morel et al., 2020; Sunda, 2012). From a proxy perspective, this flexibility may cause uncertainty in paleoproductivity estimates; the more variable the Me:C stoichiometry of organisms within an ecosystem, the more uncertain the paleoproductivity estimate derived from that Me. (The corollary being that the more rigid the stoichiometry, the more robust the paleoproductivity estimate.) An extreme example concerns nonessential elements (e.g., Ag, Ba), or metals that are only essential for certain groups of organisms within an ecosystem (e.g., Mo for nitrogen fixers). Productivity estimates derived from the export of these nonessential elements are potentially most susceptible to decoupling from productivity cycles as their export is not intrinsically tied to the overall functioning of an ecosystem.

Similarly, the reactor models assume that nutrient uptake is well described by a single and fixed isotope separation factor, Δ_{p-r} . A number of studies showed that this assumption is violated for Zn; different phytoplankton (e.g., Köbberich & Vance, 2017, 2019) and—depending on environmental conditions—even a single organism (e.g., John et al., 2007; Köbberich & Vance, 2017) can exhibit a range of Δ_{p-r} . Whether such behavior is also seen for other metal isotope systems is unknown, but could be important given that calculation of f is dependent on Δ_{p-r} (Equations 12–14).

Biological processes can potentially exert an additional control on bioactive metal isotope distributions through remineralization—the regeneration of POC to inorganic nutrients. In the case of a scarce nutrient, such as Fe, individual organisms (e.g., Saito et al., 2011) and even entire ecosystems (e.g., Rafter et al., 2017) have evolved mechanisms to retain certain nutrients. Likewise, macro- and micronutrients may be regenerated by heterotrophic organisms at different rates (e.g., Ohnemus et al., 2019; Twining et al., 2014), which could affect the Me:C stoichiometry of exported POC and thus the accuracy of Me-derived C export fluxes. Even less is known about the role of heterotrophs in fractionating POC-associated metal isotope compositions, which could be significant for some metals (e.g., Cd, Janssen et al., 2019).

Lastly, many of the metals reviewed here form complexes with organic ligands. For some metals, such as Fe and Cu, almost the entire oceanic inventory is bound to organic ligands. The effect of ligands on trace metal cycling is an area of active research, and is potentially important from the perspective of modulating isotope fractionation during uptake by plankton and into secondary Me sinks. Where known, these effects are discussed in the relevant sections.

2.3.2. Chemical

There are several chemical transformations that can modulate marine trace metal distributions without affecting C, such as scavenging and precipitation–dissolution reactions. Scavenging, meaning adsorption and desorption, can alter Me:C relationships by redistributing metals, but not C. Originally developed in the context of dissolved and particulate thorium isotopes (Bacon & Anderson, 1982), reversible scavenging is now suggested to play a role in the vertical cycling of other metals, including Cu (e.g., Little et al., 2013), Fe (e.g., Abadie et al., 2017), and Zn (e.g., Weber et al., 2018). Reversible scavenging is a continuous process that occurs between particle surfaces and dissolved species. While this process can occur at any depth, scavenging intensity is positively correlated with the quantity of particles, and so is typically most important in the upper water column. Likewise, while dissolved metals may be scavenged by any class of particle (e.g., opal, lithogenics), certain particle types may preferentially scavenge certain elements (e.g., Lerner et al., 2018). Scavenging may even affect trace metals cycled predominantly by organic matter; secondary

phases may scavenge metals during remineralization, which can affect trace metal distributions in the upper water column (e.g., Zn, John & Conway, 2014; Co, Hawco et al., 2018; Fe, Tagliabue et al., 2019).

Precipitation and dissolution of minerals is also a consideration for certain trace metals. The relative importance of mineral cycling depends on the metal and the redox environment. For example, Ba is primarily cycled by the mineral barite, rather than POC, and the thermodynamics of precipitation vary throughout the ocean (e.g., Rushdi et al., 2000). Changes in the ambient redox environment, such as in an oxygen minimum zone (OMZ), may even enhance dissolved–particulate transformations for certain trace metals. Some metals, such as Fe, may have large sources in OMZs associated with the reductive dissolution of particulate Fe–Mn oxides. Other metals may experience enhanced removal in OMZs via precipitation into sulfide minerals (e.g., Zn, Cu, Cd, Mo, Ni, Ag; Bianchi et al., 2018; Helz et al., 1996; Guinoiseau et al., 2019; Janssen et al., 2014; Kramer et al., 2011; McKay & Pedersen, 2008; Vance et al., 2016). The net effect of these non-POC-associated transformations is that processes other than POC cycling may redistribute trace metals, but not C, within the ocean interior. If significant, these processes could drive the ocean to a different Me:C stoichiometry and/or dissolved metal isotope composition that could impact calculations of export and f , respectively, when using the nutrient utilization framework described in Section 2.2.

2.3.3. Physical

The physical circulation of the ocean exerts a major control on many oceanic TEI distributions and we describe this influence on our nine trace metals in detail in later sections. In addition to circulation, there are also scale dependencies that can affect trace metal-based productivity estimates at both small and large scales, as well as other, non-productivity metal sinks. At the local to regional scale, Me point sources may be significant if they mask any POC-related Me drawdown. While perhaps less significant for C, point sources—rivers, dust, desorption from particles, sediments, and hydrothermalism—may be significant terms in local and regional trace metal budgets if the magnitude is comparable to the dissolved supply from ocean circulation. Examples include dust-derived Cu to surface planktonic communities (e.g., Paytan et al., 2009) and hydrothermally derived Fe to the deep ocean (e.g., Resing et al., 2015). Consideration of these external sources is particularly important when productivity estimates are derived close to such point sources and for metals with residence times that are less than (or similar to) the mixing time of the ocean (~ 1 kyr).

At the basin scale, the location of a site can influence the calculation of f . Close to an upwelling source of metal, such as in the modern Southern Ocean, f is, by definition, close to one and decreases downstream into the low latitudes. Given this dependence, it follows that a change in ocean circulation geometry could influence the spatial pattern of f without any net changes in productivity. This is particularly important to consider from a paleoceanographic perspective, since records are typically generated from fixed locations (i.e., sediment cores), making it challenging to determine if variations in f originated from overlying changes in ocean circulation or productivity. One solution to this challenge is to obtain an independent constraint on ocean circulation, such as from another isotope system or using a model. Alternatively, the spatial pattern of f could be discerned from multi-site reconstructions of Me isotope distributions.

On a global scale, the assumption of steady state can affect how productivity is estimated from Me reactor models. The input and output fluxes of a metal through the ocean should balance, regardless of productivity. Likewise, the flux-weighted metal isotope composition of inputs and outputs should also balance. Thus, at large scales, the isotopic composition of a sedimented Me should reflect the average input $\delta^i\text{Me}$, regardless of mean ocean f . Such a situation is possible because the flux terms interact. As an example, we return to the metal in Figure 3. We will assume that this metal follows SS behavior and that biological productivity is the only sink of this metal from seawater. If the mean marine input of this metal possessed $\delta^i\text{Me} = -0.1\text{‰}$, the system would only be in steady state if, on a global basis, $f = 0.8$. However, if mean global f were to decrease to 0.2 (i.e., a smaller fraction of this nutrient Me is left unused), mean global $\delta^i\text{Me}_p$ would increase from -0.1‰ to $+0.2\text{‰}$, which no longer matches the input $\delta^i\text{Me}$ of -0.1‰ . Such an imbalance cannot be sustained indefinitely, since the ocean would be losing more “heavy” Me than is being added. As such, the ocean would gradually compensate by a lowering of $\delta^i\text{Me}_{R,0}$ to 0.0‰ . In turn, mean ocean $\delta^i\text{Me}_p$ would return to values $\approx -0.1\text{‰}$, even if f remained at 0.2. This example illustrates how ocean-scale processes can influence the relationship between trace metals and productivity, even if productivity is the main sink of a metal from a system.

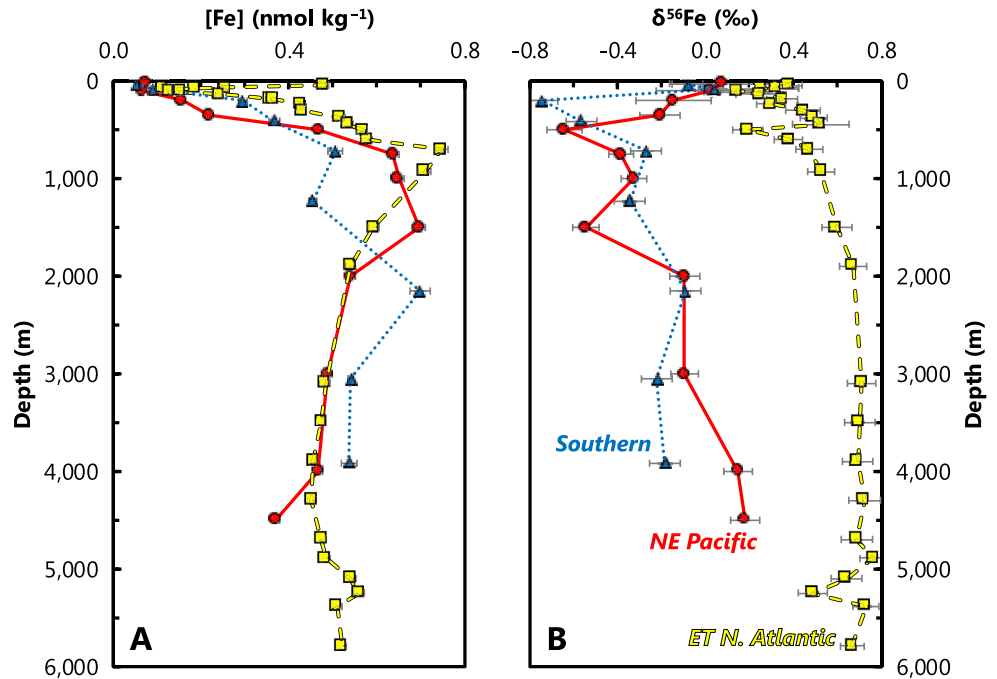


Figure 5. Representative profiles of dissolved Fe concentrations ($[Fe]$); (a) and Fe isotopic compositions ($\delta^{56}Fe$); (b). Data from the Eastern Tropical North Atlantic (squares, dashed line; Conway & John, 2014a), Northeast Pacific (circles, solid line; Conway & John, 2015a), and Southern Oceans (triangles, dotted line; Abadie et al., 2017). Station locations as per Figure 1. This comparison illustrates that despite possessing similar dissolved concentration profiles, the isotopic behavior of Fe is markedly different between basins.

Lastly, the relationship between Me and productivity— $\delta^i Me_{R,0}$, and potentially, $[Me_{R,0}]$ —can also be influenced by non-productivity Me sinks. Indeed, non-productivity sink terms are of considerable significance for many of the trace metals reviewed here. The significance of these terms may offer another, indirect means to constrain paleoproductivity: If non-productivity Me sinks possess different Δ_{P-R} and/or Me:C to productivity-related sinks, mean deep ocean $\delta^i Me$ and/or $[Me]$ will be sensitive to the relative balance of Me burial between the various sink terms, analogous to the canonical C cycle mass balance (e.g., Berner et al., 2000). For example, if assuming fixed Me inputs over time and that whole-ocean productivity abruptly decreased, the relative significance of non-productivity Me sinks would increase to compensate for the decrease in productivity. This compensation could drive deep ocean $\delta^i Me$ and/or $[Me]$ to new values that are sensitive to the balance between productivity and Me burial by other sinks. This multi-sink framework underpins the use of many TEI-based redox proxies (e.g., TI, Owens et al., 2017; U, Montoya-Pino et al., 2010), though this approach is relatively unexplored in the context of reconstructing paleoproductivity.

The review of each metal isotope system follows.

3. Iron

Iron plays a key role within phytoplankton as an electron carrier for photosynthesis and respiration processes, as well as within enzymes necessary for photosynthesis and nitrogen fixation (Morel & Price, 2003). However, in oxygenated seawater, Fe(II) is rapidly oxidized to Fe(III), which is highly insoluble (Liu & Millero, 2002). Low Fe solubility coupled to intense biological demand generally results in sub-nanomolar $[Fe]$ throughout the oceans, approaching the low picomolar range in some surface regions far from Fe sources, such as the vast Southern Ocean and North Pacific (e.g., Figure 5; Chever et al., 2010; Klunder et al., 2011; Schlitzer et al., 2018). Consequently, biological production in about 30% of the modern surface ocean is thought to be limited primarily by Fe (Moore et al., 2013), principally in upwelling regions where deep water is depleted in Fe relative to the macronutrients nitrate (NO_3^-) and phosphate (PO_4^{3-} ; e.g., Boyd et al., 2017; Moore, 2016). By limiting primary productivity (e.g., Martin & Fitzwater, 1988), inadequate Fe supply can

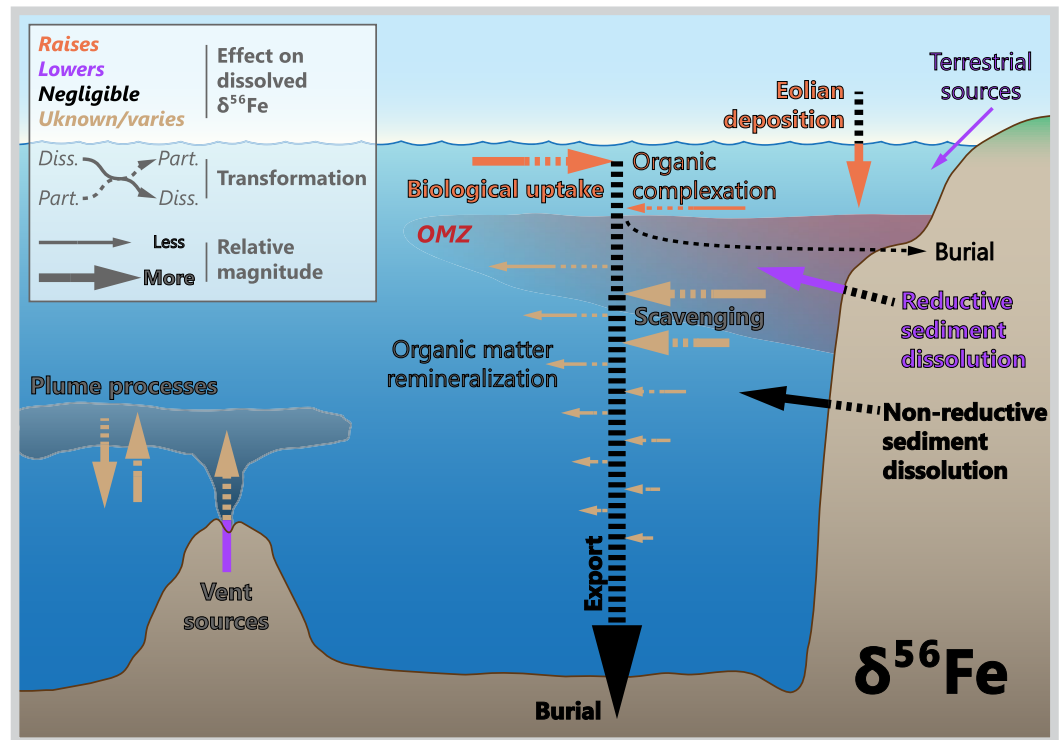


Figure 6. Processes driving Fe isotope variations in modern seawater. The ocean's internal cycle of Fe is perhaps the most complex of the trace metals discussed here, exhibiting several significant sources, sinks, and transformations not directly associated with biological productivity.

potentially influence the exchange of carbon between the ocean and atmosphere. Changing supplies of Fe from sources such as atmospheric dust, hydrothermal venting, or sedimentary release to the surface oceans through geological time can exert a significant control on both the distribution of primary productivity in the oceans and thus the global carbon cycle. For example, changes in supply of atmospheric dust to the Fe-limited Southern Ocean has been shown to correlate with climate variability on millennial time scales and has also been invoked to explain at least part of the dramatic sawtooth glacial–interglacial shifts in atmospheric carbon dioxide (Martin, 1990; Martínez-García et al., 2011, 2014; Sigman & Boyle, 2000).

The strong link between Fe supply and primary productivity suggests that ratios of Fe to other elements and/or Fe isotope ratios ($\delta^{56}\text{Fe}$) might be useful proxies for paleoproductivity. However, in the vast majority of settings, $\delta^{56}\text{Fe}$ and Fe flux records do not reflect paleoproductivity; instead, the influence of the major Fe sources and their redox-driven cycling exert far stronger controls over marine Fe geochemistry compared to biological productivity. Thus, a simple reactor framework, as outlined in Section 2.2.1, cannot be applied to $\delta^{56}\text{Fe}$. However, we note that there are a number of promising archives of past Fe isotope chemistry, particularly for the deep ocean, and we anticipate that these records will prove most valuable as context for interpreting other proxy records, or for generating novel hypotheses regarding the connections between Fe sources, biological productivity, and global climate.

3.1. Marine Distribution

The distribution of dissolved Fe in seawater is driven by a mixture of competing processes, including: biological uptake and regeneration; distinct sources of Fe at shallow, intermediate, and deep depths; adsorption–desorption processes onto organic and lithogenic particles; dissolution and precipitation processes; and, complexation with organic ligands (Figure 6; e.g., Boyd & Ellwood, 2010; Labatut et al., 2014; Tagliabue et al., 2017). As a result, [Fe] display what has historically been termed a hybrid-type depth profile in the open ocean, which exhibits a number of similarities between different ocean basins (Figure 5). Dissolved

Fe is drawn down in surface waters by biological uptake, and [Fe] can even be as low as $0.01 \text{ nmol kg}^{-1}$ in Fe-limited regions (Schlitzer et al., 2018). In comparatively “dustier” regions of the oceans, such as the North Atlantic, surface [Fe] can be as high as 2 nmol kg^{-1} following dust deposition events (Sedwick et al., 2005). Below the surface mixed layer, regeneration of biogenic material, reversible particle scavenging, and complexation by organic ligands act to keep the background deep ocean [Fe] between $0.4\text{--}0.6 \text{ nmol kg}^{-1}$ (e.g., Lauderdale et al., 2020). Against this background, however, it has been known for decades that [Fe] in deeper waters are elevated near point sources such as sedimentary margins (Johnson et al., 1997). Recently, a range of studies, including those conducted as part of the GEOTRACES program, have illuminated this picture, showing that deep sources of Fe—such as sedimentary and hydrothermal release—are widespread, may have distinct traceable $\delta^{56}\text{Fe}$ source signatures, and that this Fe can be transported over large distances through the ocean interior (e.g., Conway & John, 2014a; Radic et al., 2011; Resing et al., 2015; Nishioka et al., 2020; Saito et al., 2013). Despite exhibiting well-defined maxima close to point sources, [Fe] distributions at shallow and intermediate depths are extremely variable and models have struggled to reproduce these variations (e.g., Tagliabue et al., 2016). The extent to which deeply sourced Fe is supplied to surface seawater is thus equivocal (e.g., Roshan et al., 2020; Tagliabue et al., 2010).

The origin of [Fe] variability in the shallow and intermediate ocean is thought to reflect local differences in the competition between uptake, regeneration, sources, and scavenging. The same processes influence $\delta^{56}\text{Fe}$; however, unlike the modest variations in [Fe], $\delta^{56}\text{Fe}$ exhibits dramatic variability between—and even within—ocean basins (Figure 5; Schlitzer et al., 2018). Such water column variability in $\delta^{56}\text{Fe}$, from isotope compositions as light as -4‰ (Charette et al., 2020), to as heavy as $+2\text{‰}$ (Ellwood et al., 2020), is thought to be driven by an interplay between different Fe sources with distinct Fe isotope compositions, biological uptake, Fe complexation to organic ligands in surface waters, and non-reductive release of dissolved Fe from particles (notably lithogenic particles) during desorption and/or ligand-promoted dissolution (e.g., Abadie et al., 2017; Conway & John, 2014a; Ellwood et al., 2020; Figure 6). These processes can render remarkably different $\delta^{56}\text{Fe}$ profiles, even when profiles of [Fe] are similar, such as in the examples from the Northeast Pacific, Eastern Tropical North Atlantic, and the Weddell Sea of the Southern Ocean (Figure 5). In the North Pacific and North Atlantic examples, the deep distribution of $\delta^{56}\text{Fe}$ is considered to be most strongly influenced by the dominant regional Fe source—dust in the Atlantic and the continental margins in the Pacific (Conway & John, 2014a; 2015b). In the Weddell Sea, the deep $\delta^{56}\text{Fe}$ distribution has been attributed to regeneration of isotopically light biogenic Fe at depth (Abadie et al., 2017), or, more recently, to the addition of isotopically light Fe from regional sedimentary release (Sieber et al., 2021). Thus, $\delta^{56}\text{Fe}$ appears to provide the most insight into the relative contributions of various Fe sources at the basin scale (e.g., Conway & John, 2014a), as well as for internal Fe-cycling processes such as uptake and regeneration.

Despite synthesis of numerous studies of both small- (e.g., Coale, 1991; Coale et al., 2003; Martin et al., 1990) and large-scale iron fertilization events (e.g., de Baar et al., 2005; Boyd & Ellwood, 2010; Boyd et al., 2007; Urban et al., 2020), there are still uncertainties in how changing Fe supply to the surface ocean may affect phytoplankton growth in Fe-limited regions, and/or nitrogen fixers under NO_3^- limitation. These uncertainties have led to several gaps in our ability to link Fe cycling directly to climate change (Misumi et al., 2014). One major challenge is assessing what portion of the dissolved Fe pool is available for uptake by different microbes, termed “bioavailable” Fe. Such uncertainties on Fe supply, speciation, and bioavailability in the surface ocean are compounded by limitations in our ability to constrain the supply of dissolved Fe in upwelled deep waters. For example, while the ratio of C to macronutrients such N and P in the deep ocean is well known and the residence time and distribution can be accurately reproduced based on apparent oxygen utilization (AOU), this is not the case for Fe. Only around 10%–15% of cellular Fe (Fe:C = 18–33 $\mu\text{mol:mol}$) appears to be regenerated in the deep ocean (Fe:C 4–6 $\mu\text{mol:mol}$; Twining & Baines, 2013). This lack of regeneration leads to a much weaker correlation between [Fe] and AOU, even in regions far from Fe sources (Rijkenberg et al., 2014) and to upwelled deep waters being relatively depleted in dissolved Fe relative to macronutrients (e.g., Moore, 2016). Since incubation experiments show that Fe associated with sinking organic matter from the subsurface is efficiently regenerated (Velasquez et al., 2016), much of the released Fe must be rapidly scavenged (Tagliabue et al., 2019). Despite this scavenging, vertical transport is still thought to be the major source of dissolved Fe for phytoplankton in most Fe-limited regions, highlighting the complex interplay between Fe supply (sources, stabilization, and transport) and demand (biological uptake, scavenging).

3.2. Driving Processes

3.2.1. Biological

Initial studies of processes that fractionate Fe isotopes were optimistic that $\delta^{56}\text{Fe}$ would make for a powerful proxy of physiological “biosignatures” (Beard et al., 1999), especially once measurement of $\delta^{56}\text{Fe}$ was extended to seawater by Lacan et al. (2008). However, much of this early optimism faded once it was found that other factors were also important in setting dissolved $\delta^{56}\text{Fe}$, such as external Fe sources (e.g., John et al., 2012; Radic et al., 2011; Section 3.2.2). Moreover, organisms exhibit significant variability in Fe:C ratios (e.g., Twining & Baines, 2013), suggesting that Fe cycling may be partially decoupled from ecosystem productivity. Despite this more complicated picture, there is a growing body of evidence suggesting that phytoplankton preferentially incorporate light Fe isotopes from seawater and, in some circumstances, render detectable changes in dissolved $\delta^{56}\text{Fe}$. For example, studies from isolated eddies, the Mertz Polynya, and the open Southern Ocean showed that surface $\delta^{56}\text{Fe}$, at picomolar [Fe], are isotopically heavy ($>+1\text{‰}$), which has been attributed to the combination of surface uptake, regeneration, and organic complexation (Ellwood et al., 2015, 2020; Sieber et al., 2021). Estimates for the magnitude of fractionation due to biological uptake, $\Delta_{\text{P-R}}$, ranges between -0.1 (Radic et al., 2011) and -1.0‰ (Ellwood et al., 2020; Sieber et al., 2021). The magnitude and direction of any Fe isotope fractionation during uptake may depend on the phytoplankton species, uptake mechanism, and Fe species consumed. Additional research is required on all three fronts.

Below the surface, dissolved $\delta^{56}\text{Fe}$ primarily reflects the isotope composition of regional Fe sources, and is not substantially influenced by the remineralization of organic matter (Figure 6; e.g., Abadie et al., 2017; Conway & John, 2014a; John, Helgoe, Townsend, Weber et al., 2018; Labatut et al., 2014; Sieber et al., 2021). These results indicate that there remains the possibility for using $\delta^{56}\text{Fe}$ of surface seawater to reconstruct productivity in some oceanographic settings, though any such reconstructions would need to consider the role of other Fe-cycling processes and the degree to which they might erase any diagnostic productivity signatures, discussed next.

3.2.2. Chemical

The chemical behavior of Fe in seawater is complex and has the potential to decouple Fe cycling from macronutrients and therefore productivity. Unlike the macronutrients, which are present as aqueous ions in solution, Fe is scarcely soluble in seawater, and much of what constitutes “dissolved” Fe—operationally defined as that which can pass through a 0.2 or 0.4 μm filter—is in actuality a ‘soup’ of organic complexes, nanoparticles, colloids, and a small fraction of truly ionic Fe. The controls governing, and the extent to which exchange occurs between these forms of dissolved Fe, are areas of focused interest (e.g., Fitzsimmons & Boyle, 2014; Fitzsimmons et al., 2015). Additionally, dissolved Fe is subject to strong removal via scavenging, which lowers the Fe:macronutrient ratio of waters returned to the surface via upwelling (Moore, 2016). Chemical processes can also exert a significant influence over the isotopic composition of Fe in seawater, such as through redox transformations, exchange reactions (e.g., complexation, particle interactions), and by authigenic precipitation, discussed below.

Redox transformations drive large Fe isotope effects (e.g., Anbar et al., 2005; Johnson et al., 2002; Skulan et al., 2002; Welch et al., 2003). Indeed, much of the Fe isotope variation in Earth’s ancient, more-reducing past likely derives from fractionations associated with redox transformations (see e.g., Johnson et al., 2008; Rouxel et al., 2005 and references therein). While the role of redox relative to other processes is somewhat diminished in today’s mostly oxygenated ocean, redox remains an important mediator of Fe isotope source compositions, particularly within the ocean interior. This is neatly illustrated using the example of sediment dissolution, which can occur with or without a change in the redox state of Fe (Figure 6). Bulk marine sediments typically possess a composition similar to the crustal composition of $+0.1\text{‰}$ (Beard et al., 2003; Poitrasson, 2006). However, dissolved Fe(II) derived from bacterially mediated reductive dissolution in sediments has been characterized by $\delta^{56}\text{Fe}$ between -1‰ and -3‰ (Bergquist & Boyle, 2006, 2010; Henkel et al., 2018; Homoky et al., 2009, 2013; Klar, Homoky et al., 2017; Severmann et al., 2006), whereas Fe derived from non-reductive dissolution processes is thought to be considerably heavier, between $+0.1\text{‰}$ and $+0.3\text{‰}$, and also likely to be present in the colloidal phase (Homoky et al., 2009, 2013; 2021; Radic et al., 2011). Further modification of reductive endmember compositions is possible upon contact with oxidizing seawater, potentially masking true source signatures. Oceanic water column dissolved $\delta^{56}\text{Fe}$

compositions attributed to either non-reductive (+0.1‰ to +0.4‰) or reductive (−0.3‰ to −4‰) release of Fe from sediments have now been observed in all ocean basins (Abadie et al., 2017; Charette et al., 2020; Chever et al., 2015; Conway & John, 2014a, 2015a; Fitzsimmons et al., 2016; John, Helgoe, Townsend, Weber et al., 2018; John et al., 2012; Labatut et al., 2014; Klar, Homoky et al., 2017; Klar et al., 2018; Radic et al., 2011; Rolison et al., 2018; Staubwasser et al., 2013).

Exchange reactions can also fractionate primary Fe isotope compositions. For example, natural lithogenic dust is thought to possess a relatively narrow range of Fe isotope compositions (i.e., $\delta^{56}\text{Fe} \approx +0.1\text{‰} \pm 0.2\text{‰}$; Chen et al., 2020; Conway et al., 2019; Mead et al., 2013; Waeles et al., 2007), reflecting the overall homogeneity of the upper continental crust. However, dissolved Fe in seawater attributed to dissolving dust particles is isotopically heavy, around +0.7‰ (Figure 6; Conway & John, 2014a). This fractionation is thought to reflect dissolution in concert with, and complexation by, strong organic ligands (Fishwick et al., 2014), which have been experimentally shown to preferentially bind heavy Fe isotopes (Dideriksen et al., 2008; Morgan et al., 2010). Fractionation effects may also arise during exchange of Fe between dissolved and particulate forms, though the magnitude of the effect depends on whether the exchange is primarily physical (negligible fractionation; e.g., Fitzsimmons et al., 2017) or chemical (from $\approx +0.3$ up to +1‰; Labatut et al., 2014; Fitzsimmons et al., 2015).

Lastly, authigenic precipitation can control the isotopic composition of Fe released by large point sources, such as hydrothermal vents and margin sediments (Figure 6). Iron in hydrothermal vent fluids possesses endmember compositions ranging from −0.7‰ to +0.1‰ (Beard et al., 2003; Bennett et al., 2009; Rouxel et al., 2008, 2016, 2018; Nasemann et al., 2018; Severmann et al., 2004; Sharma et al., 2001). However, precipitation of Fe into authigenic minerals can render significant changes in dissolved $\delta^{56}\text{Fe}$ (e.g., Bennett et al., 2009; Severmann et al., 2004). The direction of fractionation depends on—and may thus be diagnostic of—the specific transformations occurring (e.g., Horner, Williams et al., 2015; Lough et al., 2017): Fe sulfides and oxides preferentially incorporate isotopically light and heavy Fe, respectively (e.g., Rouxel et al., 2008; Skulan et al., 2002). Mineral precipitation can drive $\delta^{56}\text{Fe}$ of residual Fe stabilized in seawater to values ranging between −2.4‰ and +1.5‰, depending on the authigenic mineral produced (Conway & John, 2014a; Ellwood et al., 2015; Fitzsimmons et al., 2016, 2017; Klar, James et al., 2017; Lough et al., 2017; Rouxel et al., 2018). Analogous processes appear to operate along continental margins, whereby “light” Fe, mobilized by reductive dissolution, encounters oxidizing seawater and forms precipitates that are heavier than the source Fe (though overall still considerably lighter than background seawater; e.g., Marsay et al., 2018; Figure 6).

Additionally, the importance of local point sources on dissolved $\delta^{56}\text{Fe}$ continue to emerge, including from anthropogenic aerosol dust (e.g., Mead et al., 2013; Kurisu, Sakata et al., 2016; Kurisu, Takahashi, et al., 2016; Conway et al., 2019; Pinedo-González et al., 2020), glaciers and meltwater (e.g., Zhang et al., 2015; Stevenson et al., 2017), and rivers (e.g., Akerman et al., 2014; Bergquist & Boyle, 2006; Chen et al., 2014; Escoube et al., 2015, 2009; Fantle & DePaolo, 2004; Ilina et al., 2013; Ingri et al., 2006; Mulholland et al., 2015; Poirasson et al., 2014). These local point sources can vary dramatically over short spatial and temporal scales and with *in situ* chemical conditions. The importance of different Fe sources on dissolved $\delta^{56}\text{Fe}$ is so significant that any fractionation arising from biological uptake in the Fe-depleted surface layer, even if it were recorded in a sedimentary archive, is likely to be overprinted by even a small addition of new Fe from either above or below. Thus, records of surface seawater $\delta^{56}\text{Fe}$ are more likely to reflect the influence of different Fe sources and associated chemical transformations than productivity.

3.2.3. Physical

The residence time of Fe in seawater is substantially less than the mixing time of the global ocean (Table 1). Local and regional Fe sources can thus drive large differences in [Fe] and dissolved $\delta^{56}\text{Fe}$ between ocean basins (Figure 5). However, local source signatures—[Fe], $\delta^{56}\text{Fe}$, and perhaps Fe speciation—can be transported and retained over the scale of individual ocean basins (Figure 7; Abadie et al., 2017; Conway & John, 2014a). The discovery of significant long-range intra-basin Fe transport is arguably one of the marquee findings of the GEOTRACES program, and underpins the utility of sedimentary $\delta^{56}\text{Fe}$ to reconstruct past marine Fe sources, discussed next.

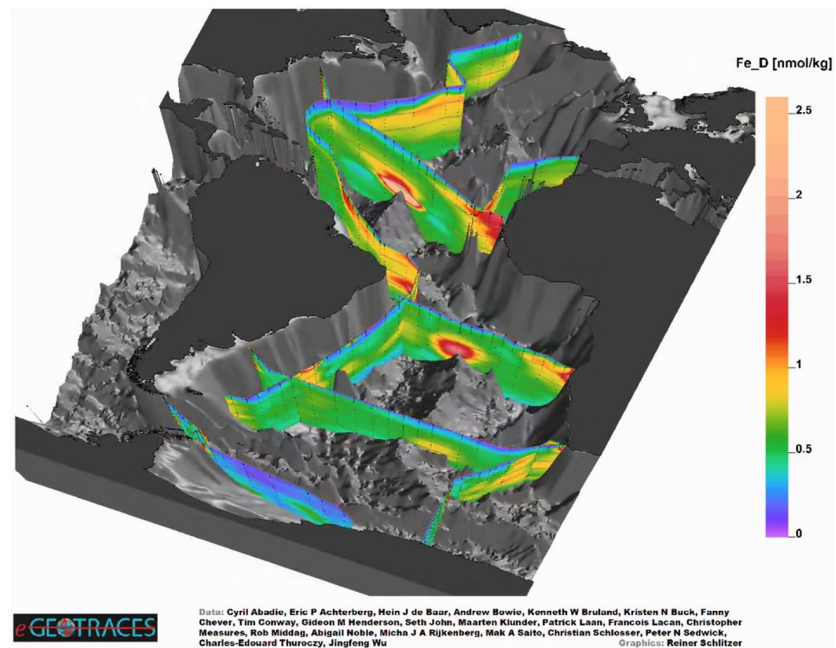


Figure 7. Three-dimensional scene depicting dissolved Fe concentrations in the Atlantic Ocean (Schlitzer, 2019). This perspective illustrates the density of GEOTRACES data in the region as well as the influence of multiple Fe “hot spots”, such as mid-ocean ridges and continental margins. Data are available in the GEOTRACES Intermediate Data Product 2017 (Schlitzer et al., 2018); names of data originators appear in the figure. Three-dimensional scenes for other trace element and isotope (TEIs) are available from <https://eGEOTRACES.org/>.

3.3. Marine Archives

3.3.1. Surface Ocean

A requirement of the application of any paleoproxy is the availability of suitable sedimentary archives. These archives must have both a high fidelity for the signal of interest and be robust to post-depositional alteration. Archives most relevant to reconstructing paleoproductivity should capture surface ocean $\delta^{56}\text{Fe}$; however, there are few—if any—reliable archives. The lack of surface water archives reflects two related challenges. First, most archives for surface seawater are derived from biominerals, such as foraminifera, diatoms, sponges, and corals. These archives possess vanishingly low Fe content compared to Ca or Si, such that Fe isotopic analysis of these substrates has proven difficult. Second, following burial, many biominerals will act as substrates for authigenic mineral formation. Many of these secondary authigenic minerals, such as clays (e.g., Badaut & Risacher, 1983) and Fe–Mn oxides (e.g., Boyle, 1981), possess Fe contents far in excess of those in the underlying biomineral, necessitating significant physical and chemical cleaning (e.g., Cheng et al., 2000).

Despite these obstacles, there are three positive signs that reconstructing past surface seawater $\delta^{56}\text{Fe}$ is possible. First, biogenic opal may contain Fe at concentrations in the $\mu\text{g g}^{-1}$ range (Ellwood & Hunter, 2000; Lal et al., 2006; Shemesh et al., 1988; Sun et al., 2016), which is tractable for $\delta^{56}\text{Fe}$ analysis. Second, the Fe content of diatoms is correlated with ambient [Fe] (Twining & Baines, 2013). Lastly, the positive relationship between the Fe content of diatoms and corresponding seawater appears to hold through sinking and sedimentation (Pichevin et al., 2014), indicating that diatoms are a potential window into past surface ocean Fe chemistry. Whether these relationships also extend to $\delta^{56}\text{Fe}$ remains to be seen, and will require additional core-top calibrations, incubation experiments, and detailed assessment of the efficacy of chemical cleaning.

3.3.2. Deep Ocean

There are several studies examining Fe sources and fluxes in the meso- and bathypelagic ocean using sedimentary archives. Given the considerable spatial variability in modern $\delta^{56}\text{Fe}$, it is likely that sedimentary reconstructions will reflect, at most, a regional view of the past Fe cycle. This means that multiple,

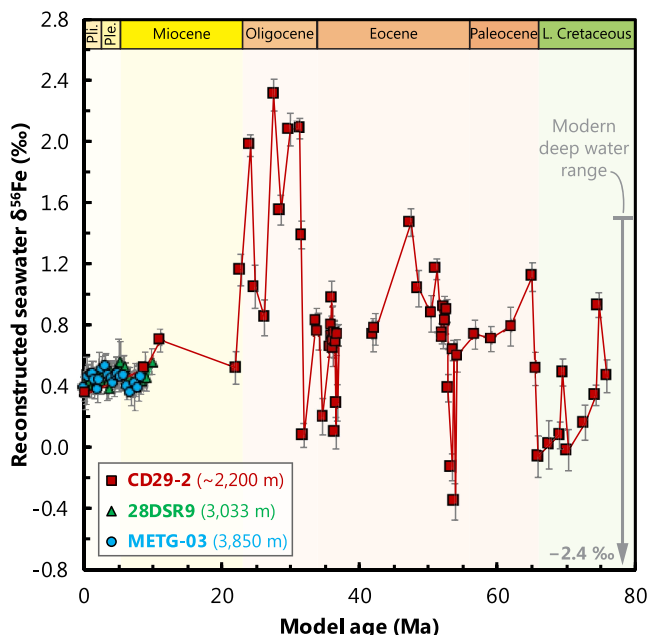


Figure 8. Ferromanganese crust records of central Pacific $\delta^{56}\text{Fe}$ since the Late Cretaceous. Records from CD29-2, 28DSR9, and METG-03 from Horner, Williams et al. (2015), Chu et al. (2006), and Liu et al. (2020), respectively. The record from CD29-2 was interpreted by Horner, Williams et al. (2015) as evidencing the importance of deep (non-eolian) Fe sources to central Pacific Fe budgets throughout much of the Cenozoic and Late Cretaceous. In contrast, the $\delta^{56}\text{Fe}$ recorded by three central Pacific Fe–Mn crusts have been similar since the late Miocene, consistent with a regional Fe source derived largely from non-reductive sediment dissolution and/or eolian deposition.

contemporaneous records will be required to diagnose whole-ocean changes in Fe cycling, but that individual records will have utility in offering basin-scale perspectives. To constrain Fe sources, researchers have examined the Fe isotope composition of Fe-rich sediments, including red clays (Dunlea et al., 2021), polymetallic nodules (Marcus et al., 2015), and Fe–Mn crusts (Chu et al., 2006; Horner, Williams et al., 2015; Levasseur et al., 2004; Liu et al., 2020; Zhu et al., 2000). Ferromanganese crusts are currently the best studied for Fe isotopes (Figure 8); Fe–Mn crusts are slowly accumulating deposits ($\sim\text{mm Myr}^{-1}$) that record ambient seawater $\delta^{56}\text{Fe}$ with a spatially invariant offset of $-0.77 \pm 0.06\text{‰}$ (Levasseur et al., 2004; Horner, Williams et al., 2015). The constancy of the offset between crusts and seawater implies that the Fe isotope composition of individual Fe–Mn crust layers can be interpreted in terms of past dissolved $\delta^{56}\text{Fe}$, and thus past Fe sources. Iron is effectively immobile in Fe–Mn crusts, with a calculated effective diffusivity $<10^{-12} \text{ cm}^2 \text{ yr}^{-1}$ (Henderson & Burton, 1999), implying that post-depositional diffusion of Fe is unlikely to reset primary $\delta^{56}\text{Fe}$ (Horner, Williams et al., 2015; Marcus et al., 2015). Curiously, however, the Fe isotopic variability of Fe–Mn deposits recovered from the central Pacific—particularly layers formed before $\sim 20 \text{ Ma}$ —exceed the range of modern deep ocean $\delta^{56}\text{Fe}$ (though only in the positive direction; Figure 8). The reasons for elevated $\delta^{56}\text{Fe}$ in the past are debated. Horner, Williams et al. (2015) report that heavy $\delta^{56}\text{Fe}$ could arise through widespread secondary modification of large Fe sources through authigenic reactions, such as sulfide precipitation. In contrast, Johnson et al. (2020) contend that the elevated $\delta^{56}\text{Fe}$ reflects extensive biological modification of dissolved Fe, driven by large-scale Fe fertilization. Regardless, the variation in these records points to a dynamic and enigmatic Fe cycle in Earth’s past, and indicates that Fe–Mn crusts have a largely untapped potential to reconstruct spatiotemporal variations in this cycle.

Other approaches are also showing promise to study Fe fluxes to the deep ocean through time. For example, researchers have constrained the rate of sedimentary accumulation of hydrothermally derived Fe and Cu using constant flux proxies such as extraterrestrial helium-3 (e.g., Middleton et al., 2016) or thorium-230 (Costa et al., 2017). These studies report that hydrothermal activity may be coherent with sea level changes on Quaternary glacial–interglacial cycles, suggesting a potentially remarkable set of connections between the solid Earth, ocean chemistry, and global climate (e.g., Cullen & Coogan, 2017). Reconstruction of hydrothermal metal fluxes over million-year timescales may also be possible using the geochemistry of pelagic clays (e.g., Dunlea et al., 2015; 2021), though such approaches are still in their infancy.

3.4. Prospects

While the marine Fe cycle is complex, Fe isotopes are proving valuable tool for untangling the many processes involved. Detailed study of the Fe cycle reveals that it is driven by a multitude of biological, physical, and chemical processes, among which productivity is but one small part. In our view, this means that it is unlikely that $\delta^{56}\text{Fe}$ can be developed as a paleoproductivity tracer. However, this does not preclude $\delta^{56}\text{Fe}$ from emerging as a powerful tracer for studying the dynamics of the Fe cycle in the modern and past oceans. Such a tracer would be especially powerful given the important connections between Fe supply and the biological productivity of the ocean.

Exploiting $\delta^{56}\text{Fe}$ will require resolving and refining several ambiguities. First, there is a clear need to better constrain the Fe isotope fractionation factor associated with biological uptake (in variable conditions and from different species) and to diagnose locations where dissolved $\delta^{56}\text{Fe}$ is most affected by productivity. Second, the fractionation factors for remineralization and scavenging are essentially unknown, though

field data suggests that the net result of these effects is relatively small (e.g., Labatut et al., 2014; Radic et al., 2011). Constraining these fractionation factors will be particularly important for developing novel archives of the past Fe cycle, such as pelagic clays (e.g., Dunlea et al., 2021). Third, any sedimentary reconstruction of past Fe isotope chemistry will need to consider the high degree of spatial variability in modern $\delta^{56}\text{Fe}$. This will necessitate spatially distributed core sampling, similar to the approach used to constrain basin-scale patterns of dust deposition over glacial–interglacial timescales (e.g., Costa et al., 2016; Winckler et al., 2016). Addressing these priorities will provide valuable constraints on the extent to which the Fe cycle has influenced primary productivity over recent geological history, and provide key insights into the potential sensitivity of Earth's climate to perturbations in marine trace element cycles.

4. Zinc

After Fe, Zn is the second most abundant transition metal in marine phytoplankton (e.g., Twining & Baines, 2013) and is involved in many cellular processes ranging from RNA synthesis to nutrient acquisition (e.g., Maret, 2001). Consistent with its importance to organisms and relatively short residence time (Table 1), [Zn] exhibits a nutrient-type distribution in the ocean most similar to that of [Si] (e.g., Bruland et al., 1978). The dissolved distribution of [Zn] is faithfully captured by certain sedimentary archives, notably those formed in the deep ocean (e.g., Marchitto et al., 2000). In contrast, there remains considerable debate surrounding the influence of biological productivity on dissolved $\delta^{66}\text{Zn}$ compared to other processes such as scavenging, ligand binding, non-productivity sinks, and anthropogenic contamination. This complexity prevents the modeling of Zn uptake via a simple reactor framework (as outlined in Section 2.2), and at present, it seems unlikely that there is a direct link between $\delta^{66}\text{Zn}$ and paleoproductivity. Despite the lack of a clear connection to productivity, there are a number of promising sedimentary archives of past seawater $\delta^{66}\text{Zn}$ that may inform on the myriad other processes that cycle Zn in seawater.

4.1. Marine Distribution

Typical surface ocean [Zn] are 0.01–0.5 nmol kg⁻¹, compared to deep water [Zn] of ~2.5 nmol kg⁻¹ in the north Atlantic and ~10 nmol kg⁻¹ in the north Pacific (Figure 9). The [Zn] distribution in the ocean generally closely follows that of the macronutrient Si (Bruland, 1980), at least partially due to the similar behavior of both elements in the Southern Ocean (de Souza et al., 2018; Middag et al., 2019; Roshan et al., 2018; Vance et al., 2017; Weber et al., 2018). The largest decouplings of [Zn] from [Si] are observed in regions remote from Southern Ocean influence, such as the north Pacific (Janssen & Cullen, 2015; Vance et al., 2019) or north Atlantic (Conway & John, 2014b).

Given the importance of Zn to organisms and the nutrient-like distribution of [Zn], it was initially expected that Zn isotope ratios would be similarly sensitive to biological processes. Indeed, culture studies consistently showed that phytoplankton assimilated isotopically light Zn from their environment (e.g., John et al., 2007; Köbberich & Vance, 2017; Samanta et al., 2018). It was therefore thought that dissolved profiles of $\delta^{66}\text{Zn}$ would exhibit profiles similar to those of the macronutrients (e.g., $\delta^{13}\text{C}$, $\delta^{15}\text{N}$, $\delta^{30}\text{Si}$; Farmer et al., 2021) and certain micronutrient metals (e.g., $\delta^{114}\text{Cd}$, $\delta^{138}\text{Ba}$; Sections 6 and 8, respectively), whereby Zn-depleted surface waters exhibit isotopically heavy compositions relative to deeper waters. In contrast, the first Zn isotope profile for seawater, obtained by Bermin et al. (2006) in the Northeast Pacific, showed that surface and deep waters exhibited Zn isotope equivalence, with a slight decrease in $\delta^{66}\text{Zn}$ just below the euphotic zone. Recent methodological improvements (e.g., Conway et al., 2013; Takano et al., 2017) have permitted detailed investigations of this surprising pattern in a number of ocean basins.

A consistent picture of the distribution of $\delta^{66}\text{Zn}$ in the ocean has since emerged. The deep ocean is almost homogeneous for $\delta^{66}\text{Zn}$, with a composition of about +0.45‰ (Figure 9; Conway & John, 2014b, 2015a; John, Helgoe, & Townsend, 2018; Lemaitre et al., 2020; Liao et al., 2020; Samanta et al., 2017; Takano et al., 2017; Sieber et al., 2020; Vance et al., 2019; R. M. Wang et al., 2019; Zhao et al., 2014). The deep ocean is thus slightly isotopically heavier than the upper continental crust (UCC), which possesses $\delta^{66}\text{Zn} = +0.3\text{‰}$ (Moynier et al., 2017). We note that Zn isotope data are reported relative to JMC-Lyon, though since this standard is now exhausted, most data are measured relative to AA-ETH or IRMM-3702 and reported relative to JMC-Lyon by means of a fixed offset of $\approx +0.3\text{‰}$ (see Archer et al., 2017; Moeller et al., 2012).

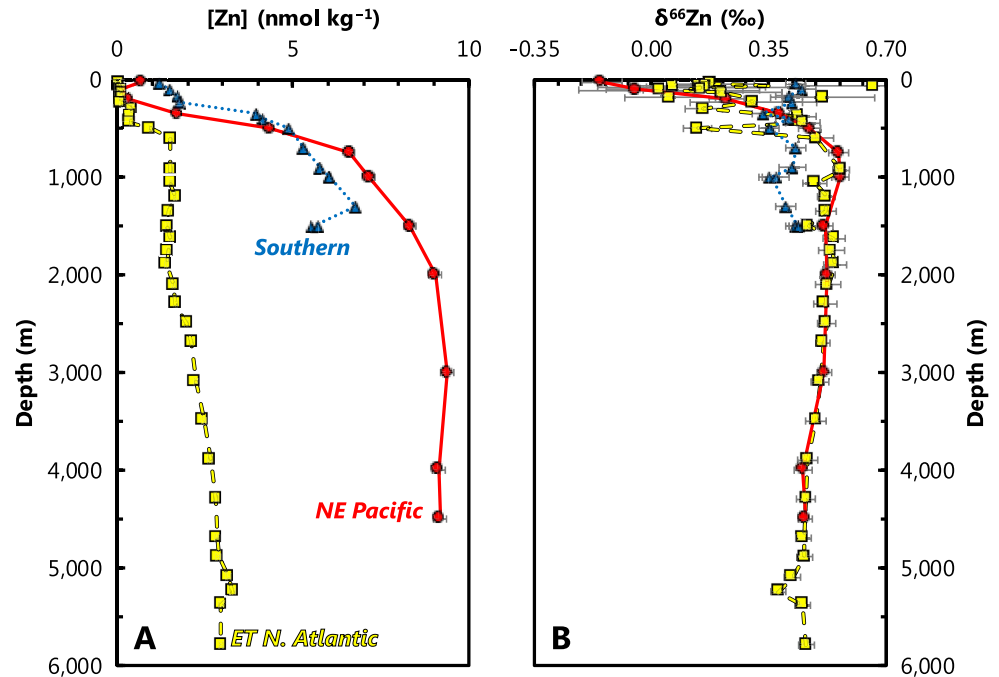


Figure 9. Representative profiles of dissolved Zn concentrations ($[Zn]$); (a) and Zn isotopic compositions ($\delta^{66}Zn$); (b). Data from the Eastern Tropical North Atlantic (squares, dashed line; Conway & John, 2014b), Northeast Pacific (circles, solid line; Conway & John, 2015a) and Southern Oceans (triangles, dotted line; R. M. Wang et al., 2019). Station locations as per Figure 1. This comparison illustrates that despite possessing distinct dissolved concentration profiles, the isotopic behavior of Zn is similar between basins.

Though most of the deep ocean is characterized by $\delta^{66}Zn = +0.45\text{‰}$, there are some deviations to values as light as -0.2‰ close to Zn point sources, such as margin sediments or hydrothermal vents (Conway & John, 2014b; Lemaitre et al., 2020). While heavy Zn isotope compositions are sometimes observed in the surface, this pattern is not seen everywhere; the upper water column is often isotopically lighter compared with deeper samples or, in the Southern Ocean and North Pacific, only very slightly fractionated toward heavier values (Conway & John, 2014b, 2015a; Lemaitre et al., 2020; Liao et al., 2020; Samanta et al., 2017; Sieber et al., 2020; Takano et al., 2017; Vance et al., 2019; R. M. Wang et al., 2019; Zhao et al., 2014). Thus, despite the nutrient-like distribution of Zn, the lack of consistent covariation between $[Zn]$ and dissolved $\delta^{66}Zn$ precludes the use of the isotope reactor framework outlined in Section 2.2. Possible reasons for the lack of “heavy” surface $\delta^{66}Zn$ values are discussed in the next section, and include: Preferential scavenging of isotopically heavy Zn on particle surfaces (e.g., John & Conway, 2014; Weber et al., 2018); isotopically light sources of Zn to the surface ocean, possibly from shallow remineralization of organic material (Samanta et al., 2017; Vance et al., 2019); and, Zn sourced from anthropogenic aerosols (Liao et al., 2020; Lemaitre et al., 2020). Given these complexities, we believe it will be extremely challenging to develop Zn isotopes as a paleoproductivity proxy.

4.2. Driving Processes

4.2.1. Biological

Zinc is a metal center in two key enzymes: Carbonic anhydrase, necessary for carbon fixation, and alkaline phosphatase, necessary for dissolved organic phosphorus uptake by marine organisms (Morel et al., 1994; Shaked et al., 2006; reviewed by Sinoir et al., 2012). Zinc also has an array of other physiological roles in marine organisms, as exemplified by the observation that Zn contents of phytoplankton cells are of similar magnitude to the micronutrient Fe (Twining & Baines, 2013).

Zinc can be growth-limiting for phytoplankton grown in culture (Anderson et al., 1978; Brand et al., 1983; Morel et al., 1994), but Zn colimitation (with Fe, Co) is rarely observed in the open ocean (e.g., Chappell

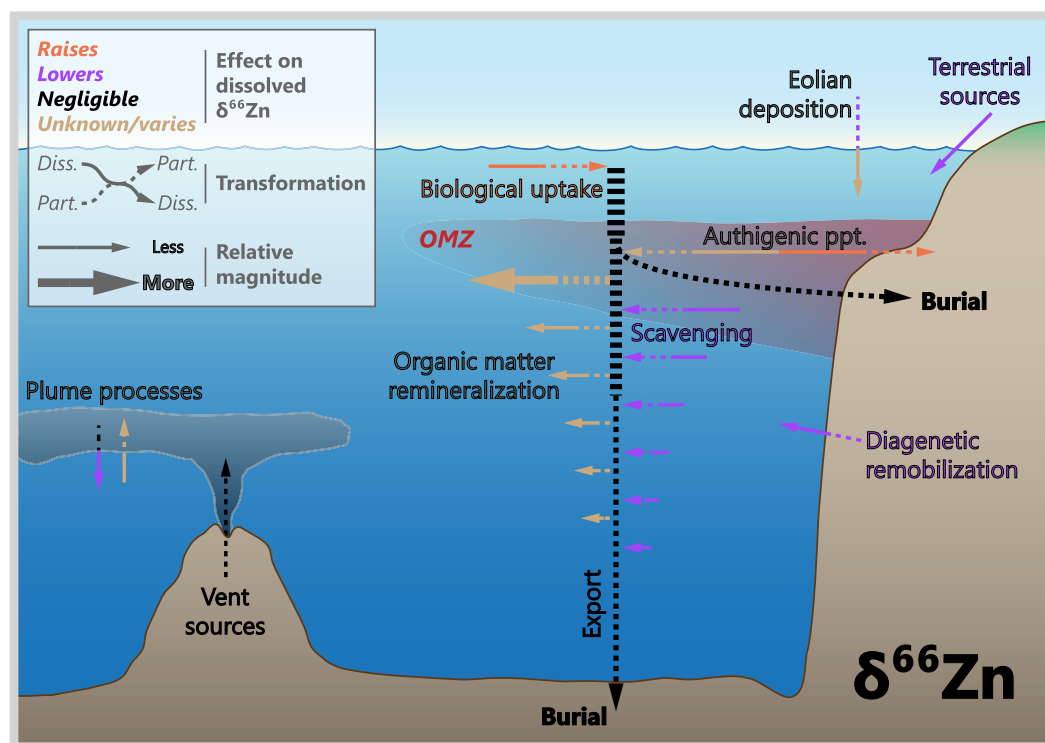


Figure 10. Processes driving Zn isotope variations in modern seawater. Though biological processes are capable of influencing dissolved $\delta^{66}\text{Zn}$, they do not appear to be the dominant driver of Zn isotope variations in the marine realm.

et al., 2016; Coale, 1991; Coale et al., 2003; Ellwood, 2004; Franck et al., 2003; Lohan et al., 2005). This difference between culture and field samples may reflect the ability of some phytoplankton to substitute Cd or Co for Zn in some enzymes when ambient dissolved [Zn] is low (e.g., Morel et al., 1994; Lee & Morel, 1995; Kellogg et al., 2020; Yee & Morel, 1996). Nevertheless, Zn availability has been shown to influence species composition and phytoplankton growth, including rates of calcification and alkaline phosphatase activity (Crawford et al., 2003; Mahaffey et al., 2014; Schulz et al., 2004; Shaked et al., 2006; Sunda & Huntsman, 1995).

Phytoplankton biomass grown in culture is typically enriched in the light isotopes of Zn (John et al., 2007; Köbberich & Vance, 2017, 2019; Samanta et al., 2018). Rather than reflecting a kinetic isotope effect expressed during uptake, recent studies suggested that Zn speciation in the media itself controls cellular $\delta^{66}\text{Zn}$; specifically, strong organic ligands present in the growth media, such as ethylenediaminetetraacetic acid, preferentially complex heavy Zn isotopes, rendering the bioavailable Zn pool isotopically light (Figure 10; John et al., 2007; Köbberich & Vance, 2017, 2019). An analogous process has also been suggested to occur between bioavailable Zn and that bound by natural organic ligands in the surface ocean, though this remains to be proven.

4.2.2. Chemical

Like most bioessential metals, Zn bioavailability is dictated by its chemical speciation (e.g., Anderson et al., 1978), which is dominated in the ocean by complexation to strong ($K' \sim 10^9\text{--}10^{11}$) organic ligands (Bruland, 1989; Donat & Bruland, 1990; Ellwood & Van Den Berg, 2000; Jakuba et al., 2012; Kim et al., 2015). Inorganic Zn is considered to make up <5% of the total Zn pool in most ocean regions, with the exception of the Southern Ocean, where strong upwelling of nutrient-rich deep waters leads to [Zn] in excess of complexing ligands (Baars & Croot, 2011). Note that while strongly complexed Zn is unlikely to be bioavailable, the presence of “weak” ligands (or more labile ligands) can enhance Zn uptake (Aristilde & Xu, 2012). Despite their potential importance to Zn isotope cycling, the role of organic (and inorganic) Zn-binding ligands in controlling dissolved and particulate $\delta^{66}\text{Zn}$ remains to be fully evaluated.

The importance of scavenging on the marine cycling of [Zn] and Zn isotopes is debated (Figure 10; e.g., John & Conway, 2014; Liao et al., 2020; Roshan et al., 2018; Weber et al., 2018). It is argued that scavenging can explain both the widespread observation of isotopically light Zn in the upper ocean, via preferential removal of heavy Zn isotopes on particles (and release at depth), and also the elevated concentration of Zn in the deep Pacific compared to that supplied by southern-sourced deep waters (Figure 9; Roshan et al., 2018; Weber et al., 2018). Indeed, Weber et al. (2018) propose that the light Zn isotope compositions exhibited by phytoplankton are a result of scavenging removing isotopically heavy Zn from surface seawater, leaving the residual bioavailable Zn pool isotopically light.

Elevated [Zn] in the deep Pacific has also been attributed to regional Zn inputs, particularly from hydrothermalism (Roshan et al., 2018), which possesses $\delta^{66}\text{Zn} < +0.45\%$ (John, Helgoe, & Townsend, 2018). Likewise, local- and regional-scale deviations toward lighter $\delta^{66}\text{Zn}$ in the deep Atlantic and Pacific have been attributed to sedimentary (Conway & John, 2014b; John et al., 2017; Lemaitre et al., 2020; Liao et al., 2020) and hydrothermal inputs (Conway & John, 2014b; John, Helgoe, & Townsend, 2018; Lemaitre et al., 2020). Anthropogenic aerosol deposition is also thought to supply significant Zn to regions of the surface ocean (e.g., Liao & Ho, 2018), with possible direct and indirect (via scavenging) regional impacts on upper ocean $\delta^{66}\text{Zn}$ values (Lemaitre et al., 2020; Liao et al., 2020).

Lastly, Janssen & Cullen (2015) suggest that decoupling of [Zn] and [Si] in the Northeast Pacific reflects the formation of Zn sulfides within particles in the North Pacific OMZ, in a manner analogous to that proposed for Cd (e.g., Janssen et al., 2014), which is discussed in more detail in Section 6.2.2. To date, however, there remains scant evidence for water column Zn-sulfide precipitation in OMZs (e.g., Conway & John, 2014b; John, Helgoe, & Townsend, 2018; Vance et al., 2019), with the patterns described by Janssen and Cullen (2015) alternatively attributed to shallower remineralization of Zn (from organic “soft parts”) relative to opal (Vance et al., 2019). That said, Zn-sulfide precipitation is undoubtedly important in euxinic basins such as the Black Sea and Cariaco Basin (Isson et al., 2018; Vance et al., 2016), and has been postulated to occur within the porewaters of oxygen deficient, organic-rich sediments (Section 4.3.4; Little et al., 2016).

4.2.3. Physical

In common with many of the trace metal isotope systems discussed here, the physical ocean circulation exerts a first order control on the distribution of [Zn] and dissolved $\delta^{66}\text{Zn}$ compositions (de Souza et al., 2018; Sieber et al., 2020; Vance et al., 2017; Weber et al., 2018). Subantarctic water masses have distinctive and low [Zn]:[PO_4^{3-}] and [Si]:[PO_4^{3-}] ratios, due to the elevated uptake of Zn and Si by diatoms in the surface of the Southern Ocean (Sarmiento et al., 2004; Vance et al., 2017). Remineralization of these Zn- and Si-rich diatoms at deeper depths imprints a correspondingly high [Zn]:[PO_4^{3-}] and high [Si]:[PO_4^{3-}] fingerprint on Antarctic bottom waters. This coupling of [Zn] and [Si] in the Southern Ocean forms the basis of the global [Zn]:[Si] correlation via the advection of southern sourced water masses toward the low latitudes, where they fill much of the ocean interior (de Souza et al., 2012; Holzer et al., 2014). The homogeneity of deep ocean dissolved Zn isotope compositions reflects the limited degree of Zn isotope fractionation on uptake by Southern Ocean diatoms (R. M. Wang et al., 2019; Zhao et al., 2014), which results in intermediate and deep southern-sourced water masses with limited or no Zn isotope contrast (Sieber et al., 2020). Although exceptions exist (see Section 4.2.2), generally, the oceanic [Zn]:[Si] correlation persists despite shallower remineralization of Zn relative to Si (Twining et al., 2014), and is especially clear in the South Atlantic, underlining that the mixing of water masses acts as the dominant control on [Zn] (de Souza et al., 2018; Middag et al., 2019; Vance et al., 2017). While Weber et al. (2018) concur with these other studies about the overall importance of ocean circulation on setting the distribution of [Zn] and [Zn]:[Si], they also argue that reversible scavenging is needed to fully explain the observed global patterns, particularly for dissolved $\delta^{66}\text{Zn}$. Further, any Zn addition from hydrothermal vents or sediments is superimposed on the circulation pattern, adding further complexity to the [Zn]:[Si] relationship (Section 4.2.2).

4.3. Sedimentary Archives

4.3.1. Ferromanganese Sediments

Manganese oxides are strong sorbents of positively charged, divalent trace metals, due to their negative layer charge at the pH of natural waters (e.g., Koschinsky & Halbach, 1995). The phyllo-manganate birnessite

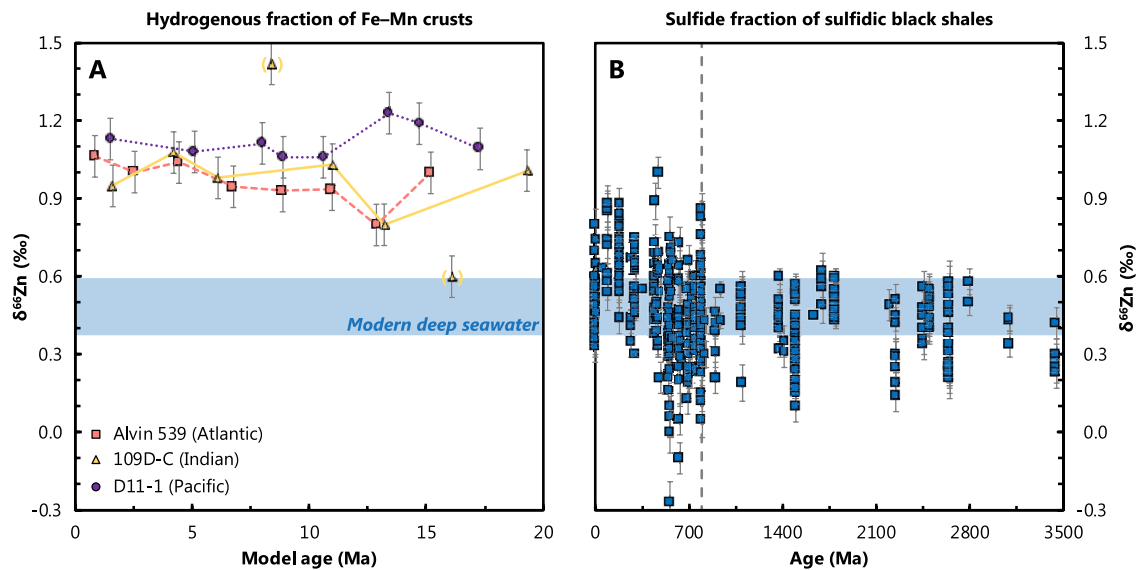


Figure 11. Records of deep ocean $\delta^{66}\text{Zn}$ through time. (a) Three records from Fe-Mn crusts recovered from the Atlantic (square, dashed line), Indian (triangle, solid line), and Pacific Oceans (circle, dotted line; Little, Vance et al., 2014). Assuming the isotopic offset between dissolved Zn in seawater and Fe-Mn crusts has remained unchanged at $\approx 0.55\text{‰}$ over this interval, these records imply only minimal Zn isotope variations in the deep ocean over the past ~ 20 Myr. Two anomalous measurements from 109D-C (in parentheses) possess low levels of authigenic Zn enrichment, indicative of detrital contamination. (b) Records recovered from the sulfide fraction of sulfidic black shales over the last 3,500 Myr (Isson et al., 2018). Assuming that sulfidic black shales record ambient seawater with no Zn isotope offset, this record can be interpreted as reflecting deep-ocean $\delta^{66}\text{Zn}$ over much of Earth's history. The dashed line indicates an apparent reorganization of the marine Zn isotope cycle around 800 Ma, interpreted by Isson et al. (2018) to reflect the rise of eukaryotes to ecological prominence.

is the main Mn- and trace element-bearing phase in oxic marine sediments (e.g., Koschinsky & Hein, 2003), as well as for several elements described here, including Zn, Cu, Ni, Cd, and Mo (though Mo exists in seawater as the molybdate anion). Ferromanganese crusts and nodules incorporate many trace elements during growth, leading to 10^6 -fold concentration enrichments relative to seawater (e.g., Arrhenius, 1963; Aplin & Cronan, 1985). As a result, Fe-Mn sediments are often one of the first marine sediment types to be targeted in the development of a new metal isotope tracer.

In the case of Zn, Fe-Mn crusts and nodules are isotopically heavy compared to seawater by $\approx +0.6\text{‰}$, exhibiting $\delta^{66}\text{Zn}$ between $+0.9\text{‰}$ and $+1.2\text{‰}$ (Figure 11; Little, Vance et al., 2014; Maréchal et al., 2000). This heavy composition is broadly consistent with inorganic sorption experiments of Zn on birnessite, with experiments at high ionic strength yielding Zn isotope offsets between sorbed and aqueous Zn of $+0.16\text{‰}$ to $+2.7\text{‰}$ (Bryan et al., 2015). However, the magnitude of fractionation observed in experiments is typically considerably larger than in natural Fe-Mn crusts and nodules, which Bryan et al. (2015) suggest may reflect sorption of Zn on birnessite via two different molecular mechanisms, each associated with different isotopic fractionation factors, as is the case for thallium (e.g., Nielsen et al., 2013). In addition, the influence of organic and inorganic speciation of Zn in seawater may play a role, though this remains to be fully evaluated (e.g., Little, Sherman et al., 2014).

Little, Vance et al. (2014) observed no marked temporal changes in $\delta^{66}\text{Zn}$ values for three Fe-Mn crusts from each of the major ocean basins over the last ~ 20 Ma. Zinc is somewhat immobile in Fe-Mn crusts, with a calculated effective diffusivity $<10^{-8} \text{ cm}^2 \text{ yr}^{-1}$, similar to Hf (Henderson & Burton, 1999) and Ba (Section 8.3). Assuming that Fe-Mn crusts preserve primary $\delta^{66}\text{Zn}$, the various records suggest that on a global basis, the marine Zn cycle has been in isotopic steady state for at least 20 Myr (Figure 11).

4.3.2. Biogenic Silica

The correlation of Zn with Si in the modern ocean led to the suggestion that Zn:Si measured in diatom opal may be a proxy for seawater $[\text{Zn}]:[\text{Si}]$ (and thus $[\text{Zn}]$) of past seawater. However, culturing and μ -XRF analyses revealed that only a small fraction (1%–3%) of the diatom Zn quota is incorporated into the opal frustules, with the remainder present in the organic 'soft parts' of the diatom cells (Ellwood & Hunter, 2000;

Twining et al., 2004). The Zn concentration in opal, $[Zn]_{\text{opal}}$, better reflects bioavailable Zn concentrations in seawater than dissolved $[Zn]:[Si]$ (Ellwood & Hunter, 2000). Thus, if the mechanisms of Zn incorporation into biogenic opal can be understood and calibrated, a $[Zn]_{\text{opal}}$ proxy of Zn bioavailability could help shed light on micronutrient limitation of the biological pump.

Andersen et al. (2011) analyzed Zn isotopes ($\delta^{66}Zn_{\text{opal}}$) and Zn:Si_{opal} in diatom opal isolated from core top sediments from the Southern Ocean. They observed isotopically heavy Zn in opal (from +0.7‰ to +1.5‰), and an inverse relationship between $\delta^{66}Zn_{\text{opal}}$ and Zn:Si_{opal}. Consistent with culturing studies, core top Zn:Si_{opal} appears to be linked to bioavailable Zn concentrations in ambient surface seawater. The authors suggested that $\delta^{66}Zn_{\text{opal}}$ should also reflect the isotope composition of bioavailable Zn in surface seawater, which should be isotopically heavy due to the predicted preferential incorporation of light Zn isotopes into phytoplankton organic matter. In this view, the extent of uptake—nutrient utilization—would be recorded by the systematics of Zn:Si_{opal} and $\delta^{66}Zn_{\text{opal}}$. While promising, this study predated the recent surge in seawater $\delta^{66}Zn$ measurements. Measurements of Southern Ocean seawater $\delta^{66}Zn$ have not borne out early predictions of isotopically heavy residual surface waters (Figure 9), with little to no fractionation observed (Sieber et al., 2020; R. M. Wang et al., 2019; Zhao et al., 2014).

In apparent contrast to diatoms, Hendry and Andersen (2013) showed that sponge spicules can faithfully record seawater $\delta^{66}Zn$. Sponges are primarily deep-sea organisms. Hence, if the controls on diatom Zn:Si and $\delta^{66}Zn_{\text{opal}}$ can be understood, a combination of Zn:Si and $\delta^{66}Zn$ measurements in diatoms and sponges (as used for Si isotopes; Farmer et al., 2021) could provide a vertically resolved view of the past ocean global Zn cycle, including the role of Southern Ocean processes in the biological carbon pump.

4.3.3. Carbonates

Carbonates may provide an alternative archive for $[Zn]$ (as Zn:Ca) and $\delta^{66}Zn$. For example, Marchitto et al. (2000) showed that Zn:Ca ratios in benthic foraminifera are sensitive to bottom water dissolved $[Zn]$. However, the Zn content in individual microfossil shells is extremely low (typically <0.1 ng per test); at this level, with current analytical capabilities and blank contributions, many tens to hundreds of benthic foraminifera would be required for a single Zn isotope measurement.

To circumvent the issue of low Zn contents of individual shells, Pichat et al. (2003) utilized a selective carbonate dissolution procedure on bulk sediment from the equatorial Pacific, mostly consisting of coccoliths. These authors argued that isotopically heavy $\delta^{66}Zn$ in carbonates reflected surface seawater, with values modulated by changes in biological productivity due to varying seasonal insolation. Similarly isotopically heavy Zn in ancient carbonates has also been argued to reflect strong biological utilization in surface waters (Kunzmann et al., 2013; cf. John et al., 2017; Liu et al., 2017). More recently, Zhao et al. (2021) surveyed carbonates from the Great Bahama Bank, observing carbonate-bound $\delta^{66}Zn$ ranging from $\approx -0.5\%$ to $+1.1\%$. Given the local seawater value of $\approx +0.1\%$, this large range is surprising, and implies that a number of additional factors must fractionate Zn isotopes during incorporation into and recovery from carbonates. These factors include: Stable isotope fractionation during Zn incorporation into $CaCO_3$, contamination from non- $CaCO_3$ phases (e.g., lithogenic or authigenic phases), and methodological issues (e.g., non-quantitative selective leaching leading to stable isotope fractionation; e.g., Revels et al., 2015). Overall, the relationship between bulk carbonate and seawater $\delta^{66}Zn$ is not straightforward.

Despite the difficulty in interpreting bulk carbonate $\delta^{66}Zn$, phase-specific (particularly, aragonitic) $CaCO_3$ archives appear more promising. For example, Zhao et al. (2021) identify carbonate ooids as a promising archive of past seawater $\delta^{66}Zn$. Likewise, Little et al. (2021) showed that deep-sea coral skeletons record intermediate- and deep-ocean $\delta^{66}Zn$. Given the large size of specimens and their global distribution, combined with the ability to assign precise ages to individual specimens, deep-sea corals may provide an archive of seawater compositions that are amenable to Zn isotope analysis. However, recent Zn isotope studies of shallow-water zooanthellate corals suggests that the relationship with seawater $\delta^{66}Zn$ is complicated by temperature and photosynthetic effects (Ferrier-Pagès et al., 2018; Xiao et al., 2020).

4.3.4. Organic-Rich Sediments

The isotope composition of Zn in organic-rich sediments deposited along productive continental margins is typically $\approx +0.1\%$, which is lighter than ambient seawater by $\sim 0.4\%$ (Little et al., 2016). This light $\delta^{66}Zn$

signature likely arises from one of two processes. In the first process, isotopically light Zn is preferentially removed from seawater during precipitation of sulfides (Fujii, Moynier, Pons, & Albarède, 2011; Vance et al., 2016). This precipitation may occur directly from seawater and into sediments, or possibly within reducing microenvironments that develop within particles sinking through low-(O₂) water columns (Bianchi et al., 2018; Janssen & Cullen, 2015; Little et al., 2016; Vance et al., 2016). Regardless, so long as Zn removal is non-quantitative, these processes act to bury isotopically light Zn from the ocean. In the euxinic Black Sea, where Zn drawdown with sulfides is quantitative, sedimentary $\delta^{66}\text{Zn}$ is expected to reflect the deep seawater composition from above the chemocline (analogous to Mo; Section 7; Vance et al., 2016), and euxinic black shales represent a promising archive of past deep seawater $\delta^{66}\text{Zn}$. This prediction was confirmed by Isson et al. (2018), who reported that sulfide-bound Zn in black shales from the euxinic Cariaco Basin exhibited the expected deep seawater-like $\delta^{66}\text{Zn}$ of $+0.5 \pm 0.1\%$. Using this calibration, Isson et al. (2018) analyzed $\delta^{66}\text{Zn}$ in hundreds of euxinic black shales generating a 3,500 Myr record of deep-ocean Zn isotope evolution (Figure 11b). Though a full discussion of this data set is beyond the scope of our review, this record reveals a shift in deep ocean $\delta^{66}\text{Zn}$ around 800 Ma, which Isson et al. (2018) interpret as reflecting a reorganization of the marine Zn cycle driven by the rising ecological prominence of eukaryotes.

A second process that can deliver isotopically light Zn to sediments is organic matter. That is, presuming that phytoplankton assimilate isotopically light Zn from seawater, the export of this organic matter to sediments can bury light Zn in margin settings (John et al., 2017; Little et al., 2016). If dominant, this biologically driven process might suggest some utility for $\delta^{66}\text{Zn}$ in organic-rich sediments to reconstruct paleo-productivity, especially in low-oxygen settings. Alternatively, if the scavenging-centered view proposed by Weber et al. (2018) is correct, the $\delta^{66}\text{Zn}$ of exported Zn—while still light relative to deep seawater—would not represent a simple measure of either Zn uptake or primary productivity. This view implies that there would be considerable spatial complexity in the $\delta^{66}\text{Zn}$ delivered to sediments that depends on factors such as scavenging intensity relative to upwelling, which is not directly linked to biological productivity. Moreover, Weber et al. (2018) even suggest that some regions of the ocean might bury isotopically heavy organic matter-associated Zn, either due to variability in surface water $\delta^{66}\text{Zn}$ resulting from scavenging, or via burial of isotopically heavy Zn adsorbed to organic matter.

Overall, the uncertainties in Zn delivery mechanisms and the indirect connections between $\delta^{66}\text{Zn}$ and primary productivity means that there are considerable obstacles to interpreting organic-rich sedimentary $\delta^{66}\text{Zn}$ as a direct tracer of productivity.

4.4. Prospects

Despite the complexities and remaining unknowns in oceanic $\delta^{66}\text{Zn}$ cycling reviewed above, we note that there are systematic variations in sedimentary Zn isotope compositions recorded in geologic archives on Myr and Gyr timescales. In addition to the organic sediment record of Isson et al. (2018), described above, Yan et al. (2019) compiled three $\delta^{66}\text{Zn}$ datasets from contemporaneous Ediacaran (635 Ma, Marinoan) post-glacial cap carbonates (John et al., 2017; Kunzmann et al., 2013; Lv et al., 2018), which show systematic changes in Zn isotope compositions over this period of marked global change. Second, Sweere et al. (2018) presented data showing marked shifts in carbonate-bound Zn isotope compositions in several geological sections spanning a Cretaceous Ocean Anoxic Event (OAE 2). While there is no consensus on the causes of these intriguing isotopic shifts within carbonates (e.g., the role of redox vs. source/sinks vs. productivity), the coherency of the records is encouraging and their full interpretation awaits identification of the driving processes.

On longer timescales, the importance of Earth's overall redox state on marine Zn isotope systematics requires elucidation. There are several other explanations for the shift in deep-ocean $\delta^{66}\text{Zn}$ at ≈ 800 Ma besides a switch to more eukaryotic-dominated oceans, such as changes in Zn speciation, variations in other Zn sinks, or diagenesis (see Isson et al., 2018); indeed, we are not aware of any studies exploring how primary sedimentary $\delta^{66}\text{Zn}$ may be modified by diagenetic processes. Moreover, the assumption that the high affinity for Zn exhibited by eukaryotes translates into higher eukaryotic Zn:C (compared to prokaryotes) is not supported by culture data, which showed that cyanobacterial Zn:C is comparable to—or can even exceed that of—eukaryotes grown under the same conditions (Köbberich & Vance, 2019). Thus, developing a more

complete interpretation of $\delta^{66}\text{Zn}$ in the sedimentary record requires building a more complete understanding of the biological and biologically mediated processes cycling $\delta^{66}\text{Zn}$ in the upper water column.

Lastly, we recommend that future studies target coupled dissolved and particulate phase $\delta^{66}\text{Zn}$ data, in concert with detailed biological and chemical speciation data. To date, particulate phase $\delta^{66}\text{Zn}$ data has proven challenging to obtain due to pervasive Zn contamination. Zinc isotope characterization of sediments and sediment porewater is needed to constrain the role of early diagenetic reactions, as well as their importance to the mass balance of Zn isotopes in the ocean. Sediment studies would also benefit from further investigation of whether specific phases offer more robust archives of past seawater $\delta^{66}\text{Zn}$, potentially exploiting selective extraction methods. We also recommend revisiting published records in light of recent seawater $\delta^{66}\text{Zn}$ data.

5. Copper

As with Fe and Zn, Cu is used in a number of cellular processes, most notably electron transport (e.g., Twinning & Baines, 2013). Unlike Fe and Zn however, Cu is toxic to phytoplankton, even at extremely low free $[\text{Cu}^{2+}]$ (pM; Brand et al., 1986). Dissolved Cu—in seawater and within marine organisms—is thus strongly regulated by organic complexes that maintain low free $[\text{Cu}^{2+}]$ (e.g., Moffett & Dupont, 2007; Waldron & Robinson, 2009). Some archives have shown promise for recording aspects of surface and deep ocean $\delta^{65}\text{Cu}$, such as organic-rich sediments and authigenic Fe–Mn oxides, respectively. Despite the strong biological control over marine [Cu] distributions, our present understanding of the biogeochemical cycle of Cu suggests there is no clear route to developing [Cu] or $\delta^{65}\text{Cu}$ as paleoproductivity proxies, and Cu cannot be modeled within the simple reactor framework (Section 2.2). However, there are a number of sensitivities in the marine Cu isotope cycle that are indirectly related to paleoproductivity that may render $\delta^{65}\text{Cu}$ as a proxy of processes related to metal complexation by organic ligands and/or marine redox evolution.

5.1. Marine Distribution

The distribution of Cu in the ocean has been described as “hybrid-type,” because it is intermediate between nutrient- and scavenged-type elements (Bruland & Lohan, 2003). Depth profiles of [Cu] typically show approximately linear increases with depth (e.g., Boyle et al., 1977; Figure 12a). Surface [Cu] are typically about 0.5–1 nmol kg⁻¹, compared to deep Atlantic [Cu] of ~2.5 nmol kg⁻¹ and deep Pacific [Cu] of ~4 nmol kg⁻¹ (Figure 12). Unlike the other metals discussed here (with the possible exception of Cr), and despite the existence of a large seawater [Cu] data set, some discrepancy still exists in the [Cu] measured by different techniques; methodological details such as storage time, acidification strength, strong oxidation (or not) prior to analysis are all thought to be potentially important, and further intercomparison efforts are needed (Posacka et al., 2017). Nevertheless, the [Cu] distribution pattern has been attributed to a combination of biological uptake and remineralization, benthic flux from sediments (e.g., Boyle et al., 1977; Little et al., 2018; Roshan & Wu, 2015a), and/or reversible scavenging (Little et al., 2013; Richon & Tagliabue, 2019). These processes are superimposed on the first-order distribution established via the physical ocean circulation (Roshan & Wu, 2015a).

Copper isotopes are reported as relative to the NIST SRM 976 standard, though due to a shortage of this material, two other certified reference standards are now available: ERM-AE633 ($\delta^{65}\text{Cu}_{\text{SRM976}} = -0.01 \pm 0.05\%$) and ERM-AE647 ($\delta^{65}\text{Cu}_{\text{SRM976}} = +0.21 \pm 0.05\%$; Moeller et al., 2012; Moynier et al., 2017). For consistency and ease of comparison, Moynier et al. (2017) recommend that future data be reported relative to NIST SRM 976. We adopt this convention. The analysis of Cu isotopes in seawater is challenging, due to both Cu's strong organic complexation, and only two isotopes precluding the use of a double spike technique (reviewed in Little et al., 2018). The data presented to date indicate that deep seawater $\delta^{65}\text{Cu}$ values are isotopically heavy (at about +0.7‰; Figure 12b) compared to the upper continental crust (UCC; at about +0.1‰; Table 1; Moynier et al., 2017). Lighter Cu isotope compositions in the upper water column and along margins are thought to reflect local sources of isotopically light Cu (e.g., aerosols, riverine particulates, and sediments; Little et al., 2018; Takano et al., 2014). While sample treatment may be a concern for quantitative [Cu] measurements (Posacka et al., 2017), it remains unclear to what extent this might also be an issue for measurements of $\delta^{65}\text{Cu}$ made using different techniques, depending on storage time, acidification and

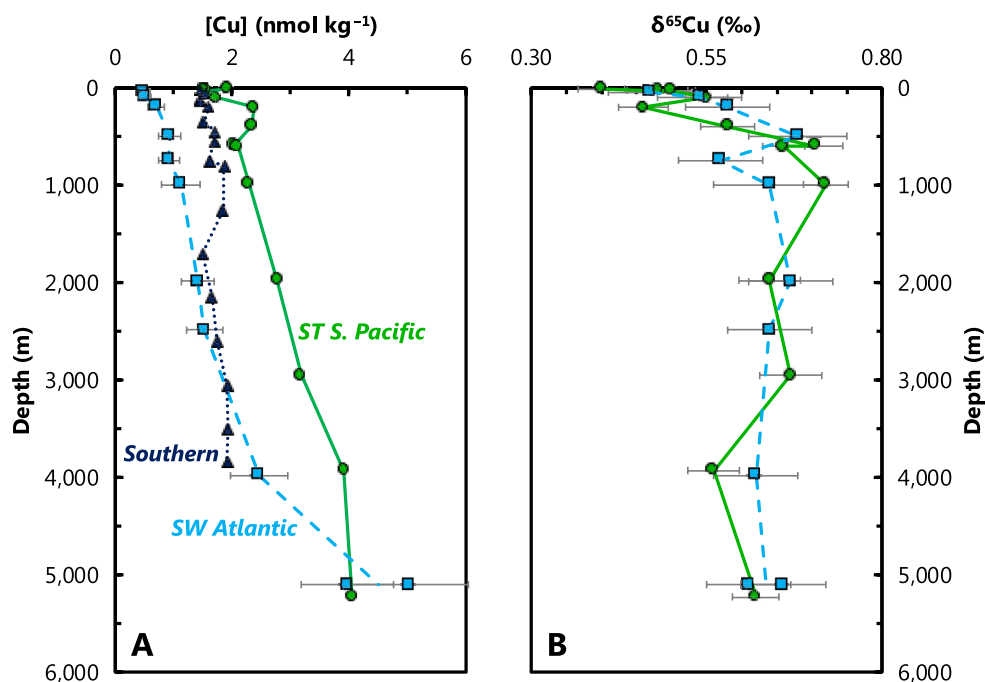


Figure 12. Representative profiles of dissolved Cu concentrations ($[Cu]$); (a) and Cu isotope compositions ($\delta^{65}\text{Cu}$); (b). Data from the Southwest Atlantic (squares, dashed line; Little et al., 2018), Subtropical South Pacific (circles, solid line; Takano et al., 2017) and Southern Oceans (triangles, dotted line; Boye et al., 2012). Station locations as per Figure 1. This comparison illustrates that the isotopic behavior of Cu is similar between basins, reflecting the importance of complexation by strong organic ligands. Note that there are no Cu isotope data available for the Southern Ocean at this time.

oxidation with UV or H_2O_2 prior to analysis (see discussion in Little et al., 2018). Reassuringly, however, Little et al. did note that despite potential underestimation of $[Cu]$ by some methods, a general homogeneity of seawater $\delta^{65}\text{Cu}$ persists between labs and geographic location and depth of samples (Little et al., 2018; Yang et al., 2020; Figure 12). As such, the expected methodological effects of incomplete Cu recovery on $\delta^{65}\text{Cu}$ may be slight, though it remains unclear how the size of this effect might vary with sample location and oceanographic conditions (e.g., in surface waters or those with low $[\text{O}_2]$). As the seawater $\delta^{65}\text{Cu}$ data set continues to grow, we echo the calls of previous authors for further intercalibration of methods (e.g., Baconnais et al., 2019; Little et al., 2018; Posacka et al., 2017).

5.2. Driving Processes

5.2.1. Biological

Copper is bioessential, but cellular Cu contents are ~ 2 – 10 fold lower than the micronutrients Fe and Zn (Twining & Baines, 2013). The redox-active behavior of Cu (existing as Cu^{2+} or Cu^+ in biological systems) enables its role in electron transport, for example in the Cu-containing proteins plastocyanin and cytochrome c oxidase (Ridge et al., 2008). Iron-limited phytoplankton tend to increase their Cu uptake, either due to the replacement of Fe-containing with Cu-containing enzymes (e.g., Peers and Price, 2006), or the involvement of Cu in the high affinity Fe uptake systems (Annett et al., 2008; Guo et al., 2012; Maldonado et al., 2006). Despite its biological function, Cu is also extremely toxic due to the formation of reactive oxygen species, which pose a threat to DNA, lipids, and proteins (Ridge et al., 2008). Copper toxicity thresholds vary by phytoplankton group, with smaller organisms generally more sensitive than larger ones (e.g., cyanobacteria cf. diatoms; Brand et al., 1986), and coastal strains more resistant than open ocean strains (e.g., Peers et al., 2005).

A small number of studies have investigated Cu isotope fractionation during cellular uptake or cell surface adsorption by microorganisms (Cadiou et al., 2017; Coutaud et al., 2018, 2019; Navarrete et al., 2011;

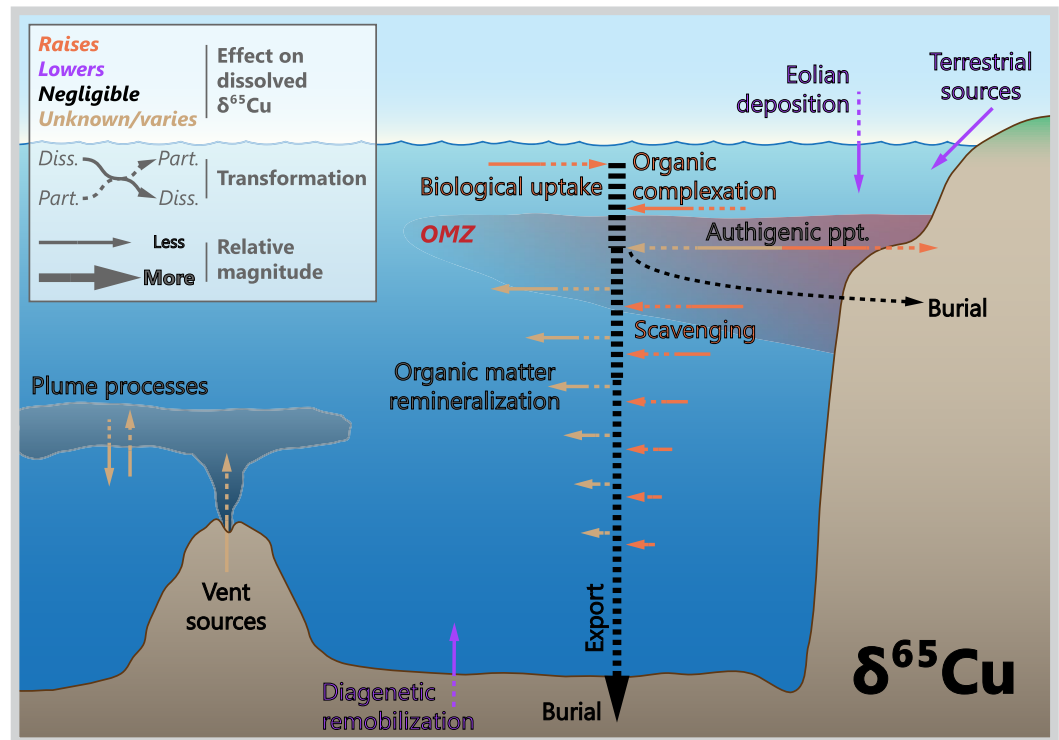


Figure 13. Processes driving Cu isotope variations in modern seawater. Biological productivity exerts only a modest impact on the marine Cu isotope cycle and thus there is no obvious route to developing Cu isotopes (or Cu concentrations) as a paleoproductivity proxy.

Pokrovsky et al., 2008). The results of these experiments are somewhat variable, with enrichment of either light or heavy Cu isotopes observed during assimilation and adsorption. However, assimilation in culture generally favors light Cu isotopes (Cadiou et al., 2017; Navarrete et al., 2011; Figure 13). The complexity in Cu isotopic behavior has been attributed to small changes in Cu speciation or redox during uptake and/or release of Cu (Coutaud et al., 2018, 2019).

5.2.2. Chemical

In seawater, the vast majority of Cu is complexed to strong organic ligands (more than 99.8% complexed in surface Northeast Pacific), which lower free $[\text{Cu}^{2+}]$ to below toxic levels (e.g., Coale & Bruland, 1988, 1990; Moffett & Dupont, 2007). It is thought that ligands are primarily produced by biota for the purpose of Cu detoxification (e.g., Moffett & Brand, 1996; Moffett et al., 1990), although recent work suggests that strongly complexed Cu is bioavailable to some eukaryotes, which appear to have a higher cellular Cu requirement (and higher thresholds of Cu toxicity) than prokaryotes (Semeniuk et al., 2009, 2015).

Both theory and experiments predict preferential complexation of heavy isotopes by strong organic ligands (Fujii et al., 2013; Ryan et al., 2014; Sherman, 2013; Sherman et al., 2015), and organic complexation is thought to play a key role in the modern oceanic budget and distribution of Cu isotopes (Little et al., 2018; Little, Vance et al., 2014; Takano et al., 2014; Thompson & Ellwood, 2014; Vance et al., 2008). The small pool of non-complexed Cu^{2+} in seawater is thus expected to be isotopically light (e.g., Little et al., 2018; Little, Sherman et al., 2014).

Based on a surface complexation model with the phyllo-manganate birnessite, the principal scavenging phase of divalent trace metals in oxic sediments, Sherman & Peacock (2010) calculated that $[\text{Cu}]$ in deep waters should be orders of magnitude lower than is actually observed. They attribute this difference to the chelation of “essentially all dissolved Cu” by organic ligands (Sherman & Peacock, 2010), consistent with observations (e.g., Heller & Croot, 2015; Jacquot & Moffett, 2015; Moffett & Dupont, 2007). Nevertheless, some form or forms of scavenging are also thought to play a role in the oceanic Cu distribution.

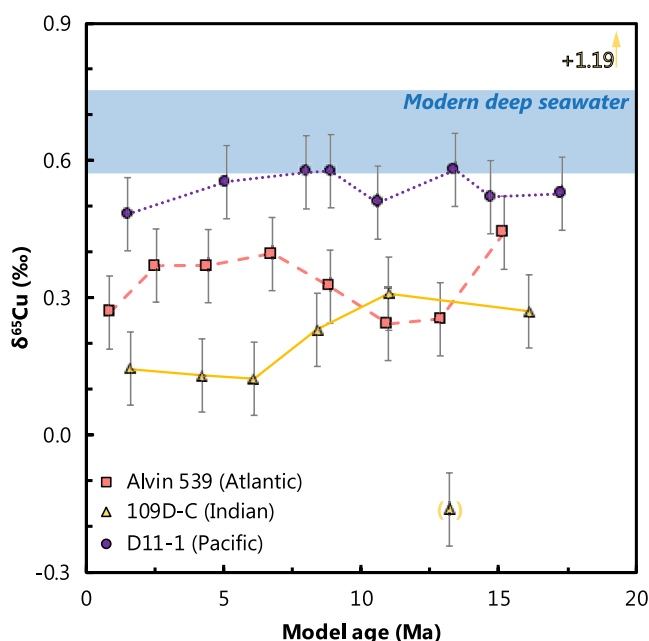


Figure 14. Deep ocean $\delta^{65}\text{Cu}$ constancy over the past 20 Myr. These records are derived from Fe–Mn crusts recovered from the Atlantic (square, dashed line), Indian (triangle, solid line), and Pacific Oceans (circle, dotted line; data from Little, Vance et al., 2014). Assuming the isotopic offset between dissolved Cu in seawater and Fe–Mn crusts has remained unchanged at $\approx 0.35\text{‰}$ over this time, these records imply that the inter-basin Cu isotope variations observed in modern crusts and the Cu isotope cycle itself have remained relatively stable for at least 20 Myr. Two samples from 109D-C possess low levels of authigenic Cu enrichment indicating detrital contamination (parentheses, arrow; see Little, Vance et al., 2014).

Reversible scavenging, a term used to describe the equilibrium between a scavenged and dissolved metal pool, has been proposed as the driving process behind the generally monotonic, linear increases in [Cu] with depth (Little et al., 2013; Richon & Tagliabue, 2019; Figure 12). In some regions with high particulate loads (e.g., some hydrothermal plumes, benthic nepheloid layers), scavenging removal of Cu has been observed (Jacquot and Moffett, 2015; Roshan & Wu, 2015a). Preferential scavenging of light Cu isotopes by particulate (e.g., oxyhydroxide) phases has also been proposed as an explanation for isotopically heavy seawater Cu isotope compositions (e.g., Takano et al., 2014), though the driving mechanisms leading to isotopically light particulate Cu remain to be fully established (see Section 5.3; Figure 13).

The shorter residence time of Cu (2–3.3 kyr; Little et al., 2017), compared to many of the other trace metals reviewed here (e.g., Cd, Zn, and Ni), mean that regional and local sources of Cu to the ocean play a relatively larger role in determining [Cu] distributions than for some other metals. Sources of Cu include aerosols (both natural and anthropogenic; e.g., Takano et al., 2014; Yang et al., 2019), benthic fluxes from sediments (e.g., Boyle et al., 1977; Heller & Croot, 2015; Roshan & Wu, 2015a; Little et al., 2018), and dissolved or particulate riverine sources (e.g., Little et al., 2018; Richon & Tagliabue, 2019; Vance et al., 2008; Figure 13). A possible small hydrothermal source has been identified in the South Pacific from the East Pacific Rise (Roshan & Wu, 2018), which is in contrast to the scavenging removal of Cu observed around hydrothermal vents elsewhere (e.g., Jacquot & Moffett, 2015).

5.2.3. Physical

Copper's shorter residence time relative to Cd, Zn, and Ni also means that the Southern Ocean and wider physical ocean circulation play a somewhat smaller role in oceanic [Cu] and $\delta^{65}\text{Cu}$ distributions compared to many of the other bioactive trace metals discussed herein. Nonetheless, the imprint of circulation is evident in certain circumstances, such as in

the Atlantic and the upper 2 km of the South Pacific where [Cu] is correlated with [Si] (Little et al., 2018; Roshan & Wu, 2015a, 2018).

5.3. Marine Archives

5.3.1. Ferromanganese Sediments

Ferromanganese sediments (crusts and nodules) exhibit Cu isotope compositions of $+0.3\text{‰}$ to $+0.5\text{‰}$ (Albarède, 2004; Little, Vance et al., 2014). This means that, on average, Fe–Mn sediments are $\sim 0.35\text{‰}$ lighter than deep seawater, which averages $+0.7\text{‰}$ (Figure 14). The explanation for this offset is uncertain, but may reflect either strong organic complexation of Cu in seawater (Little, Sherman et al., 2014), or the enrichment of light Cu isotopes on the birnessite mineral surface. The latter has been observed in inorganic experiments, whereby sorbed Cu exhibited $\delta^{65}\text{Cu}$ that was $0.45 \pm 0.18\text{‰}$ lower than $\delta^{65}\text{Cu}$ in solution (Ijichi et al., 2018). Consistent with these experiments, light isotope fractionation on sorption of Cu to birnessite has also been predicted from first-principles *ab initio* calculations (Sherman & Little, 2020). At equilibrium in seawater, however, the strong complexation and mineral sorption effects should be additive, leading to a much larger isotopic offset than the $\sim 0.35\text{‰}$ observed, suggesting that one of the two effects is not expressed in nature for reasons as yet unclear (Sherman & Little, 2020).

Little, Vance, et al. (2014) observed no marked changes in deep ocean $\delta^{65}\text{Cu}$ recovered from three Fe–Mn crusts from each of the major ocean basins over the last ~ 20 Ma. Copper is relatively immobile in Fe–Mn crusts, with a calculated effective diffusivity $\leq 10^{-9} \text{ cm}^2 \text{ yr}^{-1}$ (Henderson & Burton, 1999), similar to Ni

(Section 9.3.1). Assuming that Fe–Mn crusts preserve primary $\delta^{65}\text{Cu}$, the various records suggest that on a global basis, the marine Cu cycle has been in isotopic steady state for at least 20 Myr (Figure 14).

5.3.2. Organic-Rich Sediments

Qualitative arguments for high organic matter fluxes (i.e., higher paleoproductivity) have been made based on elevated Cu (and Ni) contents of ancient organic-rich sediments (e.g., Tribovillard et al., 2006). This approach is supported by positive correlations between Cu (and Ni, Section 9.3.2) with TOC content in modern continental margin sediments (e.g., Böning et al., 2012). For this approach to offer mechanistic insights into past export productivity, organic matter (or a biologically associated mineral phase, such as CaCO_3 or BaSO_4), must always be the primary vector for that metal to sediments. This condition is not met for Cu, nor for other chalcophile elements (e.g., Mo), thus presenting a significant challenge to the use of sedimentary Cu contents to trace past export productivity. Copper exhibits a strong reactivity toward sulfide, as illustrated by the quantitative removal of Cu from the euxinic Black Sea water column and resultant enrichment in underlying organic-rich sediments (Little et al., 2015; Tankéré et al., 2001).

Despite the strong reactivity of Cu toward sulfide, and unlike Zn (Section 4.3.4) and Mo (Section 7.2.3), Cu in euxinic sediments from the Black Sea and Cariaco Basin does not record open marine $\delta^{65}\text{Cu}$ (Little et al., 2017). In fact, authigenic Cu in modern organic-rich sediments (from both euxinic basins and continental margin settings) is generally similar in isotopic composition to Fe–Mn sediments and to suspended particulate material collected from the South Atlantic, all at about $+0.3\text{‰}$ (Ciscato et al., 2019; Little et al., 2018; Little et al., 2017). The homogeneity in authigenic sedimentary Cu isotope compositions has been suggested to reflect an equilibrium isotope fractionation in the aqueous phase between organically complexed Cu and inorganic Cu^{2+} , with the latter $\sim 0.4\text{‰}$ lighter than ligand-bound Cu, followed by near quantitative scavenging of inorganic Cu^{2+} by particulate material of any type (Little et al., 2018; Little et al., 2017). For example, in the Black Sea, transfer of Cu to the deep euxinic basin may be mediated by cycling with nanoparticulate Fe and Mn oxides at the redoxcline, linked to the benthic Fe–Mn redox shuttle (Little et al., 2017; Lyons & Severmann, 2006). If correct, this hypothesis suggests that authigenic Cu isotope compositions in marine sediments may reflect the evolution of organic complexation on geological timescales.

Ciscato et al. (2018, 2019) developed a new approach to isolate trace elements associated with two different fractions in organic-rich sediments, the “organic-pyrite fraction” (OPF) and “HF digestible fraction” (HFD). They find that the OPF of modern Peru margin sediments typically contains $>50\%$ of total Cu and is variably isotopically light compared to bulk authigenic Cu. They suggest this signature reflects incomplete sulfidation under variable water column and sedimentary redox conditions (e.g., Bianchi et al., 2018). Unlike in modern sediments, in ancient shales (ranging in age from 0.4 to 3.4 Ga) bulk Cu content does not correlate with TOC and $>80\%$ of Cu is hosted in the HFD fraction. In addition, the OPF fraction in ancient shales is markedly isotopically heavier than it is in modern sediments (Ciscato et al., 2019). This difference between modern and ancient Cu partitioning may reflect diagenetic or metamorphic processing, or it may be a primary feature relating to differences in the Cu isotope composition of seawater, or differences in the mechanism(s) of Cu sequestration into sediments.

5.4. Prospects

Despite the biological importance of Cu, the modern biogeochemical cycle of Cu suggests there is no clear route to developing Cu isotopes (or [Cu]) as a paleoproductivity proxy. Work is also urgently needed to better understand the role of processing and storage effects on the accuracy of the oceanic [Cu] database, perhaps providing the opportunity to better understand the speciation of the dissolved Cu pool. Similarly, work is needed to firmly establish the fidelity of $\delta^{65}\text{Cu}$ measurements and ensure that different datasets are directly comparable. Despite these challenges, however, it is firmly established that organic ligands play a key role in the cycling of Cu and $\delta^{65}\text{Cu}$, suggesting potential for the use of Cu isotopes in tracing the evolution of organic complexation on geological timescales. Additionally, careful sequential extraction procedures, such as those described by Ciscato et al. (2019), may allow for the direct probing of past seawater properties, such as redox state.

At present, there are few applications of Cu isotopes to study ancient biogeochemical cycles. Two black shale records indicate a shift from UCC-like to heavy Cu isotope values across the Great Oxidation Event (GOE, ~2.4 Ga; Ciscato et al., 2019; Fru et al., 2016). Chi Fru et al. (2016) interpreted this shift as reflecting the onset of oxidative weathering and waning of iron formation deposition, with the latter process driving pre-GOE seawater isotopically light due to the preferential scavenging of heavy Cu isotopes to Fe oxides. However, a recent analysis of two classic pre-GOE sequences containing iron formations do not support this earlier hypothesis, with $\delta^{65}\text{Cu}$ remaining close to 0‰ (Thibon et al., 2019). Thus, while the limited available data preclude confident interpretations, there are tantalizing tastes of future research directions in Cu isotope geochemistry.

6. Cadmium

The distribution of [Cd] closely correlates with the macronutrient $[\text{PO}_4^{3-}]$ in the oceans (e.g., Boyle et al., 1976; Bruland, 1980). The nutrient-like properties of [Cd] and attendant correlations with $[\text{PO}_4^{3-}]$ have been documented in multiple ocean basins, in multiple dimensions (i.e., vertically, spatially, and temporally), and are faithfully captured by certain sediments (e.g., Boyle, 1981). Moreover, many marine microbes assimilate isotopically light Cd from their environment (e.g., Lacan et al., 2006), consistent with the direction and magnitude of Cd isotope fractionation in seawater (e.g., Ripperger et al., 2007). Though the overall geochemical distribution of Cd is promising from the perspective of tracing paleoproductivity, there are three main uncertainties that require resolving. Broadly, these relate to uncertainties surrounding: How, why, and which organisms contribute to Cd cycling in seawater; the significance of the decoupling between Cd and major nutrients in sinking particles, particularly in low $[\text{O}_2]$ settings; and, identification of sedimentary archives that capture surface water $\delta^{114}\text{Cd}$. Despite these uncertainties, the first-order features of marine Cd geochemistry are characteristic of a nutrient-type element, meaning that Cd can be modeled in a simple reactor scheme (see Section 2.2), and that the distributions of [Cd] and $\delta^{114}\text{Cd}$ appear broadly connected to underlying patterns of productivity.

6.1. Marine Distribution

Away from major upwelling regions, surface water [Cd] are typically between 1 and 100 pmol kg^{-1} , but can reach as low as 30 fmol kg^{-1} (Schlitzer et al., 2018; Figure 15). The majority of this small surface inventory is thought to be complexed by strong organic ligands (e.g., Bruland, 1992; Ellwood, 2004). In intermediate and deep waters, [Cd] are significantly elevated relative to surface waters, ranging from 0.5 nmol kg^{-1} in intermediate and deep waters in the north Atlantic to almost 1.2 nmol kg^{-1} in the oldest deep waters of the north Pacific (Schlitzer et al., 2018). As with Zn (Section 3), the overall distribution of (Cd) throughout the oceans is driven principally by biological and physical processes in the Southern Ocean, and the lateral circulation of Southern Ocean water masses (e.g., Baars et al., 2014; Middag et al., 2018; Sieber, Conway, de Souza, Hassler et al., 2019; Xie et al., 2017). Thus, the shape of vertical [Cd] profiles at lower latitudes arises largely from horizontal transport and mixing of high-Cd Southern Ocean-sourced water masses, with a modest contribution from regeneration of sinking particles (i.e., 5%–40%; Middag et al., 2018). These processes result in Cd having a “nutrient-type” one-dimensional water column profile, with a progressive increase in intermediate and deep water [Cd] along the pathways of meridional overturning circulation (e.g., de Baar et al., 1994; Middag et al., 2018).

The past decade has seen an explosion in the number of studies employing Cd stable isotopes to investigate marine Cd cycling. The majority of extant Cd isotope data are reported relative to the NIST SRM 3108 standard, though several earlier studies, reviewed by Rehkämper et al. (2012), were reported relative to other in-house materials. Cross-calibration of these materials is described in detail by Abouchami et al. (2013). While the earliest study of Cd isotope variations in seawater was unable to unambiguously identify systematic patterns in the water column, the authors noted that cultures of phytoplankton preferentially incorporated isotopically light Cd relative to the media (Lacan et al., 2006). Assuming biological processes were responsible for Cd uptake, this observation led to two key predictions for marine Cd isotope systematics: That Cd-depleted surface waters should exhibit isotopically “heavier” compositions than Cd-replete deep waters; and, that the degree of isotopic fractionation should be proportional to the extent of Cd removal into particles. Indeed, this is precisely the pattern that was first reported by Ripperger et al. (2007).

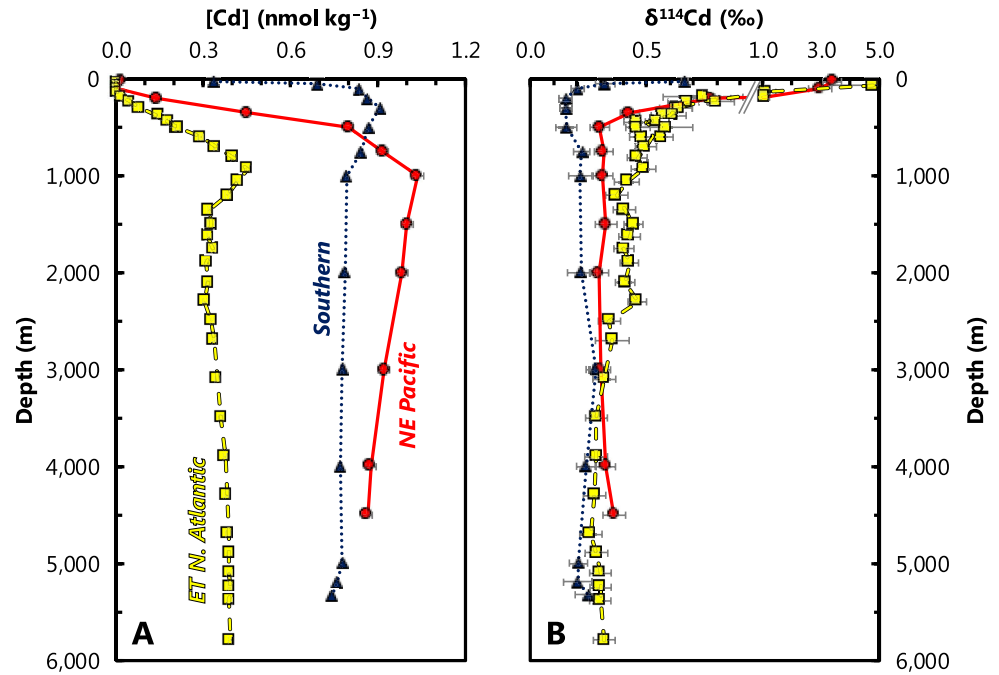


Figure 15. Representative profiles of dissolved Cd concentrations ($[Cd]$); (a) and Cd isotope compositions ($\delta^{114}Cd$); (b). Data from the Eastern Tropical North Atlantic (squares, dashed line; Conway & John, 2015b), Northeast Pacific (circles, solid line; Conway & John, 2015a), and Southern Oceans (triangles, dotted line; Abouchami et al., 2014). Station locations as per Figure 1. Note the break in scale in $\delta^{114}Cd$ above 1‰, illustrating the extreme isotopic compositions observed in the most Cd-depleted surface samples. Notably, such extreme compositions are generally not observed in the similarly Cd-depleted surface waters of the Southern Hemisphere gyres (e.g., Gault-Ringold et al., 2012; George et al., 2019; Xie et al., 2017), nor in the surface of the high latitude Southern Ocean, where dissolved $[Cd]$ is elevated (e.g., Abouchami et al., 2011, 2014). This comparison illustrates that the processes leading to distinct dissolved concentration profiles effect only modest changes in dissolved $\delta^{114}Cd$ between basins.

Subsequent studies have corroborated this general one-dimensional pattern in the Southern (e.g., Abouchami et al., 2011, 2014; Sieber, Conway, de Souza, Hassler et al., 2019; Xue et al., 2013), Atlantic (e.g., Bryan et al., 2021; Conway & John, 2015a; Xie et al., 2017; Xie, Galer et al., 2019; Xue et al., 2012), Arctic (Zhang et al., 2019), and Pacific Oceans (Conway & John, 2015b; Janssen et al., 2017; John, Helgøe, & Townsend, 2018; Sieber, Conway, de Souza, Obata et al., 2019; Xie, Rehkämper et al., 2019; Yang et al., 2012, 2014, 2018). These studies have shown that the deep ocean (>500–1,000 m) is largely homogeneous in Cd isotope composition ($\delta^{114}Cd$ of +0.2‰ to +0.3‰; Figure 15). This deep water $\delta^{114}Cd$ value is heavier than the upper continental crust $\delta^{114}Cd$ composition of $\sim 0‰$ (Schmitt et al., 2009a), similar to that observed for other metals such as Zn, Ba, and Ni (Sections 3, 7, and 8). Intermediate-depth waters relating to water masses such as Antarctic Intermediate Water (AAIW) exhibit slightly heavier $\delta^{114}Cd$ values (+0.4‰ to +0.5‰), with waters above these typically exhibiting heavier isotopic compositions (up to $\sim +1‰$; Figure 15). As for $[Cd]$, these one-dimensional $\delta^{114}Cd$ profile shapes arise largely from the combination of Southern Ocean biological processes and lateral circulation of water masses, as well as some contribution from local surface uptake and regeneration (Abouchami et al., 2014; Sieber, Conway, de Souza, Hassler et al., 2019).

Although the first-order distributions of $[Cd]$ and $\delta^{114}Cd$ in surface waters are consistent with intense cycling by biological processes, when considering the global database of surface $\delta^{114}Cd$ data, this simple “nutrient-like” reactor scheme with a single fractionation factor breaks down. For example, while studies have reported $\delta^{114}Cd$ values of up to +5‰ in Cd-depleted surface waters of the Northern Hemisphere gyres (Conway & John, 2015a, 2015b; Ripperger et al., 2007; Xue et al., 2012), others have reported more muted fractionation or even a switch to lighter-than-deep-ocean compositions in surface waters (Gault-Ringold et al., 2012; George et al., 2019; Janssen et al., 2017; Sieber, Conway, de Souza, Obata et al., 2019; Xie et al., 2017; Xie, Galer et al., 2019; Xie, Rehkämper et al., 2019). This range of observations suggests that the

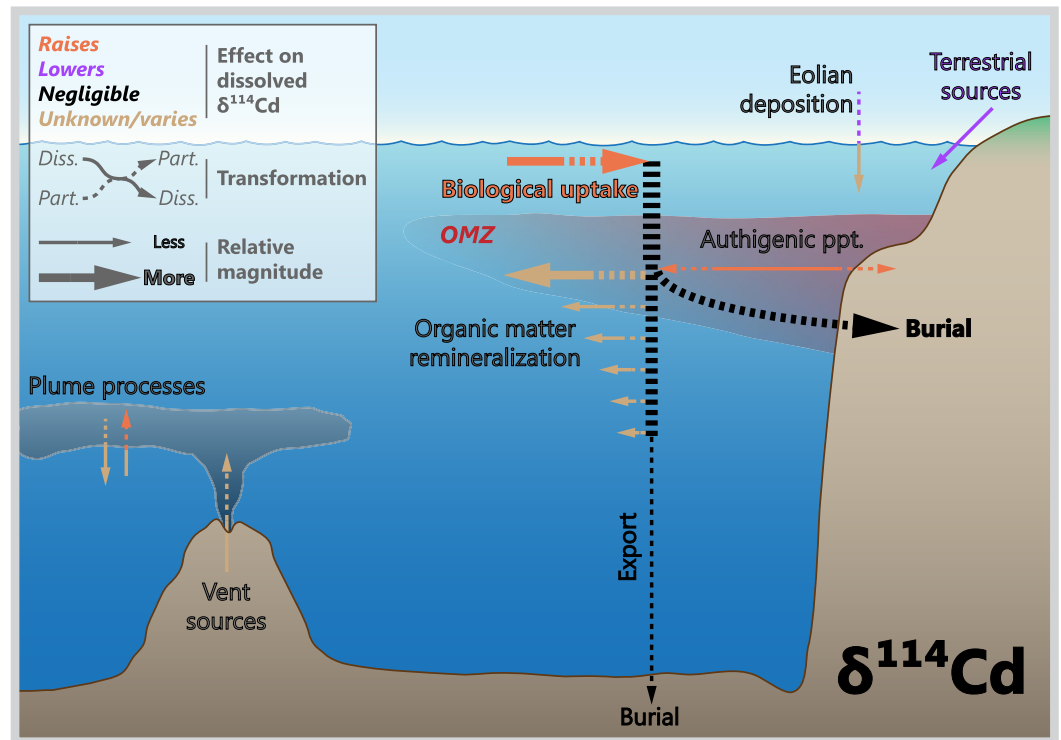


Figure 16. Processes driving Cd isotope variations in modern seawater. Biological processes exert a significant control on surface water Cd cycling, implying that $\delta^{114}\text{Cd}$ is broadly responsive to productivity. However, important redox-dependent processes remain to be fully elucidated, particularly those occurring around OMZs.

processes influencing surface Cd isotope compositions may be more complex than simple biological uptake (Figure 16). For example, interactions with ligands, effects arising from recycling of organic matter, differences in fractionation factor between different organisms, and supply of Cd from external Cd sources may all influence surface water dissolved $\delta^{114}\text{Cd}$. This raises three related questions to be addressed in the remainder of this section: What are the candidate biological processes that drive these patterns? How do other physical or chemical processes play a role in setting marine Cd distributions? Can Cd-based reconstructions of these processes be used to inform on past productivity? Further to these questions, are the extreme heavy $\delta^{114}\text{Cd}$ observed in Northern Hemisphere gyres, and so far only twice in the Southern hemisphere (Bryan et al., 2021; Sieber, Conway, de Souza, Obata et al., 2019), real, or analytical artifacts?

6.2. Driving Processes

6.2.1. Biological

As noted above, the nutrient-like distribution of [Cd] implies intense biological cycling in seawater, even though Cd is considered toxic (e.g., Waldron & Robinson, 2009). This dichotomy has inspired a significant body of research investigating the role that Cd plays in microbial physiology. These studies showed that Cd uptake by marine microbes exhibits three noteworthy dependencies. First, cellular Cd quotas are strongly positively correlated with the Cd content of their environment, both in culture (see compilation by Twining & Baines, 2013) and from oceanographic data (Middag et al., 2018). Second, microbial Cd uptake is diminished when the concentration of other divalent cations increases, particularly so for Fe, Mn, and Zn. Likewise, lower concentrations of these divalent cations cause increases in Cd uptake (e.g., Cullen et al., 2003; Sunda & Huntsman, 2000). Some diatoms have even shown capacity to substitute much of their metabolic Zn requirements with Cd (Price & Morel, 1990). Third, Cd uptake is also influenced by speciation of inorganic carbon, with low $p\text{CO}_2$ promoting higher cellular Cd quotas (e.g., Cullen et al., 1999; Cullen & Sherrell, 2005; de Baar et al., 2017). The connection between Cd and carbon speciation is particularly intriguing given the discovery of the ζ -class of carbonic anhydrase that can utilize Cd (or Zn) as the catalytic

metal (e.g., Lane et al., 2005; Xu et al., 2008). Despite these dependencies, however, the extent to which active physiological utilization of Cd controls global patterns of Cd uptake is unclear. For example, genes encoding the ζ -class of carbonic anhydrase were not found in green algae nor coccolithophores, and were similarly absent from many diatom species (Park et al., 2007). Thus, it is similarly plausible that some part of the biological Cd cycle is driven by organisms inadvertently removing Cd from seawater while attempting to source other metals (e.g., Boyle, 1988a; Horner et al., 2013), or that microbes require Cd to populate other Cd-centered metalloenzymes that await discovery.

The role of microbial physiology in mediating Cd isotope fractionation is also comparatively understudied. However, it does appear that biological fractionation of Cd isotopes is ubiquitous; fresh- (Lacan et al., 2006) and saltwater (John & Conway, 2014) green algae, incubations of unfiltered seawater (Xue et al., 2012), heterotrophic bacteria (Horner et al., 2013), and shallow marine particles (e.g., Yang et al., 2015; Janssen et al., 2019) all indicate that biological particles accumulate isotopically light Cd from their environment with a fractionation between -0.3% and -0.8% (Figure 16). The limited depth profile data of suspended particulates suggests subsequent partial respiration of already-light particulate organic matter also induces a second fractionation, further enriching light isotopes in the remnant particulate phase (Janssen et al., 2019). Additionally, the significant variability in surface water dissolved $\delta^{114}\text{Cd}$ at low [Cd]—ranging from extremely heavy compositions to deep-water like values—suggests that Cd isotope cycling is more complex than a single process removing isotopically light Cd into particulates, though our understanding of these complexities is limited.

6.2.2. Chemical

The role of chemical processes in mediating global Cd distributions is the most underconstrained of the three processes discussed in this review. Recent studies suggested that pelagic partitioning of Cd into sulfides in OMZs may constitute a significant loss term (Bianchi et al., 2018; Janssen et al., 2014; Plass et al., 2020). Moreover, the Cd isotope effect associated with sulfide precipitation identified by Guinoiseau et al. (2018) is consistent with field data, and particulate Cd is known to accumulate more rapidly in sediments that are bathed by bottom waters containing low $[\text{O}_2]$ (Figure 16; Section 5.3; e.g., van Geen et al., 1995). Collectively, these observations suggest a potential redox sensitivity in sedimentary Cd isotope distributions that deserves additional scrutiny. Indeed, the influence of sediments as the most important marine Cd sink can be seen in some water column profiles of $\delta^{114}\text{Cd}$ (Xie, Rehkämper et al., 2019). Similarly, data from the hydrothermal TAG site in the North Atlantic suggests that hydrothermal plumes may scavenge Cd from seawater, constituting a small sink of isotopically light Cd, though this does not have an observable effect on deep ocean $\delta^{114}\text{Cd}$ values outside of the plume itself (Figure 16; Conway & John, 2015b).

Other potential sources and sinks include rivers, atmospheric deposition, and sediments; however, none of these interfaces exhibit significant anomalies in [Cd] or $\delta^{114}\text{Cd}$ in GEOTRACES-era datasets. This finding is in accord with earlier research by Martin & Thomas (1994), though there exist two possible exceptions. The first concerns the role of atmospheric aerosols, which have been invoked to explain the Cd isotope composition of surface waters in the Southwest Pacific (e.g., George et al., 2019) and South China Sea (e.g., Yang et al., 2012). Modern aerosol inputs may be largely anthropogenic in origin. Anthropogenic forms of Cd exhibit a relatively narrow range of isotopic compositions that are typically—though not always (e.g., Shiel et al., 2010)—lighter than dust-derived Cd (e.g., Bridgestock et al., 2017). Second, interactions with organic ligands have also been invoked to explain the relatively muted pattern of Cd isotope fractionation in the surface of the south Atlantic Ocean (e.g., Guinoiseau et al., 2018; Xie et al., 2017), but there are as yet no corroborating field or experimental data examining the role of organic ligands in mediating Cd isotope fractionation in seawater.

6.2.3. Physical

Physical processes are similarly influential in mediating the global distribution of [Cd] and $\delta^{114}\text{Cd}$ throughout the global oceans, particularly those processes occurring in the Southern Ocean. Antarctic Intermediate and Bottom Waters possess higher [Cd]: $[\text{PO}_4^{3-}]$ than North Atlantic Deep Water (e.g., de Baar et al., 1994; Middag et al., 2018). Mixing between these southern- and northern-sourced water masses likely contributes to the well-known “kink” in the [Cd]: $[\text{PO}_4^{3-}]$ relationship (e.g., Elderfield & Rickaby, 2000; Frew & Hunter, 1992; Quay & Wu, 2015). Why northern- and southern-sourced intermediate and deep waters possess

different $[\text{Cd}]:[\text{PO}_4^{3-}]$ is debated, and likely reflects regionally distinct fractionation of Cd and P during biological uptake (e.g., Cullen et al., 2003; Sunda & Huntsman, 2000) and during remineralization (e.g., Baars et al., 2014; Roshan & Wu, 2015b). In the Atlantic, however, the importance of remineralization to deep water Cd budgets is of secondary significance: The ratio of regenerated-to-preformed $[\text{Cd}]$ is $\sim 30\%$ in the mesopelagic, and generally $<10\%$ in the deep ocean (Roshan & Wu, 2015b; Middag et al., 2018). Given the low proportion of regenerated Cd in the deep Atlantic, the ratio of $[\text{Cd}]:[\text{PO}_4^{3-}]$ and the overall distribution of $[\text{Cd}]$ are essentially governed by the $[\text{Cd}]:[\text{PO}_4^{3-}]$ of the source waters (Middag et al., 2018) and the prevailing geometry of ocean circulation, respectively (Boyle, 1988a).

Recent Cd isotope data from the South Atlantic (Xie et al., 2017), South Pacific (George et al., 2019; Sieber, Conway, de Souza, Obata et al., 2019), and Arctic (Zhang et al., 2019) also support the importance of mixing in mediating deep ocean $[\text{Cd}]$ and $\delta^{114}\text{Cd}$ distributions, though it should be noted that the isotopic contrast between mixing endmembers is small, relative to measurement precision (Figure 15; e.g., Janssen et al., 2017). For example, biological uptake of light Cd in the source regions of intermediate waters in the surface Southern Ocean results in isotopically heavy preformed $\delta^{114}\text{Cd}$ signatures being imparted to Cd-depleted intermediate water masses (e.g., $+0.45\%$ in AAIW; $+0.65\%$ in Subantarctic Mode Water, SAMW; Abouchami et al., 2014; Sieber, Conway, de Souza, Hassler et al., 2019; Xue et al., 2013). Lateral circulation of these southern-sourced water masses then transfers this signature northward to intermediate depths in the Atlantic and Pacific Oceans (e.g., Abouchami et al., 2014; Conway & John, 2015a; Sieber, Conway, de Souza, Obata et al., 2019; Xue et al., 2012). This effect is more pronounced in the North Atlantic than in the Pacific, where southward flowing NADW also carries isotopically heavy Cd southward at depths of 1,000–3,000 m (Figure 15; Conway & John, 2015a; Xue et al., 2012).

6.3. Marine Archives

6.3.1. Carbonates

There is a long history of the measurement of Cd contents of marine carbonates, particularly corals and foraminifera, most commonly reported as Cd:Ca molar ratios. In principle, carbonates are an appealing archive of ambient Cd chemistry since inorganic partition coefficients are $\gg 1$ (e.g., Tesoriero & Pankow, 1996) and the Cd:Ca of many types of carbonate exhibit a strong proportionality with ambient $[\text{Cd}]$. In practice, however, most biogenic carbonates exhibit partition coefficients closer to unity (Boyle, 1988a), and resultant Cd:Ca is also sensitive to the species (Boyle, 1992) and temperature of calcification (e.g., Rickaby & Elderfield, 1999). As such, Cd:Ca in carbonates has found the most utility where ambient $[\text{Cd}]$ —and attendant carbonate Cd:Ca—exceeds several 100 pmol kg^{-1} , such as in tracing industrial fallout (e.g., Shen et al., 1987) or in studies of Quaternary deep ocean circulation (e.g., Adkins et al., 1998; Boyle & Keigwin, 1985; Farmer et al., 2019; van Geen et al., 1992).

There are far fewer studies examining the Cd isotope composition of marine carbonates as tracers of historical Cd isotope chemistry. Inorganic partitioning experiments indicate that Cd isotopes are fractionated during incorporation into calcite by $\approx -0.5\%$ (Horner et al., 2011). The isotopic effect is temperature- and Mg-independent, but vanishes at low salinity. This inorganic calibration has been used to interpret patterns of Cd isotope fractionation preserved in bulk carbonates from the Neoproterozoic Eon (1,000–541 Ma). The variations in these sediments are interpreted as evidencing changes in biological productivity (e.g., Hohl et al., 2017) and Cd sinks through time (e.g., John et al., 2017). Applications of Cd isotopes to foraminifera to study problems in Quaternary paleoceanography are precluded by the large sample requirements; obtaining $\sim 1 \text{ ng}$ of Cd—the minimum quantity typically needed for a reasonably precise Cd isotope measurement (Ripperger & Rehkämper, 2007; Schmitt et al., 2009b)—requires picking and cleaning of 10s of mg of foraminiferal tests. Alleviation of such limitations awaits development of automated picking and screening systems (e.g., Mitra et al., 2019), or vast improvements in ion transmission efficiency for isotope ratio mass spectrometry.

6.3.2. Ferromanganese Sediments

Ferromanganese sediments have shown the most promise for recording deep ocean Cd isotope chemistry. Both ferromanganese nodules (Schmitt et al., 2009a) and crusts (Horner et al., 2010) reflect ambient seawater Cd isotope compositions with negligible fractionation (Figure 17a), consistent with Cd-Mn-oxyhydroxide

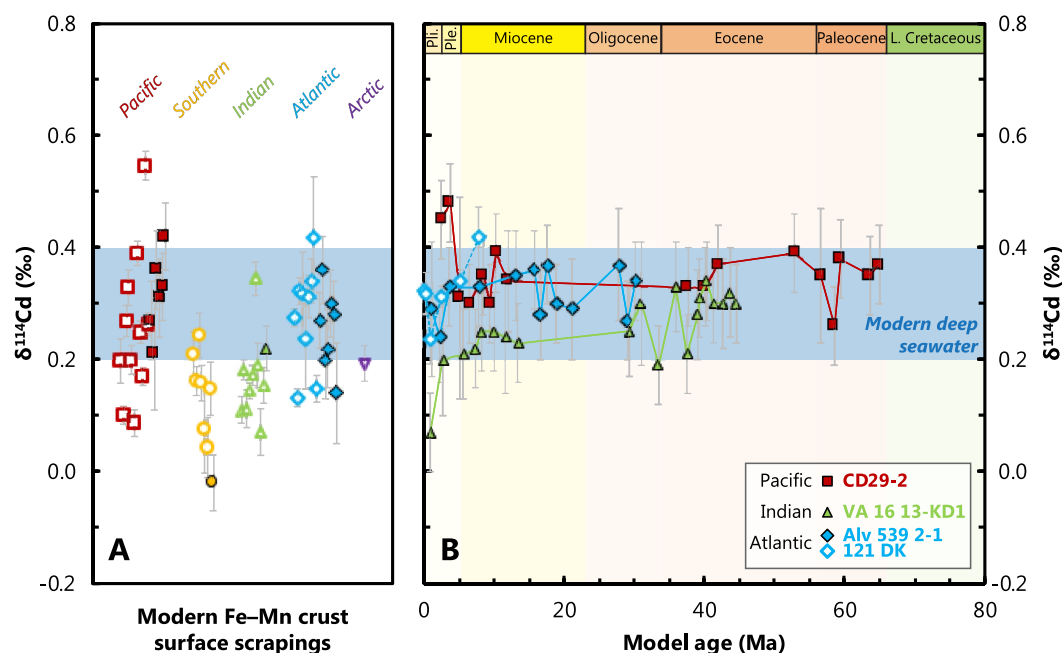


Figure 17. Ferromanganese crusts records of deep-water $\delta^{114}\text{Cd}$. (a) Compilation of “coretop” Fe–Mn crust $\delta^{114}\text{Cd}$; data from Schmitt et al. (2009a; open symbols) and Horner et al. (2010; closed symbols). In general, Southern Ocean samples exhibit lighter $\delta^{114}\text{Cd}$ than other basins, consistent with profiles of $\delta^{114}\text{Cd}$ (e.g., Figure 15). (b) Cenozoic records of deep-water $\delta^{114}\text{Cd}$ recovered from four Fe–Mn crusts; data from Murphy, 2016 (closed symbols) and Schmitt et al. (2009a; open symbols). These records have been plotted using the authors’ preferred age models, meaning that there are some differences between the chronology of CD29-2 shown here compared to Figure 8. Such differences may be immaterial however, given that Cd isotopes in Fe–Mn crusts are potentially subject to diffusive “resetting” over time (Murphy, 2016).

partitioning experiments conducted at high ionic strength that show only minor Cd isotope fractionation (Wasylenki et al., 2014). Horner et al. (2010) estimated that Cd is somewhat mobile in Fe–Mn crusts, with a predicted diffusivity $\leq 10^{-7} \text{ cm}^2 \text{ yr}^{-1}$, similar to Hf (Henderson & Burton), Mo (Section 7.3), Cr (Section 10.3.2), and Ag (Section 11.3). This rate implies that long-term records of $\delta^{114}\text{Cd}$ derived from Fe–Mn crusts are likely to exhibit some diffusive smoothing while preserving larger perturbations. As with Zn and Cu isotopes however, time-resolved records of $\delta^{114}\text{Cd}$ recovered from Fe–Mn crusts indicate minimal variation over the last 20–60 Myr (Figure 17b). The lack of variation may indicate that the sources and sinks of Cd have been in isotopic steady state throughout the Cenozoic. Alternatively, the lack of variation in $\delta^{114}\text{Cd}$ over the Cenozoic may simply reflect a “resetting” of all crust layers toward modern deep ocean Cd isotope compositions, as suggested by Murphy (2016).

6.3.3. Organic-Rich Sediments

Organic-rich sediments are the principal sink of dissolved Cd from the modern oceans (e.g., Little et al., 2015; Rosenthal et al., 1995; van Geen et al., 1995). A significant fraction of the total Cd in organic-rich sediments is derived from sinking organic matter. Accordingly, the Cd content of organic-rich sediments or of multiple paired sedimentary phases has been applied as a proxy for past productivity (e.g., Brumsack, 2006; Hohl et al., 2019). However, there is also a redox sensitivity: Cd contents are generally elevated in organic-rich sediments that are bathed by low $[\text{O}_2]$ waters (Figure 18). This enrichment likely derives from three processes. First, low $[\text{O}_2]$ environments may limit oxidation—and thus favor preservation—of settling Cd sulfide particles formed in the water column. Second, the chalcophile nature of Cd means that even trace levels of hydrogen sulfide may cause Cd to precipitate into sulfides. Thus, as organic matter is remineralized within the sediment column, any Cd liberated to porewaters is proportionally more likely to reprecipitate into sulfide minerals, relative to harder metals (and carbon), effectively “trapping” remineralized Cd in sediments (e.g., Rosenthal et al., 1995). Third, recent evidence suggests that Cd may also directly precipitate from seawater and into sediments when plumes of hydrogen sulfide interact with bottom waters (e.g., Plass

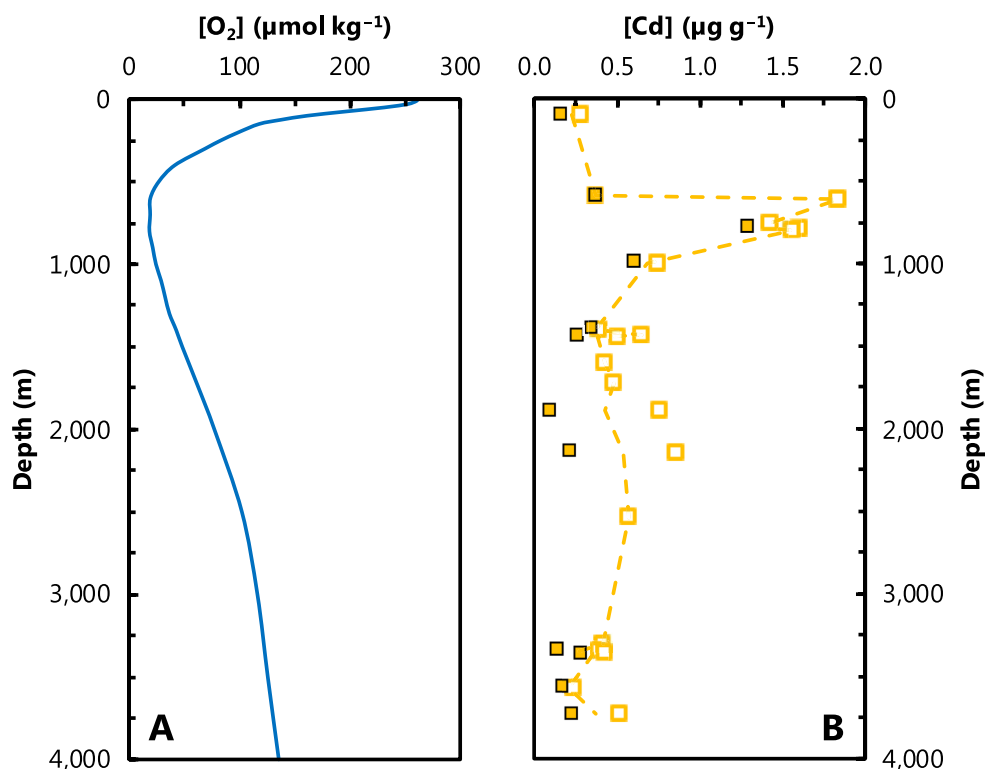


Figure 18. Cadmium concentrations in California Margin sediments. (a) Regionally representative $[O_2]$ profile from the Northeast Pacific showing broad minimum between 600–800 m. Profile from 35.5°N, 122.5°W (from World Ocean Atlas; Garcia et al., 2014). (b) Solid phase Cd concentration data from van Geen et al. (1995) for Northeast Pacific coretop (closed symbols) and “slightly deeper” (8–10 cm; open symbols) sediment samples; dashed line indicates arithmetic mean. These samples evidence a maximum in authigenic Cd deposition at the top of the oxygen minimum zone (OMZ), which may originate from processes occurring in the water or sediment column.

et al., 2020; Xie, Rehkämper et al., 2019). The relative importance of these three processes to the O_2 -dependent pattern of Cd accumulation remains to be fully elucidated.

While the contribution of organic-rich sediments to the isotopic mass balance of Cd is presently limited, their significance to the marine Cd budget suggests that, globally, the Cd isotope composition of these sediments should balance the riverine flux $\delta^{114}Cd \approx +0.1 \pm 0.1\%$ (Lambelet et al., 2013). Recent data from organic-rich sediments (Chen et al., 2021), suboxic sediments (Bryan et al., 2021), and intermediate-depth biogenic particles (Janssen et al., 2019) generally support this view, and that low $[O_2]$ settings may help to close the isotope mass balance of Cd. Alternatively, the other minor sinks of Cd—carbonates, ferromanganese oxides, clays—must possess large isotopic offsets relative to seawater, which seems unlikely given existing field and experimental data. Obtaining further calibrations of Cd isotope partitioning into recent organic-rich sediments should be considered a priority.

6.4. Prospects

The overview provided above indicates that Cd participates in marine biological processes and that its distribution is sensitive to the biological productivity of the oceans. How this sensitivity is transcribed into marine sediments remains uncertain, however. There are several additional processes that have the potential to render isotope effects that require further exploration before Cd isotopes can be solely interpreted as a productivity proxy, such as: Biological fractionation effects, authigenic transformations, and redox sensitivities. Relatedly, the fidelity of many types of marine sediment to record ambient Cd isotope chemistry remain inadequately constrained. With these two themes in mind, we suggest several areas for additional

research that may help to address the overarching question as to whether Cd isotope-based reconstructions can be used to inform on past ocean productivity.

6.4.1. Modern

Several questions persist regarding the modern Cd isotope cycle. We list five of the most pressing below and offer possible remedies to each. First, are the “extreme” (i.e., $\delta^{114}\text{Cd}$ of + 5‰; Figure 15) values seen in surface waters of the Northern Hemisphere gyres real? That is, are these heavy compositions true oceanographic features that are generally absent from the Southern Hemisphere, or do they represent analytical artifacts unique to MC-ICP-MS? This question remains to be answered, and will require measurement of the same low [Cd] surface samples by multiple MC-ICP-MS and MC-TIMS groups. To date, this exercise has proven difficult because of the difficulty of collecting surface low [Cd] seawater (where heavy $\delta^{114}\text{Cd}$ has been reported by MC-ICP-MS) in sufficient quantities to permit analysis by multiple groups.

Second, to what extent do local Cd isotope compositions in surface waters reflect larger-scale processes versus local features? While available data consistently show biological Cd uptake removes isotopically light Cd, not all surface waters show the expected progressive increase in $\delta^{114}\text{Cd}$ with decreasing [Cd]. Addressing this issue will require elucidating the role of external sources (e.g., dust, margin sediments), organismal uptake, ligands, and mixing, which would benefit from conducting additional experimentation with plankton, coupling of isotope methods with electrochemistry, and numerical modeling, respectively.

Third, is there a “Redfield” stoichiometry for Cd in organic matter? If so, what controls it? Existing culture (Ho et al., 2003) and field (Ohnemus et al., 2017) data suggest a wide range of cellular Cd:P, which have been suggested as reflecting species and local supply ratios, respectively (in addition to the aforementioned feedback interactions). Further experimentation with model organisms is needed.

Fourth, it is unclear if cells must possess a true physiological use for Cd in order to contribute to Cd isotope fractionation in seawater. The uptake of Cd into cells is widespread, whereas the genes encoding the ζ -class of carbonic anhydrases are not. The importance of this enzyme to Cd geochemistry could be tested by characterizing the Cd isotope composition of organisms that are known to produce Cd-containing carbonic anhydrases and comparing against those that cannot. Such experiments may also benefit from use of mutant cell lines with targeted knockouts or by culturing phytoplankton in the presence of carbonic anhydrase inhibitors.

Last, how are the light Cd isotope compositions seen in suspended biogenic particles above OMZs related to those within OMZ layers and to those putatively accumulating in sediments? Does biogenic particulate Cd reach sediments? Do particulate Cd isotope signatures within OMZ particles relate to sulfide precipitation and what is their influence on the global mass balance? What controls the Cd isotope composition of these particles? Addressing these questions will require examining the Cd isotope composition of particles from oxygenated oceanographic regions, identifying whether processes associated with particle regeneration affect Cd isotope compositions, and surveying core-top sediments.

6.4.2. Paleo

As with the modern cycle, several ambiguities persist, though the most pressing relates to archives. Indeed, it appears that a major obstacle preventing the widespread application of Cd isotope-based proxies in paleo-oceanography has been the lack of suitable archives. Concerning carbonates, the main difficulty is isolation of sufficient quantities of foraminiferal-bound Cd to reconstruct past seawater $\delta^{114}\text{Cd}$. This difficulty might be solved by first testing whether species matters for reconstructing $\delta^{114}\text{Cd}$, or whether mixed foraminiferal assemblages can be used. For organic-rich sediments, the role of biology itself must be considered. That is, how important might it be that different organisms exhibit different magnitudes of Cd isotope fractionation (and Cd:C stoichiometry)? If important, how best to interpret Cd isotope records—species, evolutionary innovations, productivity?

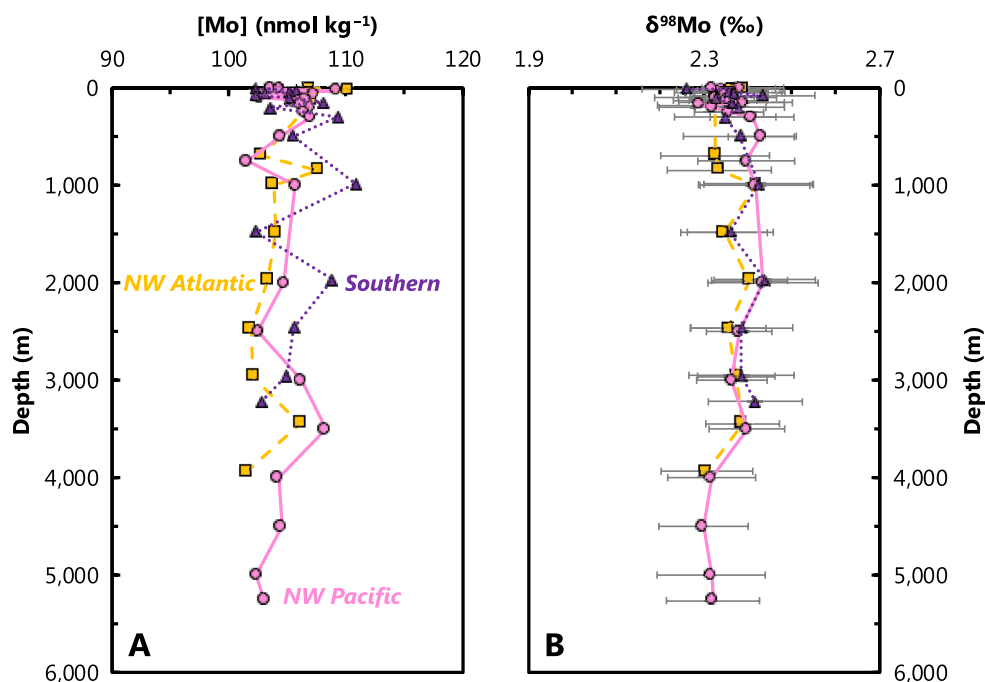


Figure 19. Representative profiles of dissolved Mo concentrations ($[Mo]$); (a) and Mo isotope compositions ($\delta^{98}Mo$); (b). Data from the Northwest Atlantic (squares, dashed line), Southern (triangles, dotted line), and Northwest Pacific Oceans (circles, solid line; all data from Nakagawa et al., 2012). Station locations as per Figure 1. This comparison illustrates that the dissolved behavior of Mo is essentially invariant throughout the global oceans.

7. Molybdenum

Molybdenum is a cofactor in several key enzymes in the nitrogen cycle, and Mo availability in the ancient oceans may have helped shape the Precambrian biosphere (e.g., Anbar & Knoll, 2002). Today, Mo is the scarcest of the essential trace metals in phytoplankton (Equation 3), but is one of the most abundant transition metals in the ocean (Collier, 1985; Morris, 1975; Bruland, 1983). Indeed, Mo possesses a long residence time ($\sim 440,000$ yr; Miller et al., 2011; Table 1), is conservative with respect to salinity, and exhibits a uniform isotopic composition in oxygenated seawater (e.g., Barling et al., 2001; Siebert et al., 2003; Figure 19). Given the lack of $[Mo]$ and $\delta^{98}Mo$ variability in the modern ocean, the isotope reactor framework outlined in Section 2.2 cannot be applied to Mo and thus there is no simple way to link $\delta^{98}Mo$ with paleoproductivity. Despite this, Mo is a widely used tracer of paleoredox conditions, and emerging fossil-specific measurements of $\delta^{98}Mo$ provide a promising future means to reconstruct high-resolution records of ocean oxygenation.

7.1. Marine Distribution

Based on 168 seawater samples from the Atlantic, Pacific, and Southern Oceans analyzed by Nakagawa et al. (2012), the average salinity-normalized $[Mo]$ and $\delta^{98}Mo$ of the ocean are 107 ± 6 nmol kg $^{-1}$ and $+2.36 \pm 0.10$ ‰, respectively (both values ± 2 SD; Figure 19).

Given that no significant gradients in $[Mo]$ are expected, there are few new open ocean $\delta^{98}Mo$ data measured as part of GEOTRACES. However, $[Mo]$ has been measured on two GEOTRACES transects (GP16 and GA02), demonstrating four intriguing instances where $[Mo]$ deviated from an otherwise conservative distribution. These instances are briefly described below and covered in detail by Ho et al. (2018). First, the most significant $[Mo]$ anomalies ($\sim 5\%$ drawdown) are associated with intense scavenging by particulate Fe hydroxides and oxyhydroxides close to the Peruvian OMZ. Second, Mo is slightly drawn down ($< 5\%$) in some samples directly above the East Pacific Rise hydrothermal ridge crest, again mostly likely driven by scavenging onto hydrothermally derived Fe–Mn oxides. Some Mo drawdown is also observed in some far-field hydrothermal samples, though the mechanism is unclear. Third, following normalization to a salinity

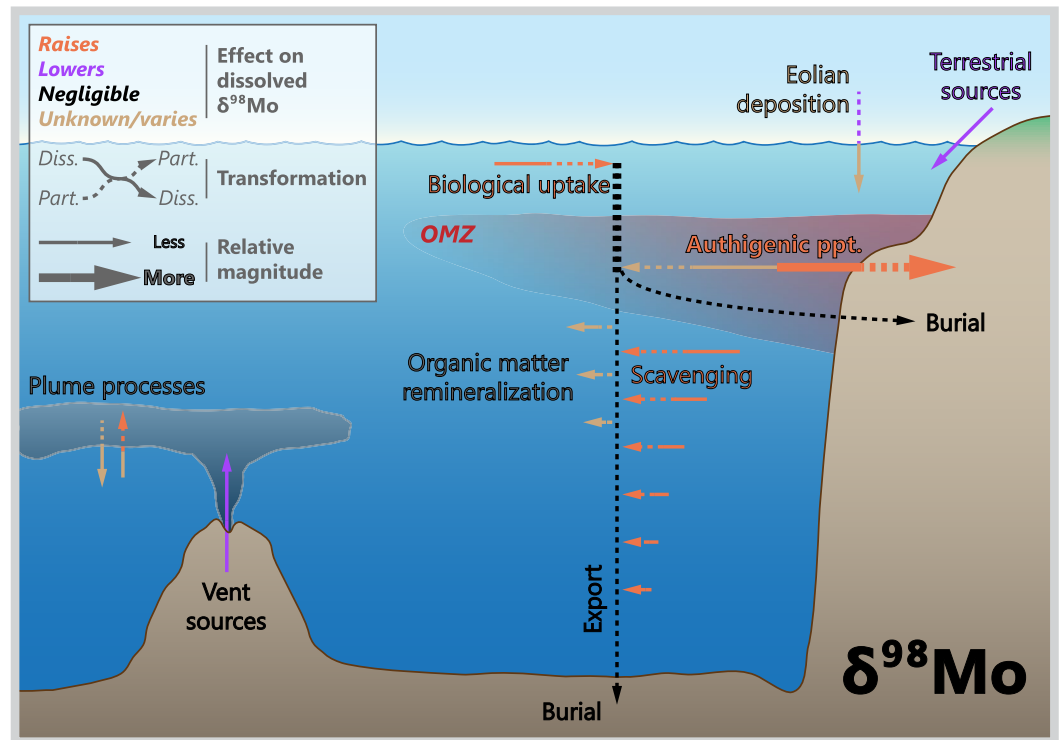


Figure 20. Processes driving Mo isotope variations in modern seawater. While biological processes may exert a slight influence on surface water Mo distributions, the main drivers of marine Mo cycling are related to the balance between scavenging pathways, which are redox dependent.

of 35, surface seawater shows a minor Mo drawdown, implying either biological uptake or adsorption to biotic particles. Though not a true oceanographic feature, a fourth type of [Mo] anomaly is also noteworthy: Bottle storage artifacts. Ho et al. (2018) found that many samples with initially low values showed an increase in [Mo] with increasing storage time, implying a change in Mo speciation to a form that is detectable by ICP-MS. In contrast to the relative constancy of [Mo] in open ocean settings, a number of studies show striking [Mo] variations in coastal and estuarine systems (e.g., Dalai et al., 2005; Dellwig et al., 2007; Joung & Shiller, 2016; Wang et al., 2016) as well as in modern restricted settings, such as the Black and Baltic Seas (Nägler et al., 2011).

7.2. Driving Processes

7.2.1. Biological

Molybdenum is an essential micronutrient required by enzymes that catalyze key reactions in the global C, N, and S cycles (Mendel & Bittner, 2006). Importantly, Mo is a cofactor of the primary nitrogenase enzyme complex, meaning that Mo is required for energy-efficient nitrogen fixation. Additionally, Mo is required for over 30 other enzymes that control biologically essential redox processes (Kendall et al., 2017). Despite its biological importance, biological activity does not significantly influence the distribution of Mo in seawater (Figure 20). Results from the GEOTRACES GP16 section do, however, suggest some Mo removal by biological uptake and/or adsorption onto biogenic particles within regions of elevated chlorophyll (Ho et al., 2018). Experimental data indicate that biological uptake of Mo imparts a small negative isotope fractionation on the order of -0.3‰ (Wasylenki et al., 2007; Figure 20).

Enhanced removal of Mo from seawater in regions with high export of organic carbon likely explains some of the nonconservative behavior observed in modern coastal regions. A significant relationship between Mo and total organic carbon content is observed in marine euxinic sediments (e.g., Algeo & Lyons, 2006; Helz et al., 1996; Lyons et al., 2009; McManus et al., 2006), though this appears to be more a function of

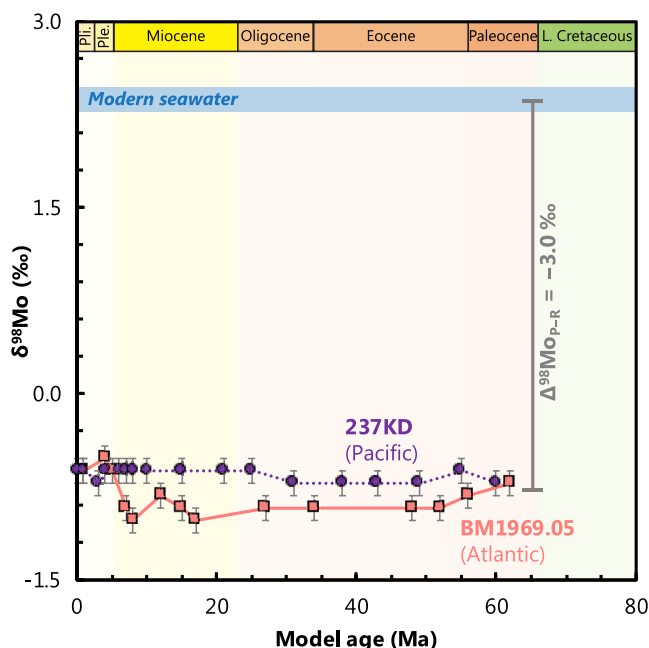


Figure 21. Two Fe–Mn records of $\delta^{98}\text{Mo}$ spanning the Cenozoic. Data from the Atlantic (squares, solid line) and Pacific Oceans (circles, dotted line; Siebert et al., 2003). Assuming that these Fe–Mn crusts have always formed with an offset $\approx -3.0\%$ with respect to dissolved Mo in seawater, these records indicate that the $\delta^{98}\text{Mo}$ of seawater has minimally varied over the Cenozoic (Anbar, 2004; Siebert et al., 2003). However, given the effective diffusivity of Mo in Fe–Mn crusts, it is possible that the lack of variation may also reflect post-depositional resetting to modern-like values.

euxinia rather than organic C burial. Furthermore, it has been shown that Mo interactions with organic matter can control Mo cycling in both soils (King et al., 2014, 2016; Marks et al., 2015; Siebert et al., 2015; Wichard et al., 2009) and marine sediments (Tessin et al., 2019; Wagner et al., 2017). The formation of Mo complexes containing organic ligands has been proposed as an explanation for the correlation between sedimentary Mo and organic carbon, suggesting that organic matter may play an important role in both the delivery and burial of Mo in sediments (Wagner et al., 2017).

7.2.2. Chemical

Due to the long residence time and abundance of Mo, nonconservative Mo behavior is typically localized to areas with high particle concentrations, such as close to the continental margin, in the euphotic ocean, or around hydrothermal vents (e.g., Goto et al., 2020). In the modern oxic water column, Mo is present primarily as the oxyanion molybdate (MoO_4^{2-}) and Mo sorption onto Mn oxyhydroxides represents the most significant modern Mo sink (Figure 20; Bertine & Turekian, 1973; Scott & Lyons, 2012). Since the Fe–Mn oxide sink preferentially removes Mo from seawater with an isotopic effect of $\approx -3.0\%$ (Barling et al., 2001; Siebert et al., 2003; Figure 21), the fraction of Mo that is buried in Fe–Mn oxides exerts a major control over the Mo isotope composition of seawater.

In the presence of sulfide, the oxygen atoms in molybdate are progressively substituted for sulfur, producing particle reactive thiomolybdate species ($\text{MoO}_{4-x}\text{S}_x^{2-}$; Erickson & Helz, 2000; Vorlicek et al., 2015). Dissolved Mo can thus be strongly drawn down in sulfidic environments, such as the Black Sea. Importantly, this drawdown occurs with a small, but non-zero isotope effect of $\approx -0.5 \pm 0.3\%$ (i.e., isotopically light Mo is preferentially scavenged; e.g., Nägler et al., 2011). Thiomolybdate may also be scavenged from sulfidic sedimentary porewaters leading to sig-

nificant Mo accumulations within sediments deposited in anoxic and euxinic environments (e.g., Crusius et al., 1996; Emerson & Husted, 1991; Scott & Lyons, 2012). Long-term Mo burial is associated with Fe–S minerals (Chappaz et al., 2014; Vorlicek et al., 2018) and/or organic matter (Dahl et al., 2017; Tessin et al., 2019), depending on the biogeochemical conditions prevailing within a given basin.

7.2.3. Physical

The residence time of dissolved Mo is significantly longer than the mixing time of the ocean (Table 1). Thus, variations in [Mo] and dissolved $\delta^{98}\text{Mo}$ are not influenced by the geometry of modern overturning circulation. Whole ocean changes in [Mo] and dissolved $\delta^{98}\text{Mo}$ are, however, possible, and much of what we know about such changes is gleaned from studies of the geological past, particularly during periods of ocean anoxia. Based on this research, it has been suggested that during intervals of lower ocean oxygenation, the ocean Mo inventory may have been low enough to limit marine primary productivity (Algeo, 2004; Anbar & Knoll, 2002; Glass et al., 2009; Reinhard et al., 2013). This limitation has been demonstrated in certain lake ecosystems (Glass et al., 2012; Goldman, 1960). Under strongly euxinic conditions ($[\text{H}_2\text{S}]_{\text{aq}} > 11 \mu\text{M}$), thermodynamic calculations predict that tetrathiomolybdate (MoS_4^{2-}) becomes the predominant Mo species (Erickson and Helz, 2000). The transformation can result in quantitative drawdown of Mo from seawater and into sediments with negligible net isotope fractionation, a mechanism that has been evidenced in Lake Cadagno (Dahl et al., 2010), the Black Sea (e.g., Nägler et al., 2011; Neubert et al., 2008), and Kyllaren fjord (a seasonally anoxic basin off of the west coast of Norway; Noordmann et al., 2015). Indeed, the quantitative drawdown mechanism is the foundation of several paleoceanographic studies that assume that the sedimentary Mo isotopic signatures, deposited in euxinic settings, faithfully capture the $\delta^{98}\text{Mo}$ of oxygenated (surface) seawater and can be further interpreted in terms of the fraction of the seafloor that is oxygenated (e.g., Dickson, 2017; Kendall et al., 2015).

7.3. Sedimentary Archives

The majority of Mo paleoceanographic studies focus on the measurement of the Mo content and isotopic composition of bulk sediments, spanning early Earth (e.g., Arnold et al., 2004) to the Holocene (e.g., Hardisty et al., 2016; van Helmond et al., 2018). However, the vast majority of these studies applied Mo and its isotopes to trace ocean redox conditions rather than productivity (e.g., Anbar, 2004; Kendall et al., 2017). Similar to the other elements reviewed here, there are measurements of $\delta^{98}\text{Mo}$ in Fe–Mn sediments (e.g., Barling et al., 2001). Siebert et al. (2003) reported a time series from two Fe–Mn crusts implying no variations in the $\delta^{98}\text{Mo}$ of seawater, relative to modern values, over the Cenozoic (Figure 21). Molybdenum is somewhat mobile in Fe–Mn crusts, with a calculated effective diffusivity $\leq 10^{-7} \text{ cm}^2 \text{ yr}^{-1}$ (see Henderson & Burton, 1999 for calculation details), similar to Cd (Section 6.3.2), Cr (Section 10.3.2), and Ag (Section 11.3). Thus, the invariance of the Fe–Mn crust $\delta^{98}\text{Mo}$ record may imply that the relative balance of Mo sinks has not shifted by more than 10% over the Cenozoic (e.g., Anbar, 2004; Siebert et al., 2003), or could reflect some degree of post-depositional resetting.

Despite the ambiguity surrounding Fe–Mn sediments, research on biological archives of [Mo] and $\delta^{98}\text{Mo}$ has found mixed results. Research examining $\delta^{98}\text{Mo}$ in corals indicates that corals may accurately record ambient seawater Mo isotopic composition (Voegelin et al., 2009). However, later studies suggested a temperature-dependent fractionation between seawater and corals that is related to the activity of symbiotic zooxanthellae (Z. Wang et al., 2019). Moreover, bivalve shell Mo:Ca ratios have been determined to have no relationship to oceanographic conditions (Vihtakari et al., 2017), whereas Tabouret et al. (2012) suggest a mechanism related to trophic uptake, but not to ambient [Mo]. A third study proposed that Mo:Ca peaks in bivalve carbonate are controlled by ingestion of phytoplankton grown on NO_3^- (due to high Mo associated with NO_3^- reductase), indicating that bivalves may provide an archive for surface water NO_3^- uptake and a potential proxy for the balance between new and regenerated productivity (Thébault et al., 2009).

7.4. Prospects

At present, it does not appear that bulk sediment $\delta^{98}\text{Mo}$ will be useful for reconstructing biological productivity, even though Mo is cycled by organic matter, both actively (e.g., Liermann et al., 2005; Wasylenki et al., 2007) and passively (e.g., King et al., 2018; Kowalski et al., 2013). That we see no pathway to using Mo as a productivity tracer reflects, in part, the difficulty in disentangling biological processes that exert relatively modest Mo isotope fractionations from those associated with thiomolybdate transformations (Tosell, 2005), or scavenging processes that possess large fractionation effects (Figure 20; e.g., Mn- or Fe-oxide scavenging; Barling & Anbar, 2004; Brucker et al., 2009; Goldberg et al., 2009, 2012; Siebert et al., 2003; Wasylenki et al., 2008). Additionally, within the modern ocean and likely within the recent geologic past, the global ocean reservoir of Mo is too large and too well mixed for biological associated fractionations to significantly impact the global Mo isotopic composition.

The use of bulk sedimentary Mo concentrations as a proxy for export of organic carbon to the seafloor is more promising, but numerous caveats exist. Specifically, other mechanisms for enhanced delivery, sequestration, and burial complicate any efforts to quantitatively relate Mo enrichments to increased export productivity (e.g., Scholz et al., 2017). Redox conditions and, in particular, the presence of sulfide in the water column and sediment porewaters will be a primary control on Mo accumulation (e.g., Hardisty et al., 2018). Sedimentary Mo enrichments can also be produced through shuttling of Mo adsorbed to the surface of Fe and Mn oxides to the seafloor (Algeo & Lyons, 2006; Algeo & Tribovillard, 2009; Dellwig et al., 2010; Scholz et al., 2013). At a minimum, independent constraints on water column and porewater redox conditions using Fe speciation, other trace metals and/or fossil redox proxies are required before an argument can be made relating sedimentary Mo contents to export productivity. Additionally, the quantitative relationship between Mo and organic carbon may be impacted by aqueous [Mo], which may have varied over Earth's history, or if depositional environments become restricted (i.e., Mo drawdown leads to a lower Mo:TOC ratio; Algeo & Lyons, 2006). Alternatively, the utility of bulk sediment Mo content and isotopic composition may be in constraining redox conditions to improve the interpretation of other trace metal proxies that are more strongly controlled by primary and/or export productivity.

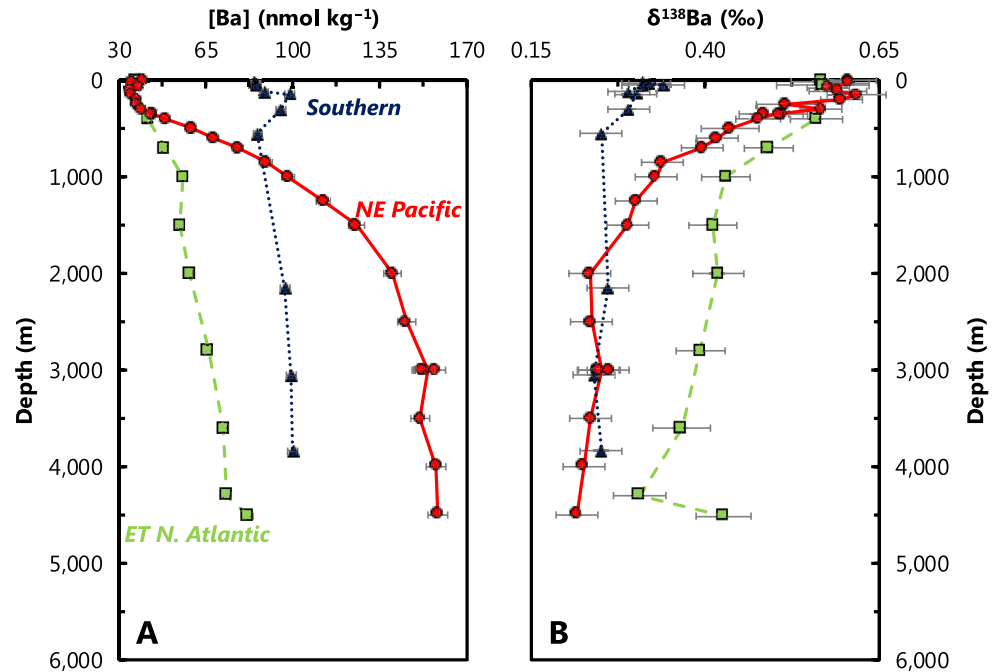


Figure 22. Representative profiles of dissolved Ba concentrations ($[Ba]$); (a) and Ba isotope compositions ($\delta^{138}Ba$); (b). Data from the Eastern Tropical North Atlantic (squares, dashed line; Bates et al., 2017), Northeast Pacific (circles, solid line; Geyman et al., 2019), and Southern Oceans (triangles, dotted lines; Hsieh & Henderson, 2017). Station locations as per Figure 1. This comparison illustrates that the oceanographic processes leading to distinct dissolved concentration profiles render significant changes in dissolved $\delta^{138}Ba$ between basins.

The most promising future avenue for Mo-based productivity proxies may emerge from fossil-specific measurements of Mo content, and perhaps $\delta^{98}Mo$. Currently, research has focused on large fossils (corals and bivalves; e.g., Thébault et al., 2009) and has led to mixed results on the utility of Mo in reconstructing productivity-related parameters. However, analytical progress may allow for measurement of smaller sample sizes, which may provide opportunities to explore new archives of past marine Mo geochemistry.

8. Barium

Like Zn, $[Ba]$ exhibits a strong correlation with $[Si]$ (e.g., Chan et al., 1977). Unlike Zn and Si however, Ba is not an essential nutrient and has no known enzymatic functions. The mechanisms underpinning the nutrient-like behavior of Ba instead relate to its cycling by the mineral $BaSO_4$ (barite), which is thought to precipitate during the microbial oxidation of sinking organic matter (e.g., Chow & Goldberg, 1960). Barite precipitation also drives a sizable, negative isotope fractionation of Ba stable isotopes (e.g., Von Allmen et al., 2010), consistent with the direction and magnitude of Ba isotope variations in seawater (e.g., Horner, Kinsley, & Nielsen, 2015). Though the connections between $[Ba]$ and productivity are thus not direct, patterns of Ba sedimentation are strongly correlated with those of export production (e.g., Eagle et al., 2003), and Ba stable isotope distributions are consistent with underlying variations in $BaSO_4$ cycling and ocean circulation (e.g., Horner & Crockford, 2021). As such, $[Ba]$ and dissolved $\delta^{138}Ba$ can be described using the reactor framework outlined in Section 2.2, and—despite some uncertainties outlined later in this section—represents a promising tool for tracing aspects of paleoproductivity.

8.1. Marine Distribution

The nutrient-like distribution of $[Ba]$ has been documented in the literature since the 1970s (e.g., Wolgemuth & Broecker, 1970; Figure 22). However, it was not until later in the decade that the GEOSECS Program fully revealed the three-dimensional marine distribution of $[Ba]$ (e.g., Chan et al., 1976, 1977). These geochemical ocean sections highlighted vertical, zonal, and meridional variations in $[Ba]$ related to

the major biogeochemical and hydrographic features of the ocean. In nutrient-depleted surface waters, [Ba] is lowest, between 35 and 45 nmol kg⁻¹. Nutrient-replete deep waters are enriched in Ba, though typically by no more than a factor of four above surface values. The spatial resolution of GEOSECS illustrated the importance of hydrography; [Ba] increases along the meridional overturning circulation from ≈50 nmol kg⁻¹ in deep waters of the North Atlantic, to ≈90 nmol kg⁻¹ in the Southern Ocean, up to ≈160 nmol kg⁻¹ in the deep Northeast Pacific (Figure 22; Chan et al., 1976, 1977).

Though it was long suspected that the major dissolved–particulate transformation of Ba was related to the mineral BaSO₄ (e.g., Chow & Goldberg, 1960; Turekian, 1968), this was not confirmed until the 1980s (e.g., Bishop, 1988; Dehairs et al., 1980). Barite crystals are now recognized as an ubiquitous component of marine particulate matter, with up to 10⁴ discrete, micron-sized crystals present per L of seawater (Dehairs et al., 1980). The distribution of particulate BaSO₄ is distinct from primary biogenic phases that exhibit ‘Martin-like’ distributions with maxima in the euphotic zone that subsequently decay along power-law trajectories (Martin et al., 1987). Instead, particulate Ba typically exhibits a minimum in the euphotic zone and the maximum slightly below, usually near the top of the mesopelagic (e.g., Ohnemus & Lam, 2015; Ohnemus et al., 2019). This distribution likely reflects the fact that neither Ba nor BaSO₄ are utilized for physiological processes by any of the major marine primary producers. Particulate Ba fluxes are nevertheless strongly correlated with export productivity in well-oxygenated environments (e.g., Bishop, 1988; Dymond & Collier, 1996; Dymond et al., 1992; Francois et al., 1995; McManus et al., 2002) and therefore sedimentary Ba content has been widely used as a proxy to reconstruct past changes in ocean export production (e.g., Francois et al., 1995; Paytan & Griffith, 2007 [and references therein]; Paytan et al., 1996; Costa et al., 2016; Winckler et al., 2016).

Recent studies of Ba stable isotope geochemistry have added a new dimension with which to study marine Ba cycling. Von Allmen et al. (2010) first reported that isotopically light Ba is preferentially incorporated into BaSO₄, with a particulate–dissolved Ba isotopic offset of ≈−0.3‰. The direction of this offset implies that residual solutions, such as seawater, should exhibit Ba isotopic compositions heavier than those of sedimented BaSO₄. This was corroborated for Atlantic seawater by Horner, Kinsley, and Nielsen (2015), showing that dissolved δ¹³⁸Ba displays a mirror image of [Ba]: Ba-depleted surface water masses exhibited “heavy” Ba isotopic compositions (≈+0.6‰), whereas Ba-replete deep waters possessed “lighter” values ≈+0.3‰ (Notably, all values are considerably heavier than the upper continental crust, which possesses δ¹³⁸Ba ≈0.0 ± 0.1‰; Nan et al., 2018.) Similar patterns have since been corroborated in other ocean basins (Bates et al., 2017; Bridgestock et al., 2018; Cao, Siebert, et al., 2020; Geyman et al., 2019; Hsieh & Henderson, 2017; Figure 22). The first order pattern is thus consistent with the removal of isotopically light Ba from surface waters and its regeneration at depth. Further, the longer a water mass remains isolated from the surface, the more isotopically light Ba is able to accumulate, hence why Ba-replete Northeast Pacific seawater ~2,000 m depth exhibits the lightest dissolved δ¹³⁸Ba yet observed in the global ocean (≈+0.2‰; Geyman et al., 2019; Figure 22).

The isotopic studies have yielded a number of novel insights into the marine Ba cycle. First, the data underscore the importance of physical mixing (i.e., ocean circulation) in mediating patterns of dissolved δ¹³⁸Ba and, by extension, [Ba]. Second, both the regression of dissolved Ba isotopic data (Bates et al., 2017; Hsieh & Henderson, 2017) and comparison of colocated seawater and particulates (Cao, Li, et al., 2020; Horner et al., 2017) imply an average particulate–dissolved Ba isotopic offset ≈−0.5‰, which is somewhat larger than the experimental results reported by Von Allmen et al. (2010). Third, marine sediments—both bulk (Bridgestock et al., 2018) and BaSO₄ isolates (Crockford et al., 2019)—faithfully reflect the ≈−0.5‰ Ba isotopic offset from surface seawater. Consequently, the mean δ¹³⁸Ba of globally sedimented BaSO₄ is ≈+0.1 ± 0.1‰ (Crockford et al., 2019). Since BaSO₄ is the dominant oceanic output (e.g., Paytan & Kastner, 1996), these data imply that mean isotopic composition of Ba delivered to the ocean should possess an average composition ≈+0.1 ± 0.1‰ (Horner & Crockford, 2021). At present however, the main Ba inputs are unable to close the marine Ba isotopic budget: Rivers, the principal Ba source to seawater, are too heavy, exhibiting compositions generally ≥+0.2‰ (e.g., Cao, Siebert, et al., 2020; Gou et al., 2020); and, ground-water discharge, while possessing the necessary light composition of ≈+0.1 ± 0.1‰, is too small a Ba flux to balance the budget (Mayfield et al., 2021). Thus, either the marine Ba isotopic budget is currently out of

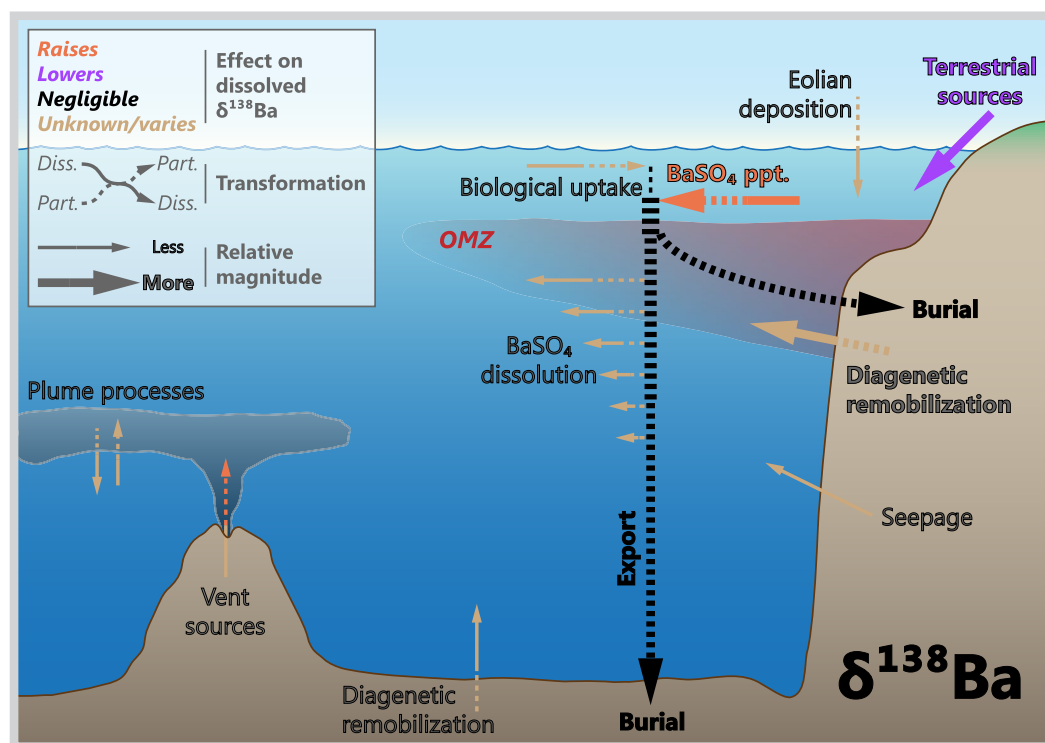


Figure 23. Processes driving Ba isotope variations in modern seawater. Though biological processes exert only a minor direct influence on $\delta^{138}\text{Ba}$, the biologically mediated cycling of BaSO_4 drives large variations in marine Ba isotope cycling, thereby connecting $\delta^{138}\text{Ba}$ to paleoproductivity.

steady state, or an additional Ba source possessing a light isotopic composition, such as estuaries (Bridge-stock et al., 2021), remains to be identified.

8.2. Driving Processes

Seawater is undersaturated with respect to BaSO_4 almost everywhere (Monnin et al., 1999; Rushdi et al., 2000). However, micro-crystalline BaSO_4 is ubiquitous in the ocean. This “barite paradox” remains an area of ongoing research. Proposed driving mechanisms broadly fall into two categories: “active” biological and “passive” chemical precipitation.

8.2.1. Biological

Several organisms are known to precipitate BaSO_4 intracellularly, possibly for the purposes of gravitropism (e.g., Gooday & Nott, 1982; Finlay et al., 1983). However, the organisms known to actively precipitate BaSO_4 are neither abundant in seawater, nor do they constitute a significant fraction of marine primary productivity. Likewise, acantharea—organisms that precipitate SrSO_4 (celestite) tests that can contain considerable quantities of Ba (e.g., Bernstein & Byrne, 2004)—are not necessary for driving significant Ba drawdown from the ocean (Esser & Volpe, 2002) nor for barite precipitation (Ganeshram et al., 2003). Thus, existing evidence does not support a significant role for active biological processes in driving the open marine Ba cycle (Figure 23).

8.2.2. Chemical

Passive chemical precipitation is likely the major contributor to particulate BaSO_4 stocks and sedimentation. We focus our discussion on those BaSO_4 formed through association with the biological pump, though we note that other types of BaSO_4 exist in the ocean and their occurrence and geochemistry are reviewed in detail elsewhere (e.g., Griffith & Paytan, 2012; Hanor, 2000). Given that seawater is largely undersaturated with respect to BaSO_4 , passive precipitation is thought to occur within particle-associated

microenvironments that are supersaturated with respect to BaSO_4 (e.g., Chow & Goldberg, 1960; Dehairs et al., 1987). The development of BaSO_4 -supersaturated microenvironments is hypothesized to relate to the heterotrophic oxidation of organic matter (Chow & Goldberg, 1960), whereby Ba and sulfate ions are concentrated in chemically isolated microzones during bacterially mediated mineralization of organic matter. Once sufficient quantities of Ba and sulfate ions have accumulated and the microenvironment becomes supersaturated, BaSO_4 precipitation occurs. Thus, passive precipitation of BaSO_4 is possible even in strongly undersaturated environments possessing low ambient sulfate concentrations (e.g., Horner et al., 2017). Continued mineralization destroys the microenvironment, ceasing precipitation and exposing BaSO_4 precipitates to undersaturated seawater where they begin to dissolve.

The widespread association between pelagic BaSO_4 and aggregates of decaying organic matter provides indirect support for this passive process (Dehairs et al., 1980; Bishop, 1988). Indeed, the peak in particulate [Ba]—and presumably BaSO_4 —abundance is found below the euphotic zone, where organic matter mineralization dominates (e.g., Sternberg et al., 2008). Though many of the microscale mechanisms remain unresolved, recent studies indicate that biofilms likely play an important role in accumulating Ba from seawater (e.g., Martinez-Ruiz et al., 2019, 2020), and can promote precipitation of BaSO_4 nanoparticles from undersaturated solutions (Deng et al., 2019).

Regardless of the precise microscale mechanism, precipitation of particulate BaSO_4 is ubiquitous in the marine realm. Given that BaSO_4 precipitation renders an apparent negative isotope fractionation of $\sim -0.5\%$, it is highly likely that BaSO_4 cycling drives much of the Ba isotope variability in the ocean (Figure 23). From a paleoproxy perspective, this is ideal; BaSO_4 formation is related to the decay of organic matter and not by the presence of any specific organism (e.g., Dehairs et al., 2008; Jacquet et al., 2007). Downward transport of particulate BaSO_4 is driven by aggregation with larger particles (Lam & Marchal, 2015) and the efficiency of this downward transport depends on the same biophysical processes that export organic matter, thus connecting the export flux of BaSO_4 to that of organic carbon (Eagle et al., 2003).

Barites formed in the ocean through this passive chemical pathway are commonly termed marine, pelagic, authigenic, or biogenic. Though none of these terms are perfect descriptors of the chemical processes involved, “marine” and “biogenic” are the most ambiguous and their use is discouraged; the former encompasses all BaSO_4 formed in the marine realm—including diagenetic, cold seep, and hydrothermal—whereas the latter could be taken to imply only those precipitates brought about by active biological processes. While “authigenic” is an informative descriptor, it has also been used to describe sedimentary BaSO_4 that formed via diagenetic redistribution on or below the seafloor (e.g., Torres et al., 1996). Thus, we recommend use of the term “pelagic” when describing chemically precipitated microcrystalline BaSO_4 , and encourage authors to include this definition in their works.

8.2.3. Physical

Dissolved [Ba] exhibits a nutrient like profile in the oceans similar to alkalinity and [Si] (Figure 22). However, the extent to which this pattern arises from nonconservative biogeochemical processes versus physical mixing remains unresolved. Results from the GEOTRACES program are facilitating renewed interest into this topic, which is being investigated using two complementary approaches. In the first, biogeochemical contributions to basin-scale [Ba] distributions are isolated using statistical methods, such as Optimum Multiparameter water mass Analysis. These statistical methods showed that mixing is dominant in the Mediterranean (Jullion et al., 2017) and North Atlantic (Le Roy et al., 2018), but that sea ice-related processes may be important in the high latitudes (Hendry et al., 2018). Second, the influence of mixing is evidenced from emerging Ba stable isotope data. Indeed, the importance of mixing has been documented vertically (Horner, Kinsley, & Nielsen, 2015), zonally (Bates et al., 2017; Bridgestock et al., 2018), and meridionally (Bates et al., 2017; Hsieh & Henderson, 2017). Together, these new approaches imply that *in situ* biogeochemical processes exert a relatively minor influence on basin-scale [Ba] distributions.

8.3. Marine Archives

Given the connections between export production and BaSO_4 fluxes, the major archive of historical changes in Ba cycling is BaSO_4 itself (e.g., Griffith & Paytan, 2012). Indeed, the sedimentary accumulation of BaSO_4 —often determined as the fraction of Ba in excess of the detrital Ba background or the deposition

rate of BaSO_4 —has been extensively used to reconstruct past changes in export production (e.g., Costa et al., 2016; Francois et al., 1995; Frank et al., 2000; Jaccard et al., 2005, 2013; Ma et al., 2014, 2015; Paytan et al., 1996; Schmitz, 1987; Winckler et al., 2016). An estimated 30% of the BaSO_4 microcrystals formed in seawater are buried in oxygenated sediments (e.g., Dymond et al., 1992), a considerably higher fraction than for organic carbon (Paytan & Kastner, 1996). However, in oligotrophic regimes where both BaSO_4 fluxes and sedimentation rates are low, prolonged exposure to undersaturated seawater results in poor preservation (Eagle et al., 2003; Serno et al., 2014). Similarly, in high productivity coastal upwelling settings, mineralization of organic matter in sediments consumes porewater O_2 , driving conditions down the redox tower and toward sulfate reduction, hampering BaSO_4 preservation (Carter et al., 2020; McManus et al., 1998; Paytan & Griffith, 2007).

The isotopic composition of Ba in sediments has been investigated as a proxy for the Ba isotope composition of the Ba source (i.e., dissolved Ba in epipelagic and upper mesopelagic seawater). Applications to date have explored the recovery of the biological carbon pump following the Paleocene–Eocene Thermal Maximum (~56 Ma; Bridgestock et al., 2019) and the origin of enigmatic sedimentary BaSO_4 deposited in the aftermath of the Marinoan glaciation (~635 Ma; Crockford et al., 2019) and Great Oxidation Event (~2,000 Ma; Hodgskiss et al., 2019). These three applications are reviewed in detail in Horner & Crockford (2021).

Unlike many of the other TEIs reviewed here, we are not aware of any studies exploring $\delta^{138}\text{Ba}$ in Fe–Mn crusts. Barium is somewhat immobile in Fe–Mn crusts, with a calculated effective diffusivity $\leq 10^{-8} \text{ cm}^2 \text{ yr}^{-1}$ (see Henderson & Burton, 1999, for calculation details), similar to Zn (Section 9.3.1). While this implies that Fe–Mn crusts have the potential to record variations in deep ocean $\delta^{138}\text{Ba}$, a significant fraction of the total Ba in Fe–Mn crusts is associated with CFA (carbonate fluorapatite; Koschinsky & Hein, 2003). Since the CFA is secondary—filling voids around the layered Fe- and Mn-oxide minerals—it is unclear if Fe–Mn crusts can be developed into a useful archive of $\delta^{138}\text{Ba}$.

Lastly, the amount of Ba in marine carbonates, typically reported as Ba:Ca, has been extensively used to reconstruct the Ba content of past environments, specifically for constraining historical patterns of upwelling and/or terrestrial runoff (e.g., Gebregiorgis et al., 2016; Lea et al., 1989). More recently, a number of studies have investigated the fidelity of surface- (Liu et al., 2019) and deep-sea corals (Hemsing et al., 2018; Geyman et al., 2019), finding that a number of species are faithful archives of ambient [Ba] and $\delta^{138}\text{Ba}$. These findings are highly promising from a proxy standpoint, as they indicate that a number of archives may be suitable for paleo Ba reconstructions.

8.4. Prospects

Barium exhibits several nutrient-like properties: First, [Ba] distributions resemble those of other nutrients and second, particulate abundances are intimately associated with the processes of organic carbon remineralization and export. Despite these connections, several aspects of Ba cycling—both in the modern and past oceans—remain unresolved. We thus suggest several areas for additional research that will help widen the applicability of Ba-based proxies in paleoceanography.

8.4.1. Modern

Several issues remain regarding the modern Ba cycle. Many of these are reviewed in detail by Horner & Crockford (2021), though we outline the four most pressing and their possible remedies here. First, to what extent do the similar distributions in [Ba], [Si], alkalinity, and ^{226}Ra reflect true biogeochemical coupling versus passive physical mixing? These correlations have been the subject of scrutiny for over 40 years (e.g., Chan et al., 1976; Chung, 1980), and recent GEOTRACES sections are facilitating a reevaluation of these relationships. As noted above, statistical analysis of Ba (and Si, Ra) distributions in regions will offer valuable insights, particularly if conducted in regions with weaker overturning circulation. Likewise, additional profiles of $\delta^{138}\text{Ba}$ from regions with strong *in situ* influences—Ba point sources (e.g., seeps, Torres et al., 1996; margin sediments, McManus et al., 1998), or point sinks (e.g., plankton blooms, Esser & Volpe, 2002)—should enable testing the importance of local processes to regional Ba isotope distributions.

Second, the Ba isotopic mass balance of the ocean must be closed. This will require detailed evaluation of other putative Ba sources, such as diagenetic remobilization (e.g., Hoppema et al., 2010), atmospheric depo-

sition, and the importance of estuarine enhancement of riverine Ba fluxes (e.g., Edmond et al., 1978; Hanor & Chan, 1977). Large intra-marine Ba point sources, such as hydrothermal vents, can drive BaSO₄ supersaturation, leading to precipitation; indeed, a recent study suggests that the net effect of such point sources may be to increase deep $\delta^{138}\text{Ba}$ through BaSO₄ precipitation, further imbalancing the Ba isotope budget (e.g., Hsieh et al., 2021; Figure 23). Barium isotope fractionation associated with other mineral sinks, such as adsorption onto Fe–Mn oxyhydroxides, also remains uncharacterized.

Third, what is the mechanism of BaSO₄ precipitation? While the microenvironment mediated model appears most likely, many microscale mechanisms of precipitation remain ambiguous: How and from what are Ba and sulfate ions liberated during mineralization? How and why are they accumulated onto biofilms? Do different substrate organisms and/or heterotrophic communities influence the amount of BaSO₄ precipitated? Addressing these questions will require additional field and laboratory studies, which can then be compared against distributions of particulate BaSO₄ in the ocean interior. Depending on their importance, these nuances may require ecological parameterizations in numerical models of Ba cycling.

Finally, additional experiments are needed to narrow estimates of the fractionation factor between BaSO₄ and seawater. Existing laboratory studies place this estimate $\approx -0.3\text{‰}$, whereas a wide range of field data suggest that it is considerably larger at $\approx -0.5\text{‰}$. Accounting for this $\approx 0.2\text{‰}$ difference is both important and justifies additional experimentation, as it indicates incomplete understanding of the processes that fractionate Ba isotopes in the marine realm.

8.4.2. Paleo

As with the modern cycle, several ambiguities persist. Assuming that BaSO₄ remains the preferred archive of past Ba cycle variations, it is imperative to constrain the effect of early diagenesis on the Ba isotope composition of sedimentary BaSO₄. Likewise, it is unknown if diagenetic BaSO₄ retains any primary Ba isotope information. Assessing these issues will require studies of co-located BaSO₄ and porewaters from environments at various stages of early diagenesis. Answering these questions is critical in establishing the validity of Ba isotopes in barite as a paleoceanographic proxy.

Additionally, there are uncertainties relating to whether BaSO₄ cycling is impacted by ambient [Ba] during BaSO₄ precipitation and burial. For example, does more BaSO₄ precipitation occur at higher ambient [Ba]? While there is evidence indicating that this is not a major influence in the modern ocean (e.g., Fagel et al., 2004; Serno et al., 2014), a relationship between ambient [Ba] and BaSO₄ precipitation is likely necessary to maintain steady state in the Ba cycle over geological timescales (e.g., Horner & Crockford, 2021). Likewise, to what extent does BaSO₄ preservation depend on ambient [Ba]? These considerations are significant when considering longer-term records, particularly when marine sulfate levels were lower-than-modern (and [Ba] presumably higher; e.g., Walker, 1983; Wei & Algeo, 2020). Finally, does the seawater temperature at the depth of POC mineralization impact the relationship between POC and BaSO₄ formation? These questions are best addressed through a combination of experimentation (e.g., cultures, precipitation), field studies in basins with large gradients in [Ba], and numerical experiments incorporating saturation state modeling.

9. Nickel

Nickel is biologically utilized, for example by diazotrophs during nitrogen fixation and by microorganisms catalyzing the breakdown of reactive oxygen species (Twining & Baines, 2013). Particularly relevant to early Earth reconstructions is the fact that methanogens have an obligate requirement for Ni. Several promising archives have been identified for marine Ni isotope chemistry, however, determination of the composition of Ni isotope ratios in seawater has lagged behind other nutrient-like metals such as Zn and Cd. Recent datasets do indicate that Ni is cycled by phytoplankton, with a resultant isotope fractionation in the euphotic zone dependent on the dominant ecology of the region. As such, Ni isotope variations are likely to be broadly responsive to biological productivity, but the assumption of a constant fractionation factor (i.e., $\Delta_{\text{p-R}}$) may be violated, which may complicate use of Ni isotopes as a quantitative paleoproductivity proxy, and the applicability of the simple reactor scheme. Additionally, the secondary sinks of Ni, such as those associated with Mn oxides, are associated with large Ni isotope fractionations, opening up the possibility of using Ni isotopes to track aspects of marine paleoredox.

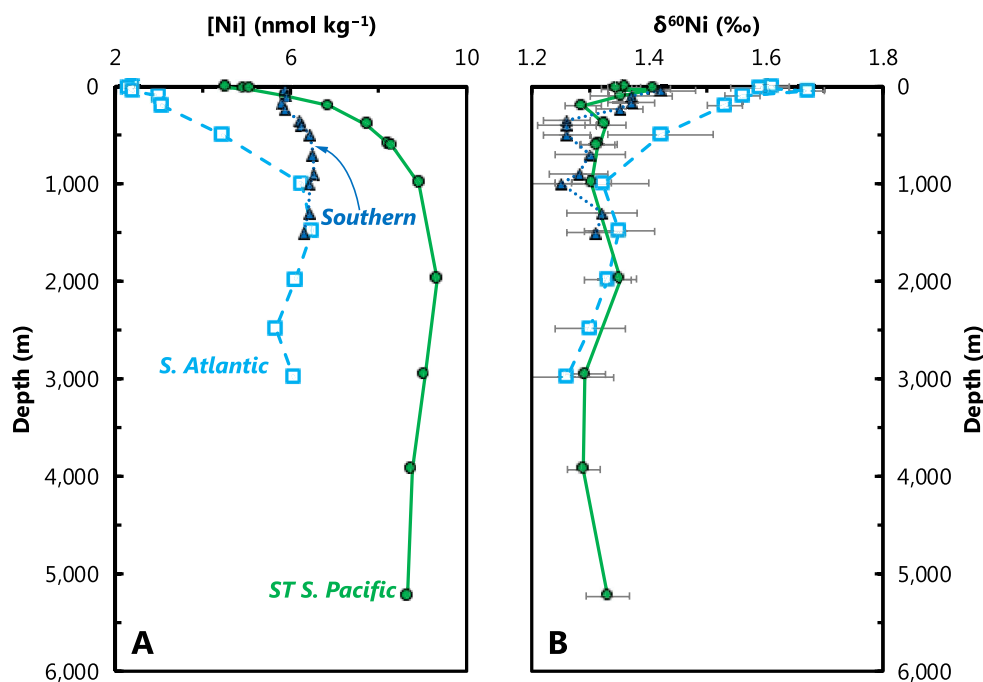


Figure 24. Representative profiles of dissolved Ni concentrations ($[\text{Ni}]$); (a) and Ni isotopic compositions ($\delta^{60}\text{Ni}$); (b). Data from the South Atlantic (squares, dashed line; Archer et al., 2020), Southern (triangles, dotted line; R. M. Wang et al., 2019), and Subtropical South Pacific Oceans (circles, solid line; Takano et al., 2017). Station locations as per Figure 1. This comparison illustrates that the oceanographic processes leading to distinct dissolved concentration profiles render only small changes in dissolved $\delta^{60}\text{Ni}$ between basins.

9.1. Marine Distribution

Nickel has a classic nutrient-type distribution in the oceans with one unusual feature: surface $[\text{Ni}]$ never drops below $\sim 1.8\text{--}2\text{ nmol kg}^{-1}$ (e.g., Bruland, 1980; Sclater et al., 1976; Figure 24). There is evidence, however, that this residual pool in surface waters is not bioavailable, as summarized recently by Archer et al. (2020). Deep water $[\text{Ni}]$ are $4\text{--}5\text{ nmol kg}^{-1}$ in the Atlantic, and $\sim 9\text{ nmol kg}^{-1}$ in the north Pacific (Figure 24).

Developing robust analytical protocols for analyzing Ni isotopes for a range of sample matrices has proven somewhat more challenging than for some of the other trace metals discussed here due to the difficulty in separating Ni from interfering elements (e.g., Fe, a major isobaric interference on ^{58}Ni). Chemical purification protocols now use a sequence of resins including anion exchange (e.g., AG MP-1M or AG1-X8, Bio-Rad) and either a Ni-specific resin (containing dimethylglyoxime) or Nobias PA-1 (Hitachi High Technologies; e.g., Cameron et al., 2009; Gueguen et al., 2013; R. M. Wang et al., 2019; Yang et al., 2020). The limited data since reported for the oceanic dissolved pool of Ni indicates relatively little variability in $\delta^{60}\text{Ni}$ at depth ($+1.2\text{‰}$ to $+1.4\text{‰}$), with a small shift toward heavier values up to $+1.7\text{‰}$ in the upper water column (Figure 24; Archer et al., 2020; Takano et al., 2017; R. M. Wang et al., 2019; Yang et al., 2020). The upper water column shift is proposed to reflect a small kinetic isotope fractionation during biological uptake. Similar to Zn, Cu, Cd, Mo, Ba, and Cr, the isotopic composition of Ni in seawater is isotopically heavy compared to the UCC (Table 1).

9.2. Driving Processes

9.2.1. Biological

To date, eight Ni-based enzyme systems have been identified (Ragsdale, 2009), including urease, which is key to the global nitrogen cycle, and methyl-CoM reductase, which catalyzes the production of all biologically generated methane on Earth. The obligate requirement of methanogens for Ni has led to interest

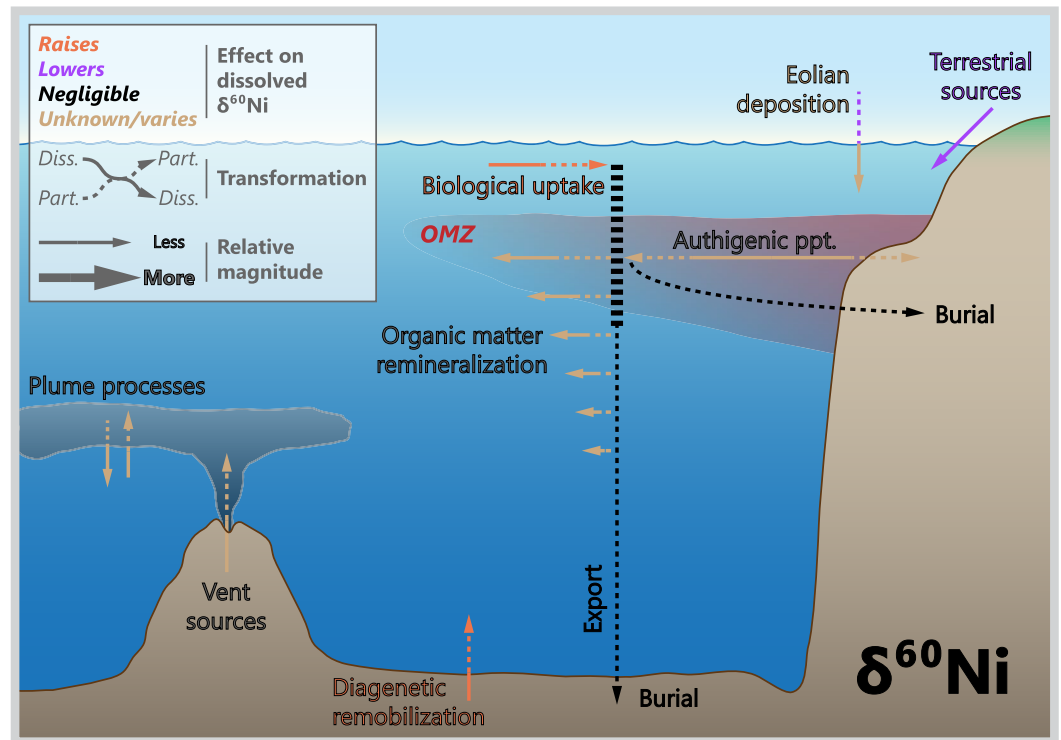


Figure 25. Processes driving Ni isotope variations in modern seawater. Biological processes are recognized to drive a small, but systematic increase in dissolved $\delta^{60}\text{Ni}$ and marine Ni isotope values are preserved in certain sediments. Other abiotic Ni cycling processes may be important however, such as sorption to Mn-oxide minerals, and the significance of these fractionations to global Ni cycling remains to be fully elucidated.

in developing Ni and $\delta^{60}\text{Ni}$ isotopes as a tracer of methane production on the early Earth (e.g., Cameron et al., 2009; Konhauser et al., 2009; S. J. Wang et al., 2019). In the modern ocean the highest Ni quotas are found in diazotrophs (N-fixers), thought to reflect the presence of Ni-Fe hydrogenases (which catalyze H_2 produced during N fixation), Ni-superoxide dismutase (Ni-SOD) and urease (Dupont, Barbeau, & Palenik, 2008; Dupont, Neupane, et al., 2008; Nuester et al., 2012; Tamagnini et al., 2002). Nickel limitation of phytoplankton grown on urea has been shown in culture and in natural assemblages, suggesting the Ni-N colimitation of phytoplankton growth may be relevant in the ocean (Dupont, Barbeau, & Palenik, 2008; Dupont et al., 2010; Price & Morel, 1991). Significant Ni is also found in diatom frustules (about 50% of diatom cellular quotas; Twining et al., 2012). The latter observation is thought to play a role in the similarity of Ni and Si oceanic distributions (Twining et al., 2012).

No culture data are available to determine the degree of Ni isotope fractionation during biological uptake. Upper ocean data suggest no fractionation or a small preference for the light isotope, equivalent to $\Delta_{\text{P-R}} \approx -0.3\text{‰}$ (Archer et al., 2020; Takano et al., 2017; Yang et al., 2020; Figure 25), consistent with the Ni isotope systematics observed in organic-rich sediments (Ciscato et al., 2018) and water column particulates (Takano et al., 2020). Interestingly, new water column data from the South Atlantic suggest distinct ecological differences in Ni drawdown and Ni isotope fractionation compared to other bioactive trace metals (e.g., Zn, Cd). Limited drawdown and Ni isotope fractionation is observed in the diatom-dominated regime south of the Polar Front in the Southern Ocean. In contrast, more marked drawdown and significant Ni isotope fractionation is observed north of the Polar Front, which has been attributed to the predominance of nitrate-limited, Ni-requiring cyanobacteria (Archer et al., 2020).

9.2.2. Chemical

Nickel is partially complexed by strong organic ligands in coastal and open ocean environments (5%–70%; e.g., Boiteau et al., 2016; Donat et al., 1994; Saito et al., 2004), though the slow water exchange kinetics of Ni make these complexation measurements particularly challenging (Hudson & Morel, 1993). Slow exchange

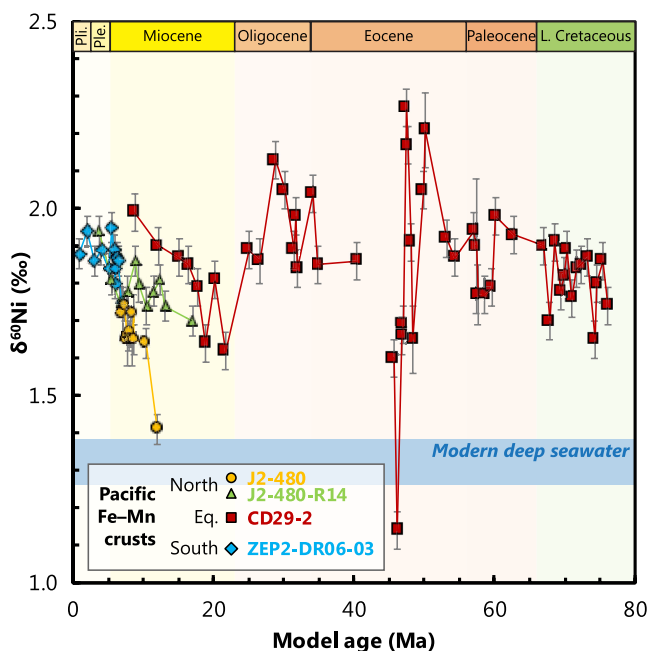


Figure 26. Four Fe–Mn records of $\delta^{60}\text{Ni}$ from the Pacific Ocean. Assuming that Fe–Mn crusts have always formed with an offset $\approx +0.5\%$ with respect to ambient dissolved Ni in seawater, these records illustrate that the Ni isotope composition of seawater has varied by only $\pm 0.2\%$ over the Cenozoic. Data for J2-480, J2-480-R14, and ZEP2-DR06-03 are from Gueguen et al. (2016). Data from CD29-2 are from Gall et al. (2013). All four records have been plotted using the authors’ preferred age model, meaning that there are some differences between the chronology of CD29-2 shown here compared to Figures 8 and 17.

kinetics may also explain the residual pool of non-bioavailable Ni in the surface ocean (e.g., Dupont et al., 2010; Mackay et al., 2002). Speciation models suggest that the remainder of the Ni is present as free Ni^{2+} and NiCl^+ , with a small fraction present as NiCO_3^0 (Turner et al., 1981; Zirino & Yamamoto, 1972).

Nickel cycling is tightly coupled to that of Mn—in sediments (Koschinsky & Hein, 2003), during removal from hydrothermal fluids (e.g., Gueguen et al., 2021), within porewaters (Klinkhammer, 1980), and across the redoxcline of the Black Sea (Vance et al., 2016). In the Black Sea, for example, Mn redox cycling is associated with preferential sorption of light Ni isotopes, with a large negative fractionation of $\approx -4\%$ (Vance et al., 2016). This large fractionation is consistent with experimental sorption of Ni on birnessite (Sorensen et al., 2020; Wasylenki et al., 2014).

Unlike the more strongly chalcophile elements such as Cd, Cu, and Zn, Ni is not strongly drawn down in the euxinic portion of the Black Sea water column (Vance et al., 2016; Tankéré et al., 2001) and in other euxinic basins (e.g., Jacobs & Emerson, 1982; Jacobs et al., 1985). However, Ni is enriched in Black Sea sediments (Little et al., 2015), with $\delta^{60}\text{Ni}$ compositions notably lighter (at $+0.3$ to $+0.6\%$) than Ni sources to the basin (at about $+1.3\%$; Vance et al., 2016). Vance et al. (2016) attributed these light isotope compositions to the scavenging of sulfidized Ni species, which are predicted to be isotopically light (Fujii, Moynier, Dauphas, & Abe, 2011).

Dissolved Ni is added to the ocean from rivers, hydrothermal vents, and dust (Figure 25). All three sources possess $\delta^{60}\text{Ni}$ between $+0.1\%$ and $+0.8\%$, which is lighter than deep ocean seawater (see recent summaries by Gueguen & Rouxel, 2021; Little et al., 2020). In general, these Ni sources are not of a sufficient magnitude to generate deviations in deep ocean dissolved $\delta^{60}\text{Ni}$, and are therefore unlikely to compromise use of $\delta^{60}\text{Ni}$ as a paleoproductivity tracer (similar to $\delta^{114}\text{Cd}$; Section 6). The main output flux of Ni from seawater is believed to be burial with Mn oxides, which

have a wide range of reported Ni isotope compositions. While hydrogenetic ferromanganese crusts are generally isotopically heavy, from about $+0.9$ to $+2.5\%$ (Gall et al., 2013; Gueguen et al., 2021, 2016), Mn-rich pelagic clays possess $\delta^{60}\text{Ni}$ between -0.8 and $+1.0\%$ (Little et al., 2020; Gueguen & Rouxel, 2021). The Ni isotope difference between sources and sinks implies the existence of a missing “heavy” Ni source. Recently, Little et al. (2020) and Gueguen & Rouxel (2021) hypothesized that this source is related to benthic release from sediments and predicted that it possesses an extremely fractionated Ni isotope composition of $\approx +3\%$.

9.2.3. Physical

The most recent estimate for the residence time of Ni in the ocean is approximately ~ 20 kyr (Little et al., 2020), considerably longer than the mixing time of the ocean. As a result, in parallel with the other bioactive trace metals discussed herein, Ni and Ni isotope distributions are modulated at first order by the geometry of physical ocean circulation. The importance of diatom uptake in the Southern Ocean in partially coupling oceanic Ni and Si (Twining et al., 2012) was introduced above, and the relative homogeneity of deep ocean Ni isotope compositions supports an important role for southern-sourced water masses in the Ni distribution (Figure 24; Archer et al., 2020; Takano et al., 2017; R. M. Wang et al., 2019).

9.3. Marine Archives

9.3.1. Ferromanganese Sediments

Ferromanganese crusts exhibit variable Ni isotope compositions (Figure 26; Gall et al., 2013; Gueguen et al., 2016a), which are, on average, slightly isotopically heavier (at $\delta^{60}\text{Ni}$ of $+1.6\%$) than seawater ($\delta^{60}\text{Ni}$ at about $+1.3\%$). Nickel is relatively immobile in Fe–Mn crusts, with a calculated effective diffusivity $\leq 10^{-9}$

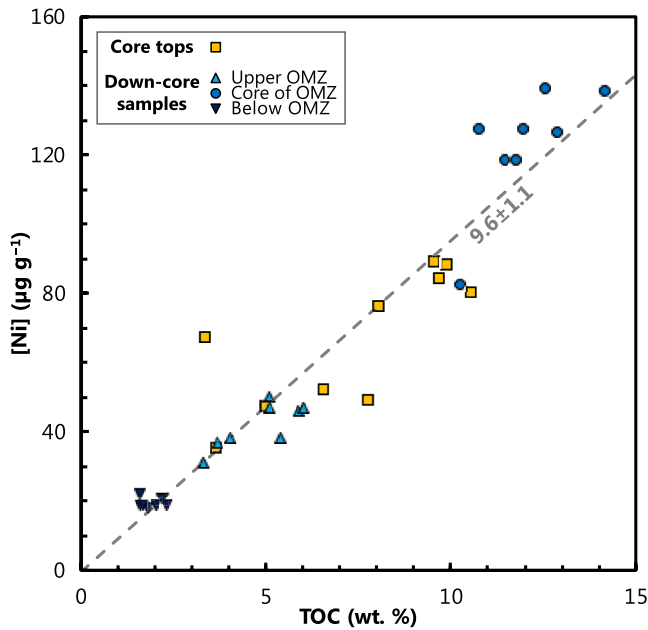


Figure 27. Correlation of Ni and TOC content in organic-rich sediments from the Peru Margin. Data from Ciscato et al. (2018). The best-fit regression of these data yields a Ni–TOC slope of 9.6 ± 1.1 (mean \pm 2 SD), similar to the “ ≈ 9 ” reported by Böning et al. (2015).

$\text{cm}^2 \text{yr}^{-1}$ (see Henderson & Burton, 1999, for calculation details), similar to Cu (Section 5.3.1), implying that Fe–Mn crusts preserve primary information about dissolved $\delta^{60}\text{Ni}$. However, experiments suggest that sorption of Ni to birnessite (the primary Ni-hosting phase in Fe–Mn sediments) should instead be associated with a large negative isotope effect of about -3 to -4‰ (Sorensen et al., 2020; Wasylenki et al., 2014). It remains unclear as to why experiment- and field-derived Ni isotope effects for Fe–Mn crusts exhibit such a large mismatch.

As discussed above, intense Mn cycling occurs across the redoxcline of the Black Sea; this cycling is associated with large variations in Ni and Ni isotopes, consistent with the experimentally observed light isotope effect on sorption to birnessite (Vance et al., 2016). Recent data from Mn-rich sediments that have undergone diagenesis also point to the preservation of a large negative Ni isotope effect, and predict a concomitant isotopically heavy benthic Ni source (Gueguen & Rouxel, 2021; Little et al., 2020).

Though promising, the development of Fe–Mn crusts as a tracer of past oceanic Ni cycling awaits a mechanistic understanding of the processes driving their variably isotopically heavy signature, as well as an awareness of the likely complicating role of diagenetic remobilization of Ni (e.g., Atkins et al., 2016; Little et al., 2020).

9.3.2. Organic-Rich Sediments

As introduced in Section 4.3.2 (Cu), qualitative arguments for high organic matter fluxes (i.e., increased paleoproductivity) have been made based on enriched Ni (and Cu) content in ancient organic-rich sediments

(e.g., Tribovillard et al., 2006). For Ni, this approach is supported by positive correlations with TOC in modern continental margin sediments (Figure 27).

Nickel does not precipitate in the presence of water column dissolved sulfide and is therefore less susceptible to decoupling from TOC fluxes compared to chalcophile elements such as Cu, Zn, and Cd. Nevertheless, Ni cycling is strongly linked to the redox cycling of Mn, potentially complicating Ni–TOC coupling in settings with active diagenetic cycling of Mn. Sedimentary and water column data from the Black Sea indicate that cycling associated with the benthic Fe–Mn redox shuttle (e.g., Lyons & Severmann, 2006) provides an alternative supply route for Ni to the deep euxinic basin in this setting (Little et al., 2015; Vance et al., 2016). Therefore, open marine settings would be the most promising from which to make estimates of the relative productivity of two different sites based on their absolute measured Ni:TOC ratios. Otherwise the degree of basin restriction will exert the primary control on nutrient supply, and therefore the degree of trace metal enrichment (Algeo & Maynard, 2008; Little et al., 2015).

Ciscato et al. (2018) investigated the distribution of Ni and its isotopes in two fractions isolated from Peru margin organic-rich sediments. The HF–HCl digestible fraction (usually containing $>80\%$ of total Ni) exhibited $\delta^{60}\text{Ni}$ values similar to modern deep seawater (at about $+1.2\text{‰}$). Meanwhile, these authors found variable Ni isotope compositions in the organic pyrite fraction, which they suggested record the fractionation imparted by biological uptake in the euphotic zone. Systematic relationships between Ni–TOC, $\delta^{60}\text{Ni}_{\text{OPF}}$, and $\delta^{13}\text{C}$ indicate that there is merit in continuing to investigate Ni and Ni isotopes as a paleoproductivity tracer (Ciscato et al., 2018).

9.4. Prospects

To date, Ni and its isotopes have been under developed as a potential paleoproductivity proxy. Recent data, both from the dissolved phase in seawater and in two different fractions isolated from anoxic organic-rich sediments, suggest promise in the coupling of Ni and C and their isotopes. However, in oxic-to-suboxic settings, Ni contents and isotopic composition of sediments are strongly influenced by the diagenetic redox cycling of Mn (e.g., Gueguen & Rouxel, 2021). We recommend additional studies of Ni contents and isotopic

compositions in sediments, focusing specifically on carbonate and siliceous biominerals, which is increasingly tractable with new and improved chemical separation and analytical techniques.

Finally, in a completely different approach, S. J. Wang et al. (2019) presented $\delta^{60}\text{Ni}$ values of Precambrian glacial diamictites, which are suggested to represent the chemical weathering residues of the UCC. They find a small shift toward heavier Ni isotope compositions across the Great Oxidation Event, which they relate to the onset of oxidative weathering of crustal sulfides. Combined with the proposed importance of Ni to the maintenance of methanogenesis during this time period (e.g., Konhauser et al., 2009), it is hoped that future Ni stable isotope analyses will shed further light on the paleoenvironmental conditions on the early Earth.

10. Chromium

Chromium (Cr) stable isotope composition ($\delta^{53}\text{Cr}$) has received significant attention over the past decade as a proxy of paleoredox conditions. These applications have generally used a framework where isotope fractionation is driven by subaerial weathering, with the partial pressure of atmospheric O_2 controlling $\delta^{53}\text{Cr}$ signatures in resultant paleorecords (e.g., Frei et al., 2009, 2014). However, subsequent studies have identified numerous challenges to this framework, including questions about the fidelity of sediment records (e.g., Frank et al., 2020; Rimmelzwaal et al., 2019; Wang et al., 2021) as well as the very processes driving Cr cycling in seawater. Indeed, recent studies suggest that the most spatially expansive Cr isotope variations in the ocean are not related to oxygen availability but rather uptake by phytoplankton (e.g., Janssen et al., 2020, 2021). This means that Cr isotopes may serve as a novel productivity tracer that is reasonably well described by the isotope reactor framework (Section 2.2). However, until recently, marine Cr data have not seen the significant improvements in quality control as other metals in the GEOTRACES repertoire, and there are currently no consensus values for [Cr] and $\delta^{53}\text{Cr}$ in GEOTRACES reference materials. Consequently, there is a degree of discrepancy among literature data that likely does not wholly represent natural variability (see discussions in Goring-Harford et al., 2018; Huang et al., 2021; Rickli et al., 2019; Moos et al., 2020; Nasemann et al., 2020), limiting our understanding of modern Cr cycling and thus paleoproxy validation. Given the issues surrounding the measurement of—and mechanisms driving—Cr isotope variation in seawater, we focus our assessment of Cr on open ocean GEOTRACES-era data that are not considered equivocal by subsequent studies. We suggest that these new insights offer an opportunity to re-assess the fidelity of different sediments as archives of past seawater $\delta^{53}\text{Cr}$.

10.1. Marine Distribution

In the ocean, [Cr] follows a nutrient-type vertical distribution (e.g., Campbell & Yeats, 1981), suggesting involvement in biological processes; however, concentration gradients with depth are minor relative to other macro- and micronutrients (Figure 28). Open ocean surface [Cr] are 2–4 nmol kg^{-1} , with lower concentrations in the oligotrophic gyres than at higher latitudes (Goring-Harford et al., 2018; Janssen et al., 2020; Moos & Boyle, 2019; Rickli et al., 2019; Scheiderich et al., 2015). Chromium is elevated in Pacific and Southern Ocean deep waters, with [Cr] of 3.5–6.0 nmol kg^{-1} (Figure 28; Huang et al., 2021; Janssen et al., 2021; Moos & Boyle, 2019; Nasemann et al., 2020; Rickli et al., 2019). Although inter-basin deep water [Cr] gradients are small relative to other trace metals (e.g., [Cd], [Zn]) and macronutrients ($[\text{PO}_4^{3-}]$, $[\text{NO}_3^-]$, and [Si]), clear increases in [Cr] are seen in deep waters advected northward from the Southern Ocean. These observations reflect, in part, a deep regeneration cycle for Cr, with maxima in the abyssal ocean (e.g., Jeandel & Minster, 1987).

The two primary redox forms of Cr in the ocean are Cr(VI), an oxyanion with limited particle reactivity, and Cr(III), a poorly soluble cation that readily adsorbs to mineral and organic phases (e.g., Semeniuk et al., 2016; Wang et al., 1997). In oxic seawater, thermodynamic calculations predict that Cr(VI) should be the only species present (Elderfield, 1970); however, Cr(III) is regularly reported as representing 5%–15% of [Cr] (e.g., Cranston & Murray, 1978; Davidson et al., 2020; Jeandel & Minster, 1987; Janssen et al., 2020), and Cr(III) abundance is elevated in OMZs and anoxic waters (Davidson et al., 2020; Huang et al., 2021; Murray et al., 1983; Rue et al., 1997). Due to the differences in solubility and reactivity of these species, redox cycling plays an important role in setting [Cr] distributions. The primary oceanic Cr reductants are ferrous

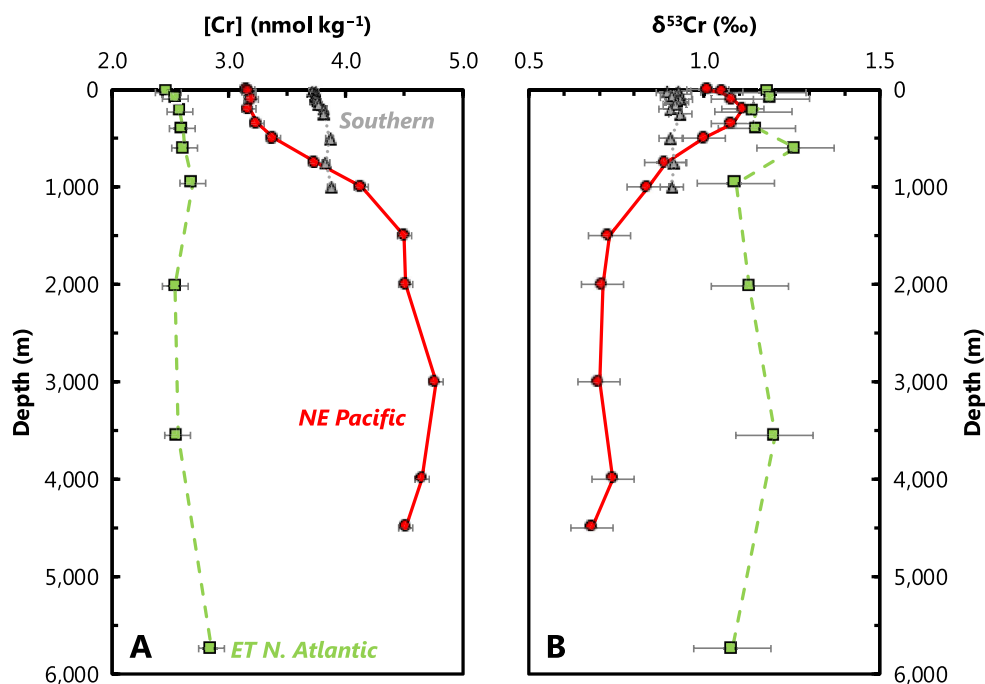


Figure 28. Representative profiles of dissolved Cr concentrations ($[Cr]$); (a) and Cr isotopic compositions ($\delta^{53}Cr$); (b). Data from the Eastern Tropical North Atlantic (squares, dashed line; Goring-Harford et al., 2018), Southern (triangles, dotted line; Rickli et al., 2019), and Northeast Pacific Oceans (circles, solid line; Moos & Boyle, 2019). Station locations as per Figure 1. These profiles illustrate that the decrease in surface ocean (Cr) from the Southern to low-latitude oceans is accompanied by a modest, but significant increase in $\delta^{53}Cr$. Likewise, deep waters with elevated (Cr) exhibit lighter $\delta^{53}Cr$, consistent with regeneration of an isotopically light Cr-bearing phase.

Fe (Pettine et al., 1998) and H_2S (Kim et al., 2001). Chromium(III) maxima in surface waters suggests that biological or photochemical processes, possibly involving dissolved organic matter, are also important (e.g., Achterberg & van den Berg, 1997; Janssen et al., 2020; Kieber & Helz, 1992); however, these processes may occur indirectly through the generation of Cr reductants such as ferrous Fe (Hug et al., 1996). The primary marine Cr oxidants are Mn oxides (Milletto et al., 2021; van der Weijden & Reith, 1982) and H_2O_2 (Pettine et al., 1991); Cr oxidation by O_2 is insignificant due to kinetic limitations. Chromium redox cycling is accompanied by isotope fractionation, with reduction consistently resulting in an enrichment of light isotopes in the reduced phase (e.g., Ellis et al., 2002; Wanner & Sonnenthal, 2013), and therefore redox cycling—biologically mediated or otherwise—is likely important for dissolved Cr stable isotope distributions as well as $[Cr]$. Fractionation during Cr oxidation is more poorly constrained, with variable fractionation patterns reported (Milletto et al., 2021; Zink et al., 2010).

Chromium stable isotope compositions are reported relative to NIST SRM 979. The pioneering study of Scheiderich et al. (2015) reported much of the first oceanographically consistent $\delta^{53}Cr$ data. These and subsequent data show enrichments of heavy isotopes in open ocean surface waters (+0.9‰ to +1.4‰) relative to most deep waters (+0.7‰ to +0.9‰; Goring-Harford et al., 2018; Janssen et al., 2020; Rickli et al., 2019; Moos & Boyle, 2019; Moos et al., 2020; Nasemann et al., 2020; Scheiderich et al., 2015; Figure 28). Importantly, the first global $\delta^{53}Cr$ compilation also identified a tight linear correlation between $\delta^{53}Cr$ and $\ln[Cr]$, suggesting that the controls on $[Cr]$ also regulate $\delta^{53}Cr$ —reduction and removal in OMZs and biological export from the surface ocean—and that these processes are accompanied by an isotope fractionation of approximately $-0.7‰$ to $-0.8‰$ (Goring-Harford et al., 2018; Janssen et al., 2020, 2021; Moos et al., 2020; Nasemann et al., 2020; Rickli et al., 2019; Scheiderich et al., 2015; Figure 29; see also reactor model, Sections 2.2 and 12.2). Subsequent studies have focused on understanding and constraining the sensitivities of these processes. Isotopic fractionation during Cr removal in OMZs has been reported both in the water column (Huang et al., 2021; Moos et al., 2020) and at the sediment-water interface (Moos et al., 2020;

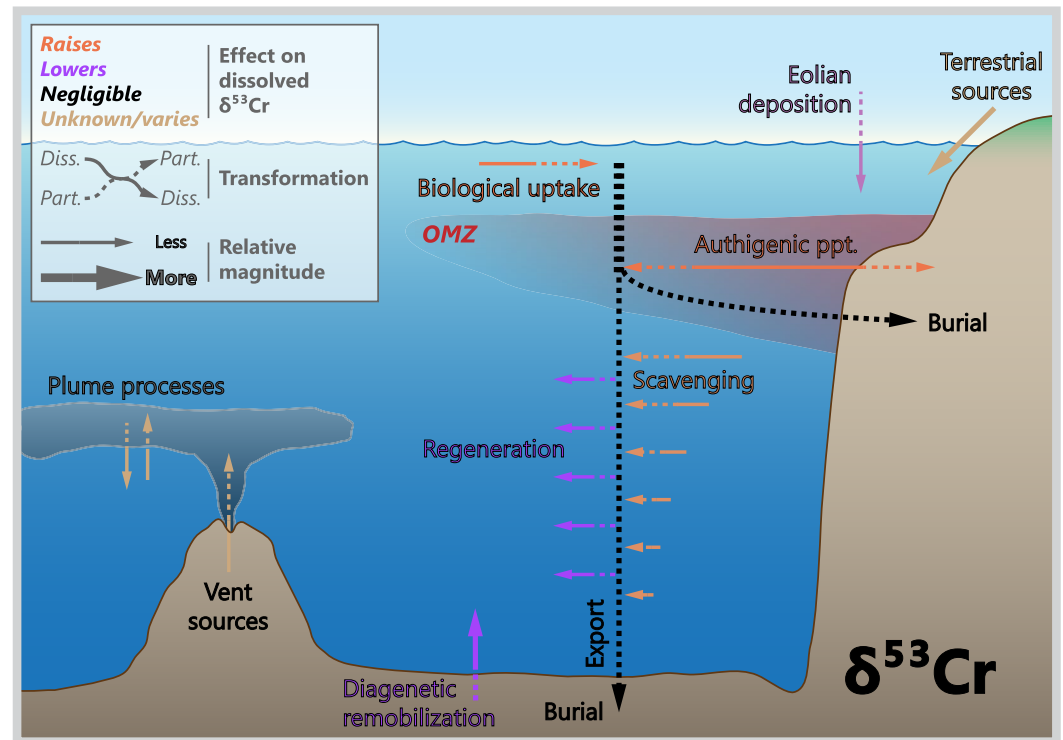


Figure 29. Processes driving Cr isotope variations in modern seawater. Though muted, biological processes exert a control on [Cr] and $\delta^{53}\text{Cr}$, and therefore $\delta^{53}\text{Cr}$ shows some response to productivity. The degree to which $\delta^{53}\text{Cr}$ may ultimately be useful as a productivity proxy will depend on how globally important productivity is relative to other controls on Cr distributions, such as Cr reduction and removal in OMZs and the fidelity of sediment records, which currently remain unresolved.

Nasemann et al., 2020). Similarly, fractionation is observed during Cr export coupled to the biological pump based on data from the open ocean (Janssen et al., 2020) and coastal waters (Goring-Harford et al., 2018).

While the understanding of [Cr] and dissolved $\delta^{53}\text{Cr}$ in the modern ocean has seen substantial improvements in the GEOTRACES-era, key uncertainties in Cr biogeochemical cycling remain. In turn, these uncertainties limit the potential of $\delta^{53}\text{Cr}$ paleoproxy applications and the identification of faithful $\delta^{53}\text{Cr}$ paleoarchives. The following sections present a more detailed summary of the marine Cr cycle and Cr archives, with a focus on the $\delta^{53}\text{Cr}$ paleoproxy outlook related to marine Cr cycling and the key remaining uncertainties.

10.2. Driving Processes

10.2.1. Biological

Although Cr(VI) can be toxic (e.g., Wong & Trevors, 1988) and there is no known biological function for Cr in marine phytoplankton, [Cr] distributions reflect biogenic controls (e.g., Campbell & Yeats, 1981). This appears to be driven not by internalization but by adsorption of Cr(III) onto phytoplankton (Semiñuk et al., 2016; Wang et al., 1997). This scavenging removes isotopically light Cr from the surface ocean (Goring-Harford et al., 2018; Janssen et al., 2020; Scheiderich et al., 2015), and has been shown to quantitatively explain patterns of oceanic [Cr] and dissolved $\delta^{53}\text{Cr}$ (Janssen et al., 2020, 2021). The magnitude of Cr export associated with the biological pump has been estimated at $\sim 0.1\text{--}1 \text{ Gmol Cr yr}^{-1}$ (Janssen et al., 2020; Jean-del & Minster, 1987), of comparable magnitude to known Cr sources (Wei et al., 2018).

10.2.2. Chemical

Chromium is reduced and removed in OMZs and anoxic waters (Davidson et al., 2020; Huang et al., 2021; Moos et al., 2020; Murray et al., 1983; Nasemann et al., 2020; Rue et al., 1997). This removal may occur in the water column (Davidson et al., 2020; Huang et al., 2021; Moos et al., 2020; Rue et al., 1997) or at the sediment–water interface, though it is presently unclear which is of greater importance (cf. Moos et al., 2020; Nasemann et al., 2020). Approximate isotope fractionation factors for OMZ Cr reduction and removal are estimated as being $\approx -0.7\%$, similar to those implied by the global dissolved $\delta^{53}\text{Cr}$ –[Cr] array. However, these fractionation factors are considerably smaller than the expectations based on laboratory constrained fractionation factors (e.g., Wanner & Sonnenthal, 2013), likely reflecting either incomplete removal or re-oxidation of Cr(III), resulting in a lower effective fractionation (Huang et al., 2021; Moos et al., 2020; Nasemann et al., 2020), and the fact that isotope reactor models will underestimate true isotope separation factors in the presence of mixing. Water column-based estimates of the OMZ Cr sink are not available, and deep water data suggest that some of the Cr removed in OMZs is released in underlying oxic waters and/or sediments (e.g., Murray et al., 1983).

10.2.3. Physical

Riverine fluxes are believed to represent the main source of Cr to the oceans, accounting for ~ 1 Gmol Cr yr^{-1} (Wei et al., 2018). High variability has been reported for riverine dissolved $\delta^{53}\text{Cr}$, though available data suggest that rivers are isotopically heavy relative to the continental crust (e.g., D'Arcy et al., 2016; Frei et al., 2014; Goring-Harford et al., 2020). The role of estuarine processes is unclear at present. Earlier studies suggested scavenging of Cr at low salinity (Campbell & Yeats, 1984; Cranston & Murray, 1980), therefore lowering of riverine Cr fluxes; however, recent data have found conservative mixing of Cr(III), Cr(VI) and $\delta^{53}\text{Cr}$ (Goring-Harford et al., 2020) or release of particulate Cr to the dissolved phase (Sun et al., 2019).

As with other trace metals (e.g., Zn, Cd, Ba; Sections 4, 6, 8), deep water circulation plays an important role in shaping [Cr] and dissolved $\delta^{53}\text{Cr}$ distributions. The advection of Cr-rich intermediate and deep waters formed in the Southern Ocean helps to explain [Cr] enrichments seen at depth in the Pacific (Figure 28a; cf. Moos & Boyle, 2019; Rickli et al., 2019). Data from NADW, while more limited, suggest it is more Cr-depleted than waters formed in the Southern Ocean (Figure 28a; cf. Goring-Harford et al., 2018; Rickli et al., 2019).

10.3. Marine Archives

10.3.1. Carbonates

Chromium(VI) is incorporated into the CaCO_3 matrix during carbonate formation (e.g., Tang et al., 2007). Because Cr(VI) dominates the [Cr] pool in the oxic ocean, this suggests that carbonates may serve as a suitable proxy for ambient dissolved $\delta^{53}\text{Cr}$, motivating numerous $\delta^{53}\text{Cr}$ -based reconstructions as well as a significant body of research to ground-truth the theory-based motivations. A recent review of $\delta^{53}\text{Cr}$ -based paleo reconstructions in carbonates can be found in Wei et al. (2020) and below we highlight relevant assessments of the utility of carbonate archives from the modern ocean.

Inorganic calcite precipitation at oceanographically relevant pH results in an enrichment of light isotopes in CaCO_3 up to 0.7‰ lighter than the solution (Füger et al., 2019), though data at an oceanographically relevant ionic strength are not available. The Cr content of carbonates is low (from <1 to ~ 10 $\mu\text{g g}^{-1}$; Holmden et al., 2016; Pereira et al., 2016; Rimmelzwaal et al., 2019), and therefore CaCO_3 is not a major Cr sink (Bonnand et al., 2013). Studies of Cr incorporated into a diverse range of biogenic carbonates show an enrichment in isotopically light Cr relative to ambient seawater, but with a wide range of fractionation factors. This fractionation is believed to reflect redox processes during Cr uptake into calcifying organisms or preceding Cr incorporation into CaCO_3 (Farkas et al., 2018; Holmden et al., 2016; Pereira et al., 2016). Marine carbonate-hosted $\delta^{53}\text{Cr}$ archives are, however, susceptible to meteoric (Wang et al., 2021) and marine diagenetic overprinting (e.g., Rimmelzwaal et al., 2019).

10.3.2. Ferromanganese Crusts

Ferromanganese crusts from the Pacific are isotopically light ($\delta^{53}\text{Cr} = -0.85\%$ to -0.15% , average = -0.42% , Wei et al., 2018) relative to North Pacific deep water ($\approx +0.7\%$ to $+0.8\%$, Moos & Boyle, 2019; Figure 28b),

equivalent to an isotope separation factor of $\approx -0.9\%$ to -1.6% . The low abundance of Cr in Fe–Mn crusts ($\sim 7 \mu\text{g g}^{-1}$) indicates that, globally, Cr removal to Fe–Mn oxides is not important in controlling [Cr] and $\delta^{53}\text{Cr}$ budgets (Wei et al., 2018). Additionally, Cr is likely somewhat mobile in Fe–Mn crusts, with a predicted diffusivity $\leq 10^{-7} \text{ cm}^2 \text{ yr}^{-1}$ (see Henderson & Burton, 1999, for calculation details), similar to Cd (Section 6.3.2), Mo (Section 7.3), and Ag (Section 11.3). This rate implies that long-term records of $\delta^{53}\text{Cr}$ derived from Fe–Mn crusts are likely to exhibit some diffusive smoothing while preserving larger perturbations. Moreover, the large range of $\delta^{53}\text{Cr}$ in modern Fe–Mn crusts, relative to the modest variations in $\delta^{53}\text{Cr}$ of surrounding intermediate and deep waters, suggests that Fe–Mn crusts are unlikely to be developed into a reliable archive for past marine $\delta^{53}\text{Cr}$.

The Cr content of other types of oxygenated sediments are generally low ($\approx 60 \mu\text{g g}^{-1}$; Gueguen et al., 2016b), with Cr:Ti ratios comparable to the continental crust. Some samples, however, do show apparent authigenic Cr enrichments of a similar magnitude to anoxic and suboxic sediments.

10.3.3. Suboxic and Anoxic Sediments

Chromium is generally enriched in suboxic and anoxic surface sediments relative to upper continental crust and oxic sediments (Gueguen et al., 2016b; Reinhard et al., 2014), with an average Cr content of surface sediments of $108 \pm 28 \mu\text{g g}^{-1}$ (1SD, $n = 12$; Bruggmann et al., 2019; Gueguen et al., 2016b), suggesting authigenic Cr enrichments in these environments may present a major Cr sink (Reinhard et al., 2013; Wei et al., 2018). Suboxic and anoxic sediment leaches targeting authigenic Cr are isotopically light relative to regional and basin-scale deepwater (Bruggmann et al., 2019; Gueguen et al., 2016b), in agreement with predictions for Cr removal in OMZs and biological export (Huang et al., 2021; Janssen et al., 2020; Moos et al., 2020; Nasemann et al., 2020). Down-core records of $\delta^{53}\text{Cr}$ in suboxic sediments demonstrate glacial-interglacial variability, which has been interpreted to reflect changes in ocean oxygenation (Gueguen et al., 2016b). However, given the relationships between biological export and ocean deoxygenation for sediment metal accumulation (e.g., Nameroff et al., 2004) and similar fractionations reported for biogenic export and OMZ removal, it may be difficult to disambiguate these two controls on sedimentary $\delta^{53}\text{Cr}$.

Initial interpretations inferred quantitative removal of Cr to anoxic sediments, suggesting they may serve as an archive of oceanic $\delta^{53}\text{Cr}$ (Reinhard et al., 2014), in a manner analogous to Zn (Section 4.3.4). However, reinterpretations of Cariaco Basin surface sediments ($\delta^{53}\text{Cr} \approx +0.4 \pm 0.1$; Gueguen et al., 2016b) alongside nearby and oceanographically consistent water column data (dissolved $\delta^{53}\text{Cr} \approx +1.2 \pm 0.1$; Goring-Harford et al., 2018; Figure 28), suggest that $\delta^{53}\text{Cr}$ in anoxic sediments may in fact be lighter than ambient seawater by $\approx 0.8 \pm 0.2\%$, which is similar to the isotope separation implied by the global dissolved [Cr]– $\delta^{53}\text{Cr}$ array ($\Delta_{\text{P-R}} \approx -0.7$ to -0.8). While a full assessment of this offset requires truly colocated water and sediment samples, existing data do not support the hypothesis that anoxic sedimentary $\delta^{53}\text{Cr}$ reflects ambient dissolved $\delta^{53}\text{Cr}$ with no isotope offset.

10.4. Prospects

Historically, $\delta^{53}\text{Cr}$ has received most attention as a paleoredox proxy, with most interpretations based on the framework that terrestrial processes result in isotopically heavy Cr reaching the oceans via rivers, without further alteration of $\delta^{53}\text{Cr}$ through oceanic cycling (e.g., Frei et al., 2009, 2014). Although this model may remain generally valid under atmospheric oxygen levels relevant to the early Earth, internal processes in the ocean, including biological productivity, dominate modern $\delta^{53}\text{Cr}$ cycling and may still be influential under strongly reducing conditions (e.g., Bauer et al., 2018).

As the body of high-quality [Cr] and dissolved $\delta^{53}\text{Cr}$ data continue to grow through GEOTRACES, two primary areas of uncertainty have emerged that are currently limiting $\delta^{53}\text{Cr}$ paleoproxy applications: A quantitative apportionment of the balance between productivity- and O_2 -related Cr cycling, and identification of archives that reliably record dissolved $\delta^{53}\text{Cr}$.

10.4.1. Modern

The most pressing issue for the Cr isotope community is to ensure that future water column data are reported according to high standards of intercalibration and quality control. In addition to this issue, several targets are needed to address specific mechanistic controls on the modern ocean Cr and $\delta^{53}\text{Cr}$ cycles. First, improved constraints on biological and OMZ-mediated Cr removal and the relative importance of these two processes would help to better understand the modern Cr biogeochemical cycle. Direct and robust determinations of fractionation factors associated with biologically mediated Cr export should be prioritized, along with a better understanding of differences in Cr removal among taxa, as well as interrogation of the mechanisms by which phytoplankton reduce and scavenge Cr. More studies have assessed fractionation factors for OMZs, but quantitative constraints are still limited and it is unclear as to what extent OMZ-related processes influence open marine (Cr) and dissolved $\delta^{53}\text{Cr}$.

Second, central to OMZ and biogenic Cr removal are understandings of how much Cr is exported with particles, how much of this reaches the seafloor, and how much is eventually buried in marine sediments. Data from marine particulates, currently limited by high filter blanks and low particulate Cr concentrations, are sorely needed to address these points. Additionally, data for marine particles may help to assess to what extent middepth scavenging outside of OMZs, known to be important for other scavenging-prone metals (e.g., Ohnemus et al., 2019, Sections 3–5), shapes Cr distributions. More data are needed from porewaters and surface sediments to better understand benthic Cr fluxes and Cr burial. Finally, some aspects of the modern global biogeochemical cycle, such as fluxes from hydrothermal vents, remain completely unconstrained.

10.4.2. Paleo

Ideal archives for $\delta^{53}\text{Cr}$ paleoproxy applications should faithfully reflect a known oceanic condition (e.g., dissolved $\delta^{53}\text{Cr}$) or processes (e.g., Cr removal in OMZs) and should have a sufficient Cr content so that sample availability is not a limiting factor. It is also clear from the $\delta^{53}\text{Cr}$ paleoproxy research to date that careful record selection is necessary to avoid samples with minimal overprinting or alteration of primary $\delta^{53}\text{Cr}$ records (e.g., Albut et al., 2018; Rimmelzwaal et al., 2019; Wang et al., 2021). Given these constraints, the following points summarize the most promising archives, which may also offer an opportunity to reevaluate literature data—mostly interpreted in terms of paleoredox—in the context of paleoproductivity.

At present, carbonate-hosted $\delta^{53}\text{Cr}$ remains a challenging archive for several reasons, including: Low Cr-Ca, taxon-dependent Cr isotope fractionations, fractionation during inorganic calcite precipitation, and potential diagenetic overprinting in marine sediments (e.g., Holmden et al., 2016; Pereira et al., 2016; Rimmelzwaal et al., 2019). Additional research is needed to assess to what extent variable taxon-dependent fractionations and diagenetic overprinting can be recognized and corrected before applying $\delta^{53}\text{Cr}$ in marine carbonates. Existing data indicate that Fe–Mn crusts are not suitable $\delta^{53}\text{Cr}$ archives (Wei et al., 2018). Other oxic sedimentary archives, such as authigenic clays, may be suitable, but little is known about the degree to which sedimentary and oceanic Cr and $\delta^{53}\text{Cr}$ exchange, the role of oxic sedimentary phases in the Cr cycle (and the relevant isotope separation factors), and the depths in the water column recorded by these phases.

Black shale records of $\delta^{53}\text{Cr}$ have been used to investigate oceanic oxygenation levels over time. However, the uncertainty regarding how faithfully anoxic and suboxic sediments record ambient conditions in the modern ocean combined with potential $\delta^{53}\text{Cr}$ homogenization among sediment phases (Frank et al., 2020) suggests more research is needed to validate shales as reliable records before further applications. Furthermore, early interpretations of quantitative removal of Cr to anoxic sediments are not supported by the current body of water column data. Consequently, more research is needed to validate the use of anoxic sediments to reconstruct water column $\delta^{53}\text{Cr}$, such as identification of suitable correction factors based on colocated water column and sediment data. Similarly, oceanographically consistent water column data are sparse relative to suboxic sedimentary measurements, complicating assessments of the impact of Cr loss to sediments. Disentangling local reduction-based accumulation from Cr delivery to suboxic and anoxic sediments via biogenic particles may be challenging, given the importance of both these processes on Cr cycling and the linkages between biological export and oxygen depletion.

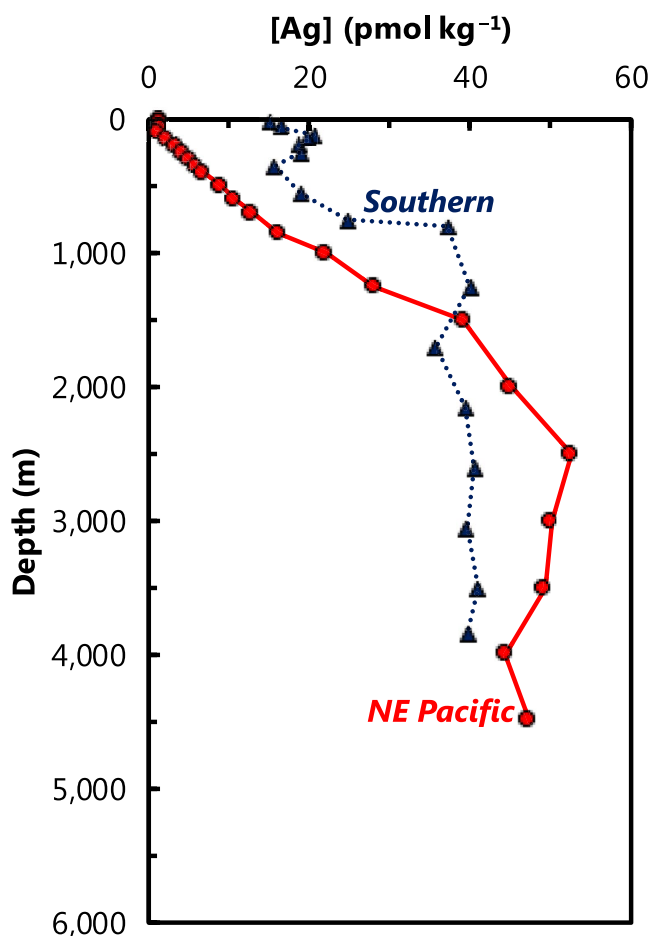


Figure 30. Representative profiles of dissolved Ag concentrations ($[Ag]$). Data from the Northeast Pacific (circles, solid line; Fischer et al., 2018) and Southern Oceans (triangles, dotted line; Boye et al., 2012). Station locations as per Figure 1. Data from the Northeast Pacific were extracted graphically using WebPlotDigitizer (Rohatgi, 2019). The authors are not aware of the existence of any Ag isotope data for seawater at this time.

11. Silver

Silver is the scarcest of the bioactive trace metals described here—within Earth's crust, in the modern ocean (Table 1), and from an observational point of view. Like Ba, Ag is an unusual candidate for a paleoproductivity proxy given that it possesses no known biological function and is most widely known for its antimicrobial properties. Despite this, $[Ag]$ exhibits a characteristic nutrient-like profile in seawater, most similar to that of $[Si]$ (or $[Zn]$, $[Ba]$; Figures 1 and 30), and Ag content in certain sediments is positively correlated with organic C. These intriguing features warrant further investigation into whether and how marine Ag cycling might reflect ocean productivity.

11.1. Marine Distribution

Dissolved Ag occurs primarily as chloride complexes in seawater (Cowan et al., 1985; Miller & Bruland, 1995) and exhibits a nutrient-type depth profile; $[Ag]$ in surface waters are typically <5 pmol kg^{-1} , and range from 5–30 pmol kg^{-1} in deep waters of the Atlantic Ocean to 50–114 pmol kg^{-1} in the Pacific Ocean (Figure 30; Boye et al., 2012; Flegal et al., 1995; Kramer et al., 2011; Rivera-Duarte et al., 1999; Ranville & Flegal, 2005; Ndung'u et al., 2001; Zhang et al., 2001, 2004). The total observed range in seawater is 0.2–115 pmol kg^{-1} (Gallon and Flegal, 2015). Despite its potential as a biogeochemical proxy, no Ag isotope data currently exist for dissolved or particulate phases in the water column, nor in marine sedimentary archives. Accordingly, we cannot directly assess the utility of $\delta^{109}Ag$ to infer paleoproductivity, though we can deduce a number of processes that are likely to influence dissolved $\delta^{109}Ag$ based on the processes known to cycle Ag (Figure 31).

11.2. Driving Processes

The typical $[Ag]$ depth profile (Figure 30) is similar to that of $[Si]$, resulting in a strong positive correlation between these elements in existing datasets. This has led researchers to suggest that Ag is taken up by diatoms, incorporated into their frustules, and then released as the frustules dissolve (e.g., Flegal et al., 1995). Silver might then be delivered to the seafloor with opal, potentially making it useful as a paleoproductivity proxy (Friedl & Pedersen, 2002). Silver is taken up by various types of phytoplankton, including diatoms (Fisher & Wentz, 1993); however, experiments conducted using the marine diatom *Thalassiosira pseudonana* show that, similar to Zn (Section 4.3.2), most of the Ag is associated with the organic fraction rather than the opal (Wagner, 2013). Moreover, the correlation between dissolved $[Ag]$ and $[Si]$ is nonlinear, indicating that other factors are at play (Zhang et al., 2001, 2004). Martin et al. (1983) also hypothesized that high particulate Ag concentration within the euphotic zone (40–70 m) off the west coast of Mexico were due to the formation of Ag-organic complexes. Interestingly, particulate Ag concentrations are even higher well below the euphotic zone, at a depth corresponding to the upper portion of the local OMZ (Martin et al., 1983). It could also be that the global $[Ag]$ – $[Si]$ correlation arises at least in part from biological processes occurring in the surface of the Southern Ocean, whereby intermediate and mode waters with low preformed $[Ag]$ are advected to lower latitudes, analogous to the mechanism proposed for $[Zn]$ – $[Si]$ (Vance et al., 2017) and $[Ba]$ – $[Si]$ coupling (Horner, Kinsley, & Nielsen, 2015). If correct, Ag is unlikely to be coupled directly to opal via a simple relationship that can be used to reconstruct past diatom productivity.

Even if driven by productivity, $[Ag]$ distributions may become decoupled from productivity by possessing different source and sink terms relative to carbon and the macronutrients (Gallon & Flegal, 2015 and references therein). For example, Ranville & Flegal (2005) and Ranville et al. (2010) invoked an anthropogenic

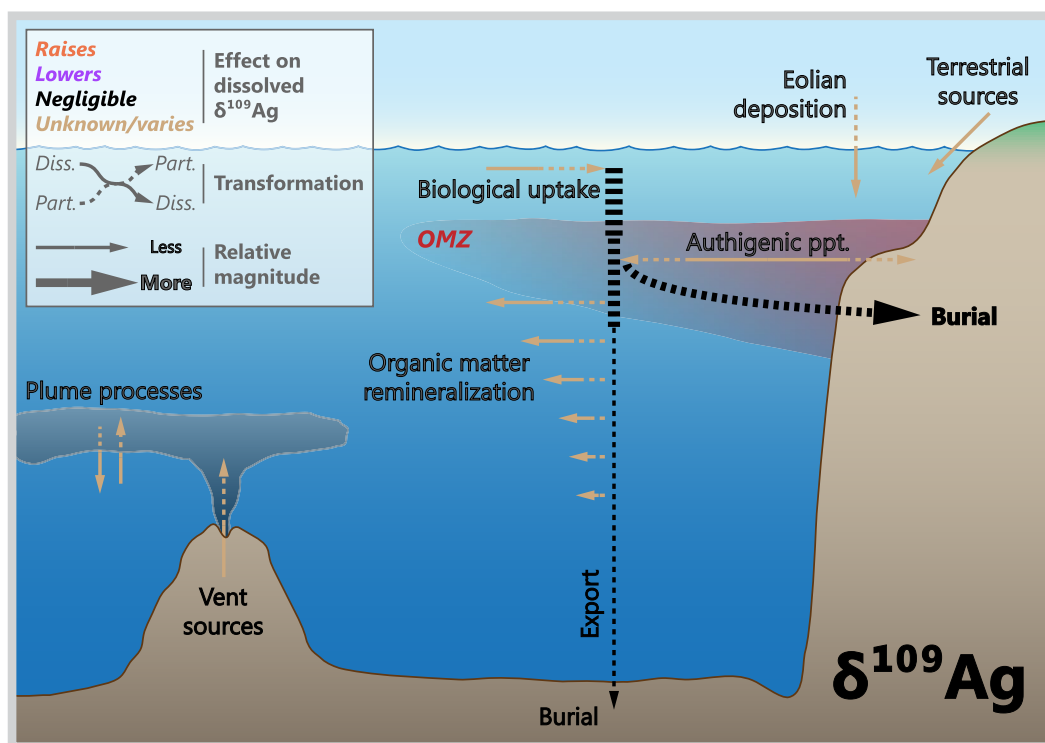


Figure 31. Processes likely to drive Ag isotope variations in modern seawater. Despite there being no Ag isotope data for seawater at this time, we can infer a number of processes that are most likely to influence dissolved $\delta^{109}\text{Ag}$ from measurements of $[\text{Ag}]$ in seawater and sediments.

aerosol source of Ag to surface and intermediate waters to explain north Pacific water column data. Other complications may arise under low $[\text{O}_2]$ environments—waters from the Northeast Pacific (Kramer et al., 2011) and southeastern Atlantic (Boye et al., 2012) exhibit a deficit in $[\text{Ag}]$ relative to $[\text{Si}]$ within their respective OMZs. These deficits imply preferential removal of Ag over Si, which may occur locally or “upstream.” If occurring locally, a putative mechanism is co-precipitation with other chalcophile elements, analogous to the sulfide-mediated mechanism proposed for Cd in OMZs (Janssen et al., 2014; Section 6.2.2). Alternatively, the deficit may reflect low preformed $[\text{Ag}]:[\text{Si}]$ in intermediate waters, which is inherited from preferential drawdown of Ag over Si in regions upstream where these intermediate waters were last ventilated. Both interpretations have implications for the use of Ag or $\delta^{109}\text{Ag}$ as a paleoproxy: The former implies a redox sensitivity that depends on the changing location, spatial extent, and intensity of low $[\text{O}_2]$ regions in the oceans over time, whereas the latter implies a sensitivity to ecology and the geometry of ocean circulation. Both interpretations warrant additional scrutiny.

11.3. Marine Archives

Bulk sediments are the main archive that has been investigated for their potential to record information about the marine Ag cycle. The Ag content of bulk sediments from open marine environments range from $\leq 100 \text{ ng g}^{-1}$ (i.e., typical lithogenic values) up to 100s of ng g^{-1} (Koide et al., 1986). In general, low Ag contents are typical of well-oxygenated sediments, while higher Ag contents are typical of sediments formed in oxygen-poor and euxinic environments. The general consensus has been that Ag enrichment in anoxic sediments is the result of post-depositional precipitation of Ag_2S (Koide et al., 1986) or possibly Ag selenide (Böning et al., 2005; Crusius & Thomson, 2003). However, high Ag content is also documented in marine sediments that are only weakly reducing (Böning et al., 2004, 2005; McKay & Pedersen, 2008; Morford et al., 2008). Furthermore, even in anoxic sediments, the degree of Ag enrichment exceeds what would be expected from post-depositional Ag precipitation alone (Böning et al., 2009; Borchers et al., 2005; McKay & Pedersen, 2008). Thus, redox-controlled, post-depositional precipitation is not the primary con-

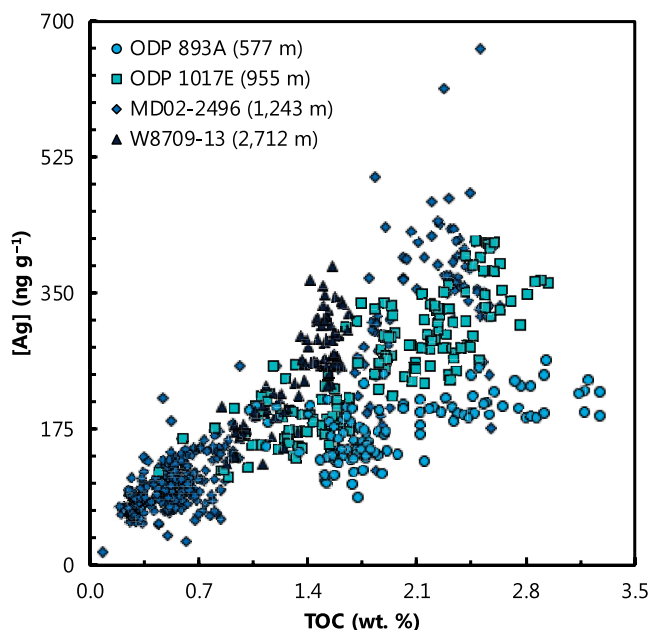


Figure 32. Concentrations of Ag and total organic carbon in sediment cores from the Northeast Pacific Ocean. These data illustrate that Ag is broadly correlated with organic matter in bulk sediments, which is promising from the perspective of developing Ag as a paleoproductivity proxy. Core MD02-2496 (Vancouver Island Margin; 48.97°N, 127.04°W, 1,243 m water depth) from Chang et al., 2014; Core W8709-13PC (Oregon Margin; 42.116°N, 125.75°W; 2,712 m water depth) from Kienast, 2003; ODP 1017E (Southern California; 34.53°N, 121.1°W; 955 m water depth) from Hendy & Pedersen, 2005; ODP 893A (Santa Barbara Basin; 34.287°N, 120.036°W; 576.5 m water depth) from Ivanochko, 2001.

control on Ag accumulation in marine sediments, implying that there must also be a flux of non-lithogenic, particulate Ag to the seafloor (McKay & Pedersen, 2008).

McKay and Pedersen (2008) hypothesized that Ag, like Ba, accumulates in organic-rich settling particles. However, in contrast to Ba, Ag precipitation requires a reduced microenvironment within the particle, which is generally only possible in waters that possess relatively low $[O_2]$ (e.g., Bianchi et al., 2018). The analysis of sediment trap samples from the Northeast Pacific show that the fluxes of particulate Ag and particulate organic carbon positively correlate (Martin et al., 1983). This correlation is also seen in surface sediments (McKay & Pedersen, 2008) and sediment cores from the Northeast Pacific (Figure 32). These data broadly support the use of particulate Ag flux as a paleoproductivity proxy, with an important caveat: The post-depositional preservation of particulate Ag requires that sedimentary porewaters remain reducing, as settling particulate Ag formed below the euphotic zone is not preserved if sediments are oxidizing (McKay and Pedersen, 2008; Morford et al., 2008). Thus, while the delivery of particulate Ag to sediments appears related to productivity (Wagner et al., 2013), Ag delivery to—and preservation within—sediments is also sensitive to $[O_2]$; firstly because low water column $[O_2]$ favors higher Ag:C of sinking particles, and secondly because low $[O_2]$ will lead to greater Ag preservation at the seafloor. By analogy to other metals (e.g., Twining & Baines, 2013), variations in surface water $[Ag]$ may also offer a third means of modulating Ag:C, though remains to be tested. These three sensitivities likely explain why different regions exhibit distinct arrays in Ag–TOC space (Figure 32). Despite these regional variations, the relationships between Ag and organic matter are promising from the point of view of tracing past productivity.

Though yet to be investigated for $\delta^{109}Ag$, Ag is predicted to be somewhat mobile in Fe–Mn crusts, with a predicted diffusivity $\leq 10^{-7} \text{ cm}^2 \text{ yr}^{-1}$ (see Henderson & Burton, 1999, for calculation details), similar to Cd (Section 6.3.2), Mo (Section 7.3), and Cr (Section 10.3.2). This rate implies that, should any long-term records be forthcoming, Fe–Mn crust based reconstructions of $\delta^{109}Ag$ are likely to exhibit some diffusive smoothing while preserving larger perturbations.

11.4. Prospects

The apparent linkages between $[Ag]$ and particulate Ag, macronutrients, and organic matter provides tantalizing evidence that Ag cycling may be related to surface productivity (Figure 30). Moreover, coretop studies indicate that the geochemical signature of this coupling is preserved under certain environmental conditions (Figure 32). Despite this progress, the study of Ag in marine biogeochemical cycles remains in its infancy, particularly compared to many of the other elements described here. Additional constraints are needed in several areas, including: The role of biogeochemical processes in mediating Ag distributions in the water column, the dominant controls on the downward transport of Ag through the oceans, and on the controls on Ag preservation in sediments. Given what has been learned from the application of the other trace metal isotope systems described here, new analytical developments in Ag isotope geochemistry could help place valuable constraints on these areas.

12. Synthesis

In this final section, we synthesize and describe the overall suitability to trace productivity (Section 12.1), explore inter-element similarities (Section 12.2), define proxy readiness (Section 12.3), and outline a number of research priorities (Section 12.4) for using Fe, Zn, Cu, Cd, Mo, Ba, Ni, Cr, and Ag and their isotopes as paleoproductivity proxies.

12.1. Overall State of the Proxies

Taking a general view, the review of each element highlights that our knowledge of bioactive trace metal isotope systematics lags behind those of trace element abundances and far behind those of macronutrient isotopes (e.g., Farmer et al., 2021). The bioactive metal isotope field is nascent; excepting Mo, the very first isotope data for seawater for all of the elements reviewed here were published within the last 15 years, or—in the case of Ag—are yet to be reported. The field is thus decades behind the trace metal concentration community. Despite the lack of detail, we can begin to classify the metals reviewed here into three broad categories: Those where there are clear and promising signs that a metal can serve as a proxy of paleoproductivity, such as for $\delta^{114}\text{Cd}$, $\delta^{138}\text{Ba}$, $\delta^{60}\text{Ni}$, and $\delta^{53}\text{Cr}$; those where a metal is unlikely to directly inform on paleoproductivity, as for $\delta^{56}\text{Fe}$, $\delta^{66}\text{Zn}$, $\delta^{65}\text{Cu}$, and $\delta^{98}\text{Mo}$; and those where simply too little is known to confidently assign utility at this time, as for $\delta^{109}\text{Ag}$.

More specifically, this review highlights the importance of ocean circulation in mediating the distribution of several bioactive trace metals and their isotopes. Key features of the isotope distributions reviewed here reflect a mixture of local (i.e., *in situ*) and regional (or *ex situ*) processes, with the latter often set far upstream of any given locality. Indeed, researchers are recognizing that, much like the macronutrients (see Farmer et al., 2021), the first-order features of many metals are not controlled locally by a given dissolved–particulate transformations, but reflect a regionally integrated history of vertical cycling and mixing that is imparted over the scale of an ocean basin, which we discuss next.

12.2. The Reactor Model Applied to Select Trace Metal Isotope Systems

Today, the Southern Ocean represents the common starting point and ultimate source of many TEIs for low latitude thermoclines (e.g., Sarmiento et al., 2004; Talley, 2013). If we assume that the reaction progress term in the reactor model is analogous to the fraction of initially supplied nutrient left unconsumed by phytoplankton, the concentration and isotope composition of a Me in the Southern Ocean can be assumed to represent the starting composition of a metal in the isotope reactor (i.e., $[\text{Me}]$ and $\delta^i\text{Me}_{\text{R},0}$ when $f = 0$). Our study suggests that four of the nine bioactive trace metals reviewed here (Cd, Ba, Ni, and Cr) are suitable candidates for the isotope reactor model, which we now use to constrain $\Delta_{\text{p-r}}$ for both Steady State (SS) and Rayleigh Distillation (RD). We assume that samples from the upper 1,000 m of the Southern Ocean represent the initial reactor conditions (Figure 33). Downstream of the Southern Ocean, we regress only those samples shallower than 200 m to ensure that the models only consider productivity-associated Me drawdown. Our example calculations are intended to be illustrative, rather than the definitive estimate of $\Delta_{\text{p-r}}$ for each metal; comprehensive, global compilations are described elsewhere for Cd (Sieber, Conway, de Souza, Hassler et al., 2019; Xie et al., 2017), Ba (Horner & Crockford, 2021; Hsieh & Henderson, 2017), Ni (Yang et al., 2020), and Cr (Rickli et al., 2019; Wei et al., 2020). Accordingly, we limit our example to the stations shown in Figure 1.

Excepting the RD model for Cd, the reactor models generate a reasonable fit to the shallow water data, with best-fit $\Delta_{\text{p-r}}$ of $-0.75 \pm 0.02\text{‰}$ (SS) and $-0.23 \pm 0.16\text{‰}$ (RD) for Cd ($n = 6$), $-0.54 \pm 0.03\text{‰}$ (SS) and $-0.35 \pm 0.03\text{‰}$ (RD) for Ba ($n = 16$), $-0.54 \pm 0.04\text{‰}$ (SS) and $-0.36 \pm 0.04\text{‰}$ (RD) for Ni ($n = 20$), and $-0.84 \pm 0.04\text{‰}$ (SS) and $-0.71 \pm 0.04\text{‰}$ (RD) for Cr ($n = 18$; all \pm represent the root-mean-square deviation). These values are generally within the accepted ranges reported for each metal, either for oceanographic data or specific experiments (e.g., culture studies, mineral precipitation). The reactor models illustrate that best-fit $\Delta_{\text{p-r}}$ for SS are larger in magnitude than for RD. This difference derives from mixing. Open-system models account for continuous uptake and removal of Me from the reactor, thus requiring a larger $\Delta_{\text{p-r}}$ to render an equivalent change in $\delta^i\text{Me}_{\text{R}}$ compared to RD. In general therefore, calculations

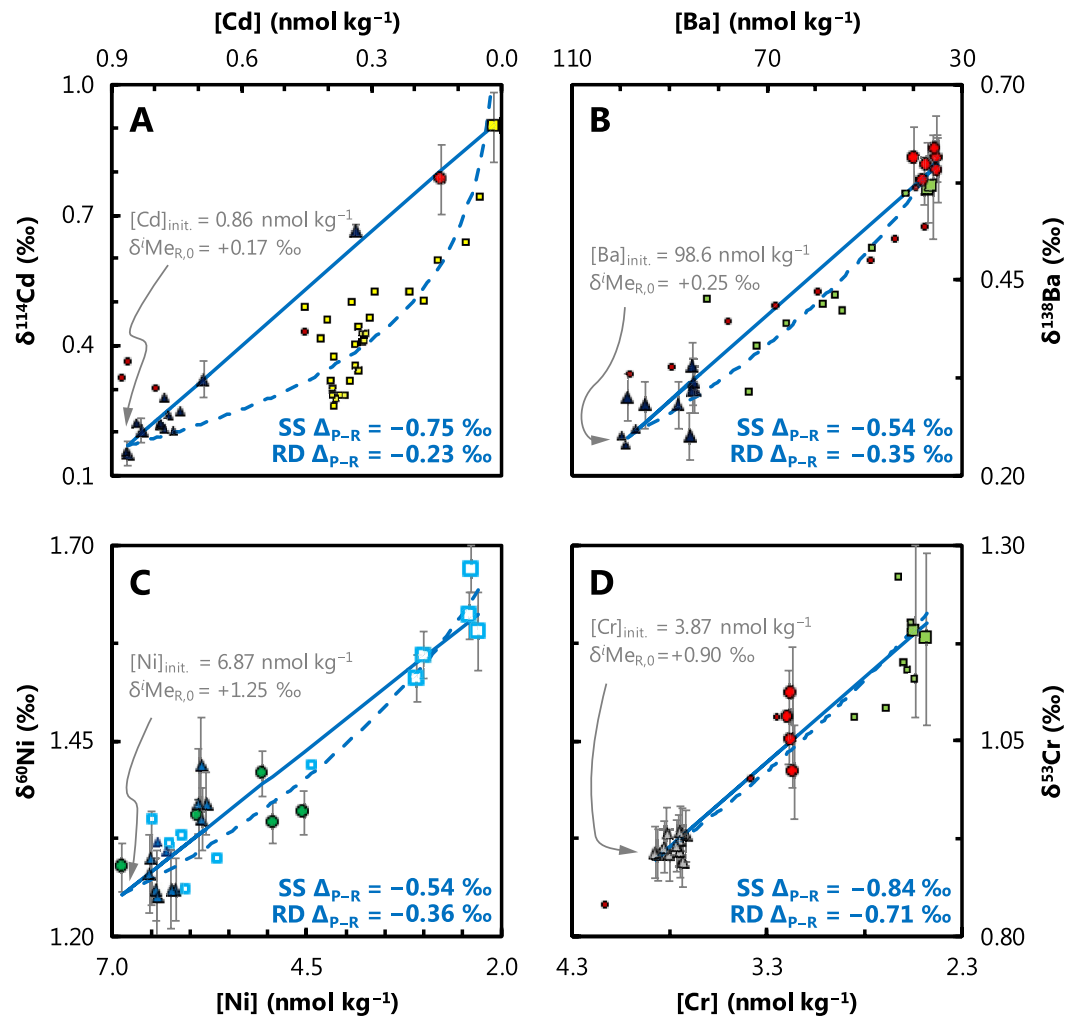


Figure 33. Reactor framework applied to select bioactive trace metal isotope systems. Station locations and symbols as per Figure 1. (a–d) Isotope reactor models for Cd (a), Ba (b), Ni (c), and Cr (d) showing evolution of the residual reactant during Me consumption. Best-fit Δ_{P-R} are shown for Steady State (SS; solid) and Rayleigh Distillation fractionation (RD; dashed lines) based on a common Southern Ocean starting point (arrow). The large and small symbols indicate data that are regressed in the model and those that are not, respectively; samples from the top 1,000 m of the Southern Ocean are included, whereas only those above 200 m are included from elsewhere. This screening focuses the regression models on productivity-associated Me drawdown, which occurs shallowly. Samples with extreme Cd isotope compositions ($\delta^{114}Cd > +1\text{‰}$) are excluded from the model given that it is unclear if these are true oceanographic features (see Section 6.4.1).

assuming SS will be closer to the underlying value of Δ_{P-R} , since the surface ocean is poorly represented by a closed-system reactor.

In practical terms, knowledge of Δ_{P-R} , derived using the reactor framework, allows for the isotope compositions of Cd, Ba, Ni, and Cr to be interpreted in terms of reflecting the balance between supply and demand for that Me in the surface ocean reactor (i.e., *f*). Though this does not confer direct information about the total quantity of nutrients consumed, it offers a means to assess the spatial pattern of nutrient utilization in Earth's past. The spatial dependency is particularly important to consider, since the geometry of ocean circulation cannot be assumed constant over time. However, if assuming that the flux of a Me to the sea-floor is proportional to export productivity, the combination of metal fluxes with metal isotopes can offer insights into patterns of paleoproductivity and circulation by constraining export and fractional nutrient use, respectively.

Table 2
Proxy Development Assessment

Section	Proxy	1. Analytical protocols?	2. Distribution in environment?	3. Driving process isolated?	4. Sedimentary archives?	5. Effect of diagenesis?	Goal: Productivity reconstruction?
3	[Fe] $\delta^{56}\text{Fe}$	Applied	Applied	Developing	Developing	Developing	Unknown
4	[Zn] $\delta^{66}\text{Zn}$	Applied	Applied	Developing	Developing	Developing	Unknown
5	[Cu] $\delta^{65}\text{Cu}$	Applied	Applied	Developing	Developing	Developing	Unknown
6	[Cd] $\delta^{114}\text{Cd}$	Applied	Applied	Developing	Developing	Developing	Unknown
7	[Mo] $\delta^{99}\text{Mo}$	Applied	Applied	Developing	Developing	Unknown	Unknown
8	[Ba] $\delta^{138}\text{Ba}$	Applied	Applied	Developing	Developing	Unknown	Unknown
9	[Ni] $\delta^{60}\text{Ni}$	Applied	Applied	Developing	Developing	Developing	Unknown
10	[Cr] $\delta^{53}\text{Cr}$	Applied	Applied	Developing	Developing	Developing	Unknown
11	[Ag] $\delta^{109}\text{Ag}$	Applied	Applied	Unknown	Unknown	Unknown	Unknown

Key
Unknown
Developing
Applied
Unlikely

Note. The progress toward five objectives is assessed for each bioactive metal proxy system and assigned a development level ranging unknown to unlikely, corresponding to the least and most certain assignments, respectively. Some trace metal isotope systems possess split designations (stripes). Definitions of each development level are described in Section 12.3 and discussed in detail for each metal system in the corresponding section.

Combined C export-*f* approaches are largely unexplored in paleoceanographic studies, and we believe they offer the best opportunity for using bioactive trace metal isotope systems to constrain paleoproductivity. These approaches will prove most powerful when the constraints on C export and *f* are derived from the same Me system, since this minimizes the importance of other metal-cycling processes. However, multi-proxy approaches may also prove useful in differentiating between productivity- and non productivity-driven variations in metal cycling. For example, Cd, Ba, Ni, and Cr isotopes are all expected to exhibit coherent variations in their distributions if productivity or ocean circulation varied. In contrast, changes in mean ocean redox state, benthic fluxes, or terrestrial sources would render distinct changes in the distribution of each Me consistent with its sensitivity to that process. The cycling of other metals that are not directly sensitive to productivity—Fe, Zn, Cu, and Mo—could also be used to provide oceanographic context for paleoproductivity records, thus helping to build a more robust picture of marine biogeochemistry at key points in Earth's history.

12.3. Proxy Readiness

We now assess the overall readiness of each bioactive trace metal isotope system to reconstruct productivity, summarized in Table 2. This exercise is analogous to the assessment of analytical techniques used in chemical oceanography described by Fassbender et al. (2017). Our assessment is similarly conducted in two dimensions. First, we identify five objectives toward the development of a reliable productivity proxy, ranging from development of the analytical capabilities necessary to measure that species, to constraining diagenetic effects, and ending with the goal of using that species to reliably reconstruct paleoproductivity itself. Second, we assess the level of development within each objective. Our reasoning behind the assignments is described above in Sections 3–11.

Reliable application of a TEI as a proxy requires that five objectives be serially met (e.g., Hillaire-Marcel & Vernal, 2007; Table 2). In practical terms, however, the final stage (proxy application) is often realized before many of the supporting objectives; variations in elemental or isotopic ratios in the sedimentary record commonly provide the motivation for developing a more holistic understanding of that isotope system in the modern environment. A common critique of this approach is that subsequent studies often invalidate

earlier interpretations. The five objectives that follow are common to the development of almost any proxy. First, it is essential to develop the analytical capability to measure the species of interest commensurate with the quantities typically encountered in the environment. In the case of trace element abundance proxies, the development and widespread adoption of ICP-MS instrumentation coupled to automated sample preparation systems has enabled low-blank, high-throughput, high-sensitivity analyses of multiple trace elements in both seawater (e.g., Wuttig et al., 2019) and sediments alike (e.g., Wefing et al., 2017). In contrast, the techniques required to measure many trace metal isotope systems have only been developed within the past decade—or are still in development—and generally remain labor intensive and time consuming. Second, it is important to map the broad vertical and spatial patterns of a TEI system in the modern ocean. The GEOTRACES program has provided a coordinated opportunity to study the basin-scale distributions of multiple TEIs. Third, the utility of a proxy is significantly increased if the driving processes are understood. These processes may be isolated through a number of approaches, including: Lab-based analogue experimentation, numerical modeling, and high-resolution spatiotemporal environmental studies. Fourth, paleoceanographic proxies require sedimentary archives—a substrate from which to reconstruct the variable of interest. The latter necessitates knowledge of how a trace metal partitions between seawater and sediment, such as through a coretop study, ideally conducted across large environmental gradients. Since many marine sedimentary archives are biogenic in origin, additional experimentation isolating “vital effects” may be necessary. Fifth, proxies are only as reliable as their archives are hardy. Diagenetic processes may alter primary environmental signatures, and recognizing these effects is imperative for reliably reconstructing past environmental conditions.

Here, we assess the level of development for each marine bioactive trace metal isotope system within each objective on a four point scale: Unknown, developing, applied, and unlikely. The levels define a continuum from least to most understood, and are a useful shorthand for illustrating where additional work is most needed. Assignment of “unknown” implies that too little is presently known to reliably assess progress toward that objective; we cannot judge if these isotope systems may or may not ultimately be useful in reconstructing ocean productivity. “Developing” objectives are those where there are pilot studies on that topic, but overall there are an insufficient number to define general rules for that system. If a trace metal isotope system is widely recognized to be useful toward some objective, it is given a score of “applied.” If the preponderance of evidence indicates that a trace metal isotope system is not suitable for reconstruction of paleoproductivity, a score of “unlikely” is given. This does not rule out future developments, such as identification of environmental control variables or new sedimentary archives, only that current data (and archives) do not support use of the isotope system toward this goal. Lastly, we recognize that there are continual refinements to analytical protocols, environmental distributions, etc. and thus, at some level, all five objectives could reasonably be described as “developing.” Rather, our assignments are intended to give a relative sense of understanding between different metal isotope systems toward the overarching goal of reconstructing past ocean productivity.

12.4. Outlook

We close by outlining three general priorities for further study. First, a number of modern ambiguities require addressing. Most notable is the apparent “missing” source and/or sink terms for the whole ocean isotopic budgets of several bioactive metals, including Cu, Cd, Ba, and Ni. Though it is possible that these missing source and sink terms represent true non-steady state imbalances in the flux of these elements to and from the ocean, we view it more likely that there are major fluxes that remain uncharacterized. The origin of these imbalances is most pressing for those elements where the output flux associated with organic matter constitutes a minor sink (e.g., Zn, Ni), as the isotopic budget of these elements is most susceptible to decoupling from productivity. Second, the significance of ocean circulation in mediating basin-scale trace metal distributions implies that paleoceanographic interpretations made from a single site cannot be uniquely interpreted in terms of either changes in productivity or ocean circulation without additional constraints. Such constraints could take the form of independent circulation estimates—from numerical models or canonical circulation proxies measured in the same samples—or by measuring trace metal isotope distributions in spatially distributed sediment samples. Third, the lack of suitable archives with which to reconstruct surface water trace metal isotopic compositions afflicts almost every element reviewed here.

Overcoming this limitation will require the most creativity; we suggest more studies testing the fidelity of non-traditional substrates (e.g., mixed foraminiferal assemblages, coccolith calcite, diatom opal), periodic reassessment of the feasibility of traditional substrates following analytical advancements (e.g., improvements in ion transmission efficiency, large-scale [automated and/or crowd-sourced] picking of monospecific foraminiferal assemblages), and development and validation of selective extraction protocols that can be used to isolate phases of interest from complex matrices. Though attempting to overcome these limitations may be considered high risk, we believe that this risk is more than justified by the reward of developing a more complete understanding of Earth's biogeochemical history.

Appendix A: GEOTRACES–PAGES Biological Productivity Working Group Members

C. Bolton (CEREGE, Univ. Aix-Marseille, CNRS, IRD, Collège de France, INRAE, Aix-en-Provence, France); E. Calvo (Institut de Ciències del Mar, CSIC, Barcelona, Spain); D. Cardinal (LOCEAN (UMR7159), Sorbonne Université, IRD, CNRS, MNHN, Paris, France); T. de Garidel-Thoron (CEREGE, Univ. Aix-Marseille, CNRS, IRD, Collège de France, INRAE Aix-en-Provence, France); S. Fietz (Department of Earth Sciences, Stellenbosch University, Stellenbosch South Africa); K. R. Hendry (School of Earth Sciences, University of Bristol, Bristol, UK); F. Marcantonio (Department of Geology and Geophysics, Texas A&M University), P. A. Rafter (Department of Earth System Science, University of California, Irvine, CA, USA); H. Ren (Department of Geosciences, National Taiwan University, Taipei, Taiwan); C. J. Somes (GEOMAR Helmholtz Centre for Ocean Research Kiel, 24105 Kiel, Germany); J. N. Sutton (Univ Brest, CNRS, IRD, Ifremer, Institut Universitaire Européen de la Mer, LEMAR, Plouzané, France); A. Torfstein (Institute of Earth Sciences, Hebrew University, Jerusalem, & InterUniversity Institute for Marine Sciences, Eilat, Israel); G. Winckler (Lamont-Doherty Earth Observatory of Columbia University, Palisades, NY, USA).

Acknowledgments

This contribution grew (and grew) out of a joint workshop between GEOTRACES and Past Global Changes (PAGES) held in Aix-en-Provence in December 2018. The workshop was funded by the U.S. National Science Foundation (NSF) through the GEOTRACES program, the international PAGES project, which received support from the Swiss Academy of Sciences and NSF, and the French program Les Envelopes Fluides et l'Environnement. The authors extend tremendous thanks to the GEOTRACES–PAGES workshop organizers, particularly Bob Anderson, Catherine Jeandel, Laurence Vidal, and Kazuyo Tachikawa. This synthesis benefited from the insights of the Associate Editor (Noah Planavsky) and from detailed and constructive reviews by Seth John and an anonymous reviewer. T. J. Horner acknowledges support from NSF; S. H. Little from the UK Natural Environment Research Council (NE/P018181/1); T. M. Conway from the University of South Florida; and, J. R. Farmer from the Max Planck Society, the Tuttle Fund of the Department of Geosciences of Princeton University, the Grand Challenges Program of the Princeton Environmental Institute, and the Andlinger Center for Energy and the Environment of Princeton University. Most importantly, we acknowledge the hundreds of scientists who have generated GEOTRACES-compliant TEI data that made this synthesis possible.

Conflict of Interest

The authors declare no conflicts of interest relevant to this study.

Data Availability Statement

The majority of the dissolved data were sourced from the GEOTRACES Intermediate Data Products in 2014 (Mawji et al., 2015) and 2017 (Schlitzer et al., 2018), and citations to the primary data sources are given in the caption for each figure. Data sources for Figure 1 are given below. Figure 1: Iron: Conway & John, 2014a (Atlantic); Conway & John, 2015a (Pacific); Abadie et al., 2017 (Southern). Zinc: Conway & John, 2014b (Atlantic); Conway & John, 2015a (Pacific); R. M. Wang et al., 2019 (Southern). Copper: Little et al., 2018 (Atlantic); Takano et al., 2017 (Pacific); Boye et al., 2012 (Southern). Cadmium: Conway and John, 2015b (Atlantic); Conway & John, 2015a (Pacific); Abouchami et al., 2014 (Southern). Molybdenum: Nakagawa et al., 2012 (all basins). Barium: Bates et al., 2017 (Atlantic); Geyman et al., 2019 (Pacific); Hsieh & Henderson, 2017 (Southern). Nickel: Archer et al., 2020 (Atlantic); Takano et al., 2017 (Pacific); R. M. Wang et al., 2019 (Southern). Chromium: Goring-Harford et al., 2018 (Atlantic); Moos & Boyle, 2019 (Pacific); Rickli et al., 2019 (Southern). Silver: Fischer et al., 2018 (Pacific); Boye et al., 2012 (Southern).

References

- Abadie, C., Lacan, F., Radic, A., Pradoux, C., & Poitrasson, F. (2017). Iron isotopes reveal distinct dissolved iron sources and pathways in the intermediate versus deep Southern Ocean. *Proceedings of the National Academy of Sciences*, 114, 858–863. <https://doi.org/10.1073/pnas.1603107114>
- Abouchami, W., Galer, S. J. G., de Baar, H. J. W., Alderkamp, A. C., Middag, R., Laan, P., et al. (2011). Modulation of the Southern Ocean cadmium isotope signature by ocean circulation and primary productivity. *Earth and Planetary Science Letters*, 305(1–2), 83–91. <https://doi.org/10.1016/j.epsl.2011.02.044>
- Abouchami, W., Galer, S. J. G., de Baar, H. J. W., Middag, R., Vance, D., Zhao, Y., et al. (2014). Biogeochemical cycling of cadmium isotopes in the Southern Ocean along the zero meridian. *Geochimica et Cosmochimica Acta*, 127, 348–367. <https://doi.org/10.1016/j.gca.2013.10.022>
- Abouchami, W., Galer, S. J. G., Horner, T. J., Rehkämper, M., Wombacher, F., Xue, Z., et al. (2013). A common reference material for cadmium isotope studies—NIST SRM 3108. *Geostandards and Geoanalytical Research*, 37(1), 5–17. <https://doi.org/10.1111/j.1751-908x.2012.00175.x>
- Achterberg, E. P., & Van Den Berg, C. M. G. (1997). Chemical speciation of chromium and nickel in the western Mediterranean. *Deep Sea Research Part II: Topical Studies in Oceanography*, 44, 693–720. [https://doi.org/10.1016/S0967-0645\(96\)00086-0](https://doi.org/10.1016/S0967-0645(96)00086-0)

- Adkins, J. F., Cheng, H., Boyle, E. A., Druffel, E. R., & Edwards, R. L. (1998). Deep-sea coral evidence for rapid change in ventilation of the deep North Atlantic 15,400 years ago. *Science*, 280(5364), 725–728. <https://doi.org/10.1126/science.280.5364.725>
- Akerman, A., Poitrasson, F., Oliva, P., Audry, S., Prunier, J., & Braun, J. J. (2014). The isotopic fingerprint of Fe cycling in an equatorial soil-plant-water system: The Nsimi watershed, South Cameroon. *Chemical Geology*, 385, 104–116. <https://doi.org/10.1016/j.chemgeo.2014.07.003>
- Albarède, F. (2004). The stable isotope geochemistry of copper and zinc. *Reviews in Mineralogy and Geochemistry*, 55(1), 409–427. <https://doi.org/10.2138/gsrmg.55.1.409>
- Albut, G., Babechuk, M. G., Kleinhanns, I. C., Bengler, M., Beukes, N. J., Steinhilber, B., et al. (2018). Modern rather than Mesoarchaean oxidative weathering responsible for the heavy stable Cr isotopic signatures of the 2.95 Ga old Ijzermijn iron formation (South Africa). *Geochimica et Cosmochimica Acta*, 228, 157–189. <https://doi.org/10.1016/j.gca.2018.02.034>
- Algeo, T. J. (2004). Can marine anoxic events draw down the trace element inventory of seawater? *Geology*, 32(12), 1057–1060. <https://doi.org/10.1130/G20896.1>
- Algeo, T. J., & Lyons, T. W. (2006). Mo-total organic carbon covariation in modern anoxic marine environments: Implications for analysis of paleoredox and paleohydrographic conditions. *Paleoceanography*, 21. <https://doi.org/10.1029/2004PA001112>
- Algeo, T. J., & Maynard, J. B. (2008). Trace-metal covariation as a guide to water-mass conditions in ancient anoxic marine environments. *Geosphere*, 4, 872. <https://doi.org/10.1130/ges00174.1>
- Algeo, T. J., & Tribovillard, N. (2009). Environmental analysis of paleoceanographic systems based on molybdenum-uranium covariation. *Chemical Geology*, 268, 211–225. <https://doi.org/10.1016/j.chemgeo.2009.09.001>
- Allredge, A. L., & Silver, M. W. (1988). Characteristics, dynamics and significance of marine snow. *Progress in Oceanography*, 20(1), 41–82. [https://doi.org/10.1016/0079-6611\(88\)90053-5](https://doi.org/10.1016/0079-6611(88)90053-5)
- Anbar, A. D. (2004). Molybdenum stable isotopes: Observations, interpretations and directions. *Reviews in Mineralogy and Geochemistry*, 55(1), 429–454. <https://doi.org/10.2138/gsrmg.55.1.429>
- Anbar, A. D., Jarzecki, A. A., & Spiro, T. G. (2005). Theoretical investigation of iron isotope fractionation between $\text{Fe}(\text{H}_2\text{O})_6^{3+}$ and $\text{Fe}(\text{H}_2\text{O})_6^{2+}$: Implications for iron stable isotope geochemistry. *Geochimica et Cosmochimica Acta*, 69, 825–837. <https://doi.org/10.1016/j.gca.2004.06.012>
- Anbar, A. D., & Knoll, A. H. (2002). Proterozoic ocean chemistry and evolution: A bioinorganic bridge? *Science*, 297, 1137–1142. <https://doi.org/10.1126/science.1069651>
- Andersen, M. B., Vance, D., Archer, C., Anderson, R. F., Ellwood, M. J., & Allen, C. S. (2011). The Zn abundance and isotopic composition of diatom frustules, a proxy for Zn availability in ocean surface seawater. *Earth and Planetary Science Letters*, 301, 137–145. <https://doi.org/10.1016/j.epsl.2010.10.032>
- Anderson, M. A., Morel, F. M. M., & Guillard, R. R. L. (1978). Growth limitation of a coastal diatom by low zinc ion activity. *Nature*, 276, 70–71. <https://doi.org/10.1038/276070a0>
- Annett, A. L., Lapi, S., Ruth, T. J., & Maldonado, M. T. (2008). The effects of Cu and Fe availability on the growth and Cu:C ratios of marine diatoms. *Limnology & Oceanography*, 53, 2451–2461. <https://doi.org/10.4319/lo.2008.53.6.2451>
- Aplin, A. C., & Cronan, D. S. (1985). Ferromanganese oxide deposits from the central Pacific Ocean. I. Encrustations from the Line Islands Archipelago. *Geochimica et Cosmochimica Acta*, 49(2), 427–436. [https://doi.org/10.1016/0016-7037\(85\)90034-1](https://doi.org/10.1016/0016-7037(85)90034-1)
- Archer, C., Andersen, M. B., Cloquet, C., Conway, T. M., Dong, S., Ellwood, M., et al. (2017). Inter-calibration of a proposed new primary reference standard AA-ETH Zn for zinc isotopic analysis. *Journal of Analytical Atomic Spectrometry*, 32(2), 415–419. <https://doi.org/10.1039/c6ja00282j>
- Archer, C., Vance, D., Milne, A., & Lohan, M. C. (2020). The oceanic biogeochemistry of nickel and its isotopes: New data from the South Atlantic and the Southern Ocean biogeochemical divide. *Earth and Planetary Science Letters*, 535, 116118. <https://doi.org/10.1016/j.epsl.2020.116118>
- Aristilde, L., Xu, Y., & Morel, F. M. M. (2012). Weak organic ligands enhance Zinc uptake in Marine phytoplankton. *Environmental Science & Technology*, 46, 5438–5445. <https://doi.org/10.1021/es300335u>
- Arnold, G. L., Anbar, A. D., Barling, J., & Lyons, T. W. (2004). Molybdenum isotope evidence for widespread anoxia in mid-Proterozoic oceans. *Science*, 304(5667), 87–90. <https://doi.org/10.1126/science.1091785>
- Arrhenius, G. (1963). *Pelagic sediments*. Scripps Institution of Oceanography, University of California.
- Atkins, A. L., Shaw, S., & Peacock, C. L. (2016). Release of Ni from birnessite during transformation of birnessite to todorokite: Implications for Ni cycling in marine sediments. *Geochimica et Cosmochimica Acta*, 189, 158–183. <https://doi.org/10.1016/j.gca.2016.06.007>
- Baars, O., Abouchami, W., Galer, S. J., Boye, M., & Croot, P. L. (2014). Dissolved cadmium in the Southern Ocean: Distribution, speciation, and relation to phosphate. *Limnology & Oceanography*, 59(2), 385–399. <https://doi.org/10.4319/lo.2014.59.2.0385>
- Baars, O., Croot, P. L., & Streu, P. (2011). The speciation of dissolved zinc in the Atlantic sector of the Southern Ocean. *Deep Sea Research Part II: Topical Studies in Oceanography*, 58, 2707–2719. <https://doi.org/10.1016/j.dsr2.2010.10.041>
- Bacon, M. P., & Anderson, R. F. (1982). Distribution of thorium isotopes between dissolved and particulate forms in the deep sea. *Journal of Geophysical Research*, 87(C3), 2045–2056. <https://doi.org/10.1029/jc087ic03p02045>
- Baconnais, I., Rouxel, O., Dulaquais, G., & Boye, M. (2019). Determination of the copper isotope composition of seawater revisited: A case study from the Mediterranean Sea. *Chemical Geology*, 511, 465–480. <https://doi.org/10.1016/j.chemgeo.2018.09.009>
- Badaut, D., & Risacher, F. (1983). Authigenic smectite on diatom frustules in Bolivian saline lakes. *Geochimica et Cosmochimica Acta*, 47(3), 363–375. [https://doi.org/10.1016/0016-7037\(83\)90259-4](https://doi.org/10.1016/0016-7037(83)90259-4)
- Barling, J., & Anbar, A. D. (2004). Molybdenum isotope fractionation during adsorption by manganese oxides. *Earth and Planetary Science Letters*, 217, 315–329. [https://doi.org/10.1016/S0012-821X\(03\)00608-3](https://doi.org/10.1016/S0012-821X(03)00608-3)
- Barling, J., Arnold, G., & Anbar, A. D. (2001). Natural mass-dependent variations in the isotopic composition of molybdenum. *Earth and Planetary Science Letters*, 193, 447–457. [https://doi.org/10.1016/S0012-821X\(01\)00514-3](https://doi.org/10.1016/S0012-821X(01)00514-3)
- Bates, S. L., Hendry, K. R., Pryer, H. V., Kinsley, C. W., Pyle, K. M., Woodward, E. M. S., & Horner, T. J. (2017). Barium isotopes reveal role of ocean circulation on barium cycling in the Atlantic. *Geochimica et Cosmochimica Acta*, 204, 286–299. <https://doi.org/10.1016/j.gca.2017.01.043>
- Bauer, K. W., Gueguen, B., Cole, D. B., Francois, R., Kallmeyer, J., Planavsky, N., & Crowe, S. A. (2018). Chromium isotope fractionation in ferruginous sediments. *Geochimica et Cosmochimica Acta*, 223, 198–215. <https://doi.org/10.1016/j.gca.2017.10.034>
- Beard, B. L., Johnson, C. M., Cox, L., Sun, H., Nealon, K. H., & Aguilar, C. (1999). Iron isotope biosignatures. *Science*, 285, 1889–1892. <https://doi.org/10.1126/science.285.5435.1889>
- Beard, B. L., Johnson, C. M., Skulan, J. L., Nealon, K. H., Cox, L., & Sun, H. (2003). Application of Fe isotopes to tracing the geochemical and biological cycling of Fe. *Chemical Geology*, 195(1–4), 87–117. [https://doi.org/10.1016/s0009-2541\(02\)00390-x](https://doi.org/10.1016/s0009-2541(02)00390-x)

- Bennett, S. A., Rouxel, O., Schmidt, K., Garbe-Schönberg, D., Statham, P. J., & German, C. R. (2009). Iron isotope fractionation in a buoyant hydrothermal plume, 5 S Mid-Atlantic Ridge. *Geochimica et Cosmochimica Acta*, 73(19), 5619–5634. <https://doi.org/10.1016/j.gca.2009.06.027>
- Berger, W. H., Smetacek, V., & Wefer, G. (1989). Ocean productivity and paleoproductivity—An overview. In W. H. Berger, V. S. Smetacek, & G. Wefer (Eds.), *Productivity of the oceans present and past: Report of the Dahlem workshop on productivity of the ocean*, Life Sciences Research Reports 44 (Vol. 1988, pp. 1–34). Berlin: Wiley & Sons, Chichester.
- Bergquist, B. A., & Boyle, E. A. (2006). Iron isotopes in the Amazon River system: Weathering and transport signatures. *Earth and Planetary Science Letters*, 248(1–2), 54–68. <https://doi.org/10.1016/j.epsl.2006.05.004>
- Bermin, J., Vance, D., Archer, C., & Statham, P. J. (2006). The determination of the isotopic composition of Cu and Zn in seawater. *Chemical Geology*, 226, 280–297. <https://doi.org/10.1016/j.chemgeo.2005.09.025>
- Berner, R. A., Petsch, S. T., Lake, J. A., Beerling, D. J., Popp, B. N., Lane, R. S., et al. (2000). Isotope fractionation and atmospheric oxygen: Implications for Phanerozoic O₂ evolution. *Science*, 287(5458), 1630–1633. <https://doi.org/10.1126/science.287.5458.1630>
- Bernstein, R. E., & Byrne, R. H. (2004). Acantharians and marine barite. *Marine Chemistry*, 86(1–2), 45–50. <https://doi.org/10.1016/j.marchem.2003.12.003>
- Bertine, K. K., & Turekian, K. K. (1973). Molybdenum in marine deposits. *Geochimica et Cosmochimica Acta*, 37(6), 1415–1434. [https://doi.org/10.1016/0016-7037\(73\)90080-x](https://doi.org/10.1016/0016-7037(73)90080-x)
- Bianchi, D., Weber, T. S., Kiko, R., & Deutsch, C. (2018). Global niche of marine anaerobic metabolisms expanded by particle microenvironments. *Nature Geoscience*, 11, 1–6. <https://doi.org/10.1038/s41561-018-0081-0>
- Bishop, J. K. (1988). The barite-opal-organic carbon association in oceanic particulate matter. *Nature*, 332(6162), 341–343. <https://doi.org/10.1038/332341a0>
- Boiteau, R. M., Till, C. P., Ruacho, A., Bundy, R. M., Hawco, N. J., McKenna, A. M., et al. (2016). Structural characterization of natural nickel and copper binding ligands along the US GEOTRACES eastern Pacific Zonal Transect. *Frontiers in Marine Science*, 3, 243. <https://doi.org/10.3389/fmars.2016.00243>
- Böning, P., Brumsack, H.-J., Böttcher, M. E., Schnetger, B., Kriete, C., Kallmeyer, J., & Borchers, S. L. (2004). Geochemistry of Peruvian near-surface sediments. *Geochimica et Cosmochimica Acta*, 68, 4429–4451. <https://doi.org/10.1016/j.gca.2004.04.027>
- Böning, P., Brumsack, H.-J., Schnetger, B., & Grunwald, M. (2009). Trace element signatures of Chilean upwelling sediments at ~36°S. *Marine Geology*, 259, 112–121. <https://doi.org/10.1016/j.margeo.2009.01.004>
- Böning, P., Cuyper, S., Grunwald, M., Schnetger, B., & Brumsack, H.-J. (2005). Geochemical characteristics of Chilean upwelling sediments at ~36°S. *Marine Geology*, 220, 1–21. <https://doi.org/10.1016/j.margeo.2005.07.005>
- Böning, P., Fröllje, H., Beck, M., Schnetger, B., & Brumsack, H. J. (2012). Underestimation of the authigenic fraction of Cu and Ni in organic-rich sediments. *Marine Geology*, 323, 24–28. <https://doi.org/10.1016/j.margeo.2012.07.004>
- Böning, P., Shaw, T., Pahnke, K., & Brumsack, H.-J. (2015). Nickel as an indicator of fresh organic matter in upwelling sediments. *Geochimica et Cosmochimica Acta*, 162, 99–108. <https://doi.org/10.1016/j.gca.2015.04.027>
- Bonnand, P., James, R. H., Parkinson, I. J., Connelly, D. P., & Fairchild, I. J. (2013). The chromium isotopic composition of seawater and marine sediments. *Earth and Planetary Science Letters*, 382, 10–20. <https://doi.org/10.1016/j.epsl.2013.09.001>
- Borchers, S. L., Schnetger, B., Böning, P., & Brumsack, H.-J. (2005). Geochemical signatures of the Namibian diatom belt: Perennial upwelling and intermittent anoxia. *Geochemistry, Geophysics, Geosystems*, 6(4), Q06006. <https://doi.org/10.1029/2004GC000886>
- Boyd, P. W., Claustre, H., Levy, M., Siegel, D. A., & Weber, T. (2019). Multi-faceted particle pumps drive carbon sequestration in the ocean. *Nature*, 568(7752), 327–335. <https://doi.org/10.1038/s41586-019-1098-2>
- Boyd, P. W., & Ellwood, M. J. (2010). The biogeochemical cycle of iron in the ocean. *Nature Geoscience*, 3(10), 675–682. <https://doi.org/10.1038/ngeo964>
- Boyd, P. W., Ellwood, M. J., Tagliabue, A., & Twining, B. S. (2017). Biotic and abiotic retention, recycling and remineralization of metals in the ocean. *Nature Geoscience*, 10(3), 167–173. <https://doi.org/10.1038/ngeo2876>
- Boyd, P. W., Jickells, T., Law, C. S., Blain, S., Boyle, E. A., Buesseler, K. O., et al. (2007). Mesoscale iron enrichment experiments 1993–2005: Synthesis and future directions. *Science*, 315(5812), 612–617. <https://doi.org/10.1126/science.1131669>
- Boye, M., Wake, D. B., Lopez Gracia, P., Bown, J., Baker, A. R., & Achterberg, E. P. (2012). Distributions of dissolved trace metals (Cd, Cu, Mn, Pb, Ag) in the southeastern Atlantic and the Southern Ocean. *Biogeochemistry*, 9, 3231–3246. <https://doi.org/10.5194/bg-9-3231-2012>
- Boyle, E. A. (1981). Cadmium, zinc, copper, and barium in foraminifera tests. *Earth and Planetary Science Letters*, 53(1), 11–35. [https://doi.org/10.1016/0012-821x\(81\)90022-4](https://doi.org/10.1016/0012-821x(81)90022-4)
- Boyle, E. A. (1988a). Cadmium: Chemical tracer of deepwater paleoceanography. *Paleoceanography*, 3(4), 471–489. <https://doi.org/10.1029/pa003i004p00471>
- Boyle, E. A. (1988b). Vertical oceanic nutrient fractionation and glacial/interglacial CO₂ cycles. *Nature*, 331(6151), 55–56. <https://doi.org/10.1038/331055a0>
- Boyle, E. A. (1992). Cadmium and δ¹³C paleochemical ocean distributions during the stage 2 glacial maximum. *Annual Review of Earth and Planetary Sciences*, 20(1), 245–287. <https://doi.org/10.1146/annurev.ea.20.050192.001333>
- Boyle, E. A., & Keigwin, L. D. (1985). Comparison of Atlantic and Pacific paleochemical records for the last 215,000 years: Changes in deep ocean circulation and chemical inventories. *Earth and Planetary Science Letters*, 76(1–2), 135–150. [https://doi.org/10.1016/0012-821x\(85\)90154-2](https://doi.org/10.1016/0012-821x(85)90154-2)
- Boyle, E. A., Sclater, F., & Edmond, J. M. (1976). On the marine geochemistry of cadmium. *Nature*, 263(5572), 42–44. <https://doi.org/10.1038/263042a0>
- Boyle, E. A., Sclater, F. R., & Edmond, J. M. (1977). The distribution of dissolved copper in the Pacific. *Earth and Planetary Science Letters*, 37, 38–54. [https://doi.org/10.1016/0012-821x\(77\)90144-3](https://doi.org/10.1016/0012-821x(77)90144-3)
- Brand, L. E., Sunda, W. G., & Guillard, R. R. L. (1983). Limitation of marine phytoplankton by zinc, manganese, and iron. *Limnology & Oceanography*, 28, 1182–1198. <https://doi.org/10.4319/lo.1983.28.6.1182>
- Brand, L. E., Sunda, W. G., & Guillard, R. R. L. (1986). Reduction of marine phytoplankton reproduction rates by copper and cadmium. *Journal of Experimental Marine Biology and Ecology*, 96, 225–250. [https://doi.org/10.1016/0022-0981\(86\)90205-4](https://doi.org/10.1016/0022-0981(86)90205-4)
- Bridgestock, L., Hsieh, Y. T., Porcelli, D., & Henderson, G. M. (2019). Increased export production during recovery from the Paleocene-Eocene thermal maximum constrained by sedimentary Ba isotopes. *Earth and Planetary Science Letters*, 510, 53–63. <https://doi.org/10.1016/j.epsl.2018.12.036>
- Bridgestock, L., Hsieh, Y. T., Porcelli, D., Homoky, W. B., Bryan, A., & Henderson, G. M. (2018). Controls on the barium isotope compositions of marine sediments. *Earth and Planetary Science Letters*, 481, 101–110. <https://doi.org/10.1016/j.epsl.2017.10.019>

- Bridgestock, L., Nathan, J., Paver, R., Hsieh, Y. T., Porcelli, D., Tanzil, J., et al. (2021). Estuarine processes modify the isotope composition of dissolved riverine barium fluxes to the ocean. *Chemical Geology*, 579, 120340. <https://doi.org/10.1016/j.chemgeo.2021.120340>
- Bridgestock, L., Rehkämper, M., van de Flierdt, T., Murphy, K., Khondoker, R., Baker, A. R., et al. (2017). The Cd isotope composition of atmospheric aerosols from the tropical Atlantic Ocean. *Geophysical Research Letters*, 44(6), 2932–2940. <https://doi.org/10.1002/2017GL072748>
- Broecker, W. S. (1982). Glacial to interglacial changes in ocean chemistry. *Progress in Oceanography*, 11, 151–197. [https://doi.org/10.1016/0079-6611\(82\)90007-6](https://doi.org/10.1016/0079-6611(82)90007-6)
- Broecker, W. S., & Peng, T. H. (1982). *Tracers in the sea*. Palisades, NY: Eldigo Press.
- Brucker, R. L. P., McManus, J., Severmann, S., & Berelson, W. M. (2009). Molybdenum behavior during early diagenesis: Insights from Mo isotopes. *Geochemistry, Geophysics, Geosystems*, 10. <https://doi.org/10.1029/2008GC002180>
- Bruggmann, S., Scholz, F., Kläbe, R. M., Canfield, D. E., & Frei, R. (2019). Chromium isotope cycling in the water column and sediments of the Peruvian continental margin. *Geochimica et Cosmochimica Acta*, 257, 224–242. <https://doi.org/10.1016/j.gca.2019.05.001>
- Bruland, K. W. (1980). Oceanographic distributions of cadmium, zinc, nickel, and copper in the North Pacific. *Earth and Planetary Science Letters*, 47(2), 176–198. [https://doi.org/10.1016/0012-821x\(80\)90035-7](https://doi.org/10.1016/0012-821x(80)90035-7)
- Bruland, K. W. (1983). Trace elements in sea-water. *Chemical Oceanography*, 8, 157–220. <https://doi.org/10.1016/B978-0-12-588608-6.50009-2>
- Bruland, K. W. (1989). Complexation of zinc by natural organic ligands in the central North Pacific. *Limnology & Oceanography*, 34, 269–285. <https://doi.org/10.4319/lo.1989.34.2.0269>
- Bruland, K. W. (1992). Complexation of cadmium by natural organic ligands in the central North Pacific. *Limnology & Oceanography*, 37(5), 1008–1017. <https://doi.org/10.4319/lo.1992.37.5.1008>
- Bruland, K. W., Knauer, G. A., & Martin, J. H. (1978). Zinc in north-east Pacific water. *Nature*, 271(5647), 741–743. <https://doi.org/10.1038/271741a0>
- Bruland, K. W., & Lohan, M. C. (2003). Controls of trace metals in seawater. In *Treatise on geochemistry* (pp. 23–47). Elsevier. <https://doi.org/10.1016/b0-08-043751-6/06105-3>
- Brumsack, H. J. (2006). The trace metal content of recent organic carbon-rich sediments: Implications for Cretaceous black shale formation. *Palaeogeography, Palaeoclimatology, Palaeoecology*, 232(2–4), 344–361. <https://doi.org/10.1016/j.palaeo.2005.05.011>
- Bryan, A. L., Dickson, A. J., Dowdall, F., Homoky, W. B., Porcelli, D., & Henderson, G. M. (2021). Controls on the cadmium isotope composition of modern marine sediments. *Earth and Planetary Science Letters*, 565, 116946. <https://doi.org/10.1016/j.epsl.2021.116946>
- Bryan, A. L., Dong, S., Wilkes, E. B., & Wasylenki, L. E. (2015). Zinc isotope fractionation during adsorption onto Mn oxyhydroxide at low and high ionic strength. *Geochimica et Cosmochimica Acta*, 157, 182–197. <https://doi.org/10.1016/j.gca.2015.01.026>
- Cadiou, J. L., Pichat, S., Bondanese, V. P., Souillard, A., Fujii, T., Albarède, F., & Oger, P. (2017). Copper transporters are responsible for copper isotopic fractionation in eukaryotic cells. *Scientific Reports*, 7(1), 1–10. <https://doi.org/10.1038/srep44533>
- Cameron, V., & Vance, D. (2014). Heavy nickel isotope compositions in rivers and the oceans. *Geochimica et Cosmochimica Acta*, 128, 195–211. <https://doi.org/10.1016/j.gca.2013.12.007>
- Cameron, V., Vance, D., Archer, C., & House, C. H. (2009). A biomarker based on the stable isotopes of nickel. *Proceedings of the National Academy of Sciences*, 106(27), 10944–10948. <https://doi.org/10.1073/pnas.0900726106>
- Campbell, J. A., & Yeats, P. A. (1981). Dissolved chromium in the northwest Atlantic Ocean. *Earth and Planetary Science Letters*, 53, 427–433. [https://doi.org/10.1016/0012-821x\(81\)90047-9](https://doi.org/10.1016/0012-821x(81)90047-9)
- Campbell, J. A., & Yeats, P. A. (1984). Dissolved chromium in the St. Lawrence estuary. *Estuarine, Coastal and Shelf Science*, 19, 513–522. [https://doi.org/10.1016/0272-7714\(84\)90013-1](https://doi.org/10.1016/0272-7714(84)90013-1)
- Cao, Z., Li, Y., Rao, X., Yu, Y., Hathorne, E. C., Siebert, C., et al. (2020). Constraining barium isotope fractionation in the upper water column of the South China Sea. *Geochimica et Cosmochimica Acta*, 288, 120–137. <https://doi.org/10.1016/j.gca.2020.08.008>
- Cao, Z., Siebert, C., Hathorne, E. C., Dai, M., & Frank, M. (2020). Corrigendum to “Constraining the oceanic barium cycle with stable barium isotopes”. *Earth and Planetary Science Letters*, 434(2016), 1–9. <https://doi.org/10.1016/j.epsl.2019.116003>
- Carlson, C. A., Hansell, D. A., Nelson, N. B., Siegel, D. A., Smethie, W. M., Khatiwala, S., et al. (2010). Dissolved organic carbon export and subsequent remineralization in the mesopelagic and bathypelagic realms of the North Atlantic basin. *Deep Sea Research Part II: Topical Studies in Oceanography*, 57(16), 1433–1445. <https://doi.org/10.1016/j.dsr2.2010.02.013>
- Carter, S. C., Paytan, A., & Griffith, E. M. (2020). Toward an improved understanding of the marine barium cycle and the application of marine barite as a paleoproductivity proxy. *Minerals*, 10(5), 421. <https://doi.org/10.3390/min10050421>
- Chan, L. H., Drummond, D., Edmond, J. M., & Grant, B. (1977). On the barium data from the Atlantic GEOSECS expedition. *Deep-Sea Research*, 24(7), 613–649. [https://doi.org/10.1016/0146-6291\(77\)90505-7](https://doi.org/10.1016/0146-6291(77)90505-7)
- Chan, L. H., Edmond, J. M., Stallard, R. F., Broecker, W. S., Chung, Y. C., Weiss, R. F., & Ku, T. L. (1976). Radium and barium at GEOSECS stations in the Atlantic and Pacific. *Earth and Planetary Science Letters*, 32(2), 258–267. [https://doi.org/10.1016/0012-821x\(76\)90066-2](https://doi.org/10.1016/0012-821x(76)90066-2)
- Chang, A. S., Pedersen, T. F., & Hendy, I. L. (2014). Effects of productivity, glaciation, and ventilation on late quaternary sedimentary redox and trace element accumulation on the Vancouver Island margin, western Canada. *Paleoceanography*, 29(7), 730–746. <https://doi.org/10.1002/2013pa002581>
- Chappaz, A., Lyons, T. W., Gregory, D. D., Reinhard, C. T., Gill, B. C., Li, C., & Large, R. R. (2014). Does pyrite act as an important host for molybdenum in modern and ancient euxinic sediments? *Geochimica et Cosmochimica Acta*, 126, 112–122. <https://doi.org/10.1016/j.gca.2013.10.028>
- Chappell, P. D., Vedmati, J., Selph, K. E., Cyr, H. A., Jenkins, B. D., Landry, M. R., & Moffett, J. W. (2016). Preferential depletion of zinc within Costra Rica upwelling dome creates conditions for zinc co-limitation of primary production. *Journal of Plankton Research*, 38, 244–255. <https://doi.org/10.1093/plankt/fbw018>
- Charette, M. A., Kipp, L. E., Jensen, L. T., Dabrowski, J. S., Whitmore, L. M., Fitzsimmons, J. N., et al. (2020). The transpolar drift as a source of riverine and shelf-derived trace elements to the central Arctic Ocean. *Journal of Geophysical Research: Oceans*, 125(5), e2019JC015920. <https://doi.org/10.1029/2019JC015920>
- Chen, J.-B., Busigny, V., Gaillardet, J., Louvat, P., & Wang, Y.-N. (2014). Iron isotopes in the Seine River (France): Natural vs anthropogenic sources. *Geochimica et Cosmochimica Acta*, 128, 128–143. <https://doi.org/10.1016/j.gca.2013.12.017>
- Chen, L., Little, S. H., Kreissig, K., Severmann, S., & McManus, J. (2021). Isotopically light Cd in sediments underlying oxygen deficient zones. *Frontiers of Earth Science*, 9, 97. <https://doi.org/10.3389/feart.2021.623720>
- Chen, T., Wenqiang, L., Gao, B., Liu, R., Li, G., Zhao, L., & Ji, J. (2020). Reactive iron isotope signatures of the East Asian dust particles: Implications for iron cycling the deep North Pacific. *Chemical Geology*, 531, 119342. <https://doi.org/10.1016/j.chemgeo.2019.119342>
- Cheng, H., Adkins, J., Edwards, R. L., & Boyle, E. A. (2000). U-Th dating of deep-sea corals. *Geochimica et Cosmochimica Acta*, 64(14), 2401–2416. [https://doi.org/10.1016/S0016-7037\(99\)00422-6](https://doi.org/10.1016/S0016-7037(99)00422-6)

- Chever, F., Bucciarelli, E., Sarthou, G., Speich, S., Arhan, M., Penven, P., & Tagliabue, A. (2010). Physical speciation of iron in the Atlantic sector of the Southern Ocean along a transect from the subtropical domain to the Weddell Sea Gyre. *Journal of Geophysical Research*, *115*, C10059. <https://doi.org/10.1029/2009JC005880>
- Chever, F., Rouxel, O. J., Croot, P. L., Ponzevera, E., Wuttig, K., & Auro, M. (2015). Total dissolvable and dissolved iron isotopes in the water column of the Peru upwelling regime. *Geochimica et Cosmochimica Acta*, *162*, 66–82. <https://doi.org/10.1016/j.gca.2015.04.031>
- Chow, T. J., & Goldberg, E. D. (1960). On the marine geochemistry of barium. *Geochimica et Cosmochimica Acta*, *20*(3–4), 192–198. [https://doi.org/10.1016/0016-7037\(60\)90073-9](https://doi.org/10.1016/0016-7037(60)90073-9)
- Chu, N., Johnson, C., Beard, B., German, C., Nesbitt, R., Frank, M., et al. (2006). Evidence for hydrothermal venting in Fe isotope compositions of the deep Pacific Ocean through time. *Earth and Planetary Science Letters*, *245*, 202–217. <https://doi.org/10.1016/j.epsl.2006.02.043>
- Chung, Y. (1980). Radium-barium-silica correlations and a two-dimensional radium model for the world ocean. *Earth and Planetary Science Letters*, *49*(2), 309–318. [https://doi.org/10.1016/0012-821x\(80\)90074-6](https://doi.org/10.1016/0012-821x(80)90074-6)
- Ciscato, E. R., Bontognali, T. R., Poulton, S. W., & Vance, D. (2019). Copper and its isotopes in organic-rich sediments: From the modern margin to Archean shales. *Geosciences*, *9*(8), 325. <https://doi.org/10.3390/geosciences9080325>
- Ciscato, E. R., Bontognali, T. R., & Vance, D. (2018). Nickel and its isotopes in organic-rich sediments: Implications for oceanic budgets and a potential record of ancient seawater. *Earth and Planetary Science Letters*, *494*, 239–250. <https://doi.org/10.1016/j.epsl.2018.04.061>
- Coale, K. H. (1991). Effects of iron, manganese, copper and zinc enrichments on productivity and biomass in the subarctic Pacific. *Limnology & Oceanography*, *36*, 1851–1864. <https://doi.org/10.4319/lo.1991.36.8.1851>
- Coale, K. H., & Bruland, K. W. (1988). Copper complexation in the Northeast Pacific. *Limnology & Oceanography*, *33*, 1084–1101. <https://doi.org/10.4319/lo.1988.33.5.1084>
- Coale, K. H., & Bruland, K. W. (1990). Spatial and temporal variability in copper complexation in the North Pacific. *Deep Sea Research Part A. Oceanographic Research Papers*, *37*, 317–336. [https://doi.org/10.1016/0198-0149\(90\)90130-n](https://doi.org/10.1016/0198-0149(90)90130-n)
- Coale, K. H., Wang, X., Tanner, S. J., & Johnson, K. S. (2003). Phytoplankton growth and biological response to iron and zinc addition in the Ross Sea and Antarctic Circumpolar Current along 170°W. *Deep Sea Research Part II: Topical Studies in Oceanography*, *50*, 635–653. [https://doi.org/10.1016/s0967-0645\(02\)00588-x](https://doi.org/10.1016/s0967-0645(02)00588-x)
- Collier, R. W. (1985). Molybdenum in the northeast Pacific Ocean. *Limnology & Oceanography*, *30*, 1351–1354. <https://doi.org/10.4319/lo.1985.30.6.1351>
- Conway, T. M., Hamilton, D. S., Shelley, R. U., Aguilar-Islas, A. M., Landing, W. M., Mahowald, N. M., & John, S. G. (2019). Tracing and constraining anthropogenic aerosol iron fluxes to the North Atlantic Ocean using iron isotopes. *Nature Communications*, *10*, 2628. <https://doi.org/10.1038/s41467-019-10457-w>
- Conway, T. M., & John, S. G. (2014a). Quantification of dissolved iron sources to the North Atlantic Ocean. *Nature*, *511*, 212–215. <https://doi.org/10.1038/nature13482>
- Conway, T. M., & John, S. G. (2014b). The biogeochemical cycling of zinc and zinc isotopes in the North Atlantic Ocean. *Global Biogeochemical Cycles*, *28*, 1111–1128. <https://doi.org/10.1002/2014gb0004862>
- Conway, T. M., & John, S. G. (2015a). The cycling of iron, zinc and cadmium in the North East Pacific Ocean—Insights from stable isotopes. *Geochimica et Cosmochimica Acta*, *164*, 262–283. <https://doi.org/10.1016/j.gca.2015.05.023>
- Conway, T. M., & John, S. G. (2015b). Biogeochemical cycling of cadmium isotopes along a high-resolution section through the North Atlantic Ocean. *Geochimica et Cosmochimica Acta*, *148*, 269–283. <https://doi.org/10.1016/j.gca.2014.09.032>
- Conway, T. M., Rosenberg, A. D., Adkins, J. F., & John, S. G. (2013). A new method for precise determination of iron, zinc and cadmium stable isotope ratios in seawater by double-spike mass spectrometry. *Analytica Chimica Acta*, *793*, 44–52. <https://doi.org/10.1016/j.aca.2013.07.025>
- Coplen, T. B. (2011). Guidelines and recommended terms for expression of stable-isotope-ratio and gas-ratio measurement results. *Rapid Communications in Mass Spectrometry*, *25*(17), 2538–2560. <https://doi.org/10.1002/rcm.5129>
- Costa, K. M., McManus, J. F., Anderson, R. F., Ren, H., Sigman, D. M., Winckler, G., et al. (2016). No iron fertilization in the equatorial Pacific Ocean during the last ice age. *Nature*, *529*(7587), 519–522. <https://doi.org/10.1038/nature16453>
- Costa, K. M., McManus, J. F., Middleton, J. L., Langmuir, C. H., Huybers, P. J., Winckler, G., & Mukhopadhyay, S. (2017). Hydrothermal deposition on the Juan de Fuca Ridge over multiple glacial-interglacial cycles. *Earth and Planetary Science Letters*, *479*, 120–132. <https://doi.org/10.1016/j.epsl.2017.09.006>
- Coutaud, M., Méheut, M., Glatzel, P., Pokrovski, G. S., Viers, J., Rols, J. L., & Pokrovsky, O. S. (2018). Small changes in Cu redox state and speciation generate large isotope fractionation during adsorption and incorporation of Cu by a phototrophic biofilm. *Geochimica et Cosmochimica Acta*, *220*, 1–18. <https://doi.org/10.1016/j.gca.2017.09.018>
- Coutaud, M., Méheut, M., Viers, J., Rols, J. L., & Pokrovsky, O. S. (2019). Copper isotope fractionation during excretion from a phototrophic biofilm. *Chemical Geology*, *513*, 88–100. <https://doi.org/10.1016/j.chemgeo.2019.02.031>
- Cowan, C. E., Jenne, E. A., & Creelius, E. A. (1985). Silver speciation in seawater: The importance of sulfide and organic complexes. In A. C. Sigleo, & A. Hattori (Eds.), *Marine and estuarine geochemistry*. Chelsea, MI: Lewis Publishers Inc.
- Cranston, R. E., & Murray, J. W. (1978). Determination of chromium species in natural waters. *Analytica Chimica Acta*, *99*, 275–282. [https://doi.org/10.1016/s0003-2670\(01\)83568-6](https://doi.org/10.1016/s0003-2670(01)83568-6)
- Cranston, R. E., & Murray, J. W. (1980). Chromium species in the Columbia River and estuary. *Limnology & Oceanography*, *25*, 1104–1112. <https://doi.org/10.4319/lo.1980.25.6.1104>
- Crawford, D. W. W., Lipsen, M. S. S., Purdie, D. A. A., Lohan, M. C. C., Statham, P. J. J., Whitney, F. A. A., et al. (2003). Influence of zinc and iron enrichments on phytoplankton growth in the northeastern subarctic Pacific. *Limnology & Oceanography*, *48*, 1583–1600. <https://doi.org/10.4319/lo.2003.48.4.1583>
- Crockford, P. W., Wing, B. A., Paytan, A., Hodgskiss, M. S., Mayfield, K. K., Hayles, J. A., et al. (2019). Barium-isotopic constraints on the origin of post-Marinoan barites. *Earth and Planetary Science Letters*, *519*, 234–244. <https://doi.org/10.1016/j.epsl.2019.05.018>
- Crusius, J., Calvert, S., Pedersen, T., & Sage, D. (1996). Rhenium and molybdenum enrichments in sediments as indicators of oxic, suboxic and sulfidic conditions of deposition. *Earth and Planetary Science Letters*, *145*, 65–78. [https://doi.org/10.1016/S0012-821X\(96\)00204-X](https://doi.org/10.1016/S0012-821X(96)00204-X)
- Crusius, J., & Thomson, J. (2003). Mobility of authigenic rhenium, silver, and selenium during postdepositional oxidation in marine sediments. *Geochimica et Cosmochimica Acta*, *67*(2), 265–273. [https://doi.org/10.1016/s0016-7037\(02\)01075-x](https://doi.org/10.1016/s0016-7037(02)01075-x)
- Cullen, J. T., Chase, Z., Coale, K. H., Fitzwater, S. E., & Sherrell, R. M. (2003). Effect of iron limitation on the cadmium to phosphorus ratio of natural phytoplankton assemblages from the Southern Ocean. *Limnology & Oceanography*, *48*(3), 1079–1087. <https://doi.org/10.4319/lo.2003.48.3.1079>

- Cullen, J. T., & Coogan, L. A. (2017). Changes in Fe oxidation rate in hydrothermal plumes as a potential driver of enhanced hydrothermal input to near-ridge sediments during glacial terminations. *Geophysical Research Letters*, *44*(23), 11–951. <https://doi.org/10.1002/2017gl074609>
- Cullen, J. T., Lane, T. W., Morel, F. M., & Sherrell, R. M. (1999). Modulation of cadmium uptake in phytoplankton by seawater CO₂ concentration. *Nature*, *402*(6758), 165–167. <https://doi.org/10.1038/46007>
- Cullen, J. T., & Sherrell, R. M. (2005). Effects of dissolved carbon dioxide, zinc, and manganese on the cadmium to phosphorus ratio in natural phytoplankton assemblages. *Limnology & Oceanography*, *50*(4), 1193–1204. <https://doi.org/10.4319/lo.2005.50.4.1193>
- da Silva, J. F., & Williams, R. J. P. (1991). *The biological chemistry of the elements: The inorganic chemistry of life*. Oxford University Press.
- Dahl, T. W., Anbar, A. D., Gordon, G. W., Rosing, M. T., Frei, R., & Canfield, D. E. (2010). The behavior of molybdenum and its isotopes across the chemocline and in the sediments of sulfidic Lake Cadagno, Switzerland. *Geochimica et Cosmochimica Acta*, *74*, 144–163. <https://doi.org/10.1016/j.gca.2009.09.018>
- Dahl, T. W., Chappaz, A., Hoek, J., McKenzie, C. J., Svane, S., & Canfield, D. E. (2017). Evidence of molybdenum association with particulate organic matter under sulfidic conditions. *Geobiology*, *15*, 311–323. <https://doi.org/10.1111/gbi.12220>
- Dalai, T. K., Nishimura, K., & Nozaki, Y. (2005). Geochemistry of molybdenum in the Chao Phraya River estuary, Thailand: Role of suboxic diagenesis and porewater transport. *Chemical Geology*, *218*, 189–202. <https://doi.org/10.1016/j.chemgeo.2005.01.002>
- D'Arcy, J., Babechuk, M. G., Dössing, L. N., Gaucher, C., & Frei, R. (2016). Processes controlling the chromium isotopic composition of river water: Constraints from basaltic river catchments. *Geochimica et Cosmochimica Acta*, *186*, 296–315. <https://doi.org/10.1016/j.gca.2016.04.027>
- Dauphas, N., John, S. G., & Rouxel, O. (2017). Iron isotope systematics. *Reviews in Mineralogy and Geochemistry*, *82*(1), 415–510. <https://doi.org/10.2138/rmg.2017.82.11>
- Davidson, A. B., Semeniuk, D. M., Koh, J., Holmden, C., Jaccard, S. L., Francois, R., & Crowe, S. A. (2020). A Mg(OH)₂ coprecipitation method for determining chromium speciation and isotopic composition in seawater. *Limnology and Oceanography: Methods*, *18*, 8–19. <https://doi.org/10.1002/lom3.10342>
- de Baar, H. J., Boyd, P. W., Coale, K. H., Landry, M. R., Tsuda, A., Assmy, P., & Buesseler, K. O. (2005). Synthesis of iron fertilization experiments: From the iron age in the age of enlightenment. *Journal of Geophysical Research*, *110*(C9). <https://doi.org/10.1029/2004jc002601>
- de Baar, H. J. W., Saager, P. M., Nolting, R. F., & van der Meer, J. (1994). Cadmium versus phosphate in the world ocean. *Marine Chemistry*, *46*(3), 261–281. [https://doi.org/10.1016/0304-4203\(94\)90082-5](https://doi.org/10.1016/0304-4203(94)90082-5)
- de Baar, H. J. W., van Heuven, S. M., Abouchami, W., Xue, Z., Galer, S. J. G., Rehkämper, M., et al. (2017). Interactions of dissolved CO₂ with cadmium isotopes in the Southern Ocean. *Marine Chemistry*, *195*, 105–121. <https://doi.org/10.1016/j.marchem.2017.06.010>
- de Souza, G. F., Khatiwala, S. P., Hain, M. P., Little, S. H., & Vance, D. (2018). On the origin of the marine zinc-silicon correlation. *Earth and Planetary Science Letters*, *492*, 22–34. <https://doi.org/10.1016/j.epsl.2018.03.050>
- de Souza, G. F., Reynolds, B. C., Rickli, J., Frank, M., Saito, M. A., Gerringa, L. J., & Bourdon, B. (2012). Southern Ocean control of silicon stable isotope distribution in the deep Atlantic Ocean. *Global Biogeochemical Cycles*, *26*(2). <https://doi.org/10.1029/2011gb004141>
- Dehairs, F., Chesselet, R., & Jedwab, J. (1980). Discrete suspended particles of barite and the barium cycle in the open ocean. *Earth and Planetary Science Letters*, *49*(2), 528–550. [https://doi.org/10.1016/0012-821x\(80\)90094-1](https://doi.org/10.1016/0012-821x(80)90094-1)
- Dehairs, F., Jacquet, S., Savoye, N., Van Mooy, B. A., Buesseler, K. O., Bishop, J. K., et al. (2008). Barium in twilight zone suspended matter as a potential proxy for particulate organic carbon remineralization: Results for the North Pacific. *Deep Sea Research Part II: Topical Studies in Oceanography*, *55*(14–15), 1673–1683. <https://doi.org/10.1016/j.dsr2.2008.04.020>
- Dehairs, F., Lambert, C. E., Chesselet, R., & Risler, N. (1987). The biological production of marine suspended barite and the barium cycle in the western Mediterranean Sea. *Biogeochemistry*, *4*(2), 119–140. <https://doi.org/10.1007/bf02180151>
- Dellwig, O., Beck, M., Lemke, A., Lunau, M., Kolditz, K., Schnetger, B., & Brumsack, H.-J. (2007). Non-conservative behaviour of molybdenum in coastal waters: Coupling geochemical, biological, and sedimentological processes. *Geochimica et Cosmochimica Acta*, *71*, 2745–2761. <https://doi.org/10.1016/j.gca.2007.03.014>
- Dellwig, O., Leipe, T., März, C., Glockzin, M., Pollehne, F., Schnetger, B., et al. (2010). A new particulate Mn-Fe-P-shuttle at the redoxcline of anoxic basins. *Geochimica et Cosmochimica Acta*, *74*, 7100–7115. <https://doi.org/10.1016/j.gca.2010.09.017>
- Deng, N., Stack, A. G., Weber, J., Cao, B., De Yoreo, J. J., & Hu, Y. (2019). Organic-mineral interfacial chemistry drives heterogeneous nucleation of Sr-rich (Ba_xSr_{1-x})SO₄ from undersaturated solution. *Proceedings of the National Academy of Sciences*, *116*(27), 13221–13226.
- Dickens, G. R., Fewless, T., Thomas, E., & Bralower, T. J. (2003). Excess barite accumulation during the Paleocene-Eocene thermal maximum: Massive input of dissolved barium from seafloor gas hydrate reservoirs. In S. L. Wing, P. D. Gingerich, B. Schmitz, & E. Thomas (Eds.), *Causes and consequences of globally warm climates in the early Paleogene* (Vol. 369, pp. 11–23). Geological Society of America Special Papers. <https://doi.org/10.1130/0-8137-2369-8.11>
- Dickson, A. J. (2017). A molybdenum-isotope perspective on Phanerozoic deoxygenation events. *Nature Geoscience*, *10*, 721–726. <https://doi.org/10.1038/NGEO3028>
- Dideriksen, K., Baker, J. A., & Stipp, S. L. S. (2008). Equilibrium Fe isotope fractionation between inorganic aqueous Fe (III) and the siderophore complex, Fe (III)-desferrioxamine B. *Earth and Planetary Science Letters*, *269*(1–2), 280–290. <https://doi.org/10.1016/j.epsl.2008.02.022>
- Donat, J. R., & Bruland, K. W. (1990). A comparison of two voltammetric techniques for determining zinc speciation in Northeast Pacific Ocean waters. *Marine Chemistry*, *28*, 301–323. [https://doi.org/10.1016/0304-4203\(90\)90050-m](https://doi.org/10.1016/0304-4203(90)90050-m)
- Donat, J. R., Lao, K. A., & Bruland, K. W. (1994). Speciation of dissolved copper and nickel in south San Francisco Bay: A multi-method approach. *Analytica Chimica Acta*, *284*, 547–571. [https://doi.org/10.1016/0003-2670\(94\)85061-5](https://doi.org/10.1016/0003-2670(94)85061-5)
- Dunlea, A. G., Murray, R. W., Sauvage, J., Spivack, A. J., Harris, R. N., & D'Hondt, S. (2015). Dust, volcanic ash, and the evolution of the South Pacific Gyre through the Cenozoic. *Paleoceanography*, *30*(8), 1078–1099. <https://doi.org/10.1002/2015pa002829>
- Dunlea, A. G., Tegler, L. A., Peucker-Ehrenbrink, B., Anbar, A. D., Romaniello, S. J., & Horner, T. J. (2021). Pelagic clays as archives of marine iron isotope chemistry. *Chemical Geology*, *575*, 120201. <https://doi.org/10.1016/j.chemgeo.2021.120201>
- Dupont, C. L., Barbeau, K., & Palenik, B. (2008). Ni uptake and limitation in marine *Synechococcus* strains. *Applied and Environmental Microbiology*, *74*(1), 23–31. <https://doi.org/10.1128/aem.01007-07>
- Dupont, C. L., Butcher, A., Valas, R. E., Bourne, P. E., & Caetano-Anolles, G. (2010). History of biological metal utilization inferred through phylogenomic analysis of protein structures. *Proceedings of the National Academy of Sciences*, *107*, 10567–10572. <https://doi.org/10.1073/pnas.0912491107>
- Dupont, C. L., Neupane, K., Shearer, J., & Palenik, B. (2008). Diversity, function and evolution of genes coding for putative Ni-containing superoxide dismutases. *Environmental Microbiology*, *10*(7), 1831–1843. <https://doi.org/10.1111/j.1462-2920.2008.01604.x>

- Dymond, J., & Collier, R. (1996). Particulate barium fluxes and their relationships to biological productivity. *Deep Sea Research Part II: Topical Studies in Oceanography*, 43(4–6), 1283–1308. [https://doi.org/10.1016/0967-0645\(96\)00011-2](https://doi.org/10.1016/0967-0645(96)00011-2)
- Dymond, J., Suess, E., & Lyle, M. (1992). Barium in deep-sea sediment: A geochemical proxy for paleoproductivity. *Paleoceanography*, 7(2), 163–181. <https://doi.org/10.1029/92pa00181>
- Eagle, M., Paytan, A., Arrigo, K. R., van Dijken, G., & Murray, R. W. (2003). A comparison between excess barium and barite as indicators of carbon export. *Paleoceanography*, 18(1), 1021. <https://doi.org/10.1029/2002PA000793>
- Edmond, J. M., Boyle, E. D., Drummond, D., Grant, B., & Mislick, T. (1978). Desorption of barium in the plume of the Zaire (Congo) River. *Netherlands Journal of Sea Research*, 12(3–4), 324–328. [https://doi.org/10.1016/0077-7579\(78\)90034-0](https://doi.org/10.1016/0077-7579(78)90034-0)
- Elderfield, H. (1970). Chromium speciation in sea water. *Earth and Planetary Science Letters*, 9, 10–16. [https://doi.org/10.1016/0012-821x\(70\)90017-8](https://doi.org/10.1016/0012-821x(70)90017-8)
- Elderfield, H., & Rickaby, R. E. M. (2000). Oceanic Cd/P ratio and nutrient utilization in the glacial Southern Ocean. *Nature*, 405(6784), 305–310. <https://doi.org/10.1038/35012507>
- Elliott, T., & Steele, R. C. (2017). The isotope geochemistry of Ni. *Reviews in Mineralogy and Geochemistry*, 82(1), 511–542. <https://doi.org/10.2138/rmg.2017.82.12>
- Ellis, A. S., Johnson, T. M., & Bullen, T. D. (2002). Chromium isotopes and the fate of hexavalent chromium in the environment. *Science*, 295, 2060–2062. <https://doi.org/10.1126/science.1068368>
- Ellwood, M. J. (2004). Zinc and cadmium speciation in subantarctic waters east of New Zealand. *Marine Chemistry*, 87(1–2), 37–58. <https://doi.org/10.1016/j.marchem.2004.01.005>
- Ellwood, M. J., & Hunter, K. A. (2000). The Incorporation of Zinc and Iron into the Frustule of the Marine Diatom *Thalassiosira pseudonana*. *Limnology & Oceanography*, 45, 1517–1524. <https://doi.org/10.4319/lo.2000.45.7.1517>
- Ellwood, M. J., Hutchins, D. A., Lohan, M. C., Milne, A., Nasemann, P., Nodder, S. D., et al. (2015). Iron stable isotopes track pelagic iron cycling during a subtropical phytoplankton bloom. *Proceedings of the National Academy of Sciences of the United States of America*, 112, E15–E20. <https://doi.org/10.1073/pnas.1421576112>
- Ellwood, M. J., Strzepek, R. F., Strutton, P. G., Trull, T. W., Fourquez, M., & Boyd, P. W. (2020). Distinct iron cycling in a Southern Ocean eddy. *Nature Communications*, 11(1), 1–8. <https://doi.org/10.1038/s41467-020-14464-0>
- Ellwood, M. J., & Van Den Berg, C. M. G. (2000). Zinc speciation in the northeastern Atlantic Ocean. *Marine Chemistry*, 68, 295–306. [https://doi.org/10.1016/s0304-4203\(99\)00085-7](https://doi.org/10.1016/s0304-4203(99)00085-7)
- Emerson, S. R., & Husted, S. S. (1991). Ocean anoxia and the concentrations of molybdenum and vanadium in seawater. *Marine Chemistry*, 34, 177–196. [https://doi.org/10.1016/0304-4203\(91\)90002-E](https://doi.org/10.1016/0304-4203(91)90002-E)
- Erickson, B. E., & Helz, G. R. (2000). Molybdenum(VI) speciation in sulfidic waters: Stability and lability of thiomolybdates. *Geochimica et Cosmochimica Acta*, 64, 1149–1158. [https://doi.org/10.1016/S0016-7037\(99\)00423-8](https://doi.org/10.1016/S0016-7037(99)00423-8)
- Escoube, R., Rouxel, O. J., Pokrovsky, O. S., Schroth, A., Max Holmes, R., & Donard, O. F. X. (2015). Iron isotope systematics in Arctic rivers. *Comptes Rendus Geoscience*, 347(7–8), 377–385. <https://doi.org/10.1016/j.crte.2015.04.005>
- Escoube, R., Rouxel, O. J., Sholkovitz, E., & Donard, O. F. X. (2009). Iron isotope systematics in estuaries: The case of North River, Massachusetts (USA). *Geochimica et Cosmochimica Acta*, 73(14), 4045–4059. <https://doi.org/10.1016/j.gca.2009.04.026>
- Esser, B. K., & Volpe, A. M. (2002). At-sea high-resolution chemical mapping: Extreme barium depletion in North Pacific surface water. *Marine Chemistry*, 79(2), 67–79. [https://doi.org/10.1016/s0304-4203\(02\)00037-3](https://doi.org/10.1016/s0304-4203(02)00037-3)
- Fagel, N., Dehairs, F., Peinert, R., Antia, A., & André, L. (2004). Reconstructing export production at the NE Atlantic margin: Potential and limits of the Ba proxy. *Marine Geology*, 204(1–2), 11–25. [https://doi.org/10.1016/s0025-3227\(03\)00371-2](https://doi.org/10.1016/s0025-3227(03)00371-2)
- Fantle, M. S., & DePaolo, D. J. (2004). Iron isotopic fractionation during continental weathering. *Earth and Planetary Science Letters*, 228(3–4), 547–562. <https://doi.org/10.1016/j.epsl.2004.10.013>
- Farkaš, J., Frýda, J., Paulukat, C., Hathorne, E. C., Matoušková, Š., Rohovec, J., et al. (2018). Chromium isotope fractionation between modern seawater and biogenic carbonates from the Great Barrier Reef, Australia: Implications for the paleo-seawater $\delta^{53}\text{Cr}$ reconstruction. *Earth and Planetary Science Letters*, 498, 140–151. <https://doi.org/10.1016/j.epsl.2018.06.032>
- Farmer, J. R., Hertzberg, J. E., Cardinal, D., Fietz, S., Hendry, K., Jaccard, S. L., et al. (2021). Assessment of C, N and Si isotopes as tracers of past ocean nutrient and carbon cycling. *Global Biogeochemical Cycles*. <https://doi.org/10.1029/2020gb006775>
- Farmer, J. R., Hönisch, B., Haynes, L. L., Kroon, D., Jung, S., Ford, H. L., et al. (2019). Deep Atlantic Ocean carbon storage and the rise of 100,000-year glacial cycles. *Nature Geoscience*, 12, 355–360. <https://doi.org/10.1038/s41561-019-0334-6>
- Fassbender, A. J., Palevsky, H. I., Martz, T. R., Ingalls, A. E., Gledhill, M., Fawcett, S. E., et al. (2017). Perspectives on chemical oceanography in the 21st century: Participants of the COME ABOARD meeting examine aspects of the field in the context of 40 years of DISCO. *Marine Chemistry*, 196, 181–190. <https://doi.org/10.1016/j.marchem.2017.09.002>
- Ferrier-Pagès, C., Sauzéat, L., & Balter, V. (2018). Coral bleaching is linked to the capacity of the animal host to supply essential metals to the symbionts. *Global Change Biology*, 24(7), 3145–3157.
- Finlay, B. J., Hetherington, N. B., & Da Vison, W. (1983). Active biological participation in lacustrine barium chemistry. *Geochimica et Cosmochimica Acta*, 47(7), 1325–1329. [https://doi.org/10.1016/0016-7037\(83\)90071-6](https://doi.org/10.1016/0016-7037(83)90071-6)
- Fischer, L., Smith, G., Hann, S., & Bruland, K. W. (2018). Ultra-trace analysis of silver and platinum in seawater by ICP-SFMS after off-line matrix separation and pre-concentration. *Marine Chemistry*, 199, 44–52. <https://doi.org/10.1016/j.marchem.2018.01.006>
- Fisher, N. S., & Went, M. (1993). The release of trace elements by dying marine phytoplankton. *Deep-Sea Research I*, 40(4), 671–694. [https://doi.org/10.1016/0967-0637\(93\)90065-b](https://doi.org/10.1016/0967-0637(93)90065-b)
- Fishwick, M. P., Sedwick, P. N., Lohan, M. C., Worsfeld, P. J., Buck, K. N., Church, T. M., & Ussher, S. J. (2014). The impact of changing surface ocean conditions on the dissolution of aerosol iron. *Global Biogeochemical Cycles*, 28(11), 1235–1250. <https://doi.org/10.1002/2014GB004921>
- Fitzsimmons, J. N., & Boyle, E. A. (2014). Both soluble and colloidal iron phases control dissolved iron variability in the tropical North Atlantic Ocean. *Geochimica et Cosmochimica Acta*, 125, 539–550. <https://doi.org/10.1016/j.gca.2013.10.032>
- Fitzsimmons, J. N., Carrasco, G. G., Wu, J., Roshan, S., Hatta, M., Measures, C. I., et al. (2015). Partitioning of dissolved iron and iron isotopes into soluble and colloidal phases along the GA03 GEOTRACES North Atlantic Transect. *Deep Sea Research Part II: Topical Studies in Oceanography*, 116, 130–151. <https://doi.org/10.1016/j.dsr2.2014.11.014>
- Fitzsimmons, J. N., Conway, T. M., Lee, J.-M., Kayser, R., Thyng, K. M., John, S. G., & Boyle, E. A. (2016). Dissolved iron and iron isotopes in the southeastern Pacific Ocean. *Global Biogeochemical Cycles*, 30(10), 1372–1395. <https://doi.org/10.1002/2015GB005357>
- Fitzsimmons, J. N., John, S. G., Marsay, C. M., Hoffman, C. L., Nicholas, S. L., Toner, B. M., et al. (2017). Iron persistence in a distal hydrothermal plume supported by dissolved–particulate exchange. *Nature Geoscience*, 10(3), 195–201. <https://doi.org/10.1038/ngeo2900>

- Flegal, A. R., Sanudo-Wilhelmy, S. A., & Scelfo, G. M. (1995). Silver in the eastern Atlantic Ocean. *Marine Chemistry*, 49, 315–320. [https://doi.org/10.1016/0304-4203\(95\)00021-i](https://doi.org/10.1016/0304-4203(95)00021-i)
- Franck, V. M., Bruland, K. W., Hutchins, D. A., & Brzezinski, M. A. (2003). Iron and zinc effects on silicic acid and nitrate uptake kinetics in three high-nutrient, low-chlorophyll (HNLC) regions. *Marine Ecology Progress Series*, 252, 15–33. <https://doi.org/10.3354/meps252015>
- Frank, A. B., Kläebe, R. M., Löhr, S., Xu, L., & Frei, R. (2020). Chromium isotope composition of organic-rich marine sediments and their mineral phases and implications for using black shales as a paleoredox archive. *Geochim. Cosmochim. Acta*, 270, 338–359. <https://doi.org/10.1016/j.gca.2019.11.035>
- Frank, M., Gersonde, R., van der Loeff, M. R., Bohrmann, G., Nürnberg, C. C., Kubik, P. W., et al. (2000). Similar glacial and interglacial export bioproductivity in the Atlantic sector of the Southern Ocean: Multiproxy evidence and implications for glacial atmospheric CO₂. *Paleoceanography*, 15(6), 642–658. <https://doi.org/10.1029/2000pa000497>
- François, R., Altabet, M. A., Yu, E. F., Sigman, D. M., Bacon, M. P., Frank, M., et al. (1997). Contribution of Southern Ocean surface-water stratification to low atmospheric CO₂ concentrations during the last glacial period. *Nature*, 389(6654), 929–935. <https://doi.org/10.1038/40073>
- François, R., Honjo, S., Manganini, S. J., & Ravizza, G. E. (1995). Biogenic barium fluxes to the deep sea: Implications for paleoproductivity reconstruction. *Global Biogeochemical Cycles*, 9(2), 289–303. <https://doi.org/10.1029/95gb00021>
- Frei, R., Gaucher, C., Poulton, S. W., & Canfield, D. E. (2009). Fluctuations in Precambrian atmospheric oxygenation recorded by chromium isotopes. *Nature*, 461, 250–253. <https://doi.org/10.1038/nature08266>
- Frei, R., Lehmann, B., Xu, L., & Frederiksen, J. A. (2020). Surface water oxygenation and bioproductivity—A link provided by combined chromium and cadmium isotopes in Early Cambrian metalliferous black shales (Nanhua Basin, South China). *Chemical Geology*, 552, 119785. <https://doi.org/10.1016/j.chemgeo.2020.119785>
- Frei, R., Poiré, D., & Frei, K. M. (2014). Weathering on land and transport of chromium to the ocean in a subtropical region (Misiones, NW Argentina): A chromium stable isotope perspective. *Chemical Geology*, 381, 110–124. <https://doi.org/10.1016/j.chemgeo.2014.05.015>
- Frew, R. D., & Hunter, K. A. (1992). Influence of Southern Ocean waters on the cadmium-phosphate properties of the global ocean. *Nature*, 360(6400), 144–146. <https://doi.org/10.1038/360144a0>
- Friedl, G., & Pedersen, T. (2002). Silver as a new tracer for diatom production. *Eawag News*, 52, 14–15.
- Froelich, P., Klinkhammer, G. P., Bender, M. L., Luedtke, N. A., Heath, G. R., Cullen, D., et al. (1979). Early oxidation of organic matter in pelagic sediments of the eastern equatorial Atlantic: Suboxic diagenesis. *Geochimica et Cosmochimica Acta*, 43(7), 1075–1090. [https://doi.org/10.1016/0016-7037\(79\)90095-4](https://doi.org/10.1016/0016-7037(79)90095-4)
- Fru, E. C., Rodríguez, N. P., Partin, C. A., Lalonde, S. V., Andersson, P., Weiss, D. J., et al. (2016). Cu isotopes in marine black shales record the Great Oxidation Event. *Proceedings of the National Academy of Sciences*, 113(18), 4941–4946. <https://doi.org/10.1073/pnas.1523544113>
- Füger, A., Bruggmann, S., Frei, R., Leis, A., Dietzel, M., & Mavromatis, V. (2019). The role of pH on Cr(VI) partitioning and isotopic fractionation during its incorporation in calcite. *Geochimica et Cosmochimica Acta*, 265, 520–532. <https://doi.org/10.1016/j.gca.2019.07.047>
- Fujii, T., Moynier, F., Abe, M., Nemoto, K., & Albarède, F. (2013). Copper isotope fractionation between aqueous compounds relevant to low temperature geochemistry and biology. *Geochimica et Cosmochimica Acta*, 110, 29–44. <https://doi.org/10.1016/j.gca.2013.02.007>
- Fujii, T., Moynier, F., Dauphas, N., & Abe, M. (2011). Theoretical and experimental investigation of nickel isotopic fractionation in species relevant to modern and ancient oceans. *Geochimica et Cosmochimica Acta*, 75(2), 469–482. <https://doi.org/10.1016/j.gca.2010.11.003>
- Fujii, T., Moynier, F., Pons, M. L., & Albarède, F. (2011). The origin of Zn isotope fractionation in sulfides. *Geochimica et Cosmochimica Acta*, 75(23), 7632–7643. <https://doi.org/10.1016/j.gca.2011.09.036>
- Gall, L., Williams, H. M., Siebert, C., Halliday, A. N., Herrington, R. J., & Hein, J. R. (2013). Nickel isotopic compositions of ferromanganese crusts and the constancy of deep ocean inputs and continental weathering effects over the Cenozoic. *Earth and Planetary Science Letters*, 375, 148–155. <https://doi.org/10.1016/j.epsl.2013.05.019>
- Gallon, C., & Flegal, A. R. (2015). Sources, fluxes, and biogeochemical cycling of silver in the oceans. In D. Whitacre (Ed.), *Reviews of environmental contamination and toxicology* (Vol. 235, pp. 27–48). Cham: Springer. https://doi.org/10.1007/978-3-319-10861-2_2
- Ganeshram, R. S., François, R., Commeau, J., & Brown-Leger, S. L. (2003). An experimental investigation of barite formation in seawater. *Geochimica et Cosmochimica Acta*, 67(14), 2599–2605. [https://doi.org/10.1016/s0016-7037\(03\)00164-9](https://doi.org/10.1016/s0016-7037(03)00164-9)
- Garcia, H. E., Locarnini, R. A., Boyer, T. P., Antonov, J. I., Baranova, O. K., Zweng, M. M., et al. (2014). World Ocean Atlas 2013. In S. Levitus, & A. Mishonov Technical (Eds.), *Dissolved oxygen, apparent oxygen utilization, and oxygen saturation* (Vol. 3, p. 27). NOAA Atlas NESDIS 75.
- Gault-Ringold, M., Adu, T., Stirling, C. H., Frew, R. D., & Hunter, K. A. (2012). Anomalous biogeochemical behavior of cadmium in Subantarctic surface waters: Mechanistic constraints from cadmium isotopes. *Earth and Planetary Science Letters*, 341, 94–103. <https://doi.org/10.1016/j.epsl.2012.06.005>
- Gebregiorgis, D., Hathorne, E. C., Sijinkumar, A. V., Nath, B. N., Nürnberg, D., & Frank, M. (2016). South Asian summer monsoon variability during the last ~54 kyrs inferred from surface water salinity and river runoff proxies. *Quaternary Science Reviews*, 138, 6–15. <https://doi.org/10.1016/j.quascirev.2016.02.012>
- George, E., Stirling, C. H., Gault-Ringold, M., Ellwood, M. J., & Middag, R. (2019). Marine biogeochemical cycling of cadmium and cadmium isotopes in the extreme nutrient-depleted subtropical gyre of the south West Pacific Ocean. *Earth and Planetary Science Letters*, 514, 84–95. <https://doi.org/10.1016/j.epsl.2019.02.031>
- Georgiev, S. V., Horner, T. J., Stein, H. J., Hannah, J. L., Bingen, B., & Rehkämper, M. (2015). Cadmium-isotopic evidence for increasing primary productivity during the Late Permian anoxic event. *Earth and Planetary Science Letters*, 410, 84–96. <https://doi.org/10.1016/j.epsl.2014.11.010>
- Geyman, B. M., Ptacek, J. L., LaVigne, M., & Horner, T. J. (2019). Barium in deep-sea bamboo corals: Phase associations, barium stable isotopes, & prospects for paleoceanography. *Earth and Planetary Science Letters*, 525, 115751. <https://doi.org/10.1016/j.epsl.2019.115751>
- Giering, S. L., Sanders, R., Lampitt, R. S., Anderson, T. R., Tamburini, C., Boutrif, M., et al. (2014). Reconciliation of the carbon budget in the ocean's twilight zone. *Nature*, 507(7493), 480–483. <https://doi.org/10.1038/nature13123>
- Glass, J. B., Axler, R. P., Chandra, S., & Goldman, C. R. (2012). Molybdenum limitation of microbial nitrogen assimilation in aquatic ecosystems and pure cultures. *Frontiers in Microbiology*, 3, 1–11. <https://doi.org/10.3389/fmicb.2012.00331>
- Glass, J. B., Wolfe-Simon, F., & Anbar, A. D. (2009). Coevolution of metal availability and nitrogen assimilation in cyanobacteria and algae. *Geobiology*, 7, 100–123. <https://doi.org/10.1111/j.1472-4669.2009.00190.x>
- Goldberg, T., Archer, C., Vance, D., & Poulton, S. W. (2009). Mo isotope fractionation during adsorption to Fe (oxyhydr)oxides. *Geochimica et Cosmochimica Acta*, 73, 6502–6516. <https://doi.org/10.1016/j.gca.2009.08.004>

- Goldberg, T., Archer, C., Vance, D., Thamdrup, B., McAnena, A., & Poulton, S. W. (2012). Controls on Mo isotope fractionations in a Mn-rich anoxic marine sediment, Gullmar Fjord, Sweden. *Chemical Geology*, 296–297, 73–82. <https://doi.org/10.1016/j.chemgeo.2011.12.020>
- Goldberg, T., Gordon, G., Izon, G., Archer, C., Pearce, C. R., McManus, J., et al. (2013). Resolution of inter-laboratory discrepancies in Mo isotope data: An intercalibration. *Journal of Analytical Atomic Spectrometry*, 28(5), 724–735. <https://doi.org/10.1039/c3ja30375f>
- Goldman, C. R. (1960). Molybdenum as a factor limiting primary productivity in Castle Lake, California. *Science*, 132, 1016–1017. <https://doi.org/10.1126/science.132.3433.1016>
- Gong, Y., Xia, Y., Huang, F., & Yu, H. (2017). Average iron isotopic compositions of the upper continental crust: Constrained by loess from the Chinese Loess Plateau. *Acta Geochimica*, 36, 125–131. <https://doi.org/10.1007/s11631-016-0131-5>
- Gooday, A. J., & Nott, J. A. (1982). Intracellular barite crystals in two xenophyophores, *Aschemonella ramuliformis* and *Galathea minima* sp. (Protozoa: Rhizopoda) with comments on the taxonomy of *A. ramuliformis*. *Journal of the Marine Biological Association of the United Kingdom*, 62(3), 595–605. <https://doi.org/10.1017/s0025315400019779>
- Goring-Harford, H. J., Klar, J. K., Donald, H. K., Pearce, C. R., Connelly, D. P., & James, R. H. (2020). Behaviour of chromium and chromium isotopes during estuarine mixing in the Beaulieu Estuary, UK. *Earth and Planetary Science Letters*, 536, 116166. <https://doi.org/10.1016/j.epsl.2020.116166>
- Goring-Harford, H. J., Klar, J. K., Pearce, C. R., Connelly, D. P., Achterberg, E. P., & James, R. H. (2018). Behaviour of chromium isotopes in the eastern sub-tropical Atlantic oxygen minimum zone. *Geochimica et Cosmochimica Acta*, 236, 41–59. <https://doi.org/10.1016/j.gca.2018.03.004>
- Goto, K. T., Sekine, Y., Shimoda, G., Hein, J. R., Aoki, S., Ishikawa, A., et al. (2020). A framework for understanding Mo isotope records of Archean and Paleoproterozoic Fe- and Mn-rich sedimentary rocks: Insights from modern marine hydrothermal Fe-Mn oxides. *Geochimica et Cosmochimica Acta*, 280, 221–236. <https://doi.org/10.1016/j.gca.2020.04.017>
- Gou, L. F., Jin, Z., Galy, A., Gong, Y. Z., Nan, X. Y., Jin, C., et al. (2020). Seasonal riverine barium isotopic variation in the middle Yellow River: Sources and fractionation. *Earth and Planetary Science Letters*, 531, 115990. <https://doi.org/10.1016/j.epsl.2019.115990>
- Griffith, E. M., & Paytan, A. (2012). Barite in the ocean—occurrence, geochemistry and palaeoceanographic applications. *Sedimentology*, 59(6), 1817–1835. <https://doi.org/10.1111/j.1365-3091.2012.01327.x>
- Gueguen, B., Reinhard, C. T., Algeo, T. J., Peterson, L. C., Nielsen, S. G., Wang, X., et al. (2016b). The chromium isotope composition of reducing and oxic marine sediments. *Geochimica et Cosmochimica Acta*, 184, 1–19. <https://doi.org/10.1016/j.gca.2016.04.004>
- Gueguen, B., & Rouxel, O. (2021). The Nickel isotope composition of the authigenic sink and the diagenetic flux in modern oceans. *Chemical Geology*, 563, 120050. <https://doi.org/10.1016/j.chemgeo.2020.120050>
- Gueguen, B., Rouxel, O., & Fouquet, Y. (2021). Nickel isotopes and rare earth elements systematics in marine hydrogenetic and hydrothermal ferromanganese deposits. *Chemical Geology*, 560, 119999. <https://doi.org/10.1016/j.chemgeo.2020.119999>
- Gueguen, B., Rouxel, O., Ponzevera, E., Bekker, A., & Fouquet, Y. (2013). Nickel isotope variations in terrestrial silicate rocks and geological reference materials measured by MC-ICP-MS. *Geostandards and Geoanalytical Research*, 37(3), 297–317. <https://doi.org/10.1111/j.1751-908x.2013.00209.x>
- Gueguen, B., Rouxel, O., Rouget, M. L., Bollinger, C., Ponzevera, E., Germain, Y., & Fouquet, Y. (2016a). Comparative geochemistry of four ferromanganese crusts from the Pacific Ocean and significance for the use of Ni isotopes as paleoceanographic tracers. *Geochimica et Cosmochimica Acta*, 189, 214–235. <https://doi.org/10.1016/j.gca.2016.06.005>
- Gueguen, B., Reinhard, C. T., Algeo, T. J., Peterson, L. C., Nielsen, S. G., Wang, X., et al. (2016). The chromium isotope composition of reducing and oxic marine sediments. *Geochimica et Cosmochimica Acta*, 184, 1–19. <https://doi.org/10.1016/j.gca.2016.04.004>
- Guinoiseau, D., Galer, S. J., & Abouchami, W. (2018). Effect of cadmium sulphide precipitation on the partitioning of Cd isotopes: Implications for the oceanic Cd cycle. *Earth and Planetary Science Letters*, 498, 300–308. <https://doi.org/10.1016/j.epsl.2018.06.039>
- Guinoiseau, D., Galer, S. J., Abouchami, W., Frank, M., Achterberg, E. P., & Haug, G. H. (2019). Importance of cadmium sulfides for biogeochemical cycling of Cd and its isotopes in oxygen deficient zones—A case study of the Angola basin. *Global Biogeochemical Cycles*, 33(12), 1746–1763. <https://doi.org/10.1029/2019gb006323>
- Guo, J., Lapi, S., Ruth, T. J., & Maldonado, M. T. (2012). The effects of iron and copper availability on the copper stoichiometry of marine phytoplankton. *Journal of Phycology*, 48, 312–325. <https://doi.org/10.1111/j.1529-8817.2012.01133.x>
- Hanor, J. S. (2000). Barite-celestine geochemistry and environments of formation. *Reviews in Mineralogy and Geochemistry*, 40(1), 193–275. <https://doi.org/10.2138/rmg.2000.40.4>
- Hanor, J. S., & Chan, L. H. (1977). Non-conservative behavior of barium during mixing of Mississippi River and Gulf of Mexico waters. *Earth and Planetary Science Letters*, 37(2), 242–250. [https://doi.org/10.1016/0012-821x\(77\)90169-8](https://doi.org/10.1016/0012-821x(77)90169-8)
- Hardisty, D. S., Lyons, T. W., Riedinger, N., Isson, T. T., Owens, J. D., Aller, R. C., et al. (2018). An evaluation of sedimentary molybdenum and iron as proxies for pore fluid paleoredox conditions. *American Journal of Science*, 318(5), 527–556. <https://doi.org/10.2475/05.2018.04>
- Hardisty, D. S., Riedinger, N., Planavsky, N. J., Asael, D., Andr n, T., Jorgensen, B. B., & Lyons, T. W. (2016). A Holocene history of dynamic water column redox conditions in the Landsort Deep, Baltic Sea. *American Journal of Science*, 316, 713–745. <https://doi.org/10.2475/08.2016.01>
- Hawco, N. J., Lam, P. J., Lee, J. M., Ohnemus, D. C., Noble, A. E., Wyatt, N. J., et al. (2018). Cobalt scavenging in the mesopelagic ocean and its influence on global mass balance: Synthesizing water column and sedimentary fluxes. *Marine Chemistry*, 201, 151–166. <https://doi.org/10.1016/j.marchem.2017.09.001>
- Hayes, C. T., Anderson, R. F., Cheng, H., Conway, T. M., Edwards, R. L., Fleisher, M. Q., et al. (2018). Replacement times of a spectrum of elements in the North Atlantic based on thorium supply. *Global Biogeochemical Cycles*, 32(9), 1294–1311. <https://doi.org/10.1029/2017gb005839>
- Hayes, J. M. (2004). *An introduction to isotopic calculations*. Woods Hole, MA: Woods Hole Oceanographic Institution. Retrieved from <https://doi.org/10.1575/1912/27058>
- Heller, M. I., & Croot, P. L. (2015). Copper speciation and distribution in the Atlantic sector of the Southern Ocean. *Marine Chemistry*, 173, 253–268. <https://doi.org/10.1016/j.marchem.2014.09.017>
- Helz, G. R., Miller, C. V., Charnock, J. M., Mosselmans, J. F. W., Patrick, R. A. D., Garner, C. D., & Vaughan, D. J. (1996). Mechanism of molybdenum removal from the sea and its concentration in black shales: EXAFS evidence. *Geochimica et Cosmochimica Acta*, 60, 3631–3642. [https://doi.org/10.1016/0016-7037\(96\)00195-0](https://doi.org/10.1016/0016-7037(96)00195-0)
- Hemings, F., Hsieh, Y. T., Bridgestock, L., Spooner, P. T., Robinson, L. F., Frank, N., & Henderson, G. M. (2018). Barium isotopes in cold-water corals. *Earth and Planetary Science Letters*, 491, 183–192. <https://doi.org/10.1016/j.epsl.2018.03.040>
- Henderson, G. M., & Burton, K. W. (1999). Using (²³⁴U/²³⁸U) to assess diffusion rates of isotope tracers in ferromanganese crusts. *Earth and Planetary Science Letters*, 170(3), 169–179. [https://doi.org/10.1016/s0012-821x\(99\)00104-1](https://doi.org/10.1016/s0012-821x(99)00104-1)

- Hendry, K. R., & Andersen, M. B. (2013). The zinc isotopic composition of siliceous marine sponges: Investigating nature's sediment traps. *Chemical Geology*, 354, 33–41. <https://doi.org/10.1016/j.chemgeo.2013.06.025>
- Hendry, K. R., Pyle, K. M., Barney Butler, G., Cooper, A., Fransson, A., Chierici, M., et al. (2018). Spatiotemporal variability of barium in Arctic sea-ice and seawater. *Journal of Geophysical Research: Oceans*, 123(5), 3507–3522. <https://doi.org/10.1029/2017jc013668>
- Hendy, I. L., & Pedersen, T. F. (2005). Is pore water oxygen content decoupled from productivity on the California Margin? Trace element results from ocean drilling program hole 1017E, San Lucia slope, California. *Paleoceanography*, 20(4). <https://doi.org/10.1029/2004pa001123>
- Henkel, S., Kasten, S., Hartmann, J. F., Silva-Busso, A., & Staubwasser, M. (2018). Iron cycling and stable Fe isotope fractionation in Antarctic shelf sediments, King George Island. *Geochimica et Cosmochimica Acta*, 237, 320–338. <https://doi.org/10.1016/j.gca.2018.06.042>
- Hillaire-Marcel, C., & De Vernal, A. (Eds.), (2007). *Proxies in late cenozoic paleoceanography*. Elsevier.
- Ho, P., Lee, J. M., Heller, M. I., Lam, P. J., & Shiller, A. M. (2018). The distribution of dissolved and particulate Mo and V along the U.S. GEOTRACES east Pacific zonal transect (GP16): The roles of oxides and biogenic particles in their distributions in the oxygen deficient zone and the hydrothermal plume. *Marine Chemistry*, 201, 242–255. <https://doi.org/10.1016/j.marchem.2017.12.003>
- Ho, T. Y., Quigg, A., Finkel, Z. V., Milligan, A. J., Wyman, K., Falkowski, P. G., & Morel, F. M. (2003). The elemental composition of some marine phytoplankton 1. *Journal of Phycology*, 39(6), 1145–1159. <https://doi.org/10.1111/j.0022-3646.2003.03-090.x>
- Hodgskiss, M. S., Crockford, P. W., Peng, Y., Wing, B. A., & Horner, T. J. (2019). A productivity collapse to end Earth's great oxidation. *Proceedings of the National Academy of Sciences*, 116(35), 17207–17212. <https://doi.org/10.1073/pnas.1900325116>
- Hohl, S. V., Galer, S. J. G., Gamper, A., & Becker, H. (2017). Cadmium isotope variations in Neoproterozoic carbonates—A tracer of biologic production? *Geochemical Perspective Letters*, 3, 32–44. <https://doi.org/10.7185/geochemlet.1704>
- Hohl, S. V., Jiang, S. Y., Wei, H. Z., Pi, D. H., Liu, Q., Viehmann, S., & Galer, S. J. (2019). Cd Isotopes trace periodic (bio) geochemical metal cycling at the verge of the Cambrian animal evolution. *Geochimica et Cosmochimica Acta*, 263, 195–214. <https://doi.org/10.1016/j.gca.2019.07.036>
- Holmden, C., Jacobson, A. D., Sageman, B. B., & Hurtgen, M. T. (2016). Response of the Cr isotope proxy to cretaceous ocean anoxic event 2 in a pelagic carbonate succession from the western interior seaway. *Geochimica et Cosmochimica Acta*, 186, 277–295. <https://doi.org/10.1016/j.gca.2016.04.039>
- Holzer, M., Primeau, F. W., DeVries, T., & Matear, R. (2014). The Southern Ocean silicon trap: Data-constrained estimates of regenerated silicic acid, trapping efficiencies, and global transport paths. *Journal of Geophysical Research: Oceans*, 119(1), 313–331. <https://doi.org/10.1002/2013jc009356>
- Homoky, W. B., Conway, T. M., John, S. G., Koenig, D., Deng, F., Tagliabue, A., & Mills, R. (2021). Iron colloids dominate sedimentary supply to the ocean interior. *Proceedings of the National Academy of Sciences of the United States of America*, 118(13), e2016078118. <https://doi.org/10.1073/pnas.2016078118>
- Homoky, W. B., John, S. G., Conway, T. M., & Mills, R. A. (2013). Distinct iron isotopic signatures and supply from marine sediment dissolution. *Nature Communications*, 4, 2143. <https://doi.org/10.1038/ncomms3143>
- Homoky, W. B., Severmann, S., Mills, R. A., Fones, G. R., & Fones, G. R. (2009). Pore-fluid Fe isotopes reflect the extent of benthic Fe redox recycling: Evidence from continental shelf and deep-sea sediments. *Geology*, 37, 751–754. <https://doi.org/10.1130/G25731A.1>
- Hoppema, M., Dehairs, F., Navez, J., Monnin, C., Jeandel, C., Fahrbach, E., & de Baar, H. J. W. (2010). Distribution of barium in the Weddell Gyre: Impact of circulation and biogeochemical processes. *Marine Chemistry*, 122(1–4), 118–129. <https://doi.org/10.1016/j.marchem.2010.07.005>
- Horner, T. J., & Crockford, P. (2021). *Barium isotopes: Drivers, dependencies, and distributions through space and time (elements in geochemical tracers in Earth system science)*. Cambridge University Press. <https://doi.org/10.1017/9781108865845>
- Horner, T. J., Kinsley, C. W., & Nielsen, S. G. (2015). Barium-isotopic fractionation in seawater mediated by barite cycling and oceanic circulation. *Earth and Planetary Science Letters*, 430, 511–522. <https://doi.org/10.1016/j.epsl.2015.07.027>
- Horner, T. J., Lee, R. B., Henderson, G. M., & Rickaby, R. E. (2013). Nonspecific uptake and homeostasis drive the oceanic cadmium cycle. *Proceedings of the National Academy of Sciences*, 110(7), 2500–2505. <https://doi.org/10.1073/pnas.1213857110>
- Horner, T. J., Pryer, H. V., Nielsen, S. G., Crockford, P. W., Gauglitz, J. M., Wing, B. A., & Ricketts, R. D. (2017). Pelagic barite precipitation at micromolar ambient sulfate. *Nature Communications*, 8(1), 1342. <https://doi.org/10.1038/s41467-017-01229-5>
- Horner, T. J., Rickaby, R. E. M., & Henderson, G. M. (2011). Isotopic fractionation of cadmium into calcite. *Earth and Planetary Science Letters*, 312(1–2), 243–253. <https://doi.org/10.1016/j.epsl.2011.10.004>
- Horner, T. J., Schönbacher, M., Rehkämper, M., Nielsen, S. G., Williams, H., Halliday, A. N., et al. (2010). Ferromanganese crusts as archives of deep water Cd isotope compositions. *Geochemistry, Geophysics, Geosystems*, 11(4), Q04001. <https://doi.org/10.1029/2009GC002987>
- Horner, T. J., Williams, H. M., Hein, J. R., Saito, M. A., Burton, K. W., Halliday, A. N., & Nielsen, S. G. (2015). Persistence of deeply sourced iron in the Pacific Ocean. *Proceedings of the National Academy of Sciences*, 112, 1292–1297. <https://doi.org/10.1073/pnas.1420188112>
- Hsieh, Y. T., Bridgestock, L., Scheuermann, P. P., Seyfried, W. E., Jr, & Henderson, G. M. (2021). Barium isotopes in mid-ocean ridge hydrothermal vent fluids: A source of isotopically heavy Ba to the ocean. *Geochimica et Cosmochimica Acta*, 292, 348–363. <https://doi.org/10.1016/j.gca.2020.09.037>
- Hsieh, Y. T., & Henderson, G. M. (2017). Barium stable isotopes in the global ocean: Tracer of Ba inputs and utilization. *Earth and Planetary Science Letters*, 473, 269–278. <https://doi.org/10.1016/j.epsl.2017.06.024>
- Huang, T., Moos, S. B., & Boyle, E. A. (2021). Trivalent chromium isotopes in the eastern tropical North Pacific oxygen-deficient zone. *Proceedings of the National Academy of Sciences*, 118(8), e1918605118. <https://doi.org/10.1073/pnas.1918605118>
- Hudson, R. J. M., & Morel, F. M. M. (1993). Trace metal transport by marine microorganisms: Implications of metal coordination kinetics. *Deep-Sea Research*, 40, 129–150. [https://doi.org/10.1016/0967-0637\(93\)90057-a](https://doi.org/10.1016/0967-0637(93)90057-a)
- Hug, S. J., Laubscher, H. U., & James, B. R. (1996). Iron (III) catalyzed photochemical reduction of chromium (VI) by oxalate and citrate in aqueous solutions. *Environmental Science & Technology*, 31(1), 160–170.
- Ijichi, Y., Ohno, T., & Sakata, S. (2018). Copper isotopic fractionation during adsorption on manganese oxide: Effects of pH and desorption. *Geochemical Journal*, 52(2), e1–e6. <https://doi.org/10.2343/geochemj.2.0516>
- Ilna, S. M., Poitrasson, F., Lapitskiy, S. A., Alekhin, Y. V., Viers, J., & Pokrovsky, O. S. (2013). Extreme iron isotope fractionation between colloids and particles of boreal and temperate organic-rich waters. *Geochimica et Cosmochimica Acta*, 101, 96–111. <https://doi.org/10.1016/j.gca.2012.10.023>
- Ingri, J., Malinovsky, D., Rodushkin, I., Baxter, D. C., Widerlund, A., Andersson, P., et al. (2006). Iron isotope fractionation in river colloidal matter. *Earth and Planetary Science Letters*, 245(3–4), 792–798. <https://doi.org/10.1016/j.epsl.2006.03.031>
- Isson, T. T., Love, G. D., Dupont, C. L., Reinhard, C. T., Zumberge, A. J., Asael, D., et al. (2018). Tracking the rise of eukaryotes to ecological dominance with zinc isotopes. *Geobiology*, 16, 341–352. <https://doi.org/10.1111/gbi.12289>

- Ivanochko, T. S. (2001). *Productivity influences on oxygenation of the santa Barbara Basin, California, during the late quaternary (Doctoral dissertation)*. University of British Columbia.
- Jaccard, S. L., Haug, G. H., Sigman, D. M., Pedersen, T. F., Thierstein, H. R., & Röhl, U. (2005). Glacial/interglacial changes in subarctic North Pacific stratification. *Science*, *308*(5724), 1003–1006. <https://doi.org/10.1126/science.1108696>
- Jaccard, S. L., Hayes, C. T., Martínez-García, A., Hodell, D. A., Anderson, R. F., Sigman, D. M., & Haug, G. H. (2013). Two modes of change in Southern Ocean productivity over the past million years. *Science*, *339*(6126), 1419–1423. <https://doi.org/10.1126/science.1227545>
- Jacobs, L., & Emerson, S. (1982). Trace metal solubility in an anoxic fjord. *Earth and Planetary Science Letters*, *60*, 237–252. [https://doi.org/10.1016/0012-821X\(82\)90006-1](https://doi.org/10.1016/0012-821X(82)90006-1)
- Jacobs, L., Emerson, S., & Skei, J. (1985). Partitioning and transport of metals across the O₂H₂S interface in a permanently anoxic basin: Framvaren Fjord, Norway. *Geochimica et Cosmochimica Acta*, *49*, 1433–1444. [https://doi.org/10.1016/0016-7037\(85\)90293-5](https://doi.org/10.1016/0016-7037(85)90293-5)
- Jacquet, S. H., Dehairs, F., Elskens, M., Savoye, N., & Cardinal, D. (2007). Barium cycling along WOCE SR3 line in the Southern Ocean. *Marine Chemistry*, *106*(1–2), 33–45. <https://doi.org/10.1016/j.marchem.2006.06.007>
- Jacquot, J. E., & Moffett, J. W. (2015). Copper distribution and speciation across the International GEOTRACES Section GA03. *Deep Sea Research Part II: Topical Studies in Oceanography*, *116*, 187–207. <https://doi.org/10.1016/j.dsr2.2014.11.013>
- Jakuba, R. W., Saito, M. A., Moffett, J. W., & Xu, Y. (2012). Dissolved zinc in the subarctic North Pacific and Bering Sea: Its distribution, speciation, and importance to primary producers. *Global Biogeochemical Cycles*, *26*, 1–15. <https://doi.org/10.1029/2010gb004004>
- Janssen, D. J., Abouchami, W., Galer, S. J. G., & Cullen, J. T. (2017). Fine-scale spatial and interannual cadmium isotope variability in the subarctic northeast Pacific. *Earth and Planetary Science Letters*, *472*, 241–252. <https://doi.org/10.1016/j.epsl.2017.04.048>
- Janssen, D. J., Abouchami, W., Galer, S. J., Purdon, K. B., & Cullen, J. T. (2019). Particulate cadmium stable isotopes in the subarctic northeast Pacific reveal dynamic Cd cycling and a new isotopically light Cd sink. *Earth and Planetary Science Letters*, *515*, 67–78. <https://doi.org/10.1016/j.epsl.2019.03.006>
- Janssen, D. J., Conway, T. M., John, S. G., Christian, J. R., Kramer, D. I., Pedersen, T. F., & Cullen, J. T. (2014). Undocumented water column sink for cadmium in open ocean oxygen-deficient zones. *Proceedings of the National Academy of Sciences*, *111*(19), 6888–6893. <https://doi.org/10.1073/pnas.1402388111>
- Janssen, D. J., & Cullen, J. T. (2015). Decoupling of zinc and silicic acid in the subarctic northeast Pacific interior. *Marine Chemistry*, *177*, 124–133. <https://doi.org/10.1016/j.marchem.2015.03.014>
- Janssen, D. J., Rickli, J., Abbott, A. N., Ellwood, M. J., Twining, B. S., Ohnemus, D. C., et al. (2021). Release from biogenic particles, benthic fluxes, and deep water circulation control Cr and $\delta^{53}\text{Cr}$ distributions in the ocean interior. *Earth and Planetary Science Letters*, *574*, 117163. <https://doi.org/10.1016/j.epsl.2021.117163>
- Janssen, D. J., Rickli, J., Quay, P. D., White, A. E., Nasemann, P., & Jaccard, S. L. (2020). Biological control of chromium redox and stable isotope composition in the surface ocean. *Global Biogeochemical Cycles*, *34*, 34. <https://doi.org/10.1029/2019GB006397>
- Jeandel, C., & Minster, J. F. (1987). Chromium behavior in the ocean: Global versus regional processes. *Global Biogeochemical Cycles*, *1*, 131–154. <https://doi.org/10.1029/GB001i002p001310.1029/gb001i002p00131>
- John, S. G., & Conway, T. M. (2014). A role for scavenging in the marine biogeochemical cycling of zinc and zinc isotopes. *Earth and Planetary Science Letters*, *394*, 159–167. <https://doi.org/10.1016/j.epsl.2014.02.053>
- John, S. G., Geis, R. W., Saito, M. A., & Boyle, E. A. (2007). Zinc isotope fractionation during high affinity and low-affinity zinc transport by the marine diatom *Thalassiosira oceanica*. *Limnology & Oceanography*, *52*, 2710–2714. <https://doi.org/10.4319/lo.2007.52.6.2710>
- John, S. G., Helgoe, J., & Townsend, E. (2018). Biogeochemical cycling of Zn and Cd and their stable isotopes in the Eastern Tropical South Pacific. *Marine Chemistry*, *201*, 256–262. <https://doi.org/10.1016/j.marchem.2017.06.001>
- John, S. G., Helgoe, J., Townsend, E., Weber, T., DeVries, T., Tagliabue, A., et al. (2018). Biogeochemical cycling of Fe and Fe stable isotopes in the eastern tropical South Pacific. *Marine Chemistry*, *201*, 66–76. <https://doi.org/10.1016/j.marchem.2017.06.003>
- John, S. G., Kunzmann, M., Townsend, E. J., & Rosenberg, A. D. (2017). Zinc and cadmium stable isotopes in the geological record: A case study from the post-snowball Earth Nuccaleena cap dolostone. *Palaeogeography, Palaeoclimatology, Palaeoecology*, *466*, 202–208. <https://doi.org/10.1016/j.palaeo.2016.11.003>
- John, S. G., Mendez, J., Moffett, J., & Adkins, J. (2012). The flux of iron and iron isotopes from San Pedro Basin sediments. *Geochimica et Cosmochimica Acta*, *93*, 14–29. <https://doi.org/10.1016/j.gca.2012.06.003>
- Johnson, C. M., Beard, B. L., & Albarède, F. (2004). Overview and general concepts. *Reviews in Mineralogy and Geochemistry*, *55*(1), 1–24. <https://doi.org/10.2138/gsrmg.55.1.1>
- Johnson, C. M., Beard, B. L., & Roden, E. E. (2008). The iron isotope fingerprints of redox and biogeochemical cycling in modern and ancient Earth. *Annual Review of Earth and Planetary Sciences*, *36*, 457–493. <https://doi.org/10.1146/annurev.earth.36.031207.124139>
- Johnson, C. M., Beard, B. L., & Weyer, S. (2020). *Iron geochemistry: An isotopic perspective*. Springer. <https://doi.org/10.1007/978-3-030-33828-2>
- Johnson, C. M., Skulan, J. L., Beard, B. L., Sun, H., Nealson, K. H., & Braterman, P. S. (2002). Isotopic fractionation between Fe(III) and Fe(II) in aqueous solutions. *Earth and Planetary Science Letters*, *195*, 141–153. [https://doi.org/10.1016/S0012-821X\(01\)00581-7](https://doi.org/10.1016/S0012-821X(01)00581-7)
- Johnson, K. S., Michael Gordon, R., & Coale, K. H. (1997). What controls dissolved iron concentrations in the world ocean? *Marine Chemistry*, *57*(3–4), 137–161. [https://doi.org/10.1016/S0304-4203\(97\)00043-1](https://doi.org/10.1016/S0304-4203(97)00043-1)
- Joung, D. J., & Shiller, A. M. (2016). Temporal and spatial variations of dissolved and colloidal trace elements in Louisiana Shelf waters. *Marine Chemistry*, *181*, 25–43. <https://doi.org/10.1016/j.marchem.2016.03.003>
- Jullion, L., Jacquet, S. H. M., & Tanhua, T. (2017). Untangling biogeochemical processes from the impact of ocean circulation: First insight on the Mediterranean dissolved barium dynamics. *Global Biogeochemical Cycles*, *31*(8), 1256–1270. <https://doi.org/10.1002/2016gb005489>
- Kellogg, M. M., McIlvin, M. R., Vedamati, J., Twining, B. S., Moffett, J. W., Marchetti, A., et al. (2020). Efficient zinc/cobalt inter-replacement in northeast Pacific diatoms and relationship to high surface dissolved Co: Zn ratios. *Limnology & Oceanography*, *65*, 2557–2582. <https://doi.org/10.1002/lno.11471>
- Kendall, B., Dahl, T. W., & Anbar, A. D. (2017). The stable isotope geochemistry of molybdenum. *Reviews in Mineralogy and Geochemistry*, *82*, 683–732. <https://doi.org/10.2138/rmg.2017.82.16>
- Kendall, B., Komiya, T., Lyons, T. W., Bates, S. M., Gordon, G. W., Romaniello, S. J., et al. (2015). Uranium and molybdenum isotope evidence for an episode of widespread ocean oxygenation during the late ediacaran period. *Geochimica et Cosmochimica Acta*, *156*, 173–193. <https://doi.org/10.1016/j.gca.2015.02.025>
- Khatiwala, S., Schmittner, A., & Muglia, J. (2019). Air-sea disequilibrium enhances ocean carbon storage during glacial periods. *Science Advances*, *5*(6), eaaw4981. <https://doi.org/10.1126/sciadv.aaw4981>
- Kieber, R. J., & Helz, G. R. (1992). Indirect photoreduction of aqueous chromium (VI). *Environmental Science & Technology*, *26*, 307–312. <https://doi.org/10.1021/es00026a010>

- Kienast, S. (2003). *Palaeoceanography of the mid-latitude north East Pacific: During the late Pleistocene (Doctoral dissertation)*. University of British Columbia.
- Kim, C., Zhou, Q., Deng, B., Thornton, E. C., & Xu, H. (2001). Chromium (VI) reduction by hydrogen sulfide in aqueous media: Stoichiometry and kinetics. *Environmental Science & Technology*, 35(11), 2219–2225. <https://doi.org/10.1021/es0017007>
- Kim, T., Obata, H., Kondo, Y., Ogawa, H., & Gamo, T. (2015). Distribution and speciation of dissolved zinc in the western North Pacific and its adjacent seas. *Marine Chemistry*, 173, 330–341. <https://doi.org/10.1016/j.marchem.2014.10.016>
- King, E. K., Perakis, S. S., & Pett-Ridge, J. C. (2018). Molybdenum isotope fractionation during adsorption to organic matter. *Geochimica et Cosmochimica Acta*, 222, 584–598. <https://doi.org/10.1016/j.gca.2017.11.014>
- King, E. K., Thompson, A., Chadwick, O. A., & Pett-Ridge, J. C. (2016). Molybdenum sources and isotopic composition during early stages of pedogenesis along a basaltic climate transect. *Chemical Geology*, 445, 54–67. <https://doi.org/10.1016/j.chemgeo.2016.01.024>
- King, E. K., Thompson, A., Hodges, C., & Pett-Ridge, J. C. (2014). Towards understanding temporal and spatial patterns of molybdenum in the critical zone. *Procedia Earth and Planetary Science*, 10, 56–62. <https://doi.org/10.1016/j.proeps.2014.08.011>
- Klar, J. K., Homoky, W. B., Statham, P. J., Birchill, A. J., Harris, E. L., Woodward, E. M. S., et al. (2017). Stability of dissolved and soluble Fe(II) in shelf sediment pore waters and release to an oxic water column. *Biogeochemistry*, 135, 1–67. <https://doi.org/10.1007/s10533-017-0309-x>
- Klar, J. K., James, R. H., Gibbs, D., Lough, A., Parkinson, I., Milton, J. A., et al. (2017). Isotopic signature of dissolved iron delivered to the Southern Ocean from hydrothermal vents in the East Scotia Sea. *Geology*, 45(4), 351–354. <https://doi.org/10.1130/G38432.1>
- Klar, J. K., Schlosser, C., Milton, J. A., Woodward, E. M. S., Lacan, F., Parkinson, I. J., et al. (2018). Sources of dissolved iron to oxygen minimum zone waters on the Senegalese continental margin in the tropical North Atlantic Ocean: Insights from iron isotopes. *Geochimica et Cosmochimica Acta*, 236, 60–78. <https://doi.org/10.1016/j.gca.2018.02.031>
- Klinkhammer, G. P. (1980). Early diagenesis in sediments from the eastern equatorial Pacific, II. Pore water metal results. *Earth and Planetary Science Letters*, 49(1), 81–101. [https://doi.org/10.1016/0012-821x\(80\)90151-x](https://doi.org/10.1016/0012-821x(80)90151-x)
- Klunder, M. B., Laan, P., Middag, R., de Baar, H. J. W., & van Ooijen, J. C. (2011). Dissolved iron in the Southern Ocean (Atlantic sector). *Deep Sea Research Part II: Topical Studies in Oceanography*, 58, 2678–2694. <https://doi.org/10.1016/j.dsr2.2010.10.042>
- Köbberich, M., & Vance, D. (2017). Kinetic control on Zn isotope signatures recorded in marine diatoms. *Geochimica et Cosmochimica Acta*, 210, 97–113. <https://doi.org/10.1016/j.gca.2017.04.014>
- Köbberich, M., & Vance, D. (2019). Zn isotope fractionation during uptake into marine phytoplankton: Implications for oceanic zinc isotopes. *Chemical Geology*, 523, 154–161. <https://doi.org/10.1016/j.chemgeo.2019.04.004>
- Koide, M., Hodge, V. F., Yang, J. S., Stallard, M., Goldberg, E. G., Calhoun, J., & Bertine, K. K. (1986). Some comparative marine chemistries of rhodium, gold, silver and molybdenum. *Applied Geochemistry*, 1, 705–714. [https://doi.org/10.1016/0883-2927\(86\)90092-2](https://doi.org/10.1016/0883-2927(86)90092-2)
- Konhäuser, K. O., Pecoits, E., Lalonde, S. V., Papineau, D., Nisbet, E. G., Barley, M. E., et al. (2009). Oceanic nickel depletion and a methanogen famine before the great oxidation event. *Nature*, 458(7239), 750–753. <https://doi.org/10.1038/nature07858>
- Koschinsky, A., & Halbach, P. (1995). Sequential leaching of marine ferromanganese precipitates: Genetic implications. *Geochimica et Cosmochimica Acta*, 59(24), 5113–5132. [https://doi.org/10.1016/0016-7037\(95\)00358-4](https://doi.org/10.1016/0016-7037(95)00358-4)
- Koschinsky, A., & Hein, J. R. (2003). Uptake of elements from seawater by ferromanganese crusts: Solid-phase associations and seawater speciation. *Marine Geology*, 198(3–4), 331–351. [https://doi.org/10.1016/s0025-3227\(03\)00122-1](https://doi.org/10.1016/s0025-3227(03)00122-1)
- Kowalski, N., Dellwig, O., Beck, M., Gräwe, U., Neubert, N., Nägler, T. F., et al. (2013). Pelagic molybdenum concentration anomalies and the impact of sediment resuspension on the molybdenum budget in two tidal systems of the North Sea. *Geochimica et Cosmochimica Acta*, 119, 198–211. <https://doi.org/10.1016/j.gca.2013.05.046>
- Kramer, D., Cullen, J. T., Christian, J. R., Johnson, W. K., & Pedersen, T. F. (2011). Silver in the subarctic northeast Pacific Ocean: Explaining the basin scale distribution of silver. *Marine Chemistry*, 123, 133–142. <https://doi.org/10.1016/j.marchem.2010.11.002>
- Kunzmann, M., Halverson, G. P., Sossi, P. A., Raub, T. D., Payne, J. L., & Kirby, J. (2013). Zn isotope evidence for immediate resumption of primary productivity after snowball Earth. *Geology*, 41, 27–30. <https://doi.org/10.1130/g33422.1>
- Kurusu, M., Sakata, K., Miyamoto, C., Takaku, Y., Iizuka, T., & Takahashi, Y. (2016). Variation of iron isotope ratios in anthropogenic materials emitted through combustion processes. *Chemistry Letters*, 45, 970–972. <https://doi.org/10.1246/cl.160451>
- Kurusu, M., Takahashi, Y., Iizuka, T., & Uematsu, M. (2016). Very low isotope ratio of iron in fine aerosols related to its contribution to the surface ocean. *Journal of Geophysical Research: Atmospheres*, 121, 11–119. <https://doi.org/10.1002/2016JD024957>
- Labatut, M., Lacan, F., Pradoux, C., Chmieleff, J., Radic, A., Murray, J. W., et al. (2014). Iron sources and dissolved-particulate interactions in the seawater of the Western Equatorial Pacific, iron isotope perspectives. *Global Biogeochemical Cycles*, 28(10), 1044–1065. <https://doi.org/10.1002/2014GB004928>
- Lacan, F., Francois, R., Ji, Y., & Sherrell, R. M. (2006). Cadmium isotopic composition in the ocean. *Geochimica et Cosmochimica Acta*, 70(20), 5104–5118. <https://doi.org/10.1016/j.gca.2006.07.036>
- Lacan, F., Radic, A., Jeandel, C., Poitras, F., Sarthou, G., Pradoux, C., & Freydisse, R. (2008). Measurement of the isotopic composition of dissolved iron in the open ocean. *Geophysical Research Letters*, 35, L24610. <https://doi.org/10.1029/2008GL035841>
- Lal, D., Charles, C., Vacher, L., Goswami, J. N., Jull, A. J. T., McHargue, L., & Finkel, R. C. (2006). Paleo-ocean chemistry records in marine opal: Implications for fluxes of trace elements, cosmogenic nuclides (¹⁰Be and ²⁶Al), and biological productivity. *Geochimica et Cosmochimica Acta*, 70, 3275–3289. <https://doi.org/10.1016/j.gca.2006.04.004>
- Lam, P. J., & Marchal, O. (2015). Insights into particle cycling from thorium and particle data. *Annual Review of Marine Science*, 7, 159–184. <https://doi.org/10.1146/annurev-marine-010814-015623>
- Lambelet, M., Rehkämper, M., van de Fliedert, T., Xue, Z., Kreissig, K., Coles, B., et al. (2013). Isotopic analysis of Cd in the mixing zone of Siberian rivers with the Arctic Ocean—New constraints on marine Cd cycling and the isotope composition of riverine Cd. *Earth and Planetary Science Letters*, 361, 64–73. <https://doi.org/10.1016/j.epsl.2012.11.034>
- Lane, T. W., Saito, M. A., George, G. N., Pickering, I. J., Prince, R. C., & Morel, F. M. (2005). Biochemistry: A cadmium enzyme from a marine diatom. *Nature*, 435(7038), 42–42. <https://doi.org/10.1038/435042a>
- Lauderdale, J. M., Braakman, R., Forget, G., Dutkiewicz, S., & Follows, M. J. (2020). Microbial feedbacks optimize ocean iron availability. *Proceedings of the National Academy of Sciences*, 117(9), 4842–4849. <https://doi.org/10.1073/pnas.1917277117>
- Le Roy, E. L., Sanial, V., Charette, M. A., van Beek, P., Lacan, F., Jacquet, S. H., et al. (2018). The ²²⁶Ra–Ba relationship in the North Atlantic during GEOTRACES-GA01. *Biogeosciences*, 15(9), 3027–3048. <https://doi.org/10.5194/bg-15-3027-2018>
- Lea, D. W., Shen, G. T., & Boyle, E. A. (1989). Coralline barium records temporal variability in equatorial Pacific upwelling. *Nature*, 340(6232), 373–376. <https://doi.org/10.1038/340373a0>
- Lee, J. G., & Morel, F. M. M. (1995). Replacement of zinc by cadmium in marine phytoplankton. *Marine Ecology Progress Series*, 127, 305–309. <https://doi.org/10.3354/meps127305>

- Lemaitre, N., de Souza, G. F., Archer, C., Wang, R. M., Planquette, H., Sarthou, G., & Vance, D. (2020). Pervasive sources of isotopically light zinc in the North Atlantic Ocean. *Earth and Planetary Science Letters*, 539, 116216. <https://doi.org/10.1016/j.epsl.2020.116216>
- Lerner, P., Marchal, O., Lam, P. J., & Solow, A. (2018). Effects of particle composition on thorium scavenging in the North Atlantic. *Geochimica et Cosmochimica Acta*, 233, 115–134. <https://doi.org/10.1016/j.gca.2018.04.035>
- Levasseur, S., Frank, M., Hein, J. R., & Halliday, A. N. (2004). The global variation in the iron isotope composition of marine hydrogenetic ferromanganese deposits: Implications for seawater chemistry? *Earth and Planetary Science Letters*, 224(1–2), 91–105. <https://doi.org/10.1016/j.epsl.2004.05.010>
- Liao, W. H., & Ho, T. Y. (2018). Particulate trace metal composition and sources in the Kuroshio adjacent to the East China Sea: The importance of aerosol deposition. *Journal of Geophysical Research: Oceans*, 123(9), 6207–6223. <https://doi.org/10.1029/2018jc014113>
- Liao, W. H., Takano, S., Yang, S. C., Huang, K. F., Sohrin, Y., & Ho, T. Y. (2020). Zn isotope composition in the water column of the Northwestern Pacific Ocean: The importance of external sources. *Global Biogeochemical Cycles*, 34(1), e2019GB006379. <https://doi.org/10.1029/2019gb006379>
- Liermann, L. J., Guynn, R. L., Anbar, A., & Brantley, S. L. (2005). Production of a molybdophore during metal-targeted dissolution of silicates by soil bacteria. *Chemical Geology*, 220, 285–302. <https://doi.org/10.1016/j.chemgeo.2005.04.013>
- Little, S. H., Archer, C., McManus, J., Najorka, J., Wegorzewski, A. V., & Vance, D. (2020). Towards balancing the oceanic Ni budget. *Earth and Planetary Science Letters*, 547, 116461. <https://doi.org/10.1016/j.epsl.2020.116461>
- Little, S. H., Archer, C., Milne, A., Schlosser, C., Achterberg, E. P., Lohan, M. C., & Vance, D. (2018). Paired dissolved and particulate phase Cu isotope distributions in the South Atlantic. *Chemical Geology*, 502, 29–43. <https://doi.org/10.1016/j.chemgeo.2018.07.022>
- Little, S. H., Sherman, D. M., Vance, D., & Hein, J. R. (2014). Molecular controls on Cu and Zn isotopic fractionation in Fe-Mn crusts. *Earth and Planetary Science Letters*, 396, 213–222. <https://doi.org/10.1016/j.epsl.2014.04.021>
- Little, S. H., Wilson, D. J., Rehkämper, M., Adkins, J. F., Robinson, L. F., & van de Flierdt, T. (2021). Cold-water corals as archives of seawater Zn and Cu isotopes. *Chemical Geology*, 578, 120304. <https://doi.org/10.1016/j.chemgeo.2021.120304>
- Little, S. H., Vance, D., Lyons, T. W., & McManus, J. (2015). Controls on trace metal authigenic enrichment in reducing sediments: Insights from modern oxygen-deficient settings. *American Journal of Science*, 315(2), 77–119. <https://doi.org/10.2475/02.2015.01>
- Little, S. H., Vance, D., McManus, J., & Severmann, S. (2016). Key role of continental margin sediments in the oceanic mass balance of Zn and Zn isotopes. *Geology*, 44, 207–210. <https://doi.org/10.1130/g37493.1>
- Little, S. H., Vance, D., McManus, J., Severmann, S., & Lyons, T. W. (2017). Copper isotope signatures in modern marine sediments. *Geochimica et Cosmochimica Acta*, 212, 253–273. <https://doi.org/10.1016/j.gca.2017.06.019>
- Little, S. H., Vance, D., Siddall, M., & Gasson, E. (2013). A modeling assessment of the role of reversible scavenging in controlling oceanic dissolved Cu and Zn distributions. *Global Biogeochemical Cycles*, 27(3), 780–791. <https://doi.org/10.1002/gbc.20073>
- Little, S. H., Vance, D., Walker-Brown, C., & Landing, W. M. (2014). The oceanic mass balance of copper and zinc isotopes, investigated by analysis of their inputs, and outputs to ferromanganese oxide sediments. *Geochimica et Cosmochimica Acta*, 125, 673–693. <https://doi.org/10.1016/j.gca.2013.07.046>
- Liu, R., Guo, B., Wang, M., Li, W., Yang, T., Ling, H., & Chen, T. (2020). Isotopic fingerprinting of dissolved iron sources in the deep western Pacific since the late Miocene. *Science China Earth Sciences*, 63, 1767–1779. <https://doi.org/10.1007/s11430-020-9648-6>
- Liu, S. A., Wu, H., Shen, S. Z., Jiang, G., Zhang, S., Lv, Y., et al. (2017). Zinc isotope evidence for intensive magmatism immediately before the end-Permian mass extinction. *Geology*, 45, 343–346. <https://doi.org/10.1130/g38644.1>
- Liu, X., & Millero, F. J. (2002). The solubility of iron in seawater. *Marine Chemistry*, 77(1), 43–54. [https://doi.org/10.1016/S0304-4203\(01\)00074-3](https://doi.org/10.1016/S0304-4203(01)00074-3)
- Liu, Y., Li, X., Zeng, Z., Yu, H. M., Huang, F., Felis, T., & Shen, C. C. (2019). Annually-resolved coral skeletal $\delta^{138}\text{Ba}/^{134}\text{Ba}$ records: A new proxy for oceanic Ba cycling. *Geochimica et Cosmochimica Acta*, 247, 27–39. <https://doi.org/10.1016/j.gca.2018.12.022>
- Lohan, M. C., Crawford, D. W., Purdie, D. A., & Statham, P. J. (2005). Iron and zinc enrichments in the northeastern subarctic Pacific: Ligand production and zinc availability in response to phytoplankton growth. *Limnology & Oceanography*, 50, 1427–1437. <https://doi.org/10.4319/lo.2005.50.5.1427>
- Lough, A. J. M., Klar, J. K., Homoky, W. B., Comer-Warner, S. A., Milton, J. A., Connelly, D. P., et al. (2017). Opposing authigenic controls on the isotopic signature of dissolved iron in hydrothermal plumes. *Geochimica et Cosmochimica Acta*, 202, 1–20. <https://doi.org/10.1016/j.gca.2016.12.022>
- Lv, Y., Liu, S. A., Wu, H., Hohl, S. V., Chen, S., & Li, S. (2018). Zn-Sr isotope records of the Ediacaran Doushantuo Formation in South China: Diagenesis assessment and implications. *Geochimica et Cosmochimica Acta*, 239, 330–345. <https://doi.org/10.1016/j.gca.2018.08.003>
- Lyons, T. W., Anbar, A. D., Severmann, S., Scott, C., & Gill, B. C. (2009). Tracking euxinia in the Ancient Ocean: A multiproxy perspective and proterozoic case study. *Annual Review of Earth and Planetary Sciences*, 37, 507–534. <https://doi.org/10.1146/annurev.earth.36.031207.124233>
- Lyons, T. W., & Severmann, S. (2006). A critical look at iron paleoredox proxies: New insights from modern euxinic marine basins. *Geochimica et Cosmochimica Acta*, 70(23), 5698–5722. <https://doi.org/10.1016/j.gca.2006.08.021>
- Ma, Z., Gray, E., Thomas, E., Murphy, B., Zachos, J., & Paytan, A. (2014). Carbon sequestration during the Palaeocene-Eocene thermal maximum by an efficient biological pump. *Nature Geoscience*, 7(5), 382–388. <https://doi.org/10.1038/ngeo2139>
- Ma, Z., Ravelo, A. C., Liu, Z., Zhou, L., & Paytan, A. (2015). Export production fluctuations in the eastern equatorial Pacific during the Pliocene-Pleistocene: Reconstruction using barite accumulation rates. *Paleoceanography*, 30(11), 1455–1469. <https://doi.org/10.1002/2015pa002860>
- Mackey, D. J., O'Sullivan, J. E., Watson, R. J., & Dal Pont, G. (2002). Trace metals in the Western Pacific: Temporal and spatial variability in the concentrations of Cd, Cu, Mn and Ni. *Deep-Sea Research Part I Oceanographic Research Papers*, 49(12), 2241–2259. [https://doi.org/10.1016/S0967-0637\(02\)00124-3](https://doi.org/10.1016/S0967-0637(02)00124-3)
- Mahaffey, C., Reynolds, S., Davis, C. E., & Lohan, M. C. (2014). Alkaline phosphatase activity in the subtropical ocean: Insights from nutrient, dust and trace metal addition experiments. *Frontiers in Marine Science*, 1, 1–13. <https://doi.org/10.3389/fmars.2014.00073>
- Maldonado, M. T., Allen, A. E., Chong, J. S., Lin, K., Leus, D., Karpenko, N., & Harris, S. L. (2006). Copper-dependent iron transport in coastal and oceanic diatoms. *Limnology & Oceanography*, 51, 1729–1743. <https://doi.org/10.4319/lo.2006.51.4.1729>
- Marchitto, T. M., Curry, W. B., & Oppo, D. W. (2000). Zinc concentrations in benthic foraminifera reflect seawater chemistry. *Paleoceanography*, 15, 299–306. <https://doi.org/10.1029/1999pa000420>
- Marcus, M. A., Edwards, K. J., Gueguen, B., Fakra, S. C., Horn, G., Jelinski, N. A., et al. (2015). Iron mineral structure, reactivity, and isotopic composition in a South Pacific Gyre ferromanganese nodule over 4 Ma. *Geochimica et Cosmochimica Acta*, 171, 61–79. <https://doi.org/10.1016/j.gca.2015.08.021>

- Maréchal, C. N., Nicolas, E., Douchet, C., & Albarède, F. (2000). Abundance of zinc isotopes as a marine biogeochemical tracer. *Geochemistry, Geophysics, Geosystems*, 1, 1015. <https://doi.org/10.1029/1999gc000029>
- Maret, W. (2001). Zinc biochemistry, physiology, and homeostasis—Recent insights and current trends. *Biometals*, 14, 187–190. <https://doi.org/10.1023/A:1012945110820>
- Mariotti, A., Germon, J. C., Hubert, P., Kaiser, P., Letolle, R., Tardieux, A., & Tardieux, P. (1981). Experimental determination of nitrogen kinetic isotope fractionation: Some principles; illustration for the denitrification and nitrification processes. *Plant and Soil*, 62, 413–430. <https://doi.org/10.1007/bf02374138>
- Marks, J. A., Perakis, S. S., King, E. K., & Pett-Ridge, J. (2015). Soil organic matter regulates molybdenum storage and mobility in forests. *Biogeochemistry*, 125, 167–183. <https://doi.org/10.1007/s10533-015-0121-4>
- Marsay, C. M., Lam, P. J., Heller, M. I., Lee, J. M., & John, S. G. (2018). Distribution and isotopic signature of ligand-leachable particulate iron along the GEOTRACES GP16 east Pacific zonal transect. *Marine Chemistry*, 201, 198–211. <https://doi.org/10.1016/j.marchem.2017.07.003>
- Martin, J. H. (1990). Glacial-interglacial CO₂ change: The iron hypothesis. *Paleoceanography*, 5, 1–13. <https://doi.org/10.1029/pa005i001p00001>
- Martin, J. H., & Fitzwater, S. E. (1988). Iron deficiency limits phytoplankton growth in the north-east Pacific subarctic. *Nature*, 331(6154), 341–343. <https://doi.org/10.1038/331341a0>
- Martin, J. H., Fitzwater, S. E., & Gordon, R. M. (1990). Iron deficiency limits phytoplankton growth in Antarctic waters. *Global Biogeochemical Cycles*, 4(1), 5–12. <https://doi.org/10.1029/gb004i001p00005>
- Martin, J. H., Knauer, G. A., & Gordon, R. M. (1983). Silver distributions and fluxes in north-east Pacific waters. *Nature*, 305, 306–309. <https://doi.org/10.1038/305306a0>
- Martin, J. H., Knauer, G. A., Karl, D. M., & Broenkow, W. W. (1987). VERTEX: Carbon cycling in the northeast Pacific. *Deep-Sea Research Part A*, 34(2), 267–285. [https://doi.org/10.1016/0198-0149\(87\)90086-0](https://doi.org/10.1016/0198-0149(87)90086-0)
- Martin, J. M., & Thomas, A. J. (1994). The global insignificance of telluric input of dissolved trace metals (Cd, Cu, Ni and Zn) to ocean margins. *Marine Chemistry*, 46(1–2), 165–178. [https://doi.org/10.1016/0304-4203\(94\)90053-1](https://doi.org/10.1016/0304-4203(94)90053-1)
- Martínez Ruíz, F. C., Paytan, A., González Muñoz, M. T., Jroundi, F., Abad, M. D. M., Lam, P. J., et al. (2020). Barite precipitation on suspended organic matter in the mesopelagic zone. *Frontiers of Earth Science*, 8, 567714. <https://doi.org/10.3389/feart.2020.567714>
- Martínez-García, A., Rosell-Melé, A., Jaccard, S. L., Geibert, W., Sigman, D. M., & Haug, G. H. (2011). Southern Ocean dust-climate coupling over the past four million years. *Nature*, 476(7360), 312–315. <https://doi.org/10.1038/nature10310>
- Martínez-García, A., Sigman, D. M., Ren, H., Anderson, R. F., Straub, M., Hodell, D. A., et al. (2014). Iron fertilization of the Subantarctic Ocean during the last ice age. *Science*, 343, 1347–1350. <https://doi.org/10.1126/science.1246848>
- Martínez-Ruiz, F., Paytan, A., González-Muñoz, M. T., Jroundi, F., Abad, M. M., Lam, P. J., et al. (2019). Barite formation in the ocean: Origin of amorphous and crystalline precipitates. *Chemical Geology*, 511, 441–451. <https://doi.org/10.1016/j.chemgeo.2018.09.011>
- Mawji, E., Schlitzer, R., Dodas, E. M., Abadie, C., Abouchami, W., Anderson, R. F., et al. (2015). The GEOTRACES intermediate data product 2014. *Marine Chemistry*, 177, 1–8. <https://doi.org/10.1016/j.marchem.2015.04.005>
- Mayfield, K. K., Eisenhauer, A., Santiago Ramos, D., Higgins, J. A., Horner, T. J., Auro, M. E., et al. (2021). Groundwater discharge impacts marine isotope budgets of Li, Mg, Ca, Sr, and Ba. *Nature Communications*, 12, 148. <https://doi.org/10.1038/s41467-020-20248-3>
- McKay, J. L., & Pedersen, T. F. (2008). The accumulation of silver in marine sediments: A link to biogenic Ba and marine productivity. *Global Biogeochemical Cycles*, 22, GB4010. <https://doi.org/10.1029/2007GB003136>
- McManus, J., Berelson, W. M., Klinkhammer, G. P., Johnson, K. S., Coale, K. H., Anderson, R. F., et al. (1998). Geochemistry of barium in marine sediments: Implications for its use as a paleoproxy. *Geochimica et Cosmochimica Acta*, 62(21–22), 3453–3473. [https://doi.org/10.1016/s0016-7037\(98\)00248-8](https://doi.org/10.1016/s0016-7037(98)00248-8)
- McManus, J., Berelson, W. M., Severmann, S., Poulson, R. L., Hammond, D. E., Klinkhammer, G. P., & Holm, C. (2006). Molybdenum and uranium geochemistry in continental margin sediments: Paleoproxy potential. *Geochimica et Cosmochimica Acta*, 70, 4643–4662. <https://doi.org/10.1016/j.gca.2006.06.1564>
- McManus, J., Dymond, J., Dunbar, R. B., & Collier, R. W. (2002). Particulate barium fluxes in the Ross Sea. *Marine Geology*, 184(1–2), 1–15. [https://doi.org/10.1016/s0025-3227\(01\)00300-0](https://doi.org/10.1016/s0025-3227(01)00300-0)
- Mead, C., Herckes, P., Majestic, B. J., & Anbar, A. D. (2013). Source apportionment of aerosol iron in the marine environment using iron isotope analysis. *Geophysical Research Letters*, 40(21), 5722–5727. <https://doi.org/10.1002/2013gl057713>
- Mendel, R. R., & Bittner, F. (2006). Cell biology of molybdenum. *Biochimica et Biophysica Acta*, 1763(7), 621–635. <https://doi.org/10.1016/j.bbamcr.2006.03.013>
- Middag, R., de Baar, H. J. W., & Bruland, K. W. (2019). The relationships between dissolved zinc and major nutrients phosphate and silicate along the GEOTRACES GA02 transect in the west Atlantic Ocean. *Global Biogeochemical Cycles*, 33, 63–84. <https://doi.org/10.1029/2018GB006034>
- Middag, R., van Heuven, S. M., Bruland, K. W., & de Baar, H. J. (2018). The relationship between cadmium and phosphate in the Atlantic Ocean unraveled. *Earth and Planetary Science Letters*, 492, 79–88. <https://doi.org/10.1016/j.epsl.2018.03.046>
- Middleton, J. L., Langmuir, C. H., Mukhopadhyay, S., McManus, J. F., & Mitrovica, J. X. (2016). Hydrothermal iron flux variability following rapid sea level changes. *Geophysical Research Letters*, 43, 3848–3856. <https://doi.org/10.1002/2016gl068408>
- Miller, C. A., Peucker-Ehrenbrink, B., Walker, B. D., & Marcantonio, F. (2011). Re-assessing the surface cycling of molybdenum and rhenium. *Geochimica et Cosmochimica Acta*, 75, 7146–7179. <https://doi.org/10.1016/j.gca.2011.09.005>
- Miller, L. A., & Bruland, K. W. (1995). Organic speciation of silver in marine waters. *Environmental Science & Technology*, 29, 2616–2621. <https://doi.org/10.1021/es00010a024>
- Millette, M., Wang, X., Planavsky, N. J., Luther, G. W., Lyons, T. W., & Tebo, B. M. (2021). Marine microbial Mn(II) oxidation mediates Cr(III) oxidation and isotope fractionation. *Geochimica et Cosmochimica Acta*, 297, 101–119. <https://doi.org/10.1016/j.gca.2021.01.008>
- Misumi, K., Lindsay, K., Moore, J. K., Doney, S. C., Bryan, F. O., Tsumune, D., & Yoshida, Y. (2014). The iron budget in ocean surface waters in the 20th and 21st centuries: Projections by the Community Earth System Model version. *Biogeosciences*, 11, 33–55. <https://doi.org/10.5194/bg-11-33-2014>
- Mitra, R., Marchitto, T. M., Ge, Q., Zhong, B., Kanakiya, B., Cook, M. S., et al. (2019). Automated species-level identification of planktic foraminifera using convolutional neural networks, with comparison to human performance. *Marine Micropaleontology*, 147, 16–24. <https://doi.org/10.1016/j.marmicro.2019.01.005>
- Moeller, K., Schoenberg, R., Pedersen, R. B., Weiss, D., & Dong, S. (2012). Calibration of the new certified reference materials ERM-AE633 and ERM-AE647 for copper and IRMM-3702 for zinc isotope amount ratio determinations. *Geostandards and Geoanalytical Research*, 36(2), 177–199. <https://doi.org/10.1111/j.1751-908x.2011.00153.x>

- Moffett, J. W., & Brand, L. E. (1996). Production of strong, extracellular Cu chelators by marine cyanobacteria in response to Cu stress. *Limnology & Oceanography*, *41*, 388–395. <https://doi.org/10.4319/lo.1996.41.3.0388>
- Moffett, J. W., & Dupont, C. (2007). Cu complexation by organic ligands in the sub-arctic NW Pacific and Bering Sea. *Deep Sea Research Part I: Oceanographic Research Papers*, *54*, 586–595. <https://doi.org/10.1016/j.dsr.2006.12.013>
- Moffett, J. W., Zika, R. G., & Brand, L. E. (1990). Distribution and potential sources and sinks of copper chelators in the Sargasso Sea. *Deep Sea Research Part A: Oceanographic Research Papers*, *37*, 27–36. [https://doi.org/10.1016/0198-0149\(90\)90027-s](https://doi.org/10.1016/0198-0149(90)90027-s)
- Monnin, C., Jeandel, C., Cattaldo, T., & Dehairs, F. (1999). The marine barite saturation state of the world's oceans. *Marine Chemistry*, *65*(3–4), 253–261. [https://doi.org/10.1016/S0304-4203\(99\)00016-x](https://doi.org/10.1016/S0304-4203(99)00016-x)
- Montoya-Pino, C., Weyer, S., Anbar, A. D., Pross, J., Oschmann, W., van de Schootbrugge, B., & Arz, H. W. (2010). Global enhancement of ocean anoxia during oceanic anoxic event 2: A quantitative approach using U isotopes. *Geology*, *38*(4), 315–318. <https://doi.org/10.1130/g30652.1>
- Moore, C. M. (2016). Diagnosing oceanic nutrient deficiency. *Philosophical Transactions of the Royal Society A: Mathematical, Physical & Engineering Sciences*, *374*(2081), 20150290. <https://doi.org/10.1098/rsta.2015.0290>
- Moore, C. M., Mills, M. M., Arrigo, K. R., Berman-Frank, I., Bopp, L., Boyd, P. W., et al. (2013). Processes and patterns of oceanic nutrient limitation. *Nature Geoscience*, *6*, 701–710. <https://doi.org/10.1038/ngeo1765>
- Moos, S. B., & Boyle, E. A. (2019). Determination of accurate and precise chromium isotope ratios in seawater samples by MC-ICP-MS illustrated by analysis of SAFe Station in the North Pacific Ocean. *Chemical Geology*, *511*, 481–493. <https://doi.org/10.1016/j.chemgeo.2018.07.027>
- Moos, S. B., Boyle, E. A., Altabet, M. A., & Bourbonnais, A. (2020). Investigating the cycling of chromium in the oxygen deficient waters of the eastern tropical north Pacific Ocean and the Santa Barbara basin using stable isotopes. *Marine Chemistry*, *221*, 103756. <https://doi.org/10.1016/j.marchem.2020.103756>
- Morel, F. M., Lam, P. J., & Saito, M. A. (2020). Trace metal substitution in marine phytoplankton. *Annual Review of Earth and Planetary Sciences*, *48*. <https://doi.org/10.1146/annurev-earth-053018-060108>
- Morel, F. M. M., & Price, N. M. (2003). The biogeochemical cycles of trace metals in the oceans. *Science*, *300*, 944–947. <https://doi.org/10.1126/science.1083545>
- Morel, F. M. M., Reinfelder, J. R., Roberts, S. B., Chamberlain, C. P., Lee, J. G., & Yee, D. (1994). Zinc and carbon co-limitation of marine phytoplankton. *Nature*, *369*, 740–742. <https://doi.org/10.1038/369740a0>
- Morford, J. L., Kalnejais, L. H., Helman, P., Yen, G., & Reinard, M. (2008). Geochemical cycling of silver in marine sediments along an offshore transect. *Marine Chemistry*, *110*, 77–88. <https://doi.org/10.1016/j.marchem.2008.02.008>
- Morgan, J. L., Wasylenki, L. E., Nuester, J., & Anbar, A. D. (2010). Fe isotope fractionation during equilibration of Fe-organic complexes. *Environmental Science & Technology*, *44*(16), 6095–6101. <https://doi.org/10.1021/es100906z>
- Morris, A. W. (1975). Dissolved molybdenum and vanadium in the northeast Atlantic Ocean. *Deep-Sea Research and Oceanographic Abstracts*, *22*, 49–54. [https://doi.org/10.1016/0011-7471\(75\)90018-2](https://doi.org/10.1016/0011-7471(75)90018-2)
- Moynier, F., Vance, D., Fujii, T., & Savage, P. (2017). The isotope geochemistry of zinc and copper. *Reviews in Mineralogy and Geochemistry*, *82*, 543–600. <https://doi.org/10.2138/rmg.2017.82.13>
- Mulholland, D. S., Poittrasson, F., Boaventura, G. R., Allard, T., Vieira, L. C., Santos, R. V., et al. (2015). Insights into iron sources and pathways in the Amazon River provided by isotopic and spectroscopic studies. *Geochimica et Cosmochimica Acta*, *150*, 142–159. <https://doi.org/10.1016/j.gca.2014.12.004>
- Murphy, K. L. (2016). *Isotopic studies in marine geochemistry (Doctoral dissertation)*. Imperial College London. <https://doi.org/10.25560/68270>
- Murray, J. W., Spell, B., & Paul, B. (1983). The contrasting geochemistry of manganese and chromium in the eastern tropical Pacific Ocean. In C. S. Wong, E. Boyle, K. W. Bruland, J. D. Burton, & E. D. Goldberg (Eds.), *Trace metals in sea water. NATO conference series (IV marine Sciences)* (Vol. 9, pp. 643–669). Boston, MA: Springer. https://doi.org/10.1007/978-1-4757-6864-0_37
- Nägler, T. F., Anbar, A. D., Archer, C., Goldberg, T., Gordon, G. W., Greber, N. D., et al. (2014). Proposal for an international molybdenum isotope measurement standard and data representation. *Geostandards and Geoanalytical Research*, *38*(2), 149–151. <https://doi.org/10.1111/ggr.2014.38.issue-3>
- Nägler, T. F., Neubert, N., Böttcher, M. E., Dellwig, O., & Schnetger, B. (2011). Molybdenum isotope fractionation in pelagic euxinia: Evidence from the modern Black and Baltic Seas. *Chemical Geology*, *289*, 1–11. <https://doi.org/10.1016/j.chemgeo.2011.07.001>
- Nakagawa, Y., Takano, S., Firdaus, M. L., Norisuye, K., Hirata, T., Vance, D., & Sohrin, Y. (2012). The molybdenum isotopic composition of the modern ocean. *Geochemical Journal*, *46*, 131–141. <https://doi.org/10.2343/geochemj.1.0158>
- Nameroff, T. J., Calvert, S. E., & Murray, J. W. (2004). Glacial-interglacial variability in the eastern tropical North Pacific oxygen minimum zone recorded by redox-sensitive trace metals. *Paleoceanography*, *19*(1), PA1010. <https://doi.org/10.1029/2003PA000912>
- Nan, X. Y., Yu, H. M., Rudnick, R. L., Gaschnig, R. M., Xu, J., Li, W.-Y., et al. (2018). Barium isotopic composition of the upper continental crust. *Geochimica et Cosmochimica Acta*, *233*, 33–49. <https://doi.org/10.1016/j.gca.2018.05.004>
- Nasemann, P., Gault-Ringold, M., Stirling, C. H., Koschinsky, A., & Sander, S. G. (2018). Processes affecting the isotopic composition of dissolved iron in hydrothermal plumes: A case study from the Vanuatu back-arc. *Chemical Geology*, *476*, 70–84. <https://doi.org/10.1016/j.chemgeo.2017.11.005>
- Nasemann, P., Janssen, D. J., Rickli, J., Grasse, P., Franck, M., & Jaccard, S. L. (2020). Chromium reduction and associated stable isotope fractionation restricted to anoxic shelf waters in the Peruvian Oxygen Minimum Zone. *Geochimica et Cosmochimica Acta*, *285*, 207–224. <https://doi.org/10.1016/j.gca.2020.06.027>
- Navarrete, J. U., Borrok, D. M., Viveros, M., & Ellzey, J. T. (2011). Copper isotope fractionation during surface adsorption and intracellular incorporation by bacteria. *Geochimica et Cosmochimica Acta*, *75*(3), 784–799. <https://doi.org/10.1016/j.gca.2010.11.011>
- Ndung'u, K., Thomas, M. A., & Flegal, A. R. (2001). Silver in the western equatorial and South Atlantic Ocean. *Deep-Sea Research II*, *48*, 2933–2945.
- Neubert, N., Nægler, T. F., & Böttcher, M. E. (2008). Sulfidity controls molybdenum isotope fractionation into euxinic sediments: Evidence from the modern Black Sea. *Geology*, *36*, 775–778. <https://doi.org/10.1130/G24959A.1>
- Nielsen, S. G., Wasylenki, L. E., Rehkämper, M., Peacock, C. L., Xue, Z., & Moon, E. M. (2013). Towards an understanding of thallium isotope fractionation during adsorption to manganese oxides. *Geochimica et Cosmochimica Acta*, *117*, 252–265. <https://doi.org/10.1016/j.gca.2013.05.004>
- Nishioka, J., Obata, H., Ogawa, H., Ono, K., Yamashita, Y., Lee, K., et al. (2020). Subpolar marginal seas fuel the North Pacific through the intermediate water at the termination of the global ocean circulation. *Proceedings of the National Academy of Sciences of the United States of America*, *117*(23), 12665–12673. <https://doi.org/10.1073/pnas.2000658117>

- Noordmann, J., Weyer, S., Montoya-Pino, C., Dellwig, O., Neubert, N., Eckert, S., et al. (2015). Uranium and molybdenum isotope systematics in modern euxinic basins: Case studies from the central Baltic Sea and the Kyllaren fjord (Norway). *Chemical Geology*, *396*, 182–195. <https://doi.org/10.1016/j.chemgeo.2014.12.012>
- Nuester, J., Vogt, S., Newville, M., Kustka, A. B., & Twining, B. S. (2012). The unique biogeochemical signature of the marine diazotroph *Trichodesmium*. *Frontiers in Microbiology*, *3*, 150. <https://doi.org/10.3389/fmicb.2012.00150>
- Ohnemus, D. C., & Lam, P. J. (2015). Cycling of lithogenic marine particles in the US GEOTRACES North Atlantic transect. *Deep Sea Research Part II: Topical Studies in Oceanography*, *116*, 283–302. <https://doi.org/10.1016/j.dsr2.2014.11.019>
- Ohnemus, D. C., Rauschenberg, S., Cutter, G. A., Fitzsimmons, J. N., Sherrell, R. M., & Twining, B. S. (2017). Elevated trace metal content of prokaryotic communities associated with marine oxygen deficient zones. *Limnology & Oceanography*, *62*(1), 3–25. <https://doi.org/10.1002/lno.10363>
- Ohnemus, D. C., Torrie, R., & Twining, B. S. (2019). Exposing the distributions and elemental associations of scavenged particulate phases in the ocean using basin-scale multi-element data sets. *Global Biogeochemical Cycles*, *33*(6), 725–748. <https://doi.org/10.1029/2018GB006145>
- Owens, J. D., Nielsen, S. G., Horner, T. J., Ostrander, C. M., & Peterson, L. C. (2017). Thallium-isotopic compositions of euxinic sediments as a proxy for global manganese-oxide burial. *Geochimica et Cosmochimica Acta*, *213*, 291–307. <https://doi.org/10.1016/j.gca.2017.06.041>
- Park, H., Song, B., & Morel, F. M. (2007). Diversity of the cadmium-containing carbonic anhydrase in marine diatoms and natural waters. *Environmental Microbiology*, *9*(2), 403–413. <https://doi.org/10.1111/j.1462-2920.2006.01151.x>
- Paytan, A. (2009). Ocean paleoproductivity. In V. Gornitz (Ed.), *Encyclopedia of paleoclimatology and ancient environments. Encyclopedia of Earth Sciences Series*. Dordrecht: Springer.
- Paytan, A., & Griffith, E. M. (2007). Marine barite: Recorder of variations in ocean export productivity. *Deep Sea Research Part II: Topical Studies in Oceanography*, *54*(5–7), 687–705. <https://doi.org/10.1016/j.dsr2.2007.01.007>
- Paytan, A., & Kastner, M. (1996). Benthic Ba fluxes in the central Equatorial Pacific, implications for the oceanic Ba cycle. *Earth and Planetary Science Letters*, *142*(3–4), 439–450. [https://doi.org/10.1016/0012-821x\(96\)00120-3](https://doi.org/10.1016/0012-821x(96)00120-3)
- Paytan, A., Kastner, M., & Chavez, F. P. (1996). Glacial to interglacial fluctuations in productivity in the equatorial Pacific as indicated by marine barite. *Science*, *274*(5291), 1355–1357. <https://doi.org/10.1126/science.274.5291.1355>
- Paytan, A., Mackey, K. R., Chen, Y., Lima, I. D., Doney, S. C., Mahowald, N., et al. (2009). Toxicity of atmospheric aerosols on marine phytoplankton. *Proceedings of the National Academy of Sciences*, *106*(12), 4601–4605. <https://doi.org/10.1073/pnas.0811486106>
- Peers, G., & Price, N. M. (2006). Copper-containing plastocyanin used for electron transport by an oceanic diatom. *Nature*, *441*, 341–344. <https://doi.org/10.1038/nature04630>
- Peers, G., Quesnel, S., & Price, N. M. (2005). Copper requirements for iron acquisition and growth of coastal and oceanic diatoms. *Limnology & Oceanography*, *50*, 1149–1158. <https://doi.org/10.4319/lo.2005.50.4.1149>
- Pereira, N. S., Vögelin, A. R., Paulukat, C., Sial, A. N., Ferreira, V. P., & Frei, R. (2016). Chromium-isotope signatures in scleractinian corals from the Rocas Atoll, Tropical South Atlantic. *Geobiology*, *14*, 54–67. <https://doi.org/10.1111/gbi.12155>
- Pettine, M., D'Ottone, L., Campanella, L., Millero, F. J., & Passino, R. (1998). The reduction of chromium (VI) by iron (II) in aqueous solutions. *Geochimica et Cosmochimica Acta*, *62*(9), 1509–1519. [https://doi.org/10.1016/s0016-7037\(98\)00086-6](https://doi.org/10.1016/s0016-7037(98)00086-6)
- Pettine, M., Millero, F. J., & La Noce, T. (1991). Chromium (III) interactions in seawater through its oxidation kinetics. *Marine Chemistry*, *34*(1–2), 29–46. [https://doi.org/10.1016/0304-4203\(91\)90012-1](https://doi.org/10.1016/0304-4203(91)90012-1)
- Pichat, S., Douchet, C., & Albarède, F. (2003). Zinc isotope variations in deep-sea carbonates from the eastern equatorial Pacific over the last 175 ka. *Earth and Planetary Science Letters*, *210*, 167–178. [https://doi.org/10.1016/s0012-821x\(03\)00106-7](https://doi.org/10.1016/s0012-821x(03)00106-7)
- Pichevin, L. E., Ganeshram, R. S., Geibert, W., Thunell, R., & Hinton, R. (2014). Silica burial enhanced by iron limitation in oceanic upwelling margins. *Nature Geoscience*, *7*(7), 541–546. <https://doi.org/10.1038/ngeo2181>
- Pinedo-González, P., Hawco, N. J., Bundy, R. M., Virginia Armbrust, E., Follows, M. J., Cael, B. B., et al. (2020). Anthropogenic Asian aerosols provide Fe to the north Pacific Ocean. *Proceedings of the National Academy of Sciences of the United States of America*, *117*, 27862–27868. <https://doi.org/10.1073/pnas.2010315117>
- Plass, A., Schlosser, C., Sommer, S., Dale, A. W., Achterberg, E. P., & Scholz, F. (2020). The control of hydrogen sulfide on benthic iron and cadmium fluxes in the oxygen minimum zone off Peru. *Biogeosciences*, *17*(13), 3685–3704. <https://doi.org/10.5194/bg-17-3685-2020>
- Poitrasson, F. (2006). On the iron isotope homogeneity level of the continental crust. *Chemical Geology*, *235*(1–2), 195–200. <https://doi.org/10.1016/j.chemgeo.2006.06.010>
- Poitrasson, F., Vieira, L. C., Seyler, P., dos Santos Pinheiro, G. M., Mulholland, D. S., Bonnet, M. P., et al. (2014). Iron isotope composition of the bulk waters and sediments from the Amazon River basin. *Chemical Geology*, *377*, 1–11. <https://doi.org/10.1016/j.chemgeo.2014.03.019>
- Pokrovsky, O. S., Viers, J., Emnova, E. E., Kompantseva, E. I., & Freyrier, R. (2008). Copper isotope fractionation during its interaction with soil and aquatic microorganisms and metal oxy (hydr) oxides: Possible structural control. *Geochimica et Cosmochimica Acta*, *72*(7), 1742–1757. <https://doi.org/10.1016/j.gca.2008.01.018>
- Posacka, A. M., Semeniuk, D. M., Whitby, H., Van Den Berg, C. M., Cullen, J. T., Orians, K., & Maldonado, M. T. (2017). Dissolved copper (dCu) biogeochemical cycling in the subarctic Northeast Pacific and a call for improving methodologies. *Marine Chemistry*, *196*, 47–61. <https://doi.org/10.1016/j.marchem.2017.05.007>
- Price, N. M., & Morel, F. M. M. (1990). Cadmium and cobalt substitution for zinc in a marine diatom. *Nature*, *344*(6267), 658–660. <https://doi.org/10.1038/344658a0>
- Price, N. M., & Morel, F. M. M. (1991). Colimitation of phytoplankton growth by nickel and nitrogen. *Limnology & Oceanography*, *50*, 1071–1077. <https://doi.org/10.4319/lo.1991.36.6.1071>
- Quay, P., & Wu, J. (2015). Impact of end-member mixing on depth distributions of $\delta^{13}\text{C}$, cadmium and nutrients in the N. Atlantic Ocean. *Deep Sea Research Part II*, *116*, 107–116. <https://doi.org/10.1016/j.dsr2.2014.11.009>
- Radic, A., Lacan, F., & Murray, J. W. (2011). Iron isotopes in the seawater of the equatorial Pacific Ocean: New constraints for the oceanic iron cycle. *Earth and Planetary Science Letters*, *306*, 1–10. <https://doi.org/10.1016/j.epsl.2011.03.015>
- Rafter, P. A., Sigman, D. M., & Mackey, K. R. (2017). Recycled iron fuels new production in the eastern equatorial Pacific Ocean. *Nature Communications*, *8*(1), 1100. <https://doi.org/10.1038/s41467-017-01219-7>
- Ragsdale, S. W. (2009). Nickel-based enzymes. *Journal of Biological Chemistry*, *284*, 18571–18575. <https://doi.org/10.1074/jbc.r900020200>
- Ranville, M. A., Cutter, G. A., Buck, C. S., Landing, W. M., Cutter, L. S., Resing, J. A., & Flegal, A. R. (2010). Aeolian contamination of Se and Ag in the North Pacific from Asian fossil fuel combustion. *Environmental Science & Technology*, *44*, 1587–1593. <https://doi.org/10.1021/es902523m>

- Ranville, M. A., & Flegal, A. R. (2005). Silver in the north Pacific Ocean. *Geochemistry, Geophysics, Geosystems*, 6(3). <https://doi.org/10.1029/2004GC000770>
- Rehkämper, M., Wombacher, F., Horner, T. J., & Xue, Z. (2012). Natural and anthropogenic Cd isotope variations. In M. Baskaran (Ed.), *Handbook of environmental isotope geochemistry* (pp. 125–154). Berlin, Heidelberg: Springer. https://doi.org/10.1007/978-3-642-10637-8_8
- Reinhard, C. T., Planavsky, N. J., Robbins, L. J., Partin, C. A., Gill, B. C., Lalonde, S. V., et al. (2013). Proterozoic ocean redox and biogeochemical stasis. *Proceedings of the National Academy of Sciences*, 110, 5357–5362. <https://doi.org/10.1073/pnas.1208622110>
- Reinhard, C. T., Planavsky, N. J., Wang, X., Fischer, W. W., Johnson, T. M., & Lyons, T. W. (2014). The isotopic composition of authigenic chromium in anoxic marine sediments: A case study from the Cariaco basin. *Earth and Planetary Science Letters*, 407, 9–18. <https://doi.org/10.1016/j.epsl.2014.09.024>
- Remmelzwaal, S. R. C., Sadekov, A. Y., Parkinson, I. J., Schmidt, D. N., Titelboim, D., Abramovich, S., et al. (2019). Post-depositional overprinting of chromium in foraminifera. *Earth and Planetary Science Letters*, 515, 100–111. <https://doi.org/10.1016/j.epsl.2019.03.001>
- Resing, J. A., Sedwick, P. N., German, C. R., Jenkins, W. J., Moffett, J. W., Sohst, B. M., & Tagliabue, A. (2015). Basin-scale transport of hydrothermal dissolved metals across the South Pacific Ocean. *Nature*, 523(7559), 200–203. <https://doi.org/10.1038/nature14577>
- Revels, B. N., Zhang, R., Adkins, J. F., & John, S. G. (2015). Fractionation of iron isotopes during leaching of natural particles by acidic and circumneutral leaches and development of an optimal leach for marine particulate iron isotopes. *Geochimica et Cosmochimica Acta*, 166, 92–104. <https://doi.org/10.1016/j.gca.2015.05.034>
- Reynolds, B. C., Frank, M., & Halliday, A. N. (2006). Silicon isotope fractionation during nutrient utilization in the North Pacific. *Earth and Planetary Science Letters*, 244(1–2), 431–443. <https://doi.org/10.1016/j.epsl.2006.02.002>
- Richon, C., & Tagliabue, A. (2019). Insights into the major processes driving the global distribution of copper in the ocean from a global model. *Global Biogeochemical Cycles*, 33(12), 1594–1610. <https://doi.org/10.1029/2019gb006280>
- Rickaby, R. E. M., & Elderfield, H. (1999). Planktonic foraminiferal Cd/Ca: Paleonutrients or paleotemperature? *Paleoceanography*, 14(3), 293–303. <https://doi.org/10.1029/1999pa900007>
- Rickli, J., Janssen, D. J., Hassler, C., Ellwood, M. J., & Jaccard, S. L. (2019). Chromium biogeochemistry and stable isotope distribution in the Southern Ocean. *Geochimica et Cosmochimica Acta*, 262, 188–206. <https://doi.org/10.1016/j.gca.2019.07.033>
- Ridge, P. G., Zhang, Y., & Gladyshev, V. N. (2008). Comparative genomic analyses of copper transporters and cuproproteomes reveal evolutionary dynamics of copper utilization and its link to oxygen. *PLoS One*, 3(1), e1378. <https://doi.org/10.1371/journal.pone.0001378>
- Rijkenberg, M. J. A., Middag, R., Laan, P., Gerringa, L. J., van Aken, H. M., Schoemann, V., et al. (2014). The distribution of dissolved iron in the West Atlantic Ocean. *PLoS One*, 9(6). <https://doi.org/10.1371/journal.pone.0101323>
- Ripperger, S., & Rehkämper, M. (2007). Precise determination of cadmium isotope fractionation in seawater by double spike MC-ICPMS. *Geochimica et Cosmochimica Acta*, 71(3), 631–642. <https://doi.org/10.1016/j.gca.2006.10.005>
- Ripperger, S., Rehkämper, M., Porcelli, D., & Halliday, A. N. (2007). Cadmium isotope fractionation in seawater—A signature of biological activity. *Earth and Planetary Science Letters*, 261(3–4), 670–684. <https://doi.org/10.1016/j.epsl.2007.07.034>
- Rivera-Duarte, I., Flegal, A. R., Sañudo-Wilhelmy, S. A., & Véron, A. J. (1999). Silver in the far North Atlantic Ocean. *Deep-Sea Research II*, 46, 979–990. [https://doi.org/10.1016/S0967-0645\(99\)00012-0](https://doi.org/10.1016/S0967-0645(99)00012-0)
- Rohatgi, A. (2019). WebPlotDigitizer (version 4.2; April 2019). Retrieved from <https://automeris.io/WebPlotDigitizer>
- Rolison, J. M., Stirling, C. H., Middag, R., Gault-Ringold, M., George, E., & Rijkenberg, M. J. A. (2018). Iron isotope fractionation during pyrite formation in a sulfidic Precambrian ocean analogue. *Earth and Planetary Science Letters*, 488, 1–13. <https://doi.org/10.1016/j.epsl.2018.02.006>
- Rosenthal, Y., Lam, P., Boyle, E. A., & Thomson, J. (1995). Authigenic cadmium enrichments in suboxic sediments: Precipitation and post-depositional mobility. *Earth and Planetary Science Letters*, 132(1–4), 99–111. [https://doi.org/10.1016/0012-821X\(95\)00056-I](https://doi.org/10.1016/0012-821X(95)00056-I)
- Roshan, S., DeVries, T., Wu, J., & Chen, G. (2018). The internal cycling of zinc in the ocean. *Global Biogeochemical Cycles*, 32(12), 1833–1849. <https://doi.org/10.1029/2018GB006045>
- Roshan, S., DeVries, T., Wu, J., John, S., & Weber, T. (2020). Reversible scavenging traps hydrothermal iron in the deep ocean. *Earth and Planetary Science Letters*, 542, 116297. <https://doi.org/10.1016/j.epsl.2020.116297>
- Roshan, S., & Wu, J. (2015a). The distribution of dissolved copper in the tropical-subtropical north Atlantic across the GEOTRACES GA03 transect. *Marine Chemistry*, 176, 189–198. <https://doi.org/10.1016/j.marchem.2015.09.006>
- Roshan, S., & Wu, J. (2015b). Cadmium regeneration within the North Atlantic. *Global Biogeochemical Cycles*, 29(12), 2082–2094. <https://doi.org/10.1002/2015gb005215>
- Roshan, S., & Wu, J. (2018). Dissolved and colloidal copper in the tropical South Pacific. *Geochimica et Cosmochimica Acta*, 233, 81–94. <https://doi.org/10.1016/j.gca.2018.05.008>
- Rouxel, O., Shanks, W. C., III, Bach, W., & Edwards, K. J. (2008). Integrated Fe-and S-isotope study of seafloor hydrothermal vents at East Pacific Rise 9–10 N. *Chemical Geology*, 252(3–4), 214–227. <https://doi.org/10.1016/j.chemgeo.2008.03.009>
- Rouxel, O., Toner, B., Germain, Y., & Glazer, B. (2018). Geochemical and iron isotopic insights into hydrothermal iron oxyhydroxide deposit formation at Loihi Seamount. *Geochimica et Cosmochimica Acta*, 220, 449–482. <https://doi.org/10.1016/j.gca.2017.09.050>
- Rouxel, O., Toner, B. M., Manganini, S. J., & German, C. R. (2016). Geochemistry and iron isotope systematics of hydrothermal plume fall-out at East Pacific Rise 9°50'N. *Chemical Geology*, 441, 212–234. <https://doi.org/10.1016/j.chemgeo.2016.08.027>
- Rouxel, O. J., Bekker, A., & Edwards, K. J. (2005). Iron isotope constraints on the Archean and Paleoproterozoic ocean redox state. *Science*, 307(5712), 1088–1091. <https://doi.org/10.1126/science.1105692>
- Rue, E. L., Smith, G. J., Cutter, G. A., & Bruland, K. W. (1997). The response of trace element redox couples to suboxic conditions in the water column. *Deep-Sea Research I*, 44(1), 113–134. [https://doi.org/10.1016/S0967-0637\(96\)00088-X](https://doi.org/10.1016/S0967-0637(96)00088-X)
- Rushdi, A. I., McManus, J., & Collier, R. W. (2000). Marine barite and celestite saturation in seawater. *Marine Chemistry*, 69(1–2), 19–31. [https://doi.org/10.1016/S0304-4203\(99\)00089-4](https://doi.org/10.1016/S0304-4203(99)00089-4)
- Ryan, B. M., Kirby, J. K., Degryse, F., Scheiderich, K., & McLaughlin, M. J. (2014). Copper isotope fractionation during equilibration with natural and synthetic ligands. *Environmental Science & Technology*, 48(15), 8620–8626. <https://doi.org/10.1021/es500764x>
- Saito, M. A., Bertrand, E. M., Dutkiewicz, S., Bulygin, V. V., Moran, D. M., Monteiro, F. M., et al. (2011). Iron conservation by reduction of metalloenzyme inventories in the marine diazotroph *Crocospaera watsonii*. *Proceedings of the National Academy of Sciences*, 108(6), 2184–2189. <https://doi.org/10.1073/pnas.1006943108>
- Saito, M. A., Moffett, J. W., & DiTullio, G. R. (2004). Cobalt and nickel in the Peru upwelling region: A major flux of labile cobalt utilized as a micronutrient. *Global Biogeochemical Cycles*, 18, 1–14. <https://doi.org/10.1029/2003gb002216>
- Saito, M. A., Noble, A. E., Tagliabue, A., Goepfert, T. J., Lamborg, C. H., & Jenkins, W. J. (2013). Slow-spreading submarine ridges in the South Atlantic as a significant oceanic iron source. *Nature Geoscience*, 6(9), 775–779. <https://doi.org/10.1038/ngeo1893>

- Samanta, M., Ellwood, M. J., Sinoir, M., & Hassler, C. S. (2017). Dissolved zinc isotope cycling in the Tasman Sea, SW Pacific Ocean. *Marine Chemistry*, 192, 1–12. <https://doi.org/10.1016/j.marchem.2017.03.004>
- Samanta, M., Ellwood, M. J., & Strzpek, R. F. (2018). Zinc isotope fractionation by *Emiliania huxleyi* cultured across a range of free zinc ion concentrations. *Limnology & Oceanography*, 63, 660–671. <https://doi.org/10.1002/lno.10658>
- Sarmiento, J. L., & Gruber, M. (2006). Carbon Cycle. In *Ocean biogeochemical dynamics* (pp. 318–358). Princeton, NJ: Princeton University Press.
- Sarmiento, J. L., Gruber, N., Brzezinski, M. A., & Dunne, J. P. (2004). High-latitude controls of thermocline nutrients and low latitude biological productivity. *Nature*, 427(6969), 56–60. <https://doi.org/10.1038/nature02127>
- Scheiderich, K., Amini, M., Holmden, C., & Francois, R. (2015). Global variability of chromium isotopes in seawater demonstrated by Pacific, Atlantic, and Arctic Ocean samples. *Earth and Planetary Science Letters*, 423, 87–97. <https://doi.org/10.1016/j.epsl.2015.04.030>
- Schlitzer, R. (2019). *eGEOTRACES - Electronic Atlas of GEOTRACES sections and Animated 3D scenes*. Retrieved from <http://egeotraces.org>
- Schlitzer, R., Anderson, R. F., Dodas, E. M., Lohan, M., Geibert, W., Tagliabue, A., et al. (2018). The GEOTRACES intermediate data product 2017. *Chemical Geology*, 493, 210–223.
- Schmitt, A. D., Galer, S. J., & Abouchami, W. (2009a). Mass-dependent cadmium isotopic variations in nature with emphasis on the marine environment. *Earth and Planetary Science Letters*, 277(1–2), 262–272. <https://doi.org/10.1016/j.epsl.2008.10.025>
- Schmitt, A. D., Galer, S. J., & Abouchami, W. (2009b). High-precision cadmium stable isotope measurements by double spike thermal ionisation mass spectrometry. *Journal of Analytical Atomic Spectrometry*, 24(8), 1079–1088. <https://doi.org/10.1039/b821576f>
- Schmitz, B. (1987). Barium, equatorial high productivity, and the northward wandering of the Indian continent. *Paleoceanography*, 2(1), 63–77. <https://doi.org/10.1029/pa002i001p00063>
- Schoenberg, R., Zink, S., Staubwasser, M., & von Blackenburg, F. (2008). The stable Cr isotope inventory of solid Earth reservoirs determined by double spike MC-ICP-MS. *Chemical Geology*, 249, 294–306. <https://doi.org/10.1016/j.chemgeo.2008.01.009>
- Scholz, F., McManus, J., & Sommer, S. (2013). The manganese and iron shuttle in a modern euxinic basin and implications for molybdenum cycling at euxinic ocean margins. *Chemical Geology*, 355, 56–68. <https://doi.org/10.1016/j.chemgeo.2013.07.006>
- Scholz, F., Siebert, C., Dale, A. W., & Frank, M. (2017). Intense molybdenum accumulation in sediments unearths a nitrogenous water column and implications for the reconstruction of paleo-redox conditions based on molybdenum isotopes. *Geochimica et Cosmochimica Acta*, 213, 400–417. <https://doi.org/10.1016/j.gca.2017.06.048>
- Schönbächler, M., Carlson, R. W., Horan, M. F., Mock, T. D., & Hauri, E. H. (2007). High precision Ag isotope measurements in geologic materials by multiple-collector ICPMS: An evaluation of dry versus wet plasma. *International Journal of Mass Spectrometry*, 261(2–3), 183–191. <https://doi.org/10.1016/j.ijms.2006.09.016>
- Schulz, K. G., Zondervan, I., Gerringa, L. J. A., Timmermans, K. R., Veldhuis, M. J. W., & Riebesell, U. (2004). Effect of trace metal availability on coccolithophorid calcification. *Nature*, 430, 673–676. <https://doi.org/10.1038/nature02631>
- Sclater, F. R., Boyle, E., & Edmond, J. M. (1976). On the marine geochemistry of nickel. *Earth and Planetary Science Letters*, 31(1), 119–128. [https://doi.org/10.1016/0012-821x\(76\)90103-5](https://doi.org/10.1016/0012-821x(76)90103-5)
- Scott, C., & Lyons, T. W. (2012). Contrasting molybdenum cycling and isotopic properties in euxinic versus non-euxinic sediments and sedimentary rocks: Refining the paleoproxies. *Chemical Geology*, 324–325, 19–27. <https://doi.org/10.1016/j.chemgeo.2012.05.012>
- Sedwick, P. N., Church, T. M., Bowie, A. R., Marsay, C. M., Ussher, S. J., Achilles, K. M., et al. (2005). Iron in the Sargasso Sea (Bermuda Atlantic Time-series Study region) during summer: Eolian imprint, spatiotemporal variability, and ecological implications. *Global Biogeochemical Cycles*, 19, GB4006. <https://doi.org/10.1029/2004GB002445>
- Semeniuk, D. M., Bundy, R. M., Payne, C. D., Barbeau, K. A., & Maldonado, M. T. (2015). Acquisition of organically complexed copper by marine phytoplankton and bacteria in the northeast subarctic Pacific Ocean. *Marine Chemistry*, 173, 222–233. <https://doi.org/10.1016/j.marchem.2015.01.005>
- Semeniuk, D. M., Cullen, J. T., Johnson, W. K., Gagnon, K., Ruth, T. J., & Maldonado, M. T. (2009). Plankton copper requirements and uptake in the subarctic northeast Pacific Ocean. *Deep Sea Research Part I: Oceanographic Research Papers*, 56(7), 1130–1142. <https://doi.org/10.1016/j.dsr.2009.03.003>
- Semeniuk, D. M., Maldonado, M. T., & Jaccard, S. L. (2016). Chromium uptake and adsorption in marine phytoplankton—Implications for the marine chromium cycle. *Geochimica et Cosmochimica Acta*, 184, 41–54. <https://doi.org/10.1016/j.gca.2016.04.021>
- Serno, S., Winckler, G., Anderson, R. F., Hayes, C. T., Ren, H., Gersonde, R., & Haug, G. H. (2014). Using the natural spatial pattern of marine productivity in the Subarctic North Pacific to evaluate paleoproductivity proxies. *Paleoceanography*, 29(5), 438–453. <https://doi.org/10.1002/2013pa002594>
- Severmann, S., Johnson, C. M., Beard, B. L., German, C. R., Edmonds, H. N., Chiba, H., & Green, D. R. H. (2004). The effect of plume processes on the Fe isotope composition of hydrothermally derived Fe in the deep ocean as inferred from the Rainbow vent site, Mid-Atlantic Ridge, 36°14' N. *Earth and Planetary Science Letters*, 225(1–2), 63–76. <https://doi.org/10.1016/j.epsl.2004.06.001>
- Severmann, S., Johnson, C. M., Beard, B. L., & McManus, J. (2006). The effect of early diagenesis on the Fe isotope compositions of porewaters and authigenic minerals in continental margin sediments. *Geochimica et Cosmochimica Acta*, 70(8), 2006–2022. <https://doi.org/10.1016/j.gca.2006.01.007>
- Severmann, S., McManus, J., Berelson, W. M., & Hammond, D. E. (2010). The continental shelf benthic iron flux and its isotope composition. *Geochimica et Cosmochimica Acta*, 74(14), 3984–4004. <https://doi.org/10.1016/j.gca.2010.04.022>
- Shaked, Y., Xu, Y., Leblanc, K., & Morel, F. M. M. (2006). Zinc availability and alkaline phosphatase activity in *Emiliania huxleyi*: Implications for Zn-P co-limitation in the ocean. *Limnology & Oceanography*, 51, 299–309. <https://doi.org/10.4319/lno.2006.51.1.0299>
- Sharma, M., Polizzotto, M., & Anbar, A. D. (2001). Iron isotopes in hot springs along the Juan de Fuca ridge. *Earth and Planetary Science Letters*, 194(1–2), 39–51. [https://doi.org/10.1016/S0012-821X\(01\)00538-6](https://doi.org/10.1016/S0012-821X(01)00538-6)
- Shemesh, A., Mortlock, R. A., Smith, R. J., & Froelich, P. N. (1988). Determination of Ge/Si in marine siliceous microfossils: Separation, cleaning and dissolution of diatoms and radiolaria. *Marine Chemistry*, 25, 305–323. [https://doi.org/10.1016/0304-4203\(88\)90113-2](https://doi.org/10.1016/0304-4203(88)90113-2)
- Shen, G. T., Boyle, E. A., & Lea, D. W. (1987). Cadmium in corals as a tracer of historical upwelling and industrial fallout. *Nature*, 328(6133), 794–796. <https://doi.org/10.1038/328794a0>
- Sherman, D. M. (2013). Equilibrium isotopic fractionation of copper during oxidation/reduction, aqueous complexation and ore-forming processes: Predictions from hybrid density functional theory. *Geochimica et Cosmochimica Acta*, 118, 85–97. <https://doi.org/10.1016/j.gca.2013.04.030>
- Sherman, D. M., & Little, S. H. (2020). Isotopic disequilibrium of Cu in marine ferromanganese crusts: Evidence from ab initio predictions of Cu isotope fractionation on sorption to birnessite. *Earth and Planetary Science Letters*, 549, 116540. <https://doi.org/10.1016/j.epsl.2020.116540>

- Sherman, D. M., Little, S. H., & Vance, D. (2015). Reply to comment on “Molecular controls on Cu and Zn isotopic fractionation in Fe-Mn crusts”. *Earth and Planetary Science Letters*, 411, 313–315. <https://doi.org/10.1016/j.epsl.2014.12.027>
- Sherman, D. M., & Peacock, C. L. (2010). Surface complexation of Cu on birnessite (δ -MnO₂): Controls on Cu in the deep ocean. *Geochimica et Cosmochimica Acta*, 74(23), 6721–6730. <https://doi.org/10.1016/j.gca.2010.08.042>
- Shiel, A. E., Weis, D., & Orians, K. J. (2010). Evaluation of zinc, cadmium and lead isotope fractionation during smelting and refining. *The Science of the Total Environment*, 408(11), 2357–2368. <https://doi.org/10.1016/j.scitotenv.2010.02.016>
- Sieber, M., Conway, T. M., de Souza, G. F., Hassler, C. S., Ellwood, M. J., & Vance, D. (2019). High-resolution Cd isotope systematics in multiple zones of the Southern Ocean from the Antarctic circumnavigation expedition. *Earth and Planetary Science Letters*, 527, 115799. <https://doi.org/10.1016/j.epsl.2019.115799>
- Sieber, M., Conway, T. M., de Souza, G. F., Hassler, C. S., Ellwood, M. J., & Vance, D. (2020). Cycling of zinc and its isotopes across multiple zones of the Southern Ocean: Insights from the Antarctic circumnavigation expedition. *Geochimica et Cosmochimica Acta*, 268, 310–324. <https://doi.org/10.1016/j.gca.2019.09.039>
- Sieber, M., Conway, T. M., de Souza, G. F., Hassler, C. S., Ellwood, M. J., & Vance, D. (2021). Isotopic fingerprinting of biogeochemical processes and iron sources in the iron-limited surface Southern Ocean. In *Earth and planetary Science letters*. Press.
- Sieber, M., Conway, T. M., de Souza, G. F., Obata, H., Takano, S., Sohrin, Y., & Vance, D. (2019). Physical and biogeochemical controls on the distribution of dissolved cadmium and its isotopes in the Southwest Pacific Ocean. *Chemical Geology*, 511, 494–509. <https://doi.org/10.1016/j.chemgeo.2018.07.021>
- Siebert, C., Nägler, T. F., von Blanckenburg, F., & Kramers, J. D. (2003). Molybdenum isotope records as a potential new proxy for paleoceanography. *Earth and Planetary Science Letters*, 211, 159–171. [https://doi.org/10.1016/S0012-821X\(03\)00189-4](https://doi.org/10.1016/S0012-821X(03)00189-4)
- Siebert, C., Pett-Ridge, J. C., Opfergelt, S., Guicharnaud, R. A., Halliday, A. N., & Burton, K. W. (2015). Molybdenum isotope fractionation in soils: Influence of redox conditions, organic matter, and atmospheric inputs. *Geochimica et Cosmochimica Acta*, 162, 1–24. <https://doi.org/10.1016/j.gca.2015.04.007>
- Sigman, D. M., Altabet, M. A., McCorkle, D. C., Francois, R., & Fischer, G. (1999). The $\delta^{15}\text{N}$ of nitrate in the Southern Ocean: Consumption of nitrate in surface waters. *Global Biogeochemical Cycles*, 13(4), 1149–1166. <https://doi.org/10.1029/1999gb900038>
- Sigman, D. M., & Boyle, E. A. (2000). Glacial/interglacial variations in atmospheric carbon dioxide. *Nature*, 407(6806), 859–869. <https://doi.org/10.1038/35038000>
- Sigman, D. M., & Hain, M. P. (2012). The Biological productivity of the ocean: Section 1. *Nature Education Knowledge*, 3(10), 21.
- Sigman, D. M., Hain, M. P., & Haug, G. H. (2010). The polar ocean and glacial cycles in atmospheric CO₂ concentration. *Nature*, 466, 47–55. <https://doi.org/10.1038/nature09149>
- Sinoir, M., Butler, E. C. V., Bowie, A. R., Mongin, M., Nesterenko, P. N., & Hassler, C. S. (2012). Zinc marine biogeochemistry in seawater: A review. *Marine and Freshwater Research*, 63, 644–657. <https://doi.org/10.1071/mf11286>
- Skulan, J. L., Beard, B. L., & Johnson, C. M. (2002). Kinetic and equilibrium Fe isotope fractionation between aqueous Fe (III) and hematite. *Geochimica et Cosmochimica Acta*, 66(17), 2995–3015. [https://doi.org/10.1016/s0016-7037\(02\)00902-x](https://doi.org/10.1016/s0016-7037(02)00902-x)
- Sorensen, J. V., Gueguen, B., Stewart, B. D., Peña, J., Rouxel, O., & Toner, B. M. (2020). Large nickel isotope fractionation caused by surface complexation reactions with hexagonal birnessite. *Chemical Geology*, 537, 119481. <https://doi.org/10.1016/j.chemgeo.2020.119481>
- Staubwasser, M., Schoenberg, R., von Blanckenburg, F., Krüger, S., & Pohl, C. (2013). Isotope fractionation between dissolved and suspended particulate Fe in the oxic and anoxic water column of the Baltic Sea. *Biogeosciences*, 10, 233–245. <https://doi.org/10.5194/bg-10-233-2013>
- Sternberg, E., Jeandel, C., Robin, E., & Souhaut, M. (2008). Seasonal cycle of suspended barite in the Mediterranean sea. *Geochimica et Cosmochimica Acta*, 72(16), 4020–4034. <https://doi.org/10.1016/j.gca.2008.05.043>
- Stevenson, E. I., Fantle, M. S., Das, S. B., Williams, H. M., & Aciego, S. M. (2017). The iron isotopic composition of subglacial streams draining the Greenland ice sheet. *Geochimica et Cosmochimica Acta*, 213, 237–254. <https://doi.org/10.1016/j.gca.2017.06.002>
- Sun, W.-P., Hu, C.-Y., Han, Z.-B., Shen, C., & Pan, J.-M. (2016). Zn/Si records in diatom opal from Prydz Bay, East Antarctica. *Marine Geology*, 381, 34–41. <https://doi.org/10.1016/j.margeo.2016.08.009>
- Sun, Z., Wang, X., & Planavsky, N. (2019). Cr isotope systematics in the Connecticut River estuary. *Chemical Geology*, 506, 29–39. <https://doi.org/10.1016/j.chemgeo.2018.12.034>
- Sunda, W. G. (2012). Feedback interactions between trace metal nutrients and phytoplankton in the ocean. *Frontiers in Microbiology*, 3(204). <https://doi.org/10.3389/fmicb.2012.00204>
- Sunda, W. G., & Huntsman, S. A. (1995). Iron uptake and growth limitation in oceanic and coastal phytoplankton. *Marine Chemistry*, 50, 189–206. [https://doi.org/10.1016/0304-4203\(95\)00035-p](https://doi.org/10.1016/0304-4203(95)00035-p)
- Sunda, W. G., & Huntsman, S. A. (2000). Effect of Zn, Mn, and Fe on Cd accumulation in phytoplankton: Implications for oceanic Cd cycling. *Limnology & Oceanography*, 45(7), 1501–1516. <https://doi.org/10.4319/lo.2000.45.7.1501>
- Sweere, T. C., Dickson, A. J., Jenkyns, H. C., Porcelli, D., Elrick, M., van den Boorn, S. H., & Henderson, G. M. (2018). Isotopic evidence for changes in the zinc cycle during oceanic anoxic event 2 (Late Cretaceous). *Geology*, 46(5), 463–466. <https://doi.org/10.1130/g40226.1>
- Sweere, T. C., Dickson, A. J., Jenkyns, H. C., Porcelli, D., & Henderson, G. M. (2020). Zinc-and cadmium-isotope evidence for redox-driven perturbations to global micronutrient cycles during oceanic anoxic event 2 (Late Cretaceous). *Earth and Planetary Science Letters*, 546, 116427. <https://doi.org/10.1016/j.epsl.2020.116427>
- Tabouret, H., Pomerleau, S., Jolivet, A., Pécuyer, C., Riso, R., Thébault, J., et al. (2012). Specific pathways for the incorporation of dissolved barium and molybdenum into the bivalve shell: An isotopic tracer approach in the juvenile Great Scallop (*Pecten maximus*). *Marine Environmental Research*, 78, 15–25. <https://doi.org/10.1016/j.marenvres.2012.03.006>
- Tagliabue, A., Aumont, O., DeAth, R., Dunne, J. P., Dutkiewicz, S., Galbraith, E., et al. (2016). How well do global ocean biogeochemistry models simulate dissolved iron distributions? *Global Biogeochemical Cycles*, 30(2), 149–174. <https://doi.org/10.1002/2015gb005289>
- Tagliabue, A., Bopp, L., Dutay, J. C., Bowie, A. R., Chever, F., Jean-Baptiste, P., et al. (2010). Hydrothermal contribution to the oceanic dissolved iron inventory. *Nature Geoscience*, 3(4), 252–256.
- Tagliabue, A., Bowie, A. R., Boyd, P. W., Buck, K. N., Johnson, K. S., & Saito, M. A. (2017). The integral role of iron in ocean biogeochemistry. *Nature*, 543(7643), 51–59. <https://doi.org/10.1038/nature21058>
- Tagliabue, A., Bowie, A. R., DeVries, T., Ellwood, M. J., Landing, W. M., Milne, A., et al. (2019). The interplay between regeneration and scavenging fluxes drives ocean iron cycling. *Nature Communications*, 10(1), 1–8. <https://doi.org/10.1038/s41467-019-12775-5>
- Takano, S., Liao, W. H., Tian, H. A., Huang, K. F., Ho, T. Y., & Sohrin, Y. (2020). Sources of particulate Ni and Cu in the water column of the northern South China Sea: Evidence from elemental and isotope ratios in aerosols and sinking particles. *Marine Chemistry*, 219, 103751. <https://doi.org/10.1016/j.marchem.2020.103751>

- Takano, S., Tanimizu, M., Hirata, T., Shin, K. C., Fukami, Y., Suzuki, K., & Sohrin, Y. (2017). A simple and rapid method for isotopic analysis of nickel, copper, and zinc in seawater using chelating extraction and anion exchange. *Analytica Chimica Acta*, *967*, 1–11. <https://doi.org/10.1016/j.aca.2017.03.010>
- Takano, S., Tanimizu, M., Hirata, T., & Sohrin, Y. (2014). Isotopic constraints on biogeochemical cycling of copper in the ocean. *Nature Communications*, *5*, 5663. <https://doi.org/10.1038/ncomms6663>
- Talley, L. D. (2013). Closure of the global overturning circulation through the Indian, Pacific, and Southern Oceans: Schematics and transports. *Oceanography*, *26*(1), 80–97. <https://doi.org/10.5670/oceanog.2013.07>
- Tamagnini, P., Axelsson, R., Lindberg, P., Oxelfelt, F., Wüschiers, R., & Lindblad, P. (2002). Hydrogenases and hydrogen metabolism of cyanobacteria. *Microbiology and Molecular Biology Reviews*, *66*(1), 1–20. <https://doi.org/10.1128/mmb.66.1.1-20.2002>
- Tang, Y., Elzinga, E. J., Lee, Y. J., & Reeder, R. J. (2007). Coprecipitation of chromate with calcite: Batch experiments and X-ray absorption spectroscopy. *Geochimica et Cosmochimica Acta*, *71*, 1480–1493. <https://doi.org/10.1016/j.gca.2006.12.010>
- Tankéré, S. P. C., Muller, F. L. L., Burton, J. D., Statham, P. J., Guieu, C., & Martin, J. M. (2001). Trace metal distributions in shelf waters of the northwestern Black Sea. *Continental Shelf Research*, *21*, 1501–1532. [https://doi.org/10.1016/s0278-4343\(01\)00013-9](https://doi.org/10.1016/s0278-4343(01)00013-9)
- Tesoriero, A. J., & Pankow, J. F. (1996). Solid solution partitioning of Sr²⁺, Ba²⁺, and Cd²⁺ to calcite. *Geochimica et Cosmochimica Acta*, *60*(6), 1053–1063. [https://doi.org/10.1016/0016-7037\(95\)00449-1](https://doi.org/10.1016/0016-7037(95)00449-1)
- Tessin, A., Chappaz, A., Hendsy, L., & Sheldon, N. (2019). Molybdenum speciation as a paleo-redox proxy: A case study from Late Cretaceous western interior Seaway black shales. *Geology*, *47*, 59–62. <https://doi.org/10.1130/G45785.1>
- Thébault, J., Chauvaud, L., L'Helguen, S., Clavier, J., Barats, A., Jacquet, S., et al. (2009). Barium and molybdenum records in bivalve shells: Geochemical proxies for phytoplankton dynamics in coastal environments? *Limnology & Oceanography*, *54*(3), 1002–1014. <https://doi.org/10.4319/lo.2009.54.3.1002>
- Thibon, F., Blichert-Toft, J., Albarede, F., Foden, J., & Tsikos, H. (2019). A critical evaluation of copper isotopes in precambrian iron formations as a paleoceanographic proxy. *Geochimica et Cosmochimica Acta*, *264*, 130–140. <https://doi.org/10.1016/j.gca.2019.08.020>
- Thompson, C. M., & Ellwood, M. J. (2014). Dissolved copper isotope biogeochemistry in the Tasman Sea, SW Pacific Ocean. *Marine Chemistry*, *165*, 1–9. <https://doi.org/10.1016/j.marchem.2014.06.009>
- Torres, M. E., Brumsack, H. J., Bohrmann, G., & Emeis, K. C. (1996). Barite fronts in continental margin sediments: A new look at barium remobilization in the zone of sulfate reduction and formation of heavy barites in diagenetic fronts. *Chemical Geology*, *127*(1–3), 125–139. [https://doi.org/10.1016/0009-2541\(95\)00090-9](https://doi.org/10.1016/0009-2541(95)00090-9)
- Tossell, J. A. (2005). Calculating the partitioning of the isotopes of Mo between oxidic and sulfidic species in aqueous solution. *Geochimica et Cosmochimica Acta*, *69*, 2981–2993. <https://doi.org/10.1016/j.gca.2005.01.016>
- Tribouillard, N., Algeo, T. J., Lyons, T., & Riboulleau, A. (2006). Trace metals as paleoredox and paleoproductivity proxies: An update. *Chemical Geology*, *232*(1–2), 12–32. <https://doi.org/10.1016/j.chemgeo.2006.02.012>
- Turekian, K. K. (1968). Deep-sea deposition of barium, cobalt and silver. *Geochimica et Cosmochimica Acta*, *32*(6), 603–612. [https://doi.org/10.1016/0016-7037\(68\)90051-3](https://doi.org/10.1016/0016-7037(68)90051-3)
- Turner, D. R., Whitfield, M., & Dickson, A. G. (1981). The equilibrium speciation of dissolved components in freshwater and sea water at 25°C and 1 atm pressure. *Geochimica et Cosmochimica Acta*, *45*, 855–881. [https://doi.org/10.1016/0016-7037\(81\)90115-0](https://doi.org/10.1016/0016-7037(81)90115-0)
- Twining, B. S., & Baines, S. B. (2013). The trace metal composition of marine phytoplankton. *Annual Review of Marine Science*, *5*, 191–215. <https://doi.org/10.1146/annurev-marine-121211-172322>
- Twining, B. S., Baines, S. B., & Fisher, N. S. (2004). Element stoichiometries of individual plankton cells collected during the Southern Ocean Iron Experiment (SOFEX). *Limnology & Oceanography*, *49*, 2115–2128. <https://doi.org/10.4319/lo.2004.49.6.2115>
- Twining, B. S., Baines, S. B., Vogt, S., & Nelson, D. M. (2012). Role of diatoms in nickel biogeochemistry in the ocean. *Global Biogeochemical Cycles*, *26*(4), GB4001. <https://doi.org/10.1029/2011GB004233>
- Twining, B. S., Nodder, S. D., King, A. L., Hutchins, D. A., LeClerc, G. R., DeBruyn, J. M., et al. (2014). Differential remineralization of major and trace elements in sinking diatoms. *Limnology & Oceanography*, *59*(3), 689–704. <https://doi.org/10.4319/lo.2014.59.3.0689>
- Urban, E. R., Jr, Bowie, A. R., Boyd, P. W., Buck, K. N., Lohan, M. C., Sander, S. G., et al. (2020). The importance of bottom-up approaches to international cooperation in ocean science. *Oceanography*, *33*(1), 11–15. <https://doi.org/10.5670/oceanog.2020.109>
- van der Weijden, C. H., & Reith, M. (1982). Chromium (III)-Chromium (VI) interconversions in seawater. *Marine Chemistry*, *11*(6), 565–572. [https://doi.org/10.1016/0304-4203\(82\)90003-2](https://doi.org/10.1016/0304-4203(82)90003-2)
- van Geen, A., Luoma, S. N., Fuller, C. C., Anima, R., Clifton, H. E., & Trumbore, S. (1992). Evidence from Cd/Ca ratios in foraminifera for greater upwelling off California 4,000 years ago. *Nature*, *358*(6381), 54–56. <https://doi.org/10.1038/358054a0>
- van Geen, A., McCorkle, D. C., & Klinkhammer, G. P. (1995). Sensitivity of the phosphate-cadmium-carbon isotope relation in the ocean to cadmium removal by suboxic sediments. *Paleoceanography*, *10*(2), 159–169. <https://doi.org/10.1029/94pa03352>
- van Helmond, N. A. G. M., Jilbert, T., & Slomp, C. P. (2018). Hypoxia in the Holocene Baltic Sea: Comparing modern versus past intervals using sedimentary trace metals. *Chemical Geology*, *493*, 478–490. <https://doi.org/10.1016/j.chemgeo.2018.06.028>
- Vance, D., Archer, C., Bermin, J., Perkins, J., Statham, P. J., Lohan, M. C., et al. (2008). The copper isotope geochemistry of rivers and the oceans. *Earth and Planetary Science Letters*, *274*, 204–213. <https://doi.org/10.1016/j.epsl.2008.07.026>
- Vance, D., de Souza, G. F., Zhao, Y., Cullen, J. T., & Lohan, M. C. (2019). The relationship between zinc, its isotopes, and the major nutrients in the North-East Pacific. *Earth and Planetary Science Letters*, *525*, 115748. <https://doi.org/10.1016/j.epsl.2019.115748>
- Vance, D., Little, S. H., Archer, C., Cameron, V., Andersen, M. B., Rijkenberg, M. J. A., & Lyons, T. W. (2016). The oceanic budgets of nickel and zinc isotopes: The importance of sulfidic environments as illustrated by the Black Sea. *Philosophical Transactions of the Royal Society A: Mathematical, Physical and Engineering Sciences*, *374*, 20150294. <https://doi.org/10.1098/rsta.2015.0294>
- Vance, D., Little, S. H., de Souza, G. F., Khatiwala, S., Lohan, M. C., & Middag, R. (2017). Silicon and zinc biogeochemical cycles coupled through the Southern Ocean. *Nature Geoscience*, *10*, 202–206. <https://doi.org/10.1038/ngeo2890>
- Velasquez, I. B., Ibsanmi, E., Maas, E. W., Boyd, P. W., Nodder, S., & Sander, S. G. (2016). Ferrioxamine siderophores detected amongst iron binding ligands produced during the remineralization of marine particles. *Frontiers in Marine Science*, *3*, 172. <https://doi.org/10.3389/fmars.2016.00172>
- Vihtakari, M., Ambrose, W. G., Jr, Renaud, P. E., Locke, V. W. L., Carroll, M. L., Berge, J., et al. (2017). A key to the past? Element ratios as environmental proxies in two Arctic bivalves. *Palaeogeography, Palaeoclimatology, Palaeoecology*, *465*, 316–332. <https://doi.org/10.1016/j.palaeo.2016.10.020>
- Voegelin, A. R., Nägler, T. F., Samankassou, E., & Villa, I. M. (2009). Molybdenum isotopic composition of modern and Carboniferous carbonates. *Chemical Geology*, *265*, 488–498. <https://doi.org/10.1016/j.chemgeo.2009.05.015>

- Volk, T., & Hoffert, M. I. (1985). Ocean carbon pumps: Analysis of relative strengths and efficiencies in ocean-driven atmospheric CO₂ changes. In E.T. Sundquist, W.S. Broecker (Eds.), *The carbon cycle and atmospheric CO₂: Natural variations Archean to present* (Vol. 32, pp. 99–110). AGU.
- Von Allmen, K., Böttcher, M. E., Samankassou, E., & Nägler, T. F. (2010). Barium isotope fractionation in the global barium cycle: First evidence from barium minerals and precipitation experiments. *Chemical Geology*, 277(1–2), 70–77. <https://doi.org/10.1016/j.chemgeo.2010.07.011>
- Vorliceck, T. P., Chappaz, A., Groskreutz, L. M., Young, N., & Lyons, T. W. (2015). A new analytical approach to determining Mo and Re speciation in sulfidic waters. *Chemical Geology*, 403, 52–57. <https://doi.org/10.1016/j.chemgeo.2015.03.003>
- Vorliceck, T. P., Helz, G. R., Chappaz, A., Vue, P., Vezina, A., & Hunter, W. (2018). Molybdenum burial mechanism in sulfidic sediments: Iron-sulfide pathway. *ACS Earth and Space Chemistry*, 2, 565–576. <https://doi.org/10.1021/acsearthspacechem.8b00016>
- Waelles, M., Baker, A. R., Jickells, T., & Hoogewerff, J. (2007). Global dust teleconnections: Aerosol iron solubility and stable isotope composition. *Environmental Chemistry*, 4(4), 233–237. <https://doi.org/10.1071/en07013>
- Wagner, M., Chappaz, A., & Lyons, T. W. (2017). Molybdenum speciation and burial pathway in weakly sulfidic environments: Insights from XAFS. *Geochimica et Cosmochimica Acta*, 206, 18–29. <https://doi.org/10.1016/j.gca.2017.02.018>
- Wagner, M., Hendy, I. L., McKay, J. L., & Pedersen, T. F. (2013). Influence of biological productivity on silver and redox-sensitive trace metal accumulation in Southern Ocean surface sediments, Pacific sector. *Earth and Planetary Science Letters*, 380, 31–40. <https://doi.org/10.1016/j.epsl.2013.08.020>
- Wagner, M. E. (2013). *Silver as a novel tracer for Late Quaternary Southern Ocean biological and geophysical processes* (PhD thesis). University of Michigan.
- Waldron, K. J., & Robinson, N. J. (2009). How do bacterial cells ensure that metalloproteins get the correct metal? *Nature Reviews Microbiology*, 7(1), 25–35. <https://doi.org/10.1038/nrmicro2057>
- Walker, J. C. (1983). Possible limits on the composition of the Archaean ocean. *Nature*, 302(5908), 518–520. <https://doi.org/10.1038/302518a0>
- Wang, C., Reinhard, C. T., Rybacki, K. S., Hardisty, D. S., Ossa, F. O., Wang, X., et al. (2021). Chromium isotope systematics and the diagenesis of marine carbonates. *Earth and Planetary Science Letters*, 562, 116824. <https://doi.org/10.1016/j.epsl.2021.116824>
- Wang, D., Xia, W., Lu, S., Wang, G., Liu, Q., Moore, W. S., & Arthur Chen, C. T. (2016). The nonconservative property of dissolved molybdenum in the western Taiwan Strait: Relevance of submarine groundwater discharges and biological utilization. *Geochemistry, Geophysics, Geosystems*, 17, 28–43. <https://doi.org/10.1002/2014GC005708>
- Wang, R. M., Archer, C., Bowie, A. R., & Vance, D. (2019). Zinc and nickel isotopes in seawater from the Indian Sector of the Southern Ocean: The impact of natural iron fertilization versus Southern Ocean hydrography and biogeochemistry. *Chemical Geology*, 511, 452–464. <https://doi.org/10.1016/j.chemgeo.2018.09.010>
- Wang, S.-J., Rudnick, R. L., Gaschnig, R. M., Wang, H., & Wasylenki, L. E. (2019). Methanogenesis sustained by sulfide weathering during the great oxidation event. *Nature Geoscience*, 12, 296–300. <https://doi.org/10.1038/s41561-019-0320-z>
- Wang, W. X., Griscom, S. B., & Fisher, N. S. (1997). Bioavailability of Cr(III) and Cr(VI) to Marine Mussels from solute and particulate pathways. *Environmental Science & Technology*, 31(2), 603–611. <https://doi.org/10.1021/es960574x>
- Wang, Z., Li, J., Wei, G., Deng, W., Chen, X., Zeng, T., et al. (2019). Biologically controlled Mo isotope fractionation in coral reef systems. *Geochimica et Cosmochimica Acta*, 262, 128–142. <https://doi.org/10.1016/j.gca.2019.07.037>
- Wanner, C., & Sonnenthal, E. L. (2013). Assessing the control on the effective kinetic Cr isotope fractionation factor: A reactive transport modeling approach. *Chemical Geology*, 337–338, 88–98. <https://doi.org/10.1016/j.chemgeo.2012.11.008>
- Wasylenki, L. E., Anbar, A. D., Liermann, L. J., Mathur, R., Gordon, G. W., & Brantley, S. L. (2007). Isotope fractionation during microbial metal uptake measured by MC-ICP-MS. *Journal of Analytical Atomic Spectrometry*, 22, 905–910. <https://doi.org/10.1039/b705476a>
- Wasylenki, L. E., Rolfe, B. A., Weeks, C. L., Spiro, T. G., & Anbar, A. D. (2008). Experimental investigation of the effects of temperature and ionic strength on Mo isotope fractionation during adsorption to manganese oxides. *Geochimica et Cosmochimica Acta*, 72, 5997–6005. <https://doi.org/10.1016/j.gca.2008.08.027>
- Wasylenki, L. E., Swihart, J. W., & Romaniello, S. J. (2014). Cadmium isotope fractionation during adsorption to Mn oxyhydroxide at low and high ionic strength. *Geochimica et Cosmochimica Acta*, 140, 212–226. <https://doi.org/10.1016/j.gca.2014.05.007>
- Weber, T., John, S. G., Tagliabue, A., & DeVries, T. (2018). Biological uptake and reversible scavenging of zinc in the global ocean. *Science*, 361, 72–76. <https://doi.org/10.1126/science.aap8532>
- Wefing, A. M., Arps, J., Blaser, P., Wienberg, C., Hebbeln, D., & Frank, N. (2017). High precision U-series dating of scleractinian cold-water corals using an automated chromatographic U and Th extraction. *Chemical Geology*, 475, 140–148. <https://doi.org/10.1016/j.chemgeo.2017.10.036>
- Wei, W., & Algeo, T. J. (2020). Secular variation in the elemental composition of marine shales since 840 Ma: Tectonic and seawater influences. *Geochimica et Cosmochimica Acta*, 287, 367–390. <https://doi.org/10.1016/j.gca.2020.01.033>
- Wei, W., Frei, R., Chen, T., Kläebe, R., Wei, G., Li, D., & Ling, H. (2018). Marine ferromanganese oxide: A potentially important sink of light chromium isotopes? *Chemical Geology*, 495, 90–103. <https://doi.org/10.1016/j.chemgeo.2018.08.006>
- Wei, W., Kläebe, R., Ling, H. F., Huang, F., & Frei, R. (2020). Biogeochemical cycle of chromium isotopes at the modern Earth's surface and its applications as a paleo-environment proxy. *Chemical Geology*, 541, 119570. <https://doi.org/10.1016/j.chemgeo.2020.119570>
- Welch, S. A., Beard, B. L., Johnson, C. M., & Braterman, P. S. (2003). Kinetic and equilibrium Fe isotope fractionation between aqueous Fe(II) and Fe(III). *Geochimica et Cosmochimica Acta*, 67, 4231–4250. [https://doi.org/10.1016/S0016-7037\(03\)00266-7](https://doi.org/10.1016/S0016-7037(03)00266-7)
- Wichard, T., Mishra, B., Myneni, S. C. B., Bellenger, J. P., & Kraepiel, A. M. L. (2009). Storage and bioavailability of molybdenum in soils increased by organic matter complexation. *Nature Geoscience*, 2, 625–629. <https://doi.org/10.1038/ngeo589>
- Willbold, M., & Elliott, T. (2017). Molybdenum isotope variations in magmatic rocks. *Chemical Geology*, 449, 253–268. <https://doi.org/10.1016/j.chemgeo.2016.12.011>
- Winckler, G., Anderson, R. F., Jaccard, S. L., & Marcantonio, F. (2016). Ocean dynamics, not dust, have controlled equatorial Pacific productivity over the past 500,000 years. *Proceedings of the National Academy of Sciences*, 113(22), 6119–6124. <https://doi.org/10.1073/pnas.1600616113>
- Wolgemuth, K., & Broecker, W. S. (1970). Barium in sea water. *Earth and Planetary Science Letters*, 8(5), 372–378. [https://doi.org/10.1016/0012-821x\(70\)90110-x](https://doi.org/10.1016/0012-821x(70)90110-x)
- Wong, P. T. S., & Trevors, J. T. (1988). Chromium toxicity to algae and bacteria. In O. J. Nriagu, & E. Nieboer (Eds.), *Chromium in the natural and human environments* (pp. 305–315). New York, NY: John Wiley and Sons.
- Woodland, S. J., Rehkämper, M., Halliday, A. N., Lee, D.-C., Hatterdorf, B., & Günther, D. (2005). Accurate measurement of silver isotopic compositions in geological materials including lowPd/Ag meteorites. *Geochimica et Cosmochimica Acta*, 69(8), 2153–2163. <https://doi.org/10.1016/j.gca.2004.10.012>

- Wuttig, K., Townsend, A. T., van der Merwe, P., Gault-Ringold, M., Holmes, T., Schallenberg, C., et al. (2019). Critical evaluation of a seaFAST system for the analysis of trace metals in marine samples. *Talanta*, *197*, 653–668. <https://doi.org/10.1016/j.talanta.2019.01.047>
- Xiao, H., Deng, W., Wei, G., Chen, J., Zheng, X., Shi, T., et al. (2020). A pilot study on zinc isotopic compositions in shallow water coral skeletons. *Geochemistry, Geophysics, Geosystems*, *21*(11), e2020GC009430. <https://doi.org/10.1029/2020gc009430>
- Xie, R. C., Rehkämper, M., Grasse, P., van de Fliedert, T., Frank, M., & Xue, Z. (2019). Isotopic evidence for complex biogeochemical cycling of Cd in the eastern tropical South Pacific. *Earth and Planetary Science Letters*, *512*, 134–146. <https://doi.org/10.1016/j.epsl.2019.02.001>
- Xie, R. C., Galer, S. J., Abouchami, W., Rijkenberg, M. J., de Baar, H. J., De Jong, J., & Andreae, M. O. (2017). Non-Rayleigh control of upper-ocean Cd isotope fractionation in the western South Atlantic. *Earth and Planetary Science Letters*, *471*, 94–103. <https://doi.org/10.1016/j.epsl.2017.04.024>
- Xie, R. C., Galer, S. J. G., Abouchami, W., & Frank, M. (2019). Limited impact of eolian and riverine sources on the biogeochemical cycling of Cd in the tropical Atlantic. *Chemical Geology*, *511*, 371–379. <https://doi.org/10.1016/j.chemgeo.2018.10.018>
- Xu, Y., Feng, L., Jeffrey, P. D., Shi, Y., & Morel, F. M. (2008). Structure and metal exchange in the cadmium carbonic anhydrase of marine diatoms. *Nature*, *452*(7183), 56–61. <https://doi.org/10.1038/nature06636>
- Xue, Z., Rehkämper, M., Horner, T. J., Abouchami, W., Middag, R., van de Fliedert, T., & de Baar, H. J. (2013). Cadmium isotope variations in the Southern Ocean. *Earth and Planetary Science Letters*, *382*, 161–172. <https://doi.org/10.1016/j.epsl.2013.09.014>
- Xue, Z., Rehkämper, M., Schönbachler, M., Statham, P. J., & Coles, B. J. (2012). A new methodology for precise cadmium isotope analyses of seawater. *Analytical and Bioanalytical Chemistry*, *402*(2), 883–893. <https://doi.org/10.1007/s00216-011-5487-0>
- Yan, B., Zhu, X., He, X., & Tang, S. (2019). Zn isotopic evolution in early Ediacaran ocean: A global signature. *Precambrian Research*, *320*, 472–483. <https://doi.org/10.1016/j.precamres.2018.11.021>
- Yang, S.-C., Hawco, N. J., Pinedo-González, P., Bian, X., Huang, K.-F., John, S. G., & John, S. G. (2020). A new purification method for Ni and Cu stable isotopes in seawater provides evidence for widespread Ni isotope fractionation by phytoplankton in the North Pacific. *Chemical Geology*, *547*, 119662. <https://doi.org/10.1016/j.chemgeo.2020.119662>
- Yang, S.-C., Lee, D.-C., & Ho, T.-Y. (2015). Cd isotopic composition in the suspended and sinking particles of the surface water of the South China Sea: The effects of biotic activities. *Earth and Planetary Science Letters*, *428*, 63–72. <https://doi.org/10.1016/j.epsl.2015.07.025>
- Yang, S.-C., Lee, D.-L., & Ho, T.-Y. (2012). The isotopic composition of Cadmium in the water column of the South China Sea. *Geochimica et Cosmochimica Acta*, *98*, 66–77. <https://doi.org/10.1016/j.gca.2012.09.022>
- Yang, S.-C., Lee, D.-L., Ho, T.-Y., Wen, L.-S., & Yang, H.-H. (2014). The isotopic composition of dissolved cadmium in the water column of the West Philippine Sea. *Frontiers in Marine Science*, *1*(61). <https://doi.org/10.3389/fmars.2014.00061>
- Yang, S.-C., Zhang, J., Sohrin, Y., & Ho, T.-Y. (2018). Cadmium cycling in the water column of the Kuroshio-Oyashio extension region: Insights from dissolved and particulate isotopic composition. *Geochimica et Cosmochimica Acta*, *233*, 66–80. <https://doi.org/10.1016/j.gca.2018.05.001>
- Yang, T., Chen, Y., Zhou, S., & Li, H. (2019). Impacts of aerosol copper on marine phytoplankton: A review. *Atmosphere*, *10*(7), 414. <https://doi.org/10.3390/atmos10070414>
- Yee, D., & Morel, F. M. M. (1996). In vivo substitution in carbonic of zinc by cobalt of a marine anhydrase diatom. *Limnology & Oceanography*, *41*, 573–577. <https://doi.org/10.4319/lo.1996.41.3.0573>
- Zhang, R., Jensen, L. T., Fitzsimmons, J. N., Sherrell, R. M., & John, S. (2019). Dissolved cadmium and cadmium stable isotopes in the western Arctic Ocean. *Geochimica et Cosmochimica Acta*, *258*, 258–273. <https://doi.org/10.1016/j.gca.2019.05.028>
- Zhang, R., John, S. G., Zhang, J., Ren, J., Wu, Y., Zhu, Z., et al. (2015). Transport and reaction of iron and iron stable isotopes in glacial meltwaters on Svalbard near Kongsfjorden: From rivers to estuary to ocean. *Earth and Planetary Science Letters*, *424*, 201–211. <https://doi.org/10.1016/j.epsl.2015.05.031>
- Zhang, Y., Amakawa, H., & Nozaki, Y. (2001). Oceanic profiles of dissolved silver: Precise measurements in the basins of western North Pacific, Sea of Okhotsk, and the Japan Sea. *Marine Chemistry*, *75*, 151–163. [https://doi.org/10.1016/s0304-4203\(01\)00035-4](https://doi.org/10.1016/s0304-4203(01)00035-4)
- Zhang, Y., Obata, H., & Nozaki, Y. (2004). Silver in the Pacific Ocean and the Bering Sea. *Geochemical Journal*, *38*, 623–633. <https://doi.org/10.2343/geochemj.38.623>
- Zhao, M., Tarhan, L. G., Zhang, Y., Hood, A., Asael, D., Reid, R. P., & Planavsky, N. J. (2021). Evaluation of shallow-water carbonates as a seawater zinc isotope archive. *Earth and Planetary Science Letters*, *553*. <https://doi.org/10.1016/j.epsl.2020.116599>
- Zhao, Y., Vance, D., Abouchami, W., & de Baar, H. J. W. (2014). Biogeochemical cycling of zinc and its isotopes in the Southern Ocean. *Geochimica et Cosmochimica Acta*, *125*, 653–672. <https://doi.org/10.1016/j.gca.2013.07.045>
- Zhu, X. K., O’Nions, R. K., Guo, Y., & Reynolds, B. C. (2000). Secular variation of iron isotopes in North Atlantic deep water. *Science*, *287*(5460). <https://doi.org/10.1126/science.287.5460.2000>
- Zink, S., Schoenberg, R., & Staubwasser, M. (2010). Isotopic fractionation and reaction kinetics between Cr(III) and Cr(VI) in aqueous media. *Geochimica et Cosmochimica Acta*, *74*, 5729–5745. <https://doi.org/10.1016/j.gca.2010.07.015>
- Zirino, A., & Yamamoto, S. (1972). A pH-dependent model for the chemical speciation of copper, zinc, cadmium, and lead in seawater. *Limnology & Oceanography*, *17*, 661–671. <https://doi.org/10.4319/lo.1972.17.5.0661>